

Establishment and optimization of a power-to-food system to produce single cell protein containing cobalamin and folate

Dissertation

der Mathematisch-Naturwissenschaftlichen Fakultät
der Eberhard Karls Universität Tübingen
zur Erlangung des Grades eines
Doktors der Naturwissenschaften
(Dr. rer. nat.)

vorgelegt von
Akanksha Mishra
aus Cuttack, Indien

Tübingen
2021

Gedruckt mit Genehmigung der Mathematisch-Naturwissenschaftlichen Fakultät der
Eberhard Karls Universität Tübingen.

Tag der mündlichen Qualifikation:

19.01.2022

Dekan:

Prof. Dr. Thilo Stehle

1. Berichterstatter:

Prof. Dr. Largus T. Angenent

2. Berichterstatterin:

Prof. Dr. Christiane Zarfl

Table of Contents

Abstract.....	2
Zusammenfassung.....	4
Outline of the thesis	7
Introduction.....	9
Carbon fixation with renewable electric power to feed the world: Power-to-protein	39
Power-to-protein: converting renewable electric power and carbon dioxide into single cell protein with a two-stage bioprocess.....	81
Establishing a power-to-food platform by demonstrating the presence of cobalamin and folate in single-cell protein synthesized from renewable electric power and carbon dioxide	125
Acknowledgement	192
Statement of contribution.....	194
Publications.....	195

Abstract

Climate change is among the deepest existential challenges facing humanity and the earth today are countering massive emissions from anthropogenic activities. As of today, several countries have enacted laws to mitigate carbon dioxide emissions from industrial activity and guide the transition to low-carbon transportation. Meanwhile the private sector has invented technologies that derive energy from renewable power instead of fossil-based sources. Unfortunately, such innovation is yet to transform the food sector. At present, the food sector contributes to one-third of the global carbon emissions. Because of land-use, livestock farming, and transportation, it is one of the biggest sources of greenhouse gases. To feed a growing population, we are still relying on traditional practices for food production at a high ecological cost.

Fortunately, several solutions are *en route* which specifically address the high-emission aspects of the food production process to make the food sector more sustainable. For instance, a UK-based company called Marlow Foods launched a product called Quorn™ that is obtained from a fungal strain called *Fusarium venenatum*. Due to its fibrous texture and high protein content, it has gained popularity as a meat-substitute. Lately, the food industry has been focusing on the cultivation of hydrogen-oxidizing bacteria at a commercial scale to synthesize microbial protein directly from carbon dioxide. In such systems, hydrogen acts as the energy carrier and could be derived from an electrolyzer operated with renewable power. This would eliminate our reliance on agriculture, therefore mitigating the carbon footprint of food production. We refer to this strategy for producing edible protein directly from carbon dioxide using renewable power as power-to-protein.

At the beginning of this thesis, we illustrate the power-to-protein concept by conducting a comparative analysis between all the systems that have been implemented to perform carbon fixation into microbial protein using renewable power. The comparison was conducted using the principles of thermodynamics on the predominant carbon fixation pathways used by the microbes involved in each system. It revealed that a two-stage system in which carbon dioxide is first converted to an intermediate, and then presented to a different bioreactor as a substrate for synthesizing microbial protein, would yield the highest biomass per unit input energy. Following this, we demonstrate its operation in a proof-of-concept study, in which the first bioreactor was operated with *Clostridium ljungdahlii* to convert carbon dioxide into acetic acid through the Wood-

Ljungdahl pathway. This new carbon source was provided to the second bioreactor for the growth of an aerobic strain of yeast, *Sachharomyces cerevisiae* to synthesize microbial protein. As this strain has already been accepted for human consumption, evidence of its growth on acetic acid renders a big advantage to the proposed system. In this operation, 25% of the total carbon from carbon dioxide was converted into yeast biomass with a protein content of 40-50%.

Finally, we tried to broaden the scope of the power-to-protein system into a power-to-food system by investigating the flux of cobalamin and folate that could be naturally produced by the microbes within the system. Although, this operation of the power-to-food system encountered severe technical issues, we were able to provide evidence that *S. cerevisiae* is capable of folate production when grown on acetic acid in the Stage 2 bioreactor. We observed a volumetric folate productivity of $16.47 \mu\text{g L}^{-1} \text{d}^{-1}$ or a folate yield of $5.85 \mu\text{g g}^{-1} \text{d}^{-1}$ after accounting for an average biomass concentration of 1.7g L^{-1} in the Stage 2 bioreactor. At this rate of production, we can provide 31% of the daily folate requirement for an average adult using just a standard serving size of yeast.

The power-to-food system for the generation of food enriched in nutrients warrants further optimizations and investigations. We have learned that the operation of such systems, optimization of the microbe's performance, and the downstream processing of the final product require a multidisciplinary approach. Nevertheless, the findings from this study have revealed the potential of such alternative processes to greatly reduce the carbon emissions from the food sector while meeting the needs of a rising population. This research is needed in a world where a sustainable system such as power-to-food may soon become the only tenable means of food production.

Zusammenfassung

Der Klimawandel gehört zu den größten existenziellen Herausforderungen, vor denen die Menschheit steht, und die Erde hat heute mit massiven Emissionen aus anthropogenen Aktivitäten zu kämpfen. Mehrere Länder haben bereits Gesetze erlassen, um die Kohlendioxid emissionen aus Industrietätigkeiten zu verringern und den Übergang zu einem kohlenstoffarmen Verkehrssystem zu fördern. In der Zwischenzeit hat der Privatsektor Technologien entwickelt, die Energie aus erneuerbaren statt aus fossilen Quellen gewinnen. Leider haben solche Innovationen den Lebensmittelsektor noch nicht verändert. Gegenwärtig trägt der Lebensmittelsektor zu einem Drittel der weltweiten Kohlenstoffemissionen bei. Aufgrund von Landnutzung, Viehzucht und Transport ist er eine der größten Quellen von Treibhausgasen. Um eine wachsende Bevölkerung zu ernähren, verlassen wir uns immer noch auf traditionelle Praktiken der Lebensmittelproduktion, was mit hohen ökologischen Kosten verbunden ist.

Glücklicherweise sind mehrere Lösungen auf dem Weg, die speziell auf die emissionsintensiven Aspekte der Lebensmittelproduktion abzielen, um den Lebensmittelsektor nachhaltiger zu gestalten. So hat beispielsweise das britische Unternehmen Marlow Foods ein Produkt namens Quorn™ auf den Markt gebracht, das aus einem Pilzstamm namens *Fusarium venenatum* gewonnen wird. Aufgrund seiner faserigen Beschaffenheit und seines hohen Proteingehalts hat es als Fleischersatz an Beliebtheit gewonnen. In letzter Zeit hat sich die Lebensmittelindustrie auf die Kultivierung von wasserstoffoxidierenden Bakterien im kommerziellen Maßstab konzentriert, um mikrobielles Protein direkt aus Kohlendioxid zu synthetisieren. In solchen Systemen dient Wasserstoff als Energieträger und könnte aus einem Elektrolyseur gewonnen werden, der mit erneuerbarer Energie betrieben wird. Dies würde unsere Abhängigkeit von der Landwirtschaft beseitigen und somit den Kohlenstoff-Fußabdruck der Lebensmittelproduktion verringern. Wir bezeichnen diese Strategie zur Herstellung von essbarem Eiweiß direkt aus Kohlendioxid mit Hilfe erneuerbarer Energie als Power-to-Protein.

Zu Beginn dieser Arbeit veranschaulichen wir das Power-to-Protein-Konzept, indem wir eine vergleichende Analyse aller Systeme durchführen, die für die Kohlenstoffbindung in mikrobiellem Eiweiß unter Verwendung erneuerbarer Energie eingesetzt werden. Der Vergleich wurde unter Anwendung der Grundsätze der Thermodynamik über die vorherrschenden

Kohlenstofffixierungswege durchgeführt, die von den in jedem System beteiligten Mikroben genutzt werden. Es zeigte sich, dass ein zweistufiges System, bei dem Kohlendioxid zunächst in ein Zwischenprodukt umgewandelt und dann einem anderen Bioreaktor als Substrat für die Synthese von mikrobiellem Protein zugeführt wird, die höchste Biomasse pro Energieeinheit liefern würde. Anschließend demonstrieren wir die Funktionsweise in einer Proof-of-Concept-Studie, in der der erste Bioreaktor mit *Clostridium ljungdahlii* betrieben wurde, um Kohlendioxid über den Wood-Ljungdahl-Weg in Essigsäure umzuwandeln. Diese neue Kohlenstoffquelle wurde dem zweiten Bioreaktor für das Wachstum eines aeroben Hefestammes, *Sachharomyces cerevisiae*, zur mikrobiellen Proteinsynthese zugeführt. Da dieser Stamm bereits für den menschlichen Verzehr zugelassen ist, stellt der Nachweis seines Wachstums auf Essigsäure einen großen Vorteil für das vorgeschlagene System dar. Bei diesem Verfahren wurden 25% des gesamten Kohlenstoffs aus Kohlendioxid in Hefebiomasse mit einem Proteingehalt von 40-50% umgewandelt.

Schließlich versuchten wir, den Anwendungsbereich des Power-to-Protein-Systems zu einem Power-to-Food-System zu erweitern, indem wir den Fluss von Cobalamin und Folat untersuchten, die von den Mikroben innerhalb des Systems auf natürliche Weise produziert werden könnten. Obwohl der Betrieb des Power-to-Food-Systems auf schwerwiegende technische Probleme stieß, konnten wir nachweisen, dass *S. cerevisiae* in der Lage ist, Folat zu produzieren, wenn es im Bioreaktor der Stufe 2 auf Essigsäure gezüchtet wird. Wir beobachteten eine volumetrische Folatproduktivität von $16,47 \mu\text{g L}^{-1} \text{d}^{-1}$ oder eine Folatausbeute von $5,85 \mu\text{g g}^{-1} \text{d}^{-1}$ nach Berücksichtigung einer durchschnittlichen Biomassekonzentration von $1,7 \text{g L}^{-1}$ im Bioreaktor der Stufe 2. Bei dieser Produktionsrate können wir 31% des täglichen Folatbedarfs eines durchschnittlichen Erwachsenen mit nur einer Standardportion Hefe decken.

Das Power-to-Food-System zur Erzeugung von mit Nährstoffen angereicherten Lebensmitteln bedarf weiterer Optimierungen und Untersuchungen. Wir haben gelernt, dass der Betrieb solcher Systeme, die Optimierung der Leistung der Mikroben und die anschließende Verarbeitung des Endprodukts einen multidisziplinären Ansatz erfordern. Nichtsdestotrotz haben die Ergebnisse dieser Studie das Potenzial solcher alternativen Verfahren aufgezeigt, die Kohlenstoffemissionen des Lebensmittelsektors erheblich zu reduzieren und gleichzeitig den Bedarf einer wachsenden Bevölkerung zu decken. Diese Forschung ist notwendig in einer Welt, in der ein nachhaltiges

System wie Power-to-Food bald die einzige vertretbare Methode der Lebensmittelproduktion sein könnte.

Outline of the thesis

In this thesis, we discuss the establishment and optimization of a power-to-food system by classifying all the steps that were involved into the following three chapters:

Chapter 1

In this chapter, we performed a comparative analysis for all the systems that illustrate the power-to-protein concept to produce microbial protein. The goal was to classify existing and prospective power-to-protein systems based on their carbon fixation pathway to reveal their energy efficiencies. We calculated the highest theoretical maximum value for microbial biomass that could be obtained from each power-to-protein system. This value was then normalized to the input energy required by each one at biochemical standard conditions. The input energy of each system was determined from the Gibbs free energy of all the reactions that are required for the conversion of carbon dioxide to biomass. The calculations divulged the advantage of a two-stage system for producing microbial protein.

Chapter 2

This chapter is dedicated to the demonstration of a proof-of-concept for the conversion of carbon dioxide into microbial protein *via* a two-stage system. Molitor *et al.* (2019) demonstrated an integrated system, where in, the first stage contained *C. ljungdahlii* to convert carbon dioxide into acetic acid with the Wood Ljungdahl pathway, while the second bioreactor contained *S. cerevisiae* to produce biomass. The highlight of this study was the technical, economical, and societal evaluation of the power-to-protein system. We adapted the capital cost and revenue of the Quorn™ process to that of the power-to-protein system. We accounted for the cost of replacing glucose with acetic acid as a carbon source and doubled the cost of fermentation due to the implementation of a two-stage system. With 7.6% increase in the cost of the final product from the power-to-protein system, we confirmed its economic viability.

Chapter 3

This chapter is focused on the transformation of the power-to-protein system into a power-to-food system. In this study we investigate whether the microbes are capable of inherently producing essential nutrients such as, cobalamin and folate, in the two-stage system. As cobalamin can be synthesized only by some species bacteria or archaea, we exploited the presence of a biocatalyst in the first bioreactor to act as a source of cobalamin for the biomass that is obtained from the Stage 2 bioreactor. We operated a power-to-food reactor, that was in principle the same system as described in the power-to-protein study, with a few modifications in the design and operational strategy. The primary objective behind this study was to capture the production and estimate the flux of cobalamin and folate *C. ljungdahlii* and *S. cerevisiae* in the power-to-food system.

Introduction

Syngas fermentation¹ represents the biological conversion of carbon monoxide (CO), carbon dioxide (CO₂), and hydrogen (H₂) into valuable organic acids and alcohol. This process is carried out by gas-fermenting microbes such as, the acetogenic bacteria. There are two key objectives behind the implementation of syngas fermentation as a carbon-recycling process: (1) minimization of the amount of energy lost during the conversion of a carbonaceous material into its final product (Phillips *et al.*, 2017) (2) valorization of the final product. The power-to-food bioreactor that is developed in the Environmental Biotechnology group at the University of Tübingen intends to these objectives by conducting H₂/CO₂ gas fermentation and the subsequent utilization of the obtained products as a substrate for microbial food production. However, in this chapter, in addition to the introduction of the power-to-food system, we have also addressed the importance of studying bubble size properties and their interaction with microbes during a gas fermentation process. We present several approaches from a congregation of studies that have successfully accomplished this through extraordinary designs and novel equipment. Investigation of bubble behavior in anaerobic processes is arguably small. Therefore, we believe that the outcome of this research can have enormous implications on the field of syngas fermentation.

The power-to-food concept

A scheme of the power-to-food system comprises of two stages, which represents different microbial processes carried out in different reactor vessels. The first stage uses a carboxydrotrophic acetogen, *Clostridium ljundahlii*, for synthesizing acetate from H₂/CO₂ fermentation. The acetate from Stage 1 bioreactor is simultaneously introduced into a Stage 2 bioreactor as a growth substrate to yeasts for the microbial production of food/nutrient. This concept has been successfully demonstrated for the growth of *Saccharomyces cerevisiae* from an earlier operation of the Power to protein reactor (Molitor *et al.*, 2019). Based on the existing studies, the amount of protein present

¹ Also known as Synthesis gas, is a mixture of 25-30% H₂, 5-15% CO₂, 0-5% CH₄, and 30-60% CO. It is produced as an intermediate during the manufacture of Synthetic Natural Gas (Couto, Rouboa, Silva, Monteiro, & Bouziane, 2013)

in these eukaryotic organisms is comparable to that found in other conventional food sources such as soybeans or meat (Bekatorou *et al.*, 2006).

S. cerevisiae is more commonly known as baker's yeast due to its application in the bread and dough making process (Jenson, 1997; Jespersen *et al.*, 1994). It contains approximately 30-33% dry materials, 6.5-9.3% nitrogen, 40.6–58.0% of proteins, 35.0–45.0% of carbohydrates, 4.0–6.0% of lipids, and 5.0–7.5% of minerals and vitamins (Bekatorou *et al.*, 2006). Recent studies have presented *S. cerevisiae* as a probiotic food supplement in animal feed (Lara-Flores *et al.*, 2003). Moreover, administration of aerobic conditions in the Stage 2 bioreactor produces a substantial amount of biomass, resulting in a higher yield of protein and vitamins.

The mycoprotein from *Fusarium venenatum* is currently being used in six European countries and is slowly spreading out in other countries as well (Garodia *et al.*, 2017). This strain contains high amounts of mycoprotein, including B complex vitamins and mineral nutrients, without reports of any toxic effects or adverse reactions in humans (Gilani & Lee, 2003). They are available in the commercial market as a meat substitute product called Quorn®, which is processed by a U.K based company called Marlow Foods Ltd. (Wiebe, 2004). There are several advantages encouraging the cultivation and consumption of meat substitutes that are prepared from the fungal mycoproteins. For instance, it reduces the uptake of plasma cholesterol (13% reduction) and low-density lipoproteins (9% reduction) (Garodia *et al.*, 2017). Additionally, the mycoprotein contains a healthy ratio polyunsaturated to saturated fatty acid and is enriched in dietary fiber with a low-fat content.

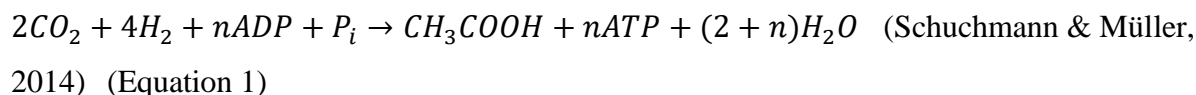
However, the power-to-food reactor is not the only exemplification of a cost-effective production of mycoprotein. Recently, Ritchie *et al.* (2017) developed a 3f-bio Technology platform that uses grain starch hydrolysate, which is generally used as a feedstock to produce ethanol in biorefineries, to produce mycoprotein. Their technology recommends splitting the same carbohydrate-rich feedstock into both ethanol and mycoprotein production processes. This would reduce the cost of the mycoprotein production process by almost 50% (Ritchie *et al.*, 2017). Nevertheless, the uniqueness of the power-to-food concept stems from the production of nutrient-rich food through the fermentation of industrial waste gases. Moreover, we will attempt to do so *via* the growth of a nutrient-producing microbe from the effluent that is generated from the gas fermentation process to strengthen the scope of the power-to-food concept. More specifically, we are interested in

comparing the concentration of vitamins produced by the system, to the amount added in the two-stage process.

The Wood-Ljungdahl pathway

The fermentation of CO₂/H₂ in the first stage of the power-to-food reactor will be carried out by *C. ljundahlii*, one of the first acetogens to produce ethanol from Syngas (Barik *et al.*, 1988; Tanner *et al.*, 1993). *C. ljundahlii* belongs to a specialized group of acetogenic bacteria, which can perform the Wood-Ljungdahl pathway for CO₂ fixation and energy conservation (Drake *et al.*, 2008). They are facultative anaerobes and use a variety of organic substrates, such as hexoses, pentoses, alcohol, and formic acid, in addition to oxidation of inorganic substrates such as H₂, CO and CO₂ (Schuchmann & Müller, 2014). An evaluation of the isotopic fractionation pattern in anaerobic organisms using the WLP pathway suggests that they may have been the first autotrophs to derive energy from inorganic substrates such as CO and H₂ (Brock, 1989).

C. thermoaceticum was selected as the model strain for studying acetogenesis (Wood, 1952). The enzymes involved in the WLP pathway were characterized using mass spectrometry (Wood, 1952). It was found that glucose gets broken down into two molecules of pyruvate *via* the Embden-Meyerhof-Pranas pathway. Thereafter, the decarboxylation of pyruvate results in the formation of two molecules of acetyl-CoA ultimately resulting in two molecules of acetate (Wood, 1952). The eight electrons that are released from the oxidation of glucose would reduce the CO₂ that is obtained from the decarboxylation of pyruvate to form acetate (Wood, 1952). Apart from the oxidation of sugars, the oxidation of H₂ will also act as a source of electrons making acetogens facultative autotrophs with the ability to convert H₂ and CO₂ (Brock, 1989). The stoichiometric reaction for acetate formation under autotrophic conditions has been shown below (Equation 1). The steps mentioned are applicable for the the heterotrophic as well as the autotrophic growth of *C. ljundahlii* (**Figure 1**).



The two carbon molecules required for the generation of one molecule of acetate come from two different branches of the WLP pathway, namely, the methyl branch and the carbonyl branch. In

the carbonyl branch, one molecule of CO₂ is reduced to one molecule of CO by the dehydrogenase/acetyl-CoA synthase enzyme (CODH/ACS). In the methyl branch, one molecule of CO₂ is converted to formate by the enzyme formate dehydrogenase. This formate then binds to the co-factor tetrahydrofolate (THF) and is converted to formyl-THF using the formyl-THF synthetase enzyme. Formyl-THF is then used to generate methenyl-THF by formyl-THF cyclohydrolase and is further reduced to methylene-THF *via* the methylene-THF dehydrogenase. Methylene-THF is reduced to methyl-THF *via* the methylene-THF reductase. Finally, a methyltransferase transfers the methyl group from methyl-THF *via* a corrinoid iron-sulphur protein (CoFeSP) to the CODH/ACS. The CO from the carbonyl branch and fuses with the Methyl-CoFeSP generated in the methyl branch followed by the attachment of CoA to form acetyl-CoA. The phosphotransacetylase enzyme produces acetyl phosphate from acetyl Co-A, which becomes a substrate for acetate kinase to produce acetate.

The reactions constituting the methyl branch in the WLP pathway are conserved in most of the acetogens (Ragsdale & Pierce, 2008). However, they differ with respect to the electron donors initiating these redox reactions (Ragsdale, 2008). For instance, *C. Ljungdahlii* and *A. woodii* use different enzymes for hydrogen oxidation, reduction of CO₂ to formate, and the conversion of methylene-THF to methyl-THF in the WLP pathway (Schuchmann & Müller, 2014). With specific regard to energy conservation in *C. Ljungdahlii*, it has been shown through predicted modelling and experimental data that *C. Ljungdahlii* uses the Rnf complex as the only coupling site for energy conservation (Schuchmann & Müller, 2014). The Rnf complex facilitates electron transfer from Fd²⁻ to NAD with the translocation of protons out into the cytoplasmic membrane (Tremblay *et al.*, 2013). The proton gradient generated activates the membrane bound ATP synthase (ATPase) to generate ATP. Nevertheless, the amount of energy conserved *via* the Rnf complex is based on the availability of the electron acceptors of hydrogenases and electron donors in the WLP pathway (Schuchmann & Müller, 2014).

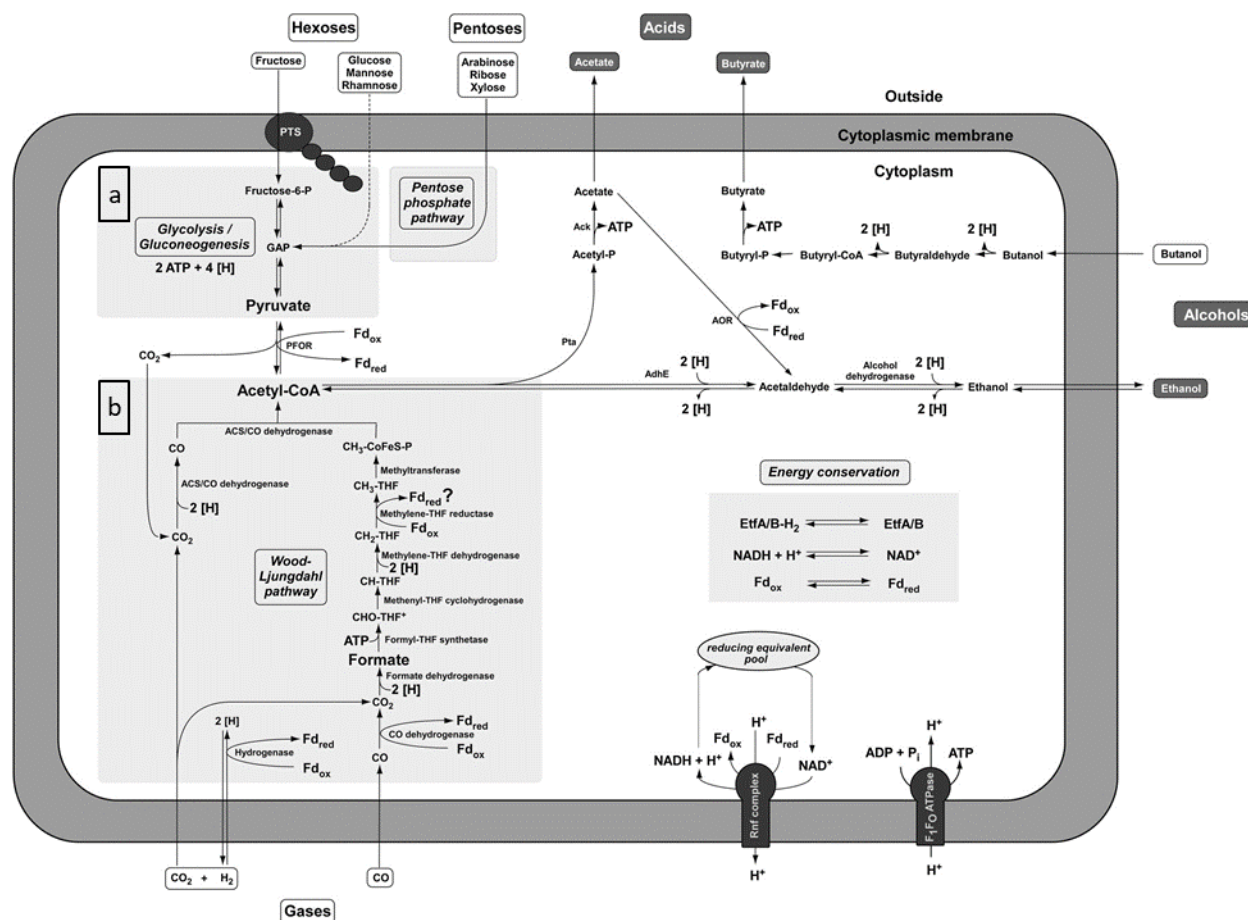


Figure 1: A scheme showing the WLP pathway in *C. ljundahlii*. The heterotrophic pathway consisting of the glycolysis and the pentose phosphate pathway and (b) shows the WLP pathway utilized during autotrophic growth. The scheme has been adapted from Köpke *et al* (2010).

Transfer of B12 and B9 vitamins from the Stage 1 bioreactor into the Stage 2 bioreactor

The chemical synthesis of vitamin B12 is tedious and consists of 70 different steps (Eschenmoser & Wintner, 1977). Therefore, at an industrial scale, the bio-synthetic fermentation process employing selected and genetically modified microbes is preferred (Martens *et al.*, 2002). Cobalamins (vitamin B₁₂) consists of adenosyl-(AdoB₁₂), methyl-(CH₃B₁₂), hydroxy-(OHB₁₂), and cyanocobalamin (CNB₁₂) (Fang *et al.*, 2017). Amongst these, adenosylcobalamin (AdoB₁₂) and cyanocobalamin (CNB₁₂) are the active forms in the human cell. In bacteria, there are two major pathways for the *de-novo* synthesis of vitamin B₁₂, based on whether these processes take place under aerobic/anaerobic conditions. For instance, *P. denitrificans* and *S. typhimurium* use the

aerobic and anaerobic pathway for the synthesis of AdoB₁₂, respectively (Fang *et al.*, 2017). In microbes, vitamin B₁₂ is used as a co-factor for synthesizing chlorophyll as well as S-adenosylmethionine, which acts a methyl donor for the synthesis of heme (Layer *et al.*, 2003). Some strains can also produce B₁₂ using the Salvage pathway that incorporates extracellular corrinoids *via* an ATP-binding cassette (ABC) and converts them into adenosylcobalamin (Escalante-Semerena, 2007).

From the standpoint of microbial production of folate (B₉) at an industrial scale, we are currently witnessing its application in the fortification of fermented dairy food and folate-containing probiotics (Vandamme & Revuelta, 2016). The biologically active form of B₉ is tetrahydrofolate (THF) (Vandamme & Revuelta, 2016). Archaea and bacteria require folate co-factors for a variety of biosynthetic processes and can synthesize it *de novo* (Rossi *et al.*, 2011). Several countries encourage folate fortification in food products to meet the daily requirements of the population (Crider *et al.*, 2011). As this strategy has proven to be a major success in USA and Canada (Jägerstad, 2012), we are motivated to study and quantify the accumulation of this substance in our power-to-food process.

The first metabolic model for *C. ljundahlii* was published by Nagarjan *et al.* (2013). Köpke *et al.* (2010) further revealed a third mode of anaerobic homoacetogenic metabolism through experimental data and *in-silico* comparisons. Based on the presence of the genes related B₁₂ biosynthesis in large clusters, they suggest that *C. ljundahlii* can synthesize it using the anaerobic pathway (Köpke *et al.*, 2010). This pathway is annotated in the KEGG database (clj00860). Furthermore, KEGG also contains information on the ABC transporters proteins (clj02010) in *C. ljundahlii* which play a role in the translocation of vitamin complexes across cell membranes (Kanehisa *et al.*, 2017; Köpke *et al.*, 2010). Although it was not verified experimentally, *C. ljundahlii* also contains genes necessary for the biosynthesis of co-factors such as, folate and riboflavin (Köpke *et al.*, 2010). Annan *et al.* (2019) performed growth experiments with *C. ljundahlii* by eliminating individual vitamins from the medium to identify the ones that are necessary for their growth. The results showed that *C. ljundahlii* is only auxotrophic for pantothenate, biotin, and thiamine and can produce B₁₂ and B₉.

Depending on the availability of B-group vitamins, fungi and yeasts could acquire it from a direct interaction with heterotrophic bacteria capable of its biosynthesis or from areas enriched with B₁₂

due to the activity of prokaryotes (Azam & Malfatti, 2007; Croft *et al.*, 2005; Kazamia *et al.*, 2012). Ectotrophic mycorrhiza² fungi require B-group vitamins for growth and thrive from a constant supply of these vitamins from the bacteria residing in the rhizosphere (Strzelczyk & Leniarska, 1985). Watanabe *et al.* (2012) isolated 1.09-2 µg/100 g dry weight of bio-active vitamin B₁₂ from a wild edible mushroom, *Cantharellus cibarius*, and suggested that it may have accumulated from the bacteria present on the surface of this wild mushroom. Several other studies, such as by Kazamia *et al.* (2012) and Croft *et al.* (2005), have demonstrated an algal-bacterial symbiosis, where algae acquired vitamin B₁₂ from bacteria. Studies carried out by Helliwell *et al.* (2016) demonstrate the conversion of pseudo-cobalamin produced by planktonic cyanobacteria into a bio-active form by several species of microalgae (Helliwell *et al.*, 2016).

Abbas (2006) discusses several studies that have benefitted from the incorporation of vitamins and proteins into the biomass of various yeast strains during fermentation. *Saccharomyces carlsbergensis* has an active transport mechanism for Pyridoxine (vitamin B6), leading to a much higher concentration in its membrane lipids in comparison to the concentrations that are present in the external media (Shane & Snell, 1976). Similarly, *S. cerevisiae* can accumulate both B6 and biotin (vitamin B7) (Rogers & Lichstein, 1969; Stolz & Vielreicher, 2003). Carlile (1995) demonstrated that a high C/N ratio enhances the accumulation of alcohols, secondary metabolites, lipids, or extracellular polysaccharides in the fungal cell wall.

Therefore, it is likely that while using the Stage 1 bioreactor as source of carbon for the Stage 2 bioreactor, we may transfer some essential vitamins, such as B9 and B12, ultimately resulting in its accumulation in cell biomass. We are interested in investigating this further during the operation of the power-to-food system by carrying out a full survey of vitamin administration and production in both the bioreactors. This would entail performing a quantifiable analysis on the total amount of B9 and B12 provided to the two reactors and the amount retrieved in the Stage 2 bioreactor.

² These species of fungi form a layer on the outermost surface of plant roots (Trappe, 1962).

Importance of bubble size properties

Martin, Richter, Saha, and Angenent (2016) calculated an average mass transfer co-efficient³ ($k_L a$) of 181 h^{-1} in their syngas fermentation reactors. The highest mass transfer was calculated to be 373 h^{-1} with a headspace carbon monoxide (CO) partial pressure of 0.0435 atm (Martin *et al.*, 2016). The value calculated for the $k_L a$ accounted for the continuous consumption of the gaseous substrate by the biomass (Martin *et al.*, 2016). Additionally, while sparging the Syngas mixture into the reactor, the diameter of the bubbles formed were roughly an order of magnitude smaller when compared to the values observed in a non-inoculated vessel containing filtered medium. Theoretically, this may have increased the $k_L a$ value by an order of magnitude with a substantial impact on substrate availability and mass transfer dynamics of the system. It is likely that the products of syngas fermentation, which are acetic acid, and ethanol, could also act as surfactants and generate smaller bubbles. However, given the amount at which these products were formed, the impact on the radius was larger than expected. These observations were indicative of an additional biological factor, such as biosurfactants, that could reduce the surface tension of the medium and reduce the radii of the gas bubbles (**Figure 2**).

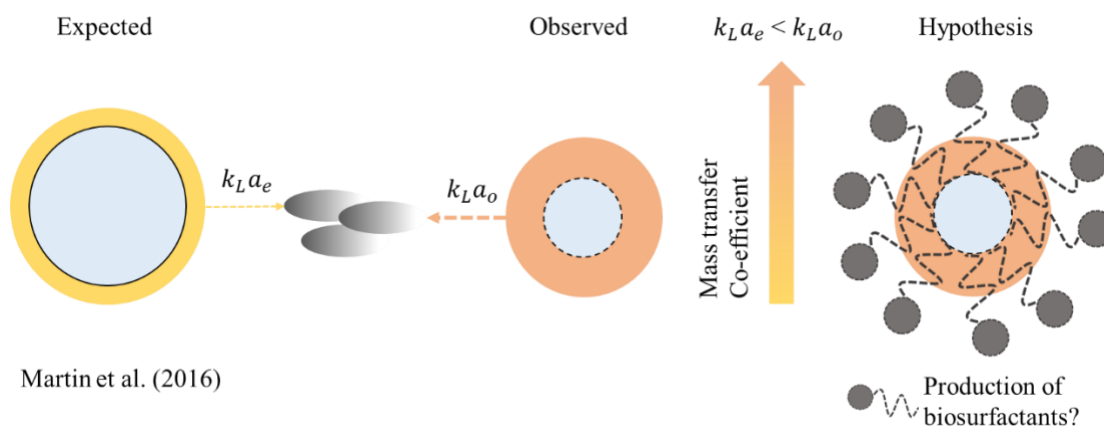


Figure 2: A graphical abstract showing the proposed hypothesis to explain the reduction in the bubble diameter below the expected value

The mass transfer or the movement of a solute across two different phases is driven by a concentration gradient. During the consumption of the gas substrates by the microbes, the availability of substrate is limited by a high cell density (Wainaina *et al.*, 2018). At the time of

³ The $k_L a$ co-efficient represents the transfer of mass from the air to a solvent.

fermentation, the CO/CO₂/H₂ gas transfer has to take place from the gas phase into the liquid medium, eventually entering the microbial cells (Phillips *et al.*, 2017). The transfer of the gaseous substrate at this interphase is governed by its concentrations in each phase, which in turn determines the fate of the enzymatic reactions that follow (Phillips *et al.*, 2017). Moreover, CO and H₂ have an extremely low solubility in water (Hougen & Watson, 1947). This could lead the microorganisms to starvation because of their inability to meet necessary energy and nutritional requirements. Therefore, an investigation into the production of potential biosurfactants by the gas fermenting microorganisms is required in parallel to the optimization of the reactor design.

In the past, different reactor designs and strategies have been proposed for achieving a higher mass transfer during syngas fermentations. Enhanced mass transfer of gases in the presence of bio-surfactant plays a key role in a US patent titled “emulsion-based fermentation for accelerated gas substrate mass transfer”. This patent presents a method in which an aqueous droplet containing microorganisms is released into an oil emulsion to which a gas substrate is introduced. During fermentation, a bio-surfactant or an amphiphilic compound is added to the oil-phase, which enables the microorganism residing in the aqueous phase to consume the gas substrate present in the oil phase (Tang *et al.*, 2017). Shen, *et al.* (2017) developed the horizontally oriented rotating packed bed (h-RPB) reactors. A key element in this design was the application of a cell biofilm that was packed into a reactor and was periodically exposed to the headspace and the liquid phase *via* rotation. This resulted in a higher mass transfer of the substrates to the biofilm. Munasinghe and Khanal (2010) compared the mass transfer of CO amongst eight different reactor configurations and concluded that the air-lift reactor configuration, containing a bulb diffuser with the smallest pore size for gas diffusion (20 µm) showed the highest mass transfer. Evidently, the diffuser with the smallest pore size generated the smallest bubbles, resulting in a higher mass transfer. This conclusion highlights the impact of bubble size properties on the overall substrate availability to the gas fermenting microorganisms.

The polypeptides produced by *Clostridium acetobutylicum*

Our current knowledge of biosurfactants is limited to research conducted under aerobic conditions. Amongst the various species that are known to generate surfactants under anaerobic conditions, one of the first microorganisms to be isolated was *Clostridium pastuerianum*. It produced four

different types of lipids with sucrose as a source of carbon and lowered the surface tension of the culture broth to a value of 55 mN/m (Cooper *et al.*, 1980).

Recently, Herman *et al.* (2017) proposed that the metabolic polypeptides produced by *Clostridium acetybutylicum* may act as signaling molecules for triggering sporulation and granulose accumulation. One of the identified polypeptides, clostrienose, displayed weak surfactant activity when produced at a concentration lower than 6 μM under batch fermentation conditions. To understand the consequences of polypeptide production in the same study, a mutant strain was generated in which the gene responsible for the formation of these metabolic polypeptides. This mutant strain showed a higher yield of ethanol due to a delay in the onset of sporulation. The results of this study establish the need to not only investigate the production of a metabolic bio-surfactant by *C. ljundahlii*, but to test its inhibitory effect on solvent production.

Biosurfactants

Surfactants are amphiphilic compounds that contain both hydrophobic (water insoluble) and hydrophilic (water soluble) groups. When they are added to solvents, they diffuse and attach to the surface of the immiscible phase, which could either be a gas or an insoluble solute. The hydrophobic tail of the surfactant will attach to the immiscible phase and the hydrophilic end will associate with the solvent. This results in the development of a micelle (**Figure 3**). The shape and the type of the micelle aggregates depend on the type of the surfactant used, especially on the structure of the hydrophilic and hydrophobic parts. Once the concentration of a surfactant reaches a critical micelle concentration (CMC), they increase the solubility of the immiscible phase by forming micelle aggregates. The ionic groups which are present on the surface of the micelle, associate with the surrounding solvent and facilitate the dissolution of the otherwise hydrophobic, immiscible solute enclosed within the micelle. Cui *et al.* (2008) have mentioned two different models for the development of micelle aggregates. These are the pseudo-phase transition model and the mass action model. The former model proposes micelle formation as a gradual change of physical properties in a system at a concentration value close to the CMC. At concentrations below the CMC, only monomers and pre-micelles are predominant in the system. The latter model advocates micelle formation as a single step process. It suggests that micelles are generated in a

single step due to a sudden change in the solution's physical properties after CMC is attained (Amato *et al.*, 2003).

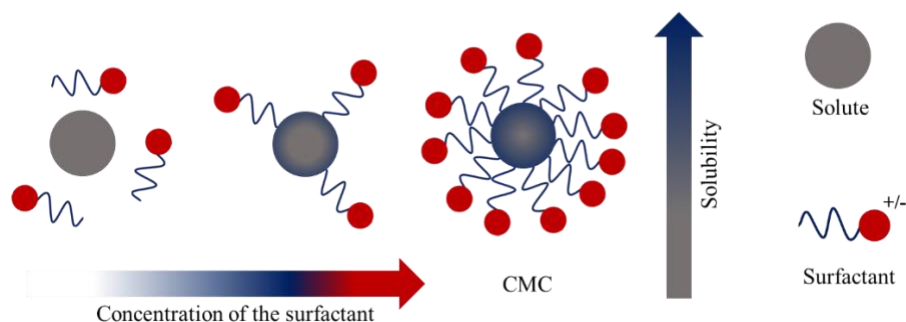


Figure 1: A diagram showing surfactants as monomers and micelles that form small aggregates in concentrations below the CMC. At concentrations close to the CMC, they start developing into larger aggregates and finally form micelles at CMC. The micelle aggregates increase the solubility of the immiscible solute.

Bacteria, yeasts, and fungi produce biosurfactants and bioemulsifiers when grown on hydrophobic carbon substrates (Gerson & Zajic, 1978). A bioemulsifier differs from a biosurfactant with respect to its mechanism. It is an additive that accelerates the suspension of one liquid in another, by increasing the dispersion of the more hydrophobic component into smaller droplets (Uzoigwe *et al.*, 2015). Meanwhile, a biosurfactant forms a layer between the solvent and the immiscible phase and increases its dissolution by reducing the surface tension of the solvent (Yin *et al.*, 2009). This is illustrated in a study by Willumsen and Karlson (1996), where no correlation was found between a biosurfactant's ability to reduce the surface tension and to form emulsions. This study was conducted on the microbiota of the PAH contaminated soils to screen to produce biosurfactants.

Most of the biosurfactants are glycolipids containing carbohydrates attached to a long-chain aliphatic acid. They can also be found in the form of lipopeptides, lipoproteins, and heteropolysachharides that are secreted by the microorganisms (Desai & Banat, 1997). Production of biosurfactants depends on the microbial strain, the source of carbon/nitrogen, the conditions provided for growth, the concentration of oxygen, and presence of metal ions (Desai & Banat, 1997). Moreover, the addition of water immiscible substrates might enhance the production of some biosurfactants (Desai & Banat, 1997). A strong biosurfactant that is derived from a microbial culture grown under oxygen limiting conditions can reduce the surface tension of the growth

medium by ≥ 40 mN/m (M. Domingues *et al.*, 2017). This criterion could be implemented to detect the production of biosurfactants by *C. ljundahlii*.

Assays for detecting biosurfactants

A multitude of methods has been developed for a reliable screening of microorganisms producing biosurfactants (V. Walter *et al.*, 2010). With respect to their structure, biosurfactants may belong to any of the diverse group of molecules, such as glycolipids, lipoproteins, lipopolysaccharides, and phospholipids (V. Walter *et al.*, 2010). V. Walter *et al.* (2010) have summarized and discussed several screening protocols test the physical properties of surfactants. The Stalagmometric method, the Pendant drop shape technique, and the Assymmetric drop shape analysis (ADSA) profile are a few examples of the described methods. The ADSA technique is widely implemented for qualitative evaluations. It monitors the surface tension of a liquid, through the geometry of the drop formed at the tip of the capillary/ pipette under gravitational force (Dilmohamud *et al.*, 2005; Tadros, 2005; Van der Vegt *et al.*, 1991). A few of the other qualitative techniques that have been discussed by Walter *et al.* (2010) will be used to detect biosurfactants in the power-to-food project. The selected assays are the Microplate assay, the Penetration assay, and the Oil spreading test (OST). The Microplate assay notes the distortion caused by the addition of tiny drops of cell culture supernatant (100 μ l) to the grids present in each well of a microtiter plate. A qualitative estimate of the concentration of the surfactant is derived from the amount of distortion observed. The Penetration Assay consists of mixing the cell culture supernatant with a red dye and placing it on microtiter plates prepared with a mixture of oil and silica gel in each well (Maczek *et al.*, 2007). If there are no biosurfactants present, the sample and the mixture form two different layers, thereby, retaining the color of the added dye. Whereas the presence of surfactant(s) would enable the mixture to enter the sample layer and turn the color of the red dye to cloudy white. Similarly, during the OST, a small volume of supernatant from the cell culture is added to a mixture of oil in water, resulting in the development of a clear zone where the surfactant dissolves the oil (Morikawa *et al.*, 2000). The OST was used in the identification and screening of biosurfactants produced from an oil-degrading bacteria isolated in a reactor treating saline oily waste (Cappello *et al.*, 2016). Furthermore, it was also employed in a pharmaceutical Wastewater in South-west Nigeria for the isolation of a surfactant producing bacteria (Adebajo, 2017).

In the recent past, scientists have attempted to develop more sophisticated techniques to analyze a more extensive set of samples. Gerc *et al.*, (2014) propose the application of metagenomic techniques to scan a diverse range of species to produce biosurfactants. For instance, the Antibiotic and Secondary Metabolite Shell (antiSMASH) identifies metabolite clusters from genomic data (Gerc *et al.*, 2014). The administration of this technique led to the discovery of a gene potentially responsible for producing biosurfactants in *Serratia marcesens* (Gerc *et al.*, 2014). Recently, Perfumo *et al.* (2018) used satellite remote sensing to capture layers of biosurfactants in the sea by its reduced surface tension. This advanced approach could potentially surpass all the methods currently practiced for microbial bioremediation of the ocean.

Although the application of qualitative screening techniques is widespread in the scientific literature, the aforementioned techniques are based on the alteration of the solvent's physical properties and do not belong to the category of high-throughput screening regimes (Jackson *et al.*, 2015). Therefore, for carrying out the quantitative analysis of biosurfactants, analytical techniques such as liquid chromatography in combination with mass spectrometry (LC-MS/MS) are more commonly employed. Płaza *et al.* (2015) attempted to screen and identify biosurfactants including the genes responsible in the *Bacillus* species through polymerase chain reaction (PCR) and LC-MS/MS techniques. Behrens *et al.* (2016) quantified the concentrations of rhamnolipid biosurfactants using a high performance liquid chromatography (HPLC) containing a charged aerosol detector. Biniarz and Łukaszewicz (2017) analyzed the presence of lipopeptides using an HPLC and an ultra-performance liquid chromatography (UPLC). Moreover, after dissolving their biological samples in methanol, they isolated the structural isoforms of these biosurfactants using a UPLC-MS. For the detection of the exact composition of the biosurfactants, we must ensure its separation from the other metabolites (Marchant & Banat, 2014). As illustrated in the studies above, this step could be carried out using an LC or HPLC. However, a detailed understanding of the biosurfactant's chemical structure is imperative to precisely determine the conditions necessary for the separation of all the components. To combat this issue, Herman *et al.* (2017) carried out an untargeted analysis in a Quadrupole Time of Flight (QTOF) LC-MS instrument to identify the metabolites that were generated during the fermentation of glucose by *C. acetobutylicum*. From the standpoint of detecting this in the power-to-food system, it is advisable to adapt a similar approach, and perform an untargeted screening analysis with an HPLC-MS for identifying the

structural composition of the biosurfactants in the samples generated from the second stage of the power-to-food reactor.

Techniques employed for the evaluation of bubble size properties

The presence of biosurfactants will have a considerable impact on bubble size properties and gas mass transfer. To establish a method that generates precise data on bubble size properties, a thorough investigation into the methods exercised in the past is necessary. Primarily, these methods can be divided into two categories, namely intrusive and non-intrusive techniques. The intrusive methods of bubble measurements involve the placement of the measurement device at the site of bubble formation, whereas the non-intrusive methods comprise of measurement techniques that operate from the external side of the vessel. Suction probes and conductivity probes are examples of intrusive techniques (Barigou & Greaves, 1991). Additionally, Saberi *et al.* (1995) introduced a method involving the immersion of two fiber optic probes to emit and receive the reflected/refracted light. The light detected by the photocell is converted into a voltage signal that provides information on the bubble shape and velocity (Saberi *et al.*, 1995). Overall, the biggest disadvantage of the intrusive techniques is the high risk of inaccurate measurements when the bubbles meet the measuring device. Therefore, utilization of non-intrusive methods is preferred for estimating bubble size properties. (Lau *et al.*, 2013). Tassin and Nikitopoulos (1995) demonstrated two non-intrusive methods, video imaging and Phase Doppler Anemometry⁴ (PDA), in a comparative study for measuring bubbles. Both the methods provided analogous bubble dimensions with minute differences.

Formation of gas bubbles and their physical properties play an important role in several industrial processes. In the last few years, this has inspired the emergence of systems designed to measure the bubble characteristics with a high precision. These systems have combined some of the intrusive and non-intrusive methods. Han *et al.* (2017) investigated the oil-in-water emulsions using a dual-sensor probe at Tianjin University. This probe was specifically designed to examine the local hold-up, bubble velocity as well as bubble size properties in a pipe with a 20 mm inner

⁴ PDA works on the principle of laser-Doppler velocimetry which states that the speed of the scattered particle crossing the optical measuring volume is calculated from the Doppler frequency (frequency emitted from the moving particle) of the scattered light (Tassin & Nikitopoulos, 1995).

diameter. Oil and surfactant solutions were injected into this pipe to observe vertical oil-in-water emulsions in multiphase flow loop facility and sensor system. The dual sensor probes give out a voltage signal based on a high and low resistivity that is dictated by the presence of either oil or water, respectively. The bubble flow parameters are calculated from the changes in the sensor's output voltage signals (Han *et al.*, 2017). Formation of bubbles during dough aeration has been measured using X-ray radiation from a synchrotron. The brightness and the beam quality of X-ray Microtomography help overcome the challenges posed by the optically opaque dough (Koksel *et al.*, 2017). Bothe *et al.* (2017) introduced the endoscopic bubble image velocimetry to study bubble size distribution, bubble velocity, and gas hold-up. It was suggested that this technique would surpass the uncertainties encountered during the calculation of the specific interfacial area, especially in the context of industrial applications. Bubble image velocimetry was used to examine the formation, coalescence, and mass transfer of bubbles as a function of changes in height and pressure. This phenomenon was tested and validated in a pilot plant at the Evonik Industries AG (Bothe *et al.*, 2017). The set-up consisted of an endoscope penetrating the vessel, in a jacketed tube, and was attached to a camera that takes ten image pairs per second. In addition to this, a laser endoscope was implemented at an angle of 90° to the first endoscope to provide illumination (Bothe *et al.*, 2017). Shadow Image Velocimetry (SIV) has also been employed to track bubbly flow under highly turbulent flow conditions. In this method, two LED pulses are powered on alternately and are in tune with a camera that takes two consecutive images (Karn *et al.*, 2015). The velocity is calculated from the distance travelled by the bubbles in the time the two consecutive images are taken. This technique has proven to overcome: (1) non-uniformities in the image background; (2) obtaining a wide range of bubble size distribution; (3) many out of focus bubble, and (4) the large clusters and overlap of bubbles (Karn *et al.*, 2015). Ferreira *et al.* (2012) studied the impact of different properties of a liquid, such as viscosity and surface tension, on the solubility and the interfacial area of the obtained bubbles *via* image analysis. In the context of their experiments, the solubility of the gas and the interfacial area of the bubbles were key determinants of the mass transfer of oxygen (Ferreira *et al.*, 2012). Based on the results, it was concluded that the surface tension had a smaller influence on the specific interfacial area when compared to the viscosity. Furthermore, the concentration profiles generated due to the presence of other bubbles in the vicinity, influenced the mass transfer and the interfacial area. Thus, by allowing us to collectively study bubble clusters, image analysis offers an additional advantage compared to the

other techniques. Honkanen *et al.* (2010) built a system consisting of a charged couple device (CCD) camera, optical fiber coupled diode laser, and a computer to study a wide range of multiphase flows in various industrial applications. This has been successfully tested in wastewater dissolved air floatation and water de-aeration channels, confirming the versatility of the image processing method.

Apart from photographic techniques, acoustic techniques have also been employed for the determination of bubble size properties. Pandit *et al.* (1992) determined the correlation of the bubble size to the frequency of the sound emitted by a gas bubble upon stimulation. Vazquez *et al.* (2005) measured bubble sizes with acoustic signals and compared the results with the ones derived from photographic techniques (image analysis). Data from this study concluded that both the techniques had an equal level of precision. The experiments were carried out by placing a hydrophone in an experimental tank at the point of origin of bubbles and recording the acoustic signals reverberating due to their formation. Kracht and Moraga (2016) calculated the Sauter diameter (d_{32}) by acoustic perturbation. Two acoustic signals were emitted, one with a high (ultrasound) frequency and the other one with a low frequency. The intensity of the response from the point of bubble generation was analyzed to determine the diameter d_{32} .

The methods adopted to evaluate the dimensions of the bubbles through digital image analysis is consistent throughout scientific literature. Lau *et al.* (2013) wrote an algorithm consisting of a set of predefined functions. The first part of the code contained the watershed function, executed to separate overlapping bubbles into individual ones. This was followed by the detection of the bubbles using a pre-defined function for recognizing the shape (specificity/roundness) of the bubbles. Ultimately, the number of individual bubbles were calculated by counting the core area of these “round” shapes. The principle behind this method is based on the difference in intensities observed between the center of the bubble and the rest of the area in a grayscale mode. They validated this method with real images collected from experiments conducted in a pseudo 2D bubble column (Lau *et al.*, 2013). The Image Segmentation function and the watershed function has been used to determine bubble size distribution in gas-liquid slug flow in horizontal pipes (do Amaral *et al.*, 2013). This code was tested on a video taken with a high-speed camera while stimulating slug flow conditions in a controlled environment (do Amaral *et al.*, 2013). Perez (2010) had developed an algorithm on MATLAB that was executed to obtain a size distribution of bubbles

in a swarm stimulated in a 2D bubble column. The studies illustrate algorithms that could potentially be applied to the power-to-food system for analyzing bubble size properties. Platforms like MATLAB and Image J are useful for performing calculations on the images taken from the power-to-food system. Implementation of pre-defined functions, like the watershed function, functions for local thresholding, and background illumination can lead to quantitative and reliable results. Nevertheless, any adaptation from an existing algorithm should be done with caution, because even the execution of an identical post-processing algorithm amongst different authors might be subjected to a substantial amount of user bias (Ferreira *et al.*, 2011).

Despite the several disadvantages and complications faced during image analysis in a fermentation system (semi-opaque or opaque conditions), the development of a photographic method that is equipped to address the optical challenges presented by such systems could produce remarkably accurate results. We are confident that by learning from the techniques implemented in the past, we can overcome similar challenges in fermentation systems. Briere *et al.* (2005) developed a system consisting of two synchronized CCD cameras, attached to a Stereomicroscope to obtain image pairs in a fermentation tank. A stroboscopic lamp was used for illumination within the multiphase fermenter vessel to capture microscopic bubbles. The characteristics of the bubbles obtained from both the images were combined using their locations and areas to estimate their spatial 3D locations. This information accounts for the depth of the bubbles and eliminates errors that would arise when two bubbles are present on different focal planes, resulting in the calculation of incorrect bubble radii (Corkidi *et al.*, 2008). To visually track the dynamics of bubble behavior in the power-to-food reactor, we suggest using a similar system with a microscope attached to a camera and an external source of illumination. This system will periodically capture images of the bubbles present at the wall of the reactor vessel. Subsequently, these images are processed by the algorithm designed to provide information on the bubble parameters.

Obtaining an ideal gas mass transfer

Once a method is developed for conducting image analysis to evaluate bubble size properties, images can be generated during the fermentation at selected time intervals. To convert this information into the gas mass transfer values, the equations described under this section should be exercised.

The mean bubble diameter (d_a) will be calculated using Equation. 2. The n represents the total number of bubbles and d_i represents the diameter of each bubble (i).

$$d_a = (\Sigma d_i)/n \text{ (Junker, 2006)} \quad \text{(Equation 2)}$$

The sauter mean diameter d_{32} is key in the measurement of mass transfer effects (Brentrup & Onken, 1979; Vega-Alvarado *et al.*, 2004). It considers the cumulative effect of the bubble volume normalized to their cumulative areas.

$$d_{32} = \Sigma n_i d_i^3 / \Sigma n_i d_i^2 \quad \text{(Equation 3)}$$

The interfacial area a is an interplay of several hydrodynamic parameters determined by physiochemical properties and vessel parameters (Garcia-Ochoa & Gomez, 2005). It can be calculated using Equation 4 given below,

$$a = \frac{6\Phi}{d_a} \quad \text{(Equation 4)}$$

Where ϕ represents the void fraction or the gas hold- up volume and is calculated using the Equation 5. If the value for the mean diameter is replaced by the Sauter diameter then the interfacial area a_{32} can be calculated (Junker, 2006).

$$\Phi = (H_G - H)/H_G \quad \text{(Saravanan, Ramamurthy, & Chandramohan, 2009)} \quad \text{(Equation 5)}$$

H_G stands for the height of liquid after aeration [m]; H = Height of liquid without aeration [m]. Its value generally ranges from 0 to 0.20.

The change in the dissolved gas concentration C_L can be calculated from the microbial uptake of the gas substrate using the equation below (Atkinson & Mavituna, 1991; Bandyopadhyay *et al.*, 1967; Rane & Sims, 1994),

$$\frac{dC_L}{dt} = -Q_g X \quad \text{(Equation 6)}$$

where $-Q_g X$ is the volumetric microbial uptake and X is the biomass. Upon integration with respect to time t this equation would yield,

$$C_{L0} - C_L = -Q_g X t \quad \text{(Equation 7)}$$

Therefore, the rate of the volumetric uptake of the gas substrate can be calculated from the change in the dissolved gas concentrations ($C_{L0} - C_L$) with respect to time t . The rate of change in dissolved gas concentration can also be calculated from a different equation (Equation 8),

$$\frac{dC_L}{dt} = k_L a (C_L^* - C_L) - Q_g X \quad (\text{Bandyopadhyay } et al., 1967; \text{Rane \& Sims, 1994}) \quad (\text{Equation 8})$$

In Equation 8, the value for C_L^* corresponds to the concentration of gas at the gas-liquid interface and is difficult to be accurately estimated. Therefore, the Equation 8 is integrated between two time points (t and t_s) to obtain,

$$\ln \left(\frac{C_{L0} - C_L}{C_{L0} - C_s} \right) = -k_L a (t - t_s) \quad (\text{Atkinson \& Mavituna, 1991}) \quad (\text{Equation 9})$$

Hence, $k_L a$ can be determined from the slop of $\ln(C_{L0} - C_L)$ versus t .

Alternatively, the gas uptake rate can also be calculated assuming initial steady state conditions.

$$Q_g X = k_L a (C_L - C_{L0}) \quad (\text{Tribe } et al., 1995) \quad (\text{Equation 10})$$

Additionally, Martin *et al.* (2016) suggested that the uptake of the gas substrate during high cell density could be limited by insufficient mass transfer through the gas liquid interface leading to negligible amounts of dissolved gases. To calculate the $k_L a$ for their system, they adopted the following equation,

$$Q_{H_2/CO} = (k_L a / H_{H_2/CO}) \cdot P_{H_2/CO}^G \quad (\text{Vega } et al., 1989) \quad (\text{Equation 11})$$

Where $Q_{H_2/CO}$ = Rate of carbon dioxide consumption [$\text{mmol L}^{-1} \text{ h}^{-1}$], $k_L a$ = Volumetric mass transfer co-efficient [h^{-1}], H = Henry's Law constant at $37^\circ\text{C} = 0.855 \text{ [L}\cdot\text{atm}\cdot\text{mmol}^{-1}]$ and $P_{H_2/CO}^G$ = Partial pressure of CO_2 in the headspace [atm].

Once the mass transfer values for H_2/CO_2 are calculated using Equations 8-11, their correlation to other parameters such as biomass concentration, the rate of substrate consumption, and the rate of product formation will be estimated. This information may lead to an optimum range of the H_2/CO_2 gas bubble sizes needed to observe a mass transfer that results in the highest yield. The data will be subsequently combined with the analytical data obtained from the measurement of certain metabolites during fermentation. This will aid in the identification of the specific compounds that

may act as biosurfactants. The set of experiments described in the final section of this dissertation is designed to capture the production of such compounds to verify our hypothesis.

Conclusion

The purpose of this review is to also provide us some insight into the key aspects of microbial fermentation processes and their potential to be implemented at a larger scale in the industry. An important advantage of the Power-to-food reactor is the utilization of H_2 , obtained from the electrolysis of water, as a source of energy for the conversion of CO_2 into an organic compound. This presents the power-to-food concept as an alternative solution to deal with the storage of renewable electricity. Moreover, the organic carbon compound produced from the power-to-food reactor could potentially act as a growth substrate for some eukaryotic microorganisms that can make nutritional supplements that is not inherently produced in the human body. The microbial production of food or food additives is promising in terms of its nutrient content, sustainability, and efficiency. This is evident in the success of commercial companies like Quorn™. Upon optimization and genetic modification, these organisms can be manipulated to generate valuable products in substantial amounts. By exploiting the consumption of a broad spectrum of substrates by nutrient-rich microorganisms, it presents an alternative platform to the industrial world to reduce their carbon footprint.

Although, the focus of this dissertation is primarily on the establishment and optimization of the Power to Food system, we wanted to also address the importance and prospects of studying bubbles size properties in the context of an anaerobic gas fermentation system. The dynamics of bubble size properties have been extensively discussed in the scientific community for a variety of industrial processes. However, an insufficient number of studies have investigated these properties in the context of H_2/CO_2 gas fermentation by acetogenic bacteria. The power-to-food reactor project gives us an incredible opportunity to explore this dynamic behaviour under the influence of microbial metabolites. The outcome will direct us to a novel strategy for making gas fermentation more cost-effective and efficient. Furthermore, genetic modification of the genes that are responsible for the prospective surface-active metabolites may increase the product yield or even modify the type of product formed.

References

- Abbas, C. A. (2006). Production of antioxidants, aromas, colours, flavours, and vitamins by yeasts *Yeasts in food and beverages* (pp. 285-334): Springer.
- Adebajo, S. O. (2017). Potential Biosurfactant-producing Bacteria from Pharmaceutical Wastewater using Simple Screening Methods in South-west, Nigeria. *Applied Environmental Research*, 39(2), 41-54.
- Amato, M., Caponetti, E., Martino, D. C., & Pedone, L. (2003). H and 19F NMR Investigation on Mixed Hydrocarbon– Fluorocarbon Micelles. *The Journal of Physical Chemistry B*, 107(37), 10048-10056.
- Arora, A., Cameotra, S. S., Kumar, R., Balomajumder, C., Singh, A. K., Santhakumari, B., Laik, S. (2016). Biosurfactant as a promoter of methane hydrate formation: thermodynamic and kinetic studies. *Scientific reports*, 6, 20893.
- Atkinson, B., & Mavituna, F. (1991). *Biochemical engineering and biotechnology handbook*: Stockton.
- Azam, F., & Malfatti, F. (2007). Microbial structuring of marine ecosystems. *Nature Reviews Microbiology*, 5(10), 782.
- Banat, I. M., Satpute, S. K., Cameotra, S. S., Patil, R., & Nyayanit, N. V. (2014). Cost effective technologies and renewable substrates for biosurfactants' production. *Frontiers in Microbiology*, 5, 697.
- Bandyopadhyay, B., Humphrey, A., & Taguchi, H. (1967). Dynamic measurement of the volumetric oxygen transfer coefficient in fermentation systems. *Biotechnology and Bioengineering*, 9(4), 533-544.
- Barigou, M., & Greaves, M. (1991). A capillary suction probe for bubble size measurement. *Measurement Science and Technology*, 2(4), 318.
- Barik, S., Prieto, S., Harrison, S., Clausen, E., & Gaddy, J. (1988). Biological production of alcohols from coal through indirect liquefaction. *Applied Biochemistry and Biotechnology*, 18(1), 363-378.
- Behrens, B., Baune, M., Jungkeit, J., Tiso, T., Blank, L. M., & Hayen, H. (2016). High performance liquid chromatography-charged aerosol detection applying an inverse gradient for quantification of rhamnolipid biosurfactants. *Journal of Chromatography A*, 1455, 125-132. doi:<https://doi.org/10.1016/j.chroma.2016.05.079>
- Bekatorou, A., Psarianos, C., & Koutinas, A. A. (2006). Production of food grade yeasts. *Food Technology & Biotechnology*, 44(3).

- Bhattacharjee, G., Barmecha, V., Pradhan, D., Naik, R., Zare, K., Mawlankar, R. B., Kumar, R. (2017). The biosurfactant Surfactin as a kinetic promoter for methane hydrate formation. *Energy Procedia*, *105*, 5011-5017.
- Biniarz, P., & Łukaszewicz, M. (2017). Direct quantification of lipopeptide biosurfactants in biological samples via HPLC and UPLC-MS requires sample modification with an organic solvent. *Applied Microbiology and Biotechnology*, *101*(11), 4747-4759.
- Borodina, I., Kildegaard, K. R., Jensen, N. B., Blicher, T. H., Maury, J., Sherstyk, S., Nielsen, J. (2015). Establishing a synthetic pathway for high-level production of 3-hydroxypropionic acid in *Saccharomyces cerevisiae* via β -alanine. *Metabolic Engineering*, *27*, 57-64. doi:<https://doi.org/10.1016/j.ymben.2014.10.003>
- Borodina, I., & Nielsen, J. (2014). Advances in metabolic engineering of yeast *Saccharomyces cerevisiae* for production of chemicals. *Biotechnology Journal*, *9*(5), 609-620. doi:[doi:10.1002/biot.201300445](https://doi.org/10.1002/biot.201300445)
- Bothe, M., Christlieb, M. A., Hoffmann, M., Tedjasukmana, O., Michaux, F., Rollbusch, P., Schlüter, M. (2017). Bubble size and bubble velocity distribution in bubble columns under industrial conditions. *The Canadian Journal of Chemical Engineering*, *95*(5), 902-912. doi:[10.1002/cjce.22759](https://doi.org/10.1002/cjce.22759)
- Brentrup, L., & Onken, U. (1979). Measurement of bubble size distribution in fermentors. *Biotechnology Letters*, *1*(10), 427-432.
- Briere, J. B., Cordova, M. S., Galindo, E., & Corkidi, G. (2005, 13-16 June 2005). *Microstereoscopic vision system for the determination of air bubbles and aqueous droplets content within oil drops in simulated processes of multiphase fermentations*. Paper presented at the Fifth International Conference on 3-D Digital Imaging and Modeling (3DIM'05).
- Brock, T. (1989). Evolutionary relationships of the autotrophic bacteria. *Autotrophic bacteria*, 499-512.
- Brumano, L. P., Antunes, F. A. F., Souto, S. G., Santos, J. C. d., Venus, J., Schneider, R., & Silva, S. S. d. (2017). Biosurfactant production by *Aureobasidium pullulans* in stirred tank bioreactor: New approach to understand the influence of important variables in the process. *Bioresource Technology*, *243*.
- Cappello, S., Volta, A., Santisi, S., Morici, C., Mancini, G., Quatrini, P., Torregrossa, M. (2016). Oil-degrading bacteria from a membrane bioreactor (BF-MBR) system for treatment of saline oily waste: Isolation, identification and characterization of the biotechnological potential. *International Biodeterioration & Biodegradation*, *110*, 235-244. doi:<https://doi.org/10.1016/j.ibiod.2015.12.028>

- Carlile, M. J. (1995). The Success of the Hypha and Mycelium. In N. A. R. Gow & G. M. Gadd (Eds.), *The Growing Fungus* (pp. 3-19). Dordrecht: Springer Netherlands.
- Cooper, D. G., Zajic, J. E., Gerson, D. F., & Manninen, K. I. (1980). Isolation and Identification of Biosurfactants Produced during Anaerobic Growth of *Clostridium pasteurianum*. *Journal of fermentation technology*, 58(1), 83-86.
- Corkidi, G., Voinson, T., Taboada, B., Córdova, M., & Galindo, E. (2008). Accurate determination of embedded particles within dispersed elements in multiphase dispersions, using a 3D micro-stereoscopic vision system. *Chemical Engineering Science*, 63(2), 317-329.
- Couto, N., Rouboa, A., Silva, V., Monteiro, E., & Bouziane, K. (2013). Influence of the biomass gasification processes on the final composition of syngas. *Energy Procedia*, 36, 596-606.
- Croft, M. T., Lawrence, A. D., Raux-Deery, E., Warren, M. J., & Smith, A. G. (2005). Algae acquire vitamin B 12 through a symbiotic relationship with bacteria. *Nature*, 438(7064), 90.
- Cui, X., Mao, S., Liu, M., Yuan, H., & Du, Y. (2008). Mechanism of Surfactant Micelle Formation. *Langmuir*, 24, 10771-10775.
- Das, A. J., Lal, S., Kumar, R., & Verma, C. (2017). Bacterial biosurfactants can be an ecofriendly and advanced technology for remediation of heavy metals and co-contaminated soil. *International Journal of Environmental Science and Technology*, 14(6).
- Desai, J. D., & Banat, I. M. (1997). Microbial production of surfactants and their commercial potential. *Microbiology and Molecular Biology Reviews*, 61(1), 47-64.
- Dilmohamud, B., Seeneevassen, J., Rughooputh, S., & Ramasami, P. (2005). Surface tension and related thermodynamic parameters of alcohols using the Traube stalagmometer. *European journal of physics*, 26(6), 1079.
- do Amaral, C. E. F., Alves, R. F., da Silva, M. J., Arruda, L. V. R., Dorini, L., Morales, R. E. M., & Pipa, D. R. (2013). Image processing techniques for high-speed videometry in horizontal two-phase slug flows. *Flow Measurement and Instrumentation*, 33, 257-264. doi:<https://doi.org/10.1016/j.flowmeasinst.2013.07.006>
- Drake, H. L., Gößner, A. S., & Daniel, S. L. (2008). Old acetogens, new light. *Annals of the New York Academy of Sciences*, 1125(1), 100-128.
- Fang, H., Kang, J., & Zhang, D. (2017). Microbial production of vitamin B12: a review and future perspectives. *Microbial Cell Factories*, 16(1), 15. doi:10.1186/s12934-017-0631-y
- Ferreira, A., Pereira, G., Teixeira, J. A., & Rocha, F. (2012). Statistical tool combined with image analysis to characterize hydrodynamics and mass transfer in a bubble column. *Chemical Engineering Journal*, 180, 216-228. doi:<https://doi.org/10.1016/j.cej.2011.09.117>

Florida, U. o. Surface tension. Retrieved from http://fsz.ifas.ufl.edu/surfacetensionandcapillarity/html/en_tensioactivos.htm

Garcia-Ochoa, F., & Gomez, E. (2005). Prediction of gas-liquid mass transfer coefficient in sparged stirred tank bioreactors. *Biotechnology and Bioengineering*, 92(6), 761-772.

Garodia, S., Naidu, P., & Nallanchakravarthula, S. (2017). QUORN: An Anticipated Novel Protein Source.

Gerc, A. J., Stanley-Wall, N. R., & Coulthurst, S. J. (2014). Role of the phosphopantetheinyltransferase enzyme, PswP, in the biosynthesis of antimicrobial secondary metabolites by *Serratia marcescens* Db10. *Microbiology*, 160(8), 1609-1617.

Gerson, D., & Zajic, J. (1978). Surfactant production from hydrocarbons by *Corynebacterium lepus*, sp. nov. and *Pseudomonas asphaltenicus*, sp. nov. *Dev. Ind. Microbiol*, 19, 577-599.

Gilani, G., & Lee, N. (2003). PROTEIN| Sources of Food-grade Protein.

Han, Y. F., Jin, N. D., Yin, Z. Q., Ren, Y. Y., & Gu, Y. (2017). Measurement of oil bubble size distribution in oil-in-water emulsions using a distributed dual-sensor probe array. *Experimental Thermal and Fluid Science*, 86, 204-223. doi:<https://doi.org/10.1016/j.expthermflusci.2017.04.009>

Helliwell, K. E., Collins, S., Kazamia, E., Purton, S., Wheeler, G. L., & Smith, A. G. (2014). Fundamental shift in vitamin B12 eco-physiology of a model alga demonstrated by experimental evolution. *The Isme Journal*, 9, 1446. doi:10.1038/ismej.2014.230

<https://www.nature.com/articles/ismej2014230#supplementary-information>

Helliwell, Katherine E., Lawrence, Andrew D., Holzer, A., Kudahl, Ulrich J., Sasso, S., Kräutler, B., Smith, Alison G. (2016). Cyanobacteria and Eukaryotic Algae Use Different Chemical Variants of Vitamin B12. *Current Biology*, 26(8), 999-1008. doi:<https://doi.org/10.1016/j.cub.2016.02.041>

Helliwell, K. E., Scaife, M. A., Sasso, S., Araujo, A. P. U., Purton, S., & Smith, A. G. (2014). Unravelling vitamin B12-responsive gene regulation in algae. *Plant physiology*, pp. 113.234369.

Helliwell, K. E., Wheeler, G. L., Leptos, K. C., Goldstein, R. E., & Smith, A. G. (2011). Insights into the evolution of vitamin B12 auxotrophy from sequenced algal genomes. *Molecular Biology and Evolution*, 28(10), 2921-2933.

Helliwell, K. E., Wheeler, G. L., & Smith, A. G. (2013). Widespread decay of vitamin-related pathways: coincidence or consequence? *Trends in Genetics*, 29(8), 469-478.

- Herman, N. A., Kim, S. J., Li, J. S., Cai, W., Koshino, H., & Zhang, W. (2017). The industrial anaerobe *Clostridium acetobutylicum* uses polyketides to regulate cellular differentiation. *Nature communications*, *8*(1), 1514.
- Hirata, Y., Ryu, M., Oda, Y., Igarashi, K., Nagatsuka, A., Furuta, T., & Sugiura, M. (2009). Novel characteristics of sophorolipids, yeast glycolipid biosurfactants, as biodegradable low-foaming surfactants. *Journal of bioscience and bioengineering*, *108*(2), 142-146.
- Honkanen, M., Eloranta, H., & Saarenrinne, P. (2010). Digital imaging measurement of dense multiphase flows in industrial processes. *Flow Measurement and Instrumentation*, *21*(1), 25-32. doi:<https://doi.org/10.1016/j.flowmeasinst.2009.11.001>
- Hougen, O. A., & Watson, K. M. (1947). *Chemical process principles*: John Wiley And Sons, Inc Chapman And Hall, Limited,; London.
- Huang, X., Mu, T., Shen, C., Lu, L., & Liu, J. (2016). Effects of bio-surfactants combined with alkaline conditions on volatile fatty acid production and microbial community in the anaerobic fermentation of waste activated sludge. *International Biodeterioration & Biodegradation*, *114*, 24-30.
- Jackson, S. A., Borchert, E., O’Gara, F., & Dobson, A. D. W. (2015). Metagenomics for the discovery of novel biosurfactants of environmental interest from marine ecosystems. *Current Opinion in Biotechnology*, *33*, 176-182. doi:<https://doi.org/10.1016/j.copbio.2015.03.004>
- Jenson, I. (1997). Bread and baker’s yeast. In B. J. B. Wood (Ed.), *Microbiology of Fermented Foods* (pp. 172-198). Boston, MA: Springer US.
- Jespersen, L., Halm, M., Kpodo, K., & Jakobsen, M. (1994). Significance of yeasts and moulds occurring in maize dough fermentation for ‘kenkey’ production. *International Journal of Food Microbiology*, *24*(1), 239-248. doi:[https://doi.org/10.1016/0168-1605\(94\)90122-8](https://doi.org/10.1016/0168-1605(94)90122-8)
- Junker, B. (2006). Measurement of bubble and pellet size distributions: past and current image analysis technology. *Bioprocess and Biosystems Engineering*, *29*(3), 185-206. doi:10.1007/s00449-006-0070-3
- Karn, A., Ellis, C., Arndt, R., & Hong, J. (2015). An integrative image measurement technique for dense bubbly flows with a wide size distribution. *Chemical Engineering Science*, *122*, 240-249. doi:<https://doi.org/10.1016/j.ces.2014.09.036>
- Kazamia, E., Czesnick, H., Nguyen, T. T. V., Croft, M. T., Sherwood, E., Sasso, S., Smith, A. G. (2012). Mutualistic interactions between vitamin B12-dependent algae and heterotrophic bacteria exhibit regulation. *Environmental Microbiology*, *14*(6), 1466-1476.
- Klosowska-Chomiczewska, I., Medrzycka, K., & Karpenko, E. (2011). *Biosurfactants–Biodegradability, toxicity, efficiency in comparison with synthetic surfactants*. Paper

- presented at the Proc. of the Polish-Swedish-Ukrainian Seminar “Research and Application of New Technologies in Wastewater Treatment and Municipal Solid Waste Disposal in Ukraine, Sweden, and Poland,” Krakow.
- Koksel, F., Strybulevych, A., Aritan, S., Page, J. H., & Scanlon, M. G. (2017). The use of synchrotron X-rays and ultrasonics for investigating the bubble size distribution and its evolution in bread dough. *Journal of Cereal Science*, 78, 10-18. doi:<https://doi.org/10.1016/j.jcs.2017.06.022>
- Köpke, M., Held, C., Hujer, S., Liesegang, H., Wiezer, A., Wollherr, A., Dürre, P. (2010). *Clostridium ljungdahlii* represents a microbial production platform based on syngas. *Proceedings of the National Academy of Sciences*, 107(29), 13087-13092.
- Kosaric, N. (1992). Biosurfactants in industry. *Pure and Applied Chemistry*, 64(11), 1731-1737.
- Kracht, W., & Moraga, C. (2016). Acoustic measurement of the bubble Sauter mean diameter d_{32} . *Minerals Engineering*, 98, 122-126. doi:<https://doi.org/10.1016/j.mineng.2016.08.001>
- Lara-Flores, M., Olvera-Novoa, M. A., Guzmán-Méndez, B. E., & López-Madrid, W. (2003). Use of the bacteria *Streptococcus faecium* and *Lactobacillus acidophilus*, and the yeast *Saccharomyces cerevisiae* as growth promoters in Nile tilapia (*Oreochromis niloticus*). *Aquaculture*, 216(1-4), 193-201.
- Lau, Y. M., Deen, N. G., & Kuipers, J. A. M. (2013). Development of an image measurement technique for size distribution in dense bubbly flows. *Chemical Engineering Science*, 94, 20-29. doi:<https://doi.org/10.1016/j.ces.2013.02.043>
- M. Domingues, P., Almeida, A., Serafim Leal, L., Gomes, N. C. M., & Cunha, Â. (2017). Bacterial production of biosurfactants under microaerobic and anaerobic conditions. *Reviews in Environmental Science and Bio/Technology*, 16(2), 239-272. doi:10.1007/s11157-017-9429-y
- Maczek, J., Junne, S., & Götz, P. (2007). Examining biosurfactant producing bacteria—an example for an automated search for natural compounds. *Application Note CyBio AG*.
- Marchant, R., & Banat, I. M. (2014). Protocols for measuring biosurfactant production in microbial cultures *Hydrocarbon and Lipid Microbiology Protocols* (pp. 119-128): Springer.
- Marsh, E. (1999). Coenzyme B12 (cobalamin)-dependent enzymes. *Essays in biochemistry*, 34, 139-154.
- Martin, M. E., Richter, H., Saha, S., & Angenent, L. T. (2016). Traits of selected clostridium strains for syngas fermentation to ethanol. *Biotechnology and Bioengineering*, 113, 531-539.

- Morikawa, M., Hirata, Y., & Imanaka, T. (2000). A study on the structure–function relationship of lipopeptide biosurfactants. *Biochimica et Biophysica Acta (BBA)-Molecular and Cell Biology of Lipids*, 1488(3), 211-218.
- Mukherjee, S., Das, P., & Sen, R. (2006). Towards commercial production of microbial surfactants. *Trends in Biotechnology*, 24(11), 509-515.
- Munasinghe, P. C., & Khanal, S. K. (2010). Syngas fermentation to biofuel: evaluation of carbon monoxide mass transfer coefficient (kLa) in different reactor configurations. *Biotechnology Progress*, 26(6), 1616-1621.
- Pandit, A. B., Varley, J., Thorpe, R. B., & Davidson, J. F. (1992). Measurement of bubble size distribution: an acoustic technique. *Chemical Engineering Science*, 47(5), 1079-1089. doi:[https://doi.org/10.1016/0009-2509\(92\)80233-3](https://doi.org/10.1016/0009-2509(92)80233-3)
- Perez, C. A., Finch, J. . (2010). Tracking velocity of multiple bubbles in a swarm. *International Journal of Mineral Processing*, 94, 147-158.
- Perfumo, A., Banat, I. M., & Marchant, R. (2018). Going Green and Cold: Biosurfactants from Low-Temperature Environments to Biotechnology Applications. *Trends in Biotechnology*, 36(3), 277-289. doi:<https://doi.org/10.1016/j.tibtech.2017.10.016>
- Phillips, J., Huhnke, R., & Atiyeh, H. (2017). Syngas Fermentation: A Microbial Conversion Process of Gaseous Substrates to Various Products. *Fermentation*, 3(2), 28.
- Plaza, G., Chojniak, J., Rudnicka, K., Paraszkiwicz, K., & Bernat, P. (2015). Detection of biosurfactants in *Bacillus* species: genes and products identification. *Journal of applied microbiology*, 119(4), 1023-1034.
- Ragsdale, S. W. (2008). Enzymology of the Wood–Ljungdahl pathway of acetogenesis. *Annals of the New York Academy of Sciences*, 1125(1), 129-136.
- Ragsdale, S. W., & Pierce, E. (2008). Acetogenesis and the Wood–Ljungdahl pathway of CO₂ fixation. *Biochimica et Biophysica Acta (BBA)-Proteins and Proteomics*, 1784(12), 1873-1898.
- Rane, K. D., & Sims, K. A. (1994). Oxygen uptake and citric acid production by *Candida lipolytica* Y 1095. *Biotechnology and Bioengineering*, 43(2), 131-137.
- Ritchie, H., Laird, J., & Ritchie, D. (2017). 3f bio: Halving the Cost of Mycoprotein Through Integrated Fermentation Processes. *Industrial Biotechnology*, 13(1), 29-31.
- Rodrigues, L., Banat, I. M., Teixeira, J., & Oliveira, R. (2006). Biosurfactants: Potential applications in medicine. *J. Antimicrob Chem*(57), 609-618.
- Rogers, T. O., & Lichstein, H. C. (1969). Characterization of the Biotin Transport System in *Saccharomyces cerevisiae*. *Journal of bacteriology*, 100(2), 557-564.

- Saberi, S., Shakourzadeh, K., Bastoul, D., & Militzer, J. (1995). Bubble size and velocity measurement in gas—liquid systems: Application of fiber optic technique to pilot plant scale. *The Canadian Journal of Chemical Engineering*, 73(2), 253-257.
- Santos, D. K. F., Rufino, R. D., Luna, J. M., Santos, V. A., & Sarubbo, L. A. (2016). Biosurfactants: multifunctional biomolecules of the 21st century. *International Journal of Molecular Sciences*, 17(3), 401.
- Saravanan, K., Ramamurthy, V., & Chandramohan, K. (2009). Gas hold up in multiple impeller agitated vessels. *Modern Applied Science*, 3(2), 49.
- Schuchmann, K., & Müller, V. (2014). Autotrophy at the thermodynamic limit of life: a model for energy conservation in acetogenic bacteria. *Nature Reviews Microbiology*, 12, 809. doi:10.1038/nrmicro3365
- Shane, B., & Snell, E. E. (1976). Transport and metabolism of vitamin B6 in the yeast *Saccharomyces carlsbergensis* 4228. *Journal of Biological Chemistry*, 251(4), 1042-1051.
- Shen, Y., Brown, R. C., & Wen, Z. (2017). Syngas fermentation by *Clostridium carboxidivorans* P7 in a horizontal rotating packed bed biofilm reactor with enhanced ethanol production. *Applied Energy*, 187(Supplement C), 585-594. doi:https://doi.org/10.1016/j.apenergy.2016.11.084
- Singh, A., Van Hamme, J. D., & Ward, O. P. (2007). Surfactants in microbiology and biotechnology: Part 2. Application aspects. *Biotechnology Advances*, 25(1), 99-121.
- Stolz, J., & Vielreicher, M. (2003). Tpn1p, the plasma membrane vitamin B6 transporter of *Saccharomyces cerevisiae*. *Journal of Biological Chemistry*, 278(21), 18990-18996.
- Strzelczyk, E., & Leniarska, U. (1985). Production of B-group vitamins by mycorrhizal fungi and actinomycetes isolated from the root zone of pine (*Pinus sylvestris* L.). *Plant and Soil*, 86(3), 387-394. doi:10.1007/bf02145459
- Tadros, T. F. (2005). Adsorption of surfactants at the air/liquid and liquid/liquid interfaces. *Applied Surfactants: Principles and Applications*, 73-84.
- Tang, S., Criddle, C., Myung, J., & Kim, M. (2017). Emulsion-based fermentation for accelerated gas substrate mass transfer: Google Patents.
- Tanner, R. S., Miller, L. M., & Yang, D. (1993). *Clostridium ljungdahlii* sp. nov., an acetogenic species in clostridial rRNA homology group I. *International Journal of Systematic and Evolutionary Microbiology*, 43(2), 232-236.
- Tassin, A. L., & Nikitopoulos, D. E. (1995). Non-intrusive measurements of bubble size and velocity. *Experiments in Fluids*, 19(2), 121-132. doi:10.1007/bf00193858

- Trappe, J. M. (1962). Fungus associates of ectotrophic mycorrhizae. *The Botanical Review*, 28(4), 538-606.
- Tremblay, P.-L., Zhang, T., Dar, S. A., Leang, C., & Lovley, D. R. (2013). The Rnf complex of *Clostridium ljungdahlii* is a proton-translocating ferredoxin: NAD⁺ oxidoreductase essential for autotrophic growth. *MBio*, 4(1), e00406-00412.
- Tribe, L., Briens, C., & Margaritis, A. (1995). Determination of the volumetric mass transfer coefficient (k_La) using the dynamic “gas out–gas in” method: analysis of errors caused by dissolved oxygen probes. *Biotechnology and Bioengineering*, 46(4), 388-392.
- Uzoigwe, C., Burgess, J. G., Ennis, C. J., & Rahman, P. K. (2015). Bioemulsifiers are not biosurfactants and require different screening approaches. *Frontiers in Microbiology*, 6, 245.
- Van der Vegt, W., Van der Mei, H., Noordmans, J., & Busscher, H. (1991). Assessment of bacterial biosurfactant production through axisymmetric drop shape analysis by profile. *Applied Microbiology and Biotechnology*, 35(6), 766-770.
- Vazquez, A., Sanchez, R., Salinas-Rodriguez, E., Soria, A., & Manasseh, R. (2005). A look at three measurement techniques for bubble size determination. *Experimental Thermal and Fluid Science*, 30(1), 49-57.
- Vega-Alvarado, L., Cordova, M., Taboada, B., Galindo, E., & Corkidi, G. (2004). *Online Sauter diameter measurement of air bubbles and oil drops in stirred bioreactors by using hough transform*. Paper presented at the International Conference Image Analysis and Recognition.
- Vega, J., Antorrena, G., Clausen, E., & Gaddy, J. (1989). Study of gaseous substrate fermentations: carbon monoxide conversion to acetate. 2. Continuous culture. *Biotechnology and Bioengineering*, 34(6), 785-793.
- Wainaina, S., Horváth, I. S., & Taherzadeh, M. J. (2018). Biochemicals from food waste and recalcitrant biomass via syngas fermentation: A review. *Bioresource Technology*, 248, 113-121. doi:<https://doi.org/10.1016/j.biortech.2017.06.075>
- Walter, V., Syldatk, C., & Hausmann, R. (2010). Screening concepts for the isolation of biosurfactant producing microorganisms *Biosurfactants* (pp. 1-13): Springer.
- Walter, V., Syldatk, C., & Hausmann, R. (2010). Screening concepts for the isolation of biosurfactant producing microorganisms. *Adv Exp Med Biol*, 672, 1-13.
- Warren, M. J., Raux, E., Schubert, H. L., & Escalante-Semerena, J. C. (2002). The biosynthesis of adenosylcobalamin (vitamin B₁₂). *Natural product reports*, 19(4), 390-412.

- Watanabe, F., SCHWARZ, J., TAKENAKA, S., Miyamoto, E., Ohishi, N., Nelle, E., Yabuta, Y. (2012). Characterization of vitamin B12 compounds in the wild edible mushrooms black trumpet (*Craterellus cornucopioides*) and golden chanterelle (*Cantharellus cibarius*). *J Nutr Sci Vitaminol (Tokyo)*, 58(6), 438-441.
- Wiebe, M. G. (2004). Quorn™ Myco-protein — Overview of a successful fungal product. *Mycologist*, 18(1), 17-20. doi:[https://doi.org/10.1017/S0269-915X\(04\)00108-9](https://doi.org/10.1017/S0269-915X(04)00108-9)
- Willumsen, P. A., & Karlson, U. (1996). Screening of bacteria, isolated from PAH-contaminated soils, for production of biosurfactants and bioemulsifiers. *Biodegradation*, 7, 415-423.
- Wood, H. G. (1952). Fermentation of 3, 4-C14-and 1-C14-labeled glucose by *Clostridium thermoaceticum*. *Journal of Biological Chemistry*, 199(2), 579-583.
- Xu, Q., Nakajima, M., Liu, Z., & Shiina, T. (2011). Biosurfactants for Microbubble Preparation and Application. *International Journal of Molecular Sciences*, 12.
- Yin, H., Qiang, J., Jia, Y., Ye, J., Peng, H., Qin, H., He, B. (2009). Characteristics of biosurfactant produced by *Pseudomonas aeruginosa* S6 isolated from oil-contaminating wastewater. *Process Biochemistry*, 44(3), 302-308.

1

Carbon fixation with renewable electric power to feed the world: Power-to-protein

Akanksha Mishra¹, Jean Nepomuscene Ntihuga¹, Bastian Molitor¹, and Largus T. Angenent^{1,2}

1. Center for Applied Geosciences, University of Tuebingen, 72070 Tuebingen, Germany

2. Max Planck Fellow, Max Planck Institute for Developmental Biology, 72076 Tübingen, Germany

Mishra, A., Ntihuga J.N., Molitor, B., & Angenent, L.T. (2020). Power-to-Protein: Carbon Fixation with Renewable Electric Power to Feed the World. *Joule*, 4(6), 1142-1147

Carbon fixation with renewable electric power to feed the world: Power-to-protein

Author Contributions

Largus T. Angenent led the discussion and oversaw the writing. Akanksha Mishra and Largus T. Angenent wrote the manuscript. Akanksha Mishra calculated the stoichiometric equations with advice from Dr. Tiaran Sun and Dr. Sofia Esquivel Elizondo about the electrochemical calculations and the applications of the electron equivalent model, respectively. Jean Nepomuscene Ntihuga drew the figure and validated all the calculations. Bastian Molitor organized the paper and edited the manuscript.

Context and Scale

Power-to-protein (PtP) is not a new idea and has roots in the space age. The concept is simple: circumventing agriculture to produce protein for animal feed or human food by fixing carbon from carbon dioxide with electric power, but without light. To do so, electrolysis has been coupled to bioreactors, resulting in the production of single-cell protein in the dark. Here, we have grouped PtP into three sections based on the different possibilities of carbon fixation without photosynthesis: (I) Calvin–Benson–Bassham cycle or reverse-Krebs cycle with hydrogen-oxidizing bacteria; (II) Wood-Ljungdahl pathway with acetate-producing bacteria; and (III) hydrogenation or electrochemical reduction with abiotic processes. We then compared the technological aspects and theoretical biomass yields of each of these PtP approaches. Single-cell protein commercialization efforts in the past have already identified the vast scale of protein production that is possible with biotechnology. Hence, many environmental and societal problems can be solved on earth with PtP when renewable electric power and clean carbon dioxide is available to all.

Introduction

We are currently amidst a multifaceted crisis regarding food production. The detrimental consequences of animal-based protein production on the environment are becoming increasingly clear (Linder, 2019). The utilization of finite resources, such as land, fossil fuels, phosphorous, and water, accompanied by greenhouse gas emissions, are primary outcomes of conventional livestock production (Poore & Nemecek, 2018). An extensive generation of ammonia *via* the Haber-Bosch process sustains the plant growth that is required to feed the many animals, but is inefficient and creates runoff from agricultural lands, resulting in eutrophication on a local and continental scale.

The production of animal protein in association with land utilization, packaging, storage, and transportation is resulting in a high market price of the final products, rendering it unattainable for the under-privileged section of our societies (Prosekov & Ivanova, 2018). This is especially true for developing and under-developed countries, where nutritious food for everyone is lacking. The implementation of renewable technologies is necessary to feed a growing human population with affordable protein and to support a circular economy rather than a fossil-based, wasteful economy.

A study by Foster and Litchfield (Foster & Litchfield, 1964) utilized electrolysis as a source of oxygen in a closed-cycle space system. They found that hydrogen, which is also generated by electrolysis, could be used in conjunction with urea and carbon dioxide to cultivate hydrogen-oxidizing bacteria as a source of single cell protein (SCP) to feed humans. This technology was proposed for long-term space exploration with astronauts, who would be the source of ammonia and carbon dioxide (Foster & Litchfield, 1964). Even though NASA has started a recent challenge to produce food (hexoses) from carbon dioxide without light through chemistry¹, here we focus only on power-to-protein (PtP) through biology. In addition, we did not focus on genetically modified microbes to be able to feed proteins directly to humans.

We define PtP as an approach to convert electric power with carbon dioxide into protein without light by coupling electrochemistry with biotechnology. We use the same terminology style as for

¹ https://www.nasa.gov/spacetechnology/centennial_challenges/co2challenge/winning-teams-design-systems-to-convert-carbon-dioxide-into-something-sweet.html

power-to-gas, which is the conversion of electric power and carbon dioxide into either hydrogen gas or methane gas (Schiebahn *et al.*, 2015). PtP can be used to produce animal feed or human food on earth, but can especially be a prospective solution to combat the aforementioned environmental and food crises when protein is produced directly for human consumption without animal production. We prospect an agricultural model without animal protein production, but with plant production for ample nutrition with grains, vegetables, fruits, and animal-replacement products, while at the same time stewarding nature.

In this Future Energy article, we explore several alternative methods for PtP by first placing them in three different sections (Sections I-III) based on the different mechanisms of carbon fixation with carbon dioxide and without photosynthesis: (I) Calvin–Benson–Bassham cycle or reverse-Krebs cycle with hydrogen-oxidizing bacteria; (II) Wood-Ljungdahl pathway with acetate-producing bacteria; and (III) hydrogenation or electrochemical reduction with abiotic processes (**Figure 1**). SCP production is an integral part of PtP, and has matured already with ample examples of industrial-scale implementation and documentation on safe utilization as a feed/food (Ritala *et al.*, 2017). We, therefore, do not review these important aspects of PtP here. We end this Future Energy article with an outlook.

Section I: Calvin–Benson–Bassham cycle or reverse-Krebs cycle

This microbial carbon fixation pathway of the Calvin–Benson–Bassham cycle or reverse-Krebs cycle requires oxygen (or possibly nitrate) as the electron acceptor. The entrée point of carbon dioxide for this PtP approach is, therefore, a bioreactor in which oxygen and hydrogen from the electrolyzer are mixed and utilized as the electron acceptor and electron donor, respectively, for autotrophic carbon fixation (**Figure 1A**). The first study of PtP by Foster and Litchfield (Foster & Litchfield, 1964) included this system setup by growing the hydrogen-oxidizing (*Knallgas*) bacterium *Cupriavidus necator*, which had before been classified as *Hydrogenomonas eutrophus*. In 1964, this was merely thought as a system to convert and recycle ammonia and carbon dioxide from humans in closed-cycle space systems.

On earth, however, there persists an incongruity between, on the one hand, having ammonia in wastewater that must be removed at great cost and energy to prevent eutrophication and, on the

other hand, producing ammonia by consuming vast quantities of natural gas during the Haber-Bosch process. This was the driving force by Matassa *et al.* (2016) to study PtP at wastewater treatment plants where carbon dioxide is available in the biogas of anaerobic digesters; and oxygen and hydrogen can be produced from an electrolyzer with electric power from burning renewable methane in biogas. In the tradition of environmental biotechnology for complex wastewaters, the researchers decided to use an open culture (microbiome) to prevent the need for axenic conditions, and therefore intrinsically choose to produce animal feed instead of human food due to the risk of pathogen contamination. They enriched for a chemolithotrophic community with an abundant (>97%) hydrogen-oxidizing bacterial population of *Sulfuricurvum* spp. (Matassa *et al.*, 2016).

These authors then teamed up with a Dutch water cycle research institute (KWR) and others to upgrade ammonia in the effluent of the sludge digester from a real wastewater treatment facility in two phases². First, the technical and economic viability of this project was investigated. This study found that, when allowed for human consumption, the produced protein could feed 36% of the population that was connected to the large Amsterdam wastewater treatment facility. In addition, they found that their PtP approach has the potential to become economically viable in the future, but that external renewable power and an external source of carbon dioxide, such as an industrial offgas, would be necessary².

Second, a pilot-scale PtP system, including an ammonia stripper, electrolyzer, and bioreactor, was built and operated at a Dutch wastewater treatment facility². Unfortunately, the design of the bioreactor was not based on already fully operating systems, such as gaseous fermenters in other industries, resulting in severe hydrogen transfer limitations and relatively low protein production rates. Regardless, important information was gained, including: (1) a lower cost for ammonia stripping than anticipated; and (2) a high sensitivity for the method of electric power production². Besides stripping ammonia from digester effluent at a centralized wastewater treatment facility, ammonia recovery from decentralized human urine collection would also be feasible as a sustainable nitrogen source (Coppens *et al.*, 2016). Another company that fits within this PtP

² Oosterholt, F., Versteeg, E., Verstraete, W., and Boere, J. (2015). Toepassing van het “Power-to-Protein” concept in de stedelijke watercyclus van Amsterdam: TKI Project Power to Protein (Nieuwegein, The Netherlands: KWR Water Cycle Institute), pp. 46; and Oosterholt, F., Broeders, E., and Zamalloa, C. (2019). Power-to-Protein: eiwitproductie in een circulaire economie: Fase 2 Pilotonderzoek (Nieuwegein, The Netherlands: KWR Water Cycle Institute).

section is NovoNutrients, Inc. (California)³, which uses microbial consortia for animal feed production.

To guarantee the use of SCP as human food, it may be a lower risk to operate the bioreactor with pure cultures rather than open cultures. From information based on the patent literature, the company Kiverdi, Inc. in California is doing exactly this as part of their Air-Protein system with hydrogen-oxidizing bacterial strains and renewable sources of ammonia, carbon dioxide, and electric power. Electrolysis provides bacteria, such as purple non-sulfur bacteria or *Knallgas* bacteria, with a controlled composition of oxygen and hydrogen in the headspace (Reed, 2018).

Similarly, a Finnish company called Solar Food, Ltd. produces protein from carbon dioxide, and ammonia, oxygen, and hydrogen, which are solely produced from electrolysis (Heikkinen & Koskinen, 2019). In an online article, it was discussed that Solar Foods reduces the nitrogen gas that is present in air by using hydrogen from electrolysis to form an ammonia solution⁴. In contrast to the conventional Haber-Bosch process of ammonia production, which uses non-renewable natural gas as a feedstock, the catalytic reduction of nitrogen using renewable electric power (*e.g.*, *via* hydrogen) makes this process more sustainable (Soloveichik, 2019). Noteworthy is that carbon dioxide could also be sourced from air in addition to the nitrogen (Sillman *et al.*, 2019).

Based on free-energy data of half reactions at biochemical standard conditions, we calculated the stoichiometric equations (including biomass as C₅H₇O₂N) and theoretical biomass yield *per* energy input for each of seven carbon-fixation processes (**Table 1**) (McCarty, 2007; Rittmann & McCarty, 2001). A comparison shows that the biomass yield *per* energy input is considerably lower for electrolysis followed by the Calvin–Benson–Bassham cycle or the reverse-Krebs cycle (9.5 mg/kJ) compared to the other overall processes (18.2-32.8 mg/kJ). Autotrophic bacterial carbon fixation with oxygen is, thus, inferior. According to our calculations, it is energetically more favourable to utilize the intermediate products acetate, methanol, or methane (from anaerobic autotrophic bacterial carbon fixation or abiotic processes) as a substrate to grow biomass with oxygen.

3 Oakbio Inc. DBA NovoNutrients, Sunnyvale, California: <https://www.novonutrients.com/novonutrients-at-indiebio-demo-day>

4 Southey, F. (2019). Solar Foods makes protein out of thin air: 'This is the most environmentally friendly food there is'. In FoodNavigator (Crawley, UK: William Reed Business Media Ltd).

However, the protein content in the bacterial biomass is also an important consideration during this comparison. Hydrogen-oxidizing bacteria consist of higher protein contents (70-75%) than yeast (40-50%) or methylotrophic microbes (45-50%), while it is similar to methanotrophic microbes (Abou-Zeid & Baghlaf, 1983; Matassa *et al.*, 2016; Molitor *et al.*, 2019a; Ritala *et al.*, 2017) (**Table 1**). The stoichiometric reactions also show that for each carbon-fixation process, enough oxygen is produced electrochemically to provide the electron acceptor for biomass growth in bioreactors.

Section II: Wood-Ljungdahl pathway

Instead of mixing oxygen and hydrogen gas from electrolysis and feeding it to a single bioreactor for SCP production, another, and possibly safer prospect, is to autotrophically fix carbon with the Wood-Ljungdahl pathway by utilizing pure cultures of acetate-producing bacteria (*i.e.*, acetogens). Molitor *et al.* (2019a) has demonstrated this concept by placing two bioreactors *in series* after electrolysis. The entrée point of carbon dioxide was the first bioreactor (**Figure 1B**), which contained a pure culture of *Clostridium ljungdahlii* under anaerobic conditions, and which performed the conversion of carbon dioxide into acetate. Subsequently, the acetate was fed into the second bioreactor to feed *Saccharomyces cerevisiae* (yeast), which converted acetate into SCP with oxygen from the electrolyzer (**Figure 1B**). In addition to safety, the considerably higher theoretical biomass yield *per* energy input for the overall electrolysis/acetate-producing bacteria/heterotrophic microbes process (24.4 mg/kJ) compared to electrolysis/hydrogen-oxidizing microbes (9.5 mg/kJ) is an important advantage (**Table 1**).

The protein production rate in the second bioreactor was approximately 18 times lower than what is currently achieved at a commercial SCP production facility in the UK, where the meat-replacing product Quorn™ is produced from sugar with the filamentous fungal strain *Fusarium venenatum* (Ritala *et al.*, 2017). Further optimization possibilities of the rates for the bench-scale SCP production within the PtP approach were discussed. For example, by utilizing a different: (1) bioreactor configuration; (2) strain for SCP production; and (3) nutrient composition, among other factors. Since both yeast and fungal SCP can be used as human food, Molitor *et al.* (Molitor *et al.*, 2019a) compared the economic viability of the hypothetical PtP approach to the company that produces Quorn™. They found, with a comparative analysis, that the SCP product from PtP would

be ~8% more expensive than Quorn™. Finally, they calculated based on data from Quorn™ that only 10,000 industrial-scale fermenter systems would be necessary to feed the entire world population of 10 billion people to satisfy their protein requirements.

LanzaTech, Inc. (Chicago, Illinois)⁵ has scaled up gas fermentation for commercial fuel production with a closely related acetogen (*Clostridium autoethanogenum*), and therefore the first bioreactor from Molitor *et al.* (2019a) for acetate production already exists at an industrial scale. With the commercial availability of electrolyzers and the Quorn™ process as the second bioreactor, all operating units seem to be available to make a relatively quick transition to an industrial scale possible when they would be coupled.

Section III: hydrogenation or electrochemical reduction with abiotic processes

Another method to perform carbon fixation is to either catalytically (*via* hydrogenation) or electrochemically reduce carbon dioxide. The entrée point of carbon dioxide is a catalytic reactor after the electrochemical cell or the electrochemical cell itself and the produced intermediates are then fed to a single bioreactor for SCP production with oxygen from the electrochemical cell (**Figure 1C**). At this moment hybrid electrochemical cells are not yet produced on a commercial scale. Companies, such as Carbon Recycling International (Iceland)⁶, therefore, rely on hydrogen from electrolysis to reduce the carbon dioxide into methanol *via* hydrogenation (power-to-methanol). This is similar to the process we already had described above for ammonia production, but then with carbon dioxide rather than di-nitrogen gas (Solar Foods). However, to our knowledge no report exists about PtP with the hydrogenation or electrochemical reduction of carbon dioxide as the carbon fixation route. Regardless, we will discuss its intermediates acetate, methanol, and methane (Ma & Kenis, 2013), because they have already been utilized as substrates for SCP production from different sources (Linder, 2019), and the coupling of the operating units from Section III is a logical next step.

⁵ LanzaTech, Inc. (Skokie, Illinois): <https://www.lanzatech.com/>

⁶ Carbon Recycling International, Kopavagur, Iceland: <https://www.carbonrecycling.is/circlenergy>

For acetate as the electrochemical intermediate, the first bioreactor with the Wood-Ljungdahl pathway would be replaced by electrochemical reduction, while the SCP production system remains the same as in Molitor *et al.* (2019a). This combined electrochemical cell/bioreactor process has the highest theoretical biomass yield *per* energy input in our calculation (32.8 mg/kJ in **Table 1**). SCP production with methanol has a longer scientific and commercial history than acetate. Researchers had, for example, utilized methanol as an organic carbon source for growing yeast as SCP in the 1980s, while others have used the methylotrophic bacterium *Methylophilus methylotrophus* (Ritala *et al.*, 2017). Finally, the oxidation of methane into SCP with methylotrophic bacteria has reached a commercial level with, for example, *Methyloccoccus capsulatus* and other bacteria being utilized by companies such as Calysta, Inc. and UniBio A/S (Ritala *et al.*, 2017). We calculated that for both methanol and methane as the intermediates, the direct electrochemical reduction has a higher theoretical biomass yield *per* energy input than the electrolyzer followed by a hydrogenation step (**Table 1**). With the same moles of biomass production per 1 mole of electrons for each of these intermediates, direct electrochemical conversion requires a lower theoretical energy input than electrolysis/hydrogenation. We also found a higher theoretical biomass yield *per* energy input for methanol vs. methane, respectively (30.4 vs. 21.8 mg/kJ **Table 1**). However, the lower protein content with methanol vs. methane (45-50% vs. 67-73% in **Table 1**) equalizes this advantage.

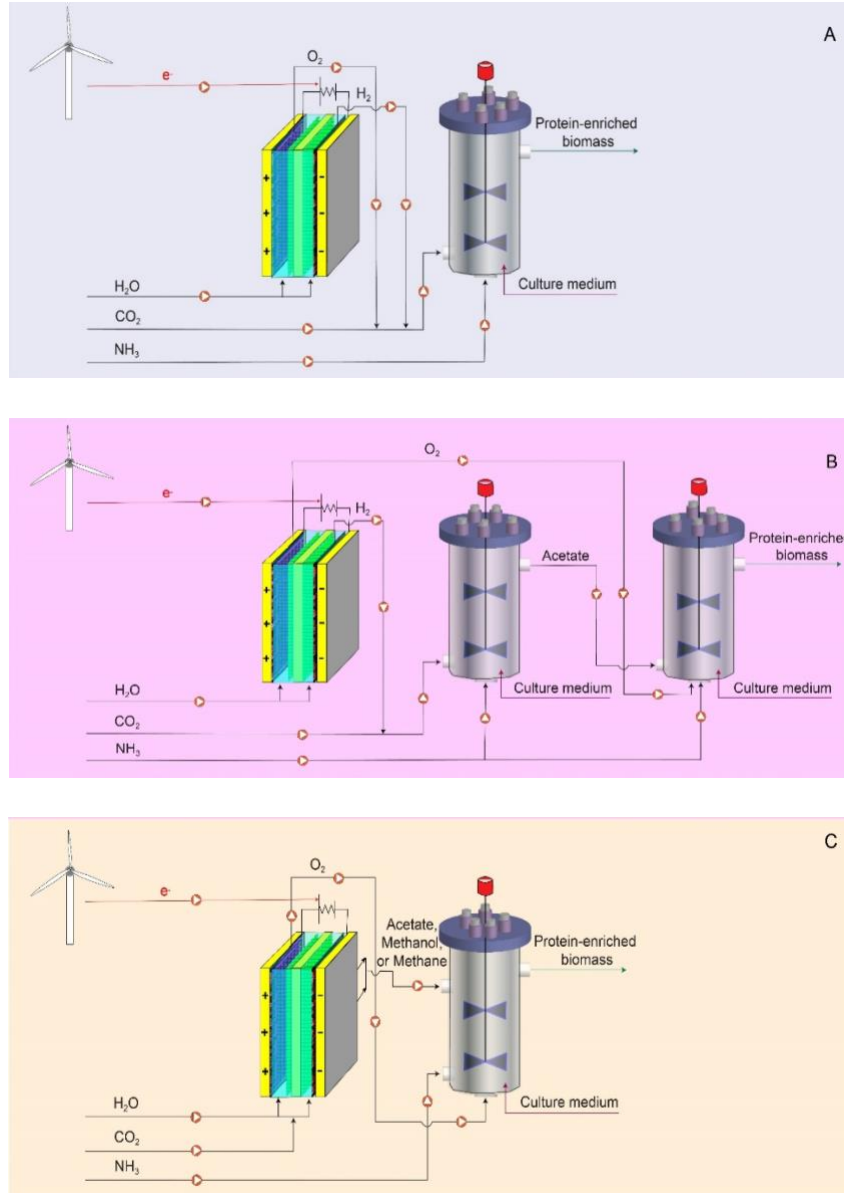


Figure 1: Conversion of renewable power and carbon dioxide to protein based on three different carbon fixation pathways. (A) An electrolyzer splits water into oxygen and hydrogen with renewable power. Carbon dioxide and both these gases are then fed into a bioreactor with aerobic hydrogen-oxidizing bacteria that fix carbon dioxide via either the Calvin-Benson-Bassham cycle or the reverse-Krebs cycle to produce biomass. (B) The hydrogen from an electrolyzer and carbon dioxide are fed into a first bioreactor with anaerobic bacteria (acetogens) that fix carbon via the Wood-Ljungdahl pathway to produce acetate. The oxygen from the electrolyzer is fed, together with this acetate, into a second bioreactor with aerobic heterotrophic microbes (yeast or fungi) to produce biomass. (C) The carbon dioxide is reduced electrochemically to fix carbon and to form oxygen and acetate, methanol, or methane, which are both fed into a bioreactor with aerobic heterotrophic, methylotrophic, or methanotrophic microbes, respectively, to produce biomass. Each bioreactor is also fed with ammonia as a nitrogen source and culture media that include other necessary nutrients and trace elements.

Table 1: A comparison of the different carbon-fixation systems for protein production in terms of their theoretical biomass yield at biochemical standard conditions.

Carbon-fixation section (I-III)	Entrée point of 1 mole of e ⁻ when box is green	Sub-process	Reaction stoichiometry (R _T)	Biomass yield per energy input (mg/kJ)	Protein content ^c
Calvin-Benson-Bassham or reverse-Krebs cycle	Electrolyzer 0.5 H ₂ O →	Hydrogen-oxidizing bacteria	0.500 H ₂ + 0.062 CO ₂ + 0.012 NH ₃ + 0.188 O ₂ → 0.012 C₅H₇O₂N + 0.475 H ₂ O	9.5	70 - 75%
	0.25 O ₂ + 0.5 H ₂	Acetate-producing bacteria	0.500 H ₂ + 0.250 CO ₂ + 0.002 NH ₃ → 0.002 C₅H₇O₂N + 0.255 H ₂ O + 0.121 CH ₃ COO ⁻ + 0.121 H ⁺	(1.2) ^b	-
Wood-Ljungdahl pathway	H ₂	Heterotrophic microbes	0.121 CH ₃ COO ⁻ + 0.121 H ⁺ + 0.087 O ₂ + 0.031 NH ₃ → 0.031 C₅H₇O₂N + 0.087 CO ₂ + 0.180 H ₂ O	24.4	40 - 50%
Hydrogenation (H)-intermediate or electrochemical reduction (ER)-intermediate with abiotic processes	Electrolyzer	(ER)-acetate ^a	0.250 H ₂ O + 0.250 CO ₂ → 0.125 CH ₃ COO ⁻ + 0.125 H ⁺ + 0.250 O ₂	32.8	40 - 50%
		Heterotrophic microbes	0.125 CH ₃ COO ⁻ + 0.125 H ⁺ + 0.090 O ₂ + 0.032 NH ₃ → 0.032 C₅H₇O₂N + 0.090 CO ₂ + 0.186 H ₂ O		
	Electrolyzer	(H)-methanol	0.500 H ₂ + 0.167 CO ₂ → 0.167 CH ₃ OH + 0.167 H ₂ O	23.7	45 - 50%
		Methylotrophic microbes	0.167 CH ₃ OH + 0.089 O ₂ + 0.032 NH ₃ → 0.032 C₅H₇O₂N + 0.269 H ₂ O + 0.005 CO ₂		
		(ER)-methanol ^a	0.333 H ₂ O + 0.167 CO ₂ → 0.167 CH ₃ OH + 0.250 O ₂	30.4	45 - 50%
		Methylotrophic microbes	0.167 CH ₃ OH + 0.089 O ₂ + 0.032 NH ₃ → 0.032 C₅H₇O₂N + 0.269 H ₂ O + 0.005 CO ₂		
	Electrolyzer	(H)-methane	0.500 H ₂ + 0.125 CO ₂ → 0.125 CH ₄ + 0.250 H ₂ O	18.2	67 - 73%
		Methanotrophic bacteria	0.125 CH ₄ + 0.143 O ₂ + 0.021 NH ₃ → 0.021 C₅H₇O₂N + 0.207 H ₂ O + 0.018 CO ₂		
		(ER)-methane ^a	0.250 H ₂ O + 0.125 CO ₂ → 0.125 CH ₄ + 0.250 O ₂	21.8	67 - 73%
		Methanotrophic bacteria	0.125 CH ₄ + 0.143 O ₂ + 0.021 NH ₃ → 0.021 C₅H₇O₂N + 0.207 H ₂ O + 0.018 CO ₂		

We assume that the source of energy in each case is renewable power and that it supplies 1 mole of electron equivalents. Each process requires a specific value of input energy (kJ) at biochemical standard conditions (pH 7, 298 K temperature, and at 1 M concentration of reactants) to transform a fraction of electron

equivalents into biomass (shown here as $C_5H_7O_2N$). Therefore, the theoretical yield of biomass for each process is normalized to its theoretical input energy to compare each process. Data from hydrogenation to acetate was not found for the correct standard conditions, and therefore this process was omitted from the table. A more detailed table (Table S1) and all the calculations (Table S2-S8) are available in the Supplementary Information.

^aEntrée point for 1 mole of e^- into direct electrochemical reduction (ER)

^bThe value of 1.2 mg/kJ is for the biomass from the acetate-producing bacteria only, and is not included here as part of the seven carbon-fixation processes. This biomass would not be utilized in the overall process (24.4 mg/kJ), and is just an indication how ineffective biomass production would be for protein production with this sub-process only.

^cReferences for these protein content values are given in the text, and acetate-producing bacteria are deliberately left out based on the previous footnote

Outlook

PtP approaches could play a pertinent role to prevent catastrophic environmental collapse, which is predicted to occur when feeding 10 billion people with animal-based protein, because conventional agriculture can be circumvented altogether. In addition, PtP can be employed in areas with a lack of affordable protein. Some of the discussed PtP approaches, such as from Sections I and II, are ready to be implemented at scale on a technological level, because off-the-shelf electrochemical systems can be combined with current commercial fermentation and/or SCP systems. More work is necessary, though, to understand the optimum energy, carbon, and nutrient flows between the electrochemical cells and bioreactors, especially to obtain realistic data for detailed life-cycle and techno-economic analyses.

It is also important to understand the societal aspects of a change in the way societies produce protein (Molitor *et al.*, 2019). A study has found that ~2.5% of all produced energy would be necessary to feed the world with protein from PtP (De Vrieze *et al.*, 2020). Therefore, a real opportunity exists to place PtP approaches within a renewable electric power grid system to help provide load management, because PtP can periodically produce and store: (1) oxygen and hydrogen gas; and/or (2) protein product, during peak supply of renewable electric power from wind and solar sources. Societies must now invest all they can into more renewable electric power production/storage and an infrastructure for carbon dioxide capture and distribution.

Acknowledgments

The authors acknowledge support from the Alexander von Humboldt Foundation in the framework of the Alexander von Humboldt Professorship endowed by the Federal Ministry of Education and Research in Germany. The authors thank Dr. Sofia Esquivel Elizondo (Max Planck Institute of Developmental Biology, Tübingen), Dr. Tianran Sun, Dr. Byoung Seung Jeon, and Isabella Cassini (all at the University of Tübingen) for help with the stoichiometric calculations.

Declaration of Interests

The authors declare no competing interests.

References

- Abou-Zeid, A.-Z. A., & Baghlaf, A. O. (1983). Methanol as the carbon source of production of single-cell proteins (SCP-s). *Zentralblatt für Mikrobiologie*, *138*(6), 451-464.
- Coppens, J., Lindeboom, R., Muys, M., Coessens, W., Alloul, A., Meerbergen, K., Vlaeminck, S. E. (2016). Nitrification and microalgae cultivation for two-stage biological nutrient valorization from source separated urine. *Bioresource Technology*, *211*, 41-50.
- De Vrieze, J., Verbeeck, K., Pikaar, I., Boere, J., Van Wijk, A., Rabaey, K., & Verstraete, W. (2020). The hydrogen gas bio-based economy and the production of renewable building block chemicals, food and energy. *New Biotechnology*, *55*, 12-18. doi:<https://doi.org/10.1016/j.nbt.2019.09.004>
- Foster, J. F., & Litchfield, J. H. (1964). A continuous culture apparatus for the microbial utilization of hydrogen produced by electrolysis of water in closed-cycle space systems. *Biotechnology and Bioengineering*, *6*(4), 441-456.
- Heikkinen, A., & Koskinen, S. (2019). Ecopreneurial Startups with Sustainable Innovations: A Case Study on the Emergence and Growth of Four Finnish Startup Companies. In:
- Linder, T. (2019). Making the case for edible microorganisms as an integral part of a more sustainable and resilient food production system. *Food Security*, *11*(2), 265-278.
- Ma, S., & Kenis, P. J. (2013). Electrochemical conversion of CO₂ to useful chemicals: current status, remaining challenges, and future opportunities. *Current Opinion in Chemical Engineering*, *2*(2), 191-199.
- Matassa, S., Verstraete, W., Pikaar, I., & Boon, N. (2016). Autotrophic nitrogen assimilation and carbon capture for microbial protein production by a novel enrichment of hydrogen-oxidizing bacteria. *Water research*, *101*, 137-146.
- McCarty, P. L. (2007). Thermodynamic electron equivalents model for bacterial yield prediction: modifications and comparative evaluations. *Biotechnology and Bioengineering*, *97*(2), 377-388.
- Molitor, B., Mishra, A., & Angenent, L. T. (2019a). Power-to-protein: converting renewable electric power and carbon dioxide into single cell protein with a two-stage bioprocess. *Energy & Environmental Science*.
- Molitor, B., Mishra, A., & Angenent, L. T. (2019b). Power-to-protein: converting renewable electric power and carbon dioxide into single cell protein with a two-stage bioprocess. *Energy & Environmental Science*, *12*(12), 3515-3521. doi:[10.1039/C9EE02381J](https://doi.org/10.1039/C9EE02381J)
- Poore, J., & Nemecek, T. (2018). Reducing food's environmental impacts through producers and consumers. *Science*, *360*(6392), 987-992. Retrieved from <https://science.sciencemag.org/content/sci/360/6392/987.full.pdf>
- Prosekov, A. Y., & Ivanova, S. A. (2018). Food security: The challenge of the present. *Geoforum*, *91*, 73-77. doi:<https://doi.org/10.1016/j.geoforum.2018.02.030>
- Reed, J. S. (2018). Use of Oxyhydrogen Microorganisms for Non-Photosynthetic Carbon Capture and Conversion of Inorganic and/or C1 Carbon Sources into Useful Organic Compounds. In: Google Patents.

- Ritala, A., Häkkinen, S. T., Toivari, M., & Wiebe, M. G. (2017). Single Cell Protein-State-of-the-Art, Industrial Landscape and Patents 2001-2016. *Frontiers in microbiology*, 8, 2009-2009. doi:10.3389/fmicb.2017.02009
- Rittmann, B. E., & McCarty, P. L. (2001). *Environmental biotechnology: principles and applications*: McGraw-Hill Education.
- Schiebahn, S., Grube, T., Robinius, M., Tietze, V., Kumar, B., & Stolten, D. (2015). Power to gas: Technological overview, systems analysis and economic assessment for a case study in Germany. *International journal of hydrogen energy*, 40(12), 4285-4294.
- Sillman, J., Nygren, L., Kahiluoto, H., Ruuskanen, V., Tamminen, A., Bajamundi, C., Vainikka, P. (2019). Bacterial protein for food and feed generated via renewable energy and direct air capture of CO₂: Can it reduce land and water use? *Global Food Security*, 22, 25-32.
- Soloveichik, G. (2019). Electrochemical synthesis of ammonia as a potential alternative to the Haber–Bosch process. *Nature Catalysis*, 2(5), 377-380.

Carbon Fixation with renewable electric power to feed the world: Power-to-protein

Supplemental Information

Akanksha Mishra¹, Jean Nepomuscene Ntihuga¹, Bastian Molitor¹, and Largus T. Angenent^{1,2}

1. Center for Applied Geosciences, University of Tuebingen, 72070 Tuebingen, Germany

2. Max Planck Fellow, Max Planck Institute for Developmental Biology, 72076 Tübingen, Germany

Adapted from: **Mishra, A., Ntihuga J.N., Molitor, B., & Angenent, L.T. (2020). Power-to-Protein: Carbon Fixation with Renewable Electric Power to Feed the World. *Joule*, 4(6), 1142-1147**

Supplemental Information

General Assumptions for all the pathways

1. The various processes described under section I, II, and III undergo a series of biochemical reactions to produce biomass. For our calculations, we assume that the energy supplied to these processes from renewable power is equivalent to 1 mole of electrons. In addition, each process also requires a minimum amount of energy (kJ) to perform all these biochemical reactions with 1 mole of electrons equivalents. This value is unique to each process and will produce either the same or a different yield of biomass. Therefore, we have estimated the biomass yield *per* input energy for each one to develop a theoretical, yet quantitative comparison of their protein production.
2. All the calculations have been performed at standard temperature (298 K) and pressure (1 atm) and pH 7
3. The Gibbs free energy/the energy input into each process has been calculated using the Thermodynamic Electron Equivalent Model (TEEM1) given in Rittmann and McCarty (2012).
4. Our model also considers the modifications that were later suggested by McCarty (2007) in TEEM2 for organic C1 compounds (methanol and methane). The modifications are as follows:
5. Accounting for the loss of energy during the conversion of the C1 carbon source first to formaldehyde and then to acetyl-CoA.
6. Also accounting for energetic cost incurred during the utilization of the mono-oxygenase enzyme for the conversion of methane to methanol for methanotrophic bacteria.
7. An additional modification that we have adapted from McCarty (2007) is the utilization of acetyl-CoA instead of pyruvate as an intermediate compound for the synthesis of biomass in all the pathways.
8. The half-reactions for each step are given in **Table S1**.
9. We have assumed an energy transfer efficiency of 60% for all the microbes involved in different processes.
10. We have also assumed the same microbial biomass composition (C₅H₇O₂N) for all the processes.

Table S1: Details of all the half-reactions involved in the seven carbon fixation processes

This table shows the entrée point of 1 mole of electron equivalents, the microbial pathway involved, and the final standard half-reactions of each step in Section I, II, and III. The variables R_d , R_a , and R_s are combined to produce a stoichiometric equation (R_f) for each process. The final equation R_f (Table 1) is then used to calculate Y_{energy} (mg/kJ), which we have defined as the amount of biomass formed from each process and normalized to its input energy.

Carbon-fixation section (I-III)	Entrée point of 1 mole of e^- when box is green	Sub-process	Oxidation half-reactions	Reduction half-reactions		Y_{energy} mg/kJ
				e^- for energy generation	e^- for biomass synthesis	
Calvin-Benson-Bassham or reverse-Krebs cycle Table S2:	Electrolyzer: $R_d: 0.5 \text{ H}_2\text{O} \rightarrow 0.25 \text{ O}_2 + \text{H}^+ + e^-$; $R_a: \text{H}^+ + e^- \rightarrow 0.5 \text{ H}_2$	Hydrogen-oxidizing bacteria $f_e: 0.751$ $f_s: 0.249$	$R_d: 0.500 \text{ H}_2 \rightarrow \text{H}^+ + e^-$	$R_a: 0.250 \text{ O}_2 + 1 \text{ H}^+ + 1 e^- \rightarrow 0.500 \text{ H}_2\text{O}$	$R_s: 0.250 \text{ CO}_2 + 0.050 \text{ NH}_3 + 1 \text{ H}^+ + 1 e^- \rightarrow 0.050 \text{ C}_5\text{H}_7\text{O}_2\text{N} + 0.400 \text{ H}_2\text{O}$	9,504
				$f_e^*R_a: 0.188 \text{ O}_2 + 0.751 \text{ H}^+ + 0.751 e^- \rightarrow 0.375 \text{ H}_2\text{O}$	$f_s^*R_s: 0.062 \text{ CO}_2 + 0.012 \text{ NH}_3 + 0.249 \text{ H}^+ + 0.249 e^- \rightarrow 0.012 \text{ C}_5\text{H}_7\text{O}_2\text{N} + 0.475 \text{ H}_2\text{O}$	
Wood-Ljungdahl pathway Table S3: Stage 1	Electrolyzer	Acetate-producing bacteria $f_c: 0.968$ $f_s: 0.033$	$R_d: 0.500 \text{ H}_2 \rightarrow \text{H}^+ + e^-$	$R_a: 0.250 \text{ CO}_2 + 0.875 \text{ H}^+ + 1 e^- \rightarrow 0.125 \text{ CH}_3\text{COO}^- + 0.250 \text{ H}_2\text{O}$	$R_s: 0.250 \text{ CO}_2 + 0.050 \text{ NH}_3 + 1 \text{ H}^+ + 1 e^- \rightarrow 0.050 \text{ C}_5\text{H}_7\text{O}_2\text{N} + 0.400 \text{ H}_2\text{O}$	1,227
				$f_c^*R_a: 0.242 \text{ CO}_2 + 0.846 \text{ H}^+ + 0.967 e^- \rightarrow 0.121 \text{ CH}_3\text{COO}^- + 0.242 \text{ H}_2\text{O}$	$f_s^*R_s: 0.008 \text{ CO}_2 + 0.002 \text{ NH}_3 + 0.033 \text{ H}^+ + 0.033 e^- \rightarrow 0.002 \text{ C}_5\text{H}_7\text{O}_2\text{N} + 0.013 \text{ H}_2\text{O}$	
Stage 2	Electrolyzer	Heterotrophic microbes $f_{e1}: 0.361$ $f_{s1}: 0.639$	$R_{d1}: 0.121 \text{ CH}_3\text{COO}^- + 0.242 \text{ H}_2\text{O} \rightarrow 0.242 \text{ CO}_2 + 0.846 \text{ H}^+ + 0.969 e^-$	$R_{a1}: 0.250 \text{ O}_2 + 1 \text{ H}^+ + 1 e^- \rightarrow 0.500 \text{ H}_2\text{O}$	$R_{s1}: 0.250 \text{ CO}_2 + 0.050 \text{ NH}_3 + 1 \text{ H}^+ + 1 e^- \rightarrow 0.050 \text{ C}_5\text{H}_7\text{O}_2\text{N} + 0.400 \text{ H}_2\text{O}$	24,356

					$f_e^* R_{a1}^* f_{e1}^b: 0.087 O_2 + 0.349 H^+ + 0.349 e^- \rightarrow 0.175 H_2O$	$f_e^* R_{s1}^* f_{s1}^b: 0.155 CO_2 + 0.031 NH_3 + 0.618 H^+ + 0.618 e^- \rightarrow 0.031 C_5H_7O_2N + 0.247 H_2O$	
Electrochemical reduction (ER)-intermediate Table S4: Stage 1	(ER)-acetate ^a			$0.500 H_2O \rightarrow 0.250 O_2 + H^+ + e^-$	$0.250 CO_2 + 0.875 H^+ + e^- \rightarrow 0.125 CH_3COO^- + 0.125 H^+ + 0.250 H_2O$	NA	
Stage 2	Heterotrophic microbes $f_e: 0.361 f_s: 0.639$		$R_{d1}: 0.125 CH_3COO^- + 0.125 H^+ + 0.250 H_2O \rightarrow 0.250 CO_2 + 0.875 H^+ + e^-$	$R_{a1}: 0.250 O_2 + 1 H^+ + 1 e^- \rightarrow 0.500 H_2O$	$R_{s1}: 0.250 CO_2 + 0.050 NH_3 + 1 H^+ + 1 e^- \rightarrow 0.050 C_5H_7O_2N + 0.400 H_2O$	32.817	
Hydrogenation (H)-intermediate Table S5: Stage 1	(H)-methanol	Electrolyzer		$0.500 H_2 \rightarrow H^+ + e^-$	$0.167 CO_2 + H^+ + e^- \rightarrow 0.167 CH_3OH + 0.167 H_2O$	NA	
Stage 2	Methylootrophic microbes $f_e: 0.355 f_s: 0.645$	Electrolyzer	$R_{d1}: 0.167 CH_3OH + 0.167 H_2O \rightarrow 0.16 CO_2 + H^+ + e^-$	$R_{a1}: 0.250 O_2 + 1 H^+ + 1 e^- \rightarrow 0.500 H_2O$	$R_{s1}: 0.250 CO_2 + 0.050 NH_3 + 1 H^+ + 1 e^- \rightarrow 0.050 C_5H_7O_2N + 0.400 H_2O$	23.666	
Electrochemical reduction (ER)-intermediate Table S6:	(ER)-methanol ^a		$R_{d1}: 0.500 H_2O \rightarrow 0.250 O_2 + H^+ + e^-$	$0.167 CO_2 + H^+ + e^- \rightarrow 0.167 CH_3OH + 0.167 H_2O$	$f_e^* R_{a1}^* f_{e1}^b: 0.089 O_2 + 0.355 H^+ + 0.355 e^- \rightarrow 0.177 H_2O$	NA	

Stage 1								
Stage 2	Methylophilic microbes $f_c: 0.355$ $f_s: 0.645$	$R_d: 0.167 \text{ CH}_3\text{OH} + 0.167 \text{ H}_2\text{O} \rightarrow 0.167 \text{ CO}_2 + \text{H}^+ + \text{e}^-$	$R_a: 0.250 \text{ O}_2 + 1 \text{ H}^+ + 1 \text{ e}^- \rightarrow 0.500 \text{ H}_2\text{O}$ $f_e^*R_a: 0.089 \text{ O}_2 + 0.355 \text{ H}^+ + 0.355 \text{ e}^- \rightarrow 0.177 \text{ H}_2\text{O}$	$R_s: 0.250 \text{ CO}_2 + 0.050 \text{ NH}_3 + 1 \text{ H}^+ + 1 \text{ e}^- \rightarrow 0.050 \text{ C}_5\text{H}_7\text{O}_2\text{N} + 0.400 \text{ H}_2\text{O}$ $f_s^*R_s: 0.161 \text{ CO}_2 + 0.032 \text{ NH}_3 + 0.645 \text{ H}^+ + 0.645 \text{ e}^- \rightarrow 0.032 \text{ C}_5\text{H}_7\text{O}_2\text{N} + 0.258 \text{ H}_2\text{O}$				30.348
Hydrogenation (H)-intermediate Table S7								
Stage 1	(H)-methane	$0.500 \text{ H}_2 \rightarrow \text{H}^+ + \text{e}^-$	$0.125 \text{ CO}_2 + \text{H}^+ + \text{e}^- \rightarrow 0.125 \text{ CH}_4 + 0.250 \text{ H}_2\text{O}$					NA
Stage 2	Methanotrophic bacteria $f_c: 0.573$ $f_s: 0.427$	$R_d: 0.125 \text{ CH}_4 + 0.250 \text{ H}_2\text{O} \rightarrow 0.125 \text{ CO}_2 + \text{H}^+ + \text{e}^-$	$R_a: 0.250 \text{ O}_2 + 1 \text{ H}^+ + 1 \text{ e}^- \rightarrow 0.500 \text{ H}_2\text{O}$ $f_e^*R_a: 0.143 \text{ O}_2 + 0.573 \text{ H}^+ + 0.573 \text{ e}^- \rightarrow 0.287 \text{ H}_2\text{O}$	$R_s: 0.250 \text{ CO}_2 + 0.050 \text{ NH}_3 + 1 \text{ H}^+ + 1 \text{ e}^- \rightarrow 0.050 \text{ C}_5\text{H}_7\text{O}_2\text{N} + 0.400 \text{ H}_2\text{O}$ $f_s^*R_s: 0.107 \text{ CO}_2 + 0.021 \text{ NH}_3 + 0.427 \text{ H}^+ + 0.427 \text{ e}^- \rightarrow 0.021 \text{ C}_5\text{H}_7\text{O}_2\text{N} + 0.171 \text{ H}_2\text{O}$				18.216
Electrochemical reduction (ER)-intermediate Table S8								
Stage 1	(ER)-methane ^a	$0.500 \text{ H}_2\text{O} \rightarrow 0.250 \text{ O}_2 + \text{H}^+ + \text{e}^-$	$0.125 \text{ CO}_2 + \text{H}^+ + \text{e}^- \rightarrow 0.125 \text{ CH}_4 + 0.250 \text{ H}_2\text{O}$					NA
Stage 2	Methanotrophic bacteria $f_c: 0.573$ $f_s: 0.427$	$R_d: 0.125 \text{ CH}_4 + 0.250 \text{ H}_2\text{O} \rightarrow 0.125 \text{ CO}_2 + \text{H}^+ + \text{e}^-$	$R_a: 0.250 \text{ O}_2 + 1 \text{ H}^+ + 1 \text{ e}^- \rightarrow 0.500 \text{ H}_2\text{O}$ $f_e^*R_a: 0.143 \text{ O}_2 + 0.573 \text{ H}^+ + 0.573 \text{ e}^- \rightarrow 0.287 \text{ H}_2\text{O}$	$R_s: 0.250 \text{ CO}_2 + 0.050 \text{ NH}_3 + 1 \text{ H}^+ + 1 \text{ e}^- \rightarrow 0.050 \text{ C}_5\text{H}_7\text{O}_2\text{N} + 0.400 \text{ H}_2\text{O}$ $f_s^*R_s: 0.107 \text{ CO}_2 + 0.021 \text{ NH}_3 + 0.427 \text{ H}^+ + 0.427 \text{ e}^- \rightarrow 0.021 \text{ C}_5\text{H}_7\text{O}_2\text{N} + 0.171 \text{ H}_2\text{O}$				21.779

^a. Entrée point for 1 mole of e^- into direct electrochemical reduction (ER)

^b. Here, Stage 1 is a biological process. The amount of acetate produced in Stage 1 is ~97% of the standard half-reaction (f_c) and can, therefore, only donate 0.96 moles of electron equivalents. This will further reduce only 97% of standard half-reaction of R_{a1} ($f_e^*R_{a1}$) and R_{s1} ($f_s^*R_{s1}$).

Table S2: Calvin-Benson-Bassham or reverse-Krebs cycle

Electron donor: Hydrogen; Electron acceptor: Oxygen

Variable	Definition	Value	Units	Calculations	Assumptions	Source
$\Delta G^{\circ}_{\text{formation}}$ Acetyl-CoA (half-reaction)		30.900	kJ/e ⁻ eq			(McCarty, 2007)
$\Delta G^{\circ}_{\text{formation}}$ Water-oxygen (half-reaction)		-78.720	kJ/e ⁻ eq			(McCarty, 2007)
$\Delta G^{\circ}_{\text{formation}}$ Hydrogen (half-reaction)		39.870	kJ/e ⁻ eq			Rittmann and McCarty (2012)
ΔG_{e}	Energy required to convert the carbon source into acetyl-CoA	109.620	kJ/e ⁻ eq	$\Delta G^{\circ}_{\text{formation}}$ Acetyl-CoA (half-reaction) - $\Delta G^{\circ}_{\text{formation}}$ Water-oxygen (half-reaction)	Considerable energy is required to reduce inorganic carbon to acetyl-CoA. In photosynthesis, the hydrogen or electrons for reducing carbon dioxide to form cellular organic matter comes from water. By analogy, to this case, we can determine the energy involved, if we take the water-oxygen reaction as the donor. Thus, for the autotrophic case, it is always taken equal to 30,900 - (-78.720) = 109.620 kJ/e ⁻ eq.	Rittmann and McCarty (2012)
Mwtbiomass	Molecular weight of biomass	113	g/mol	C = 12 g/mol; H = 1 g/mol; O = 16 g/mol; N = 14 g/mol C*5 + (H*7) + (O*2) + (N)	The biomass composition is assumed to be C ₅ H ₇ O ₂ N	Rittmann and McCarty (2012)
ΔG_{FCI}	ΔG of converting acetyl-CoA carbon to cellular biomass	3.330	kJ/g			McCarty (2007)
X	Number of electron equivalents transferred to ammonia for the synthesis of biomass	20	e ⁻ eq/mol			Rittmann and McCarty (2012)
Y	Amount of biomass obtained per unit electron equivalent	5.650	g/e ⁻ eq	Mwtbiomass/X		Rittmann and McCarty (2012)
ΔG_{FC}	Amount of energy required for the reduction of ammonia into biomass	18.814	kJ/e ⁻ eq	$\Delta G_{\text{FCI}} * Y$	We consider ammonia to be the nitrogen source.	Rittmann and McCarty (2012)
ΔG_{r}	Free energy released per equivalent of donor oxidized for energy generation	-118.590	kJ/e ⁻ eq	$\Delta G^{\circ}_{\text{formation}}$ Water-oxygen (half-reaction) - $\Delta G^{\circ}_{\text{formation}}$ Hydrogen (half-reaction)		Rittmann and McCarty (2012)

Variable	Definition	Values	Units	Calculation	Assumption	Source
ϵ	Energy transfer efficiency	0.600			The energy lost during electron transfer for biomass synthesis	Rittmann and McCarty (2012)
n	Exponent for ϵ	1		If ΔG_{ic} is negative, $n = -1$; if ΔG_{ic} is positive, $n = 1$	Depending on whether ΔG_{ic} is positive or negative, energy is either required or lost during the conversion of the carbon source to acetyl-CoA	Rittmann and McCarty (2012)
A	Donor equivalents that must be oxidized for the synthesis of biomass	3.009		$-((\Delta G_{ic}/\epsilon^n) + (\Delta G_{pc}/\epsilon))/(\Delta G_r \cdot \epsilon)$		Rittmann and McCarty (2012)
f_e	The portion of electrons from the donor going into the electron acceptor for energy generation	0.751		$A/(A+1)$		Rittmann and McCarty (2012)
f_s	The portion of electrons from the donor going into cell synthesis	0.249		$1/(A+1)$		Rittmann and McCarty (2012)
R_a	Reduction-half reaction of oxygen	See Table S1				Rittmann and McCarty (2012)
R_d	Oxidation-half reaction of hydrogen	See Table S1				Rittmann and McCarty (2012)
R_s	Half-reaction of cell synthesis	See Table S1				Rittmann and McCarty (2012)
R_f	Final equation	See Table 1		$R_f = R_d + f_e \cdot R_a + f_s \cdot R_s$		Rittmann and McCarty (2012)
d	Degree of reduction of hydrogen	2	e^- eq/mol	Number of electron equivalents transferred from 1 mole of donor		
e	Moles of hydrogen consumed	0.500	moles	Coefficient of donor in R_d		
f	Moles of biomass formed	0.0125	moles	Coefficient of biomass in $f_s \cdot R_s$		
Y_d	Biomass yield per mol electron donor	2.818	g/mol	$(f/e) \cdot M_{wt} \text{biomass}$		
Y_e	Biomass yield per mol electron	1.409	g/e eq	Y_d/d		
g	Energy input into electrolyzer with a conversion efficiency of 80%	148.238	kJ/e^- eq	$((\Delta G^\circ_{\text{formation Hydrogen (half-reaction)} - \Delta G^\circ_{\text{formation Water-oxygen (half-reaction)})})/0.8)$		
Y_{energy}	Biomass yield based on input energy	9.504	mg/kJ	$Y_e/g \cdot 1000$		

Table S3: Wood-Ljungdahl Pathway and the growth of Heterotrophic microbesElectron donor: Hydrogen; Electron acceptor: Carbon dioxide (CO₂)

Variable	Definition	Value	Units	Calculations	Assumptions	Source
$\Delta G^{\circ}_{\text{formation}}$ Acetyl-CoA (half-reaction)		30.900	kJ/e ⁻ eq			McCarty (2007)
$\Delta G^{\circ}_{\text{formation}}$ Water-oxygen (half-reaction)		-78.720	kJ/e ⁻ eq			Rittmann and McCarty (2012)
$\Delta G^{\circ}_{\text{formation}}$ Hydrogen (half-reaction)		39.870	kJ/e ⁻ eq			Rittmann and McCarty (2012)
$\Delta G^{\circ}_{\text{formation}}$ Acetate (half-reaction)	Gibbs Free energy of reduction of CO ₂ to acetate	28	kJ/e ⁻ eq	Modified from the half-reaction of acetate synthesis in Table 2.3 (Chapter 2) in Source 1 to remove the bicarbonate species; Refer Table S1 for the half-reaction		McCarty (2007)
ΔG_{ic}	Energy required to convert carbon source into acetyl-CoA	109.620	kJ/e ⁻ eq	$\Delta G^{\circ}_{\text{formation}}$ Acetyl-CoA (half-reaction) - $\Delta G^{\circ}_{\text{formation}}$ Water-oxygen(half-reaction)	Same assumption as given in Section I	McCarty (2007)
Mwtbiomass	Molecular weight of biomass	113	g/mol	C = 12 g/mol; H = 1 g/mol; O = 16 g/mol; N = 14	The biomass composition is assumed to be C ₅ H ₇ O ₂ N	Rittmann and McCarty (2012)
ΔG_{PCi}	ΔG of converting acetyl-CoA carbon to cellular biomass	3.330	kJ/g			McCarty (2007)
X	Number of electron equivalents transferred to ammonia for the synthesis of biomass	20	e ⁻ eq/mol			Rittmann and McCarty (2012)
Y	Amount of biomass obtained per unit electron	5.650	g/e ⁻ eq	Mwtbiomass/X		Rittmann and McCarty (2012)
ΔG_{PC}	Amount of energy required for the reduction of ammonia into biomass	18.814	kJ/e ⁻ eq	$\Delta G_{\text{PCi}} * Y$	We consider ammonia to be the nitrogen source.	Rittmann and McCarty (2012)
ΔG_{r}	Free energy released per equivalent of donor oxidized for energy generation	-11.870	kJ/e ⁻ eq	$\Delta G^{\circ}_{\text{formation}}$ of Acetate (half-reaction) - $\Delta G^{\circ}_{\text{formation}}$ of Hydrogen (half-reaction)		Rittmann and McCarty (2012)

Variable	Definition	Value	Units	Calculations	Assumptions	Source
ϵ	Energy transfer efficiency	0.600			The energy lost during electron transfer for biomass synthesis	Rittmann and McCarty (2012)
n	Exponent for ϵ	1		If ΔG_{ic} is negative, $n = -1$; if ΔG_{ic} is positive, $n = 1$	Depending on whether ΔG_{ic} is positive or negative, energy is either required or lost during the conversion of the carbon source to acetyl-CoA	Rittmann and McCarty (2012)
A	equivalents of hydrogen that must be oxidized for the synthesis of biomass	30.052		$-\left(\frac{\Delta G_{ic}/\epsilon^n}{(\Delta G_{PC}/\epsilon)}\right)/(\Delta G_r \cdot \epsilon)$		Rittmann and McCarty (2012)
f_e	The portion of electrons from the donor going into the electron acceptor for energy generation	0.968		$A/(A+1)$		Rittmann and McCarty (2012)
f_s	The portion of electrons from the donor going for biomass synthesis	0.033		$1/(A+1)$		Rittmann and McCarty (2012)
R_d	Oxidation-half reaction of hydrogen	See Table S1				Rittmann and McCarty (2012)
R_a	Reduction-half reaction of carbon dioxide to acetate	See Table S1				Rittmann and McCarty (2012)
R_s	Half-reaction of cell synthesis	See Table S1				Rittmann and McCarty (2012)
R_f	Final equation	See Table 1		$R_f = R_d + f_e \cdot R_a + f_s \cdot R_s$		Rittmann and McCarty (2012)
d	Degree of reduction of hydrogen	2	e ⁻ eq /mol		Number of electron equivalent transferred from 1 mole of donor	
e	Moles of donor consumed	0.500	moles	Coefficient of donor in R_d		
f	Moles of biomass formed	0.0016	moles	Coefficient of donor in $f_s \cdot R_s$		
Y_d	Biomass yield per mol electron donor	0.364	g/mol	$(f/e) \cdot M_{wt} \text{biomass}$		

Variables	Definition	Values	Units	Calculation	Assumptions	Source
Y_e	Biomass yield per mol electron	0.182	g/e ⁻ eq	Y_d/d		
g	Energy input into electrolyzer with a conversion efficiency of 80%	148,238	kJ/e ⁻ eq	$((\Delta G^{\circ}_{\text{formation}} \text{Hydrogen (half-reaction)} - \Delta G^{\circ}_{\text{formation}} \text{water-oxygen (half-reaction)})/0.8)$		
Y_{energy}	Biomass yield based on input energy	1.227	mg/kJ	$(Y_e/g)*1000$		
h	Moles of acetic acid formed	0.121	moles	Coefficient of acetate in $f_e * R_a$		
STAGE 2: GROWTH OF HETEROTROPHIC MICROBES ON ACETATE: Electron donor: Acetate; Electron acceptor: Oxygen						
R_{d1}	Oxidation-half reaction of acetate as an electron donor	See Table S1		Reverse of $R_a * f_e$		Rittmann and McCarty (2012)
R_{a1}	Reduction-half reaction of oxygen	See Table S1				Rittmann and McCarty (2012)
R_{s1}	Half-reaction of cell synthesis	See Table S1				Rittmann and McCarty (2012)
$\Delta G^{\circ}_{\text{formation}} \text{Acetate}_1$ (half-reaction)	Gibbs free energy of acetate production by the acetogens in R_{d1}	28.005	kJ/e ⁻ eq	$((\text{moles of Acetate in } R_{d1}) * \Delta G^{\circ}_{\text{formation}} \text{Acetate} + (\text{moles of Water in } R_{d1}) * \Delta G^{\circ}_{\text{formation}} \text{Water} - ((\text{moles of Hydrogen ion in } R_{d1}) * \Delta G^{\circ}_{\text{formation}} \text{Hydrogen} + (\text{moles of Carbon dioxide in } R_{d1}) * \Delta G^{\circ}_{\text{formation}} \text{Carbon dioxide})) / \text{coefficient of e}^{-} \text{ in } R_{d1}$		Values taken from Appendix A (Rittmann & McCarty, 2012)
ΔG_{ic1}	Energy required to convert carbon source into acetyl-CoA	2.895	kJ/e ⁻ eq	$\Delta G^{\circ}_{\text{formation}} \text{Acetyl-CoA (half-reaction)} - \Delta G^{\circ}_{\text{formation}} \text{Acetate}_1$ (half-reaction)		McCarty (2007)
n_1	Exponent for ΔG_{ic1}	1		Because the value of $\Delta G_{ic1} > 0$		McCarty (2007)
ΔG_{r1}	Free energy released per equivalent of acetate oxidized for energy generation	-106.725	kJ/e ⁻ eq	$\Delta G^{\circ}_{\text{formation}} \text{Water-oxygen (half-reaction)} - \Delta G^{\circ}_{\text{formation}} \text{Acetate}_1$ (half-reaction)		Rittmann and McCarty (2012)
A_1	Equivalents of acetate that must be oxidized for the synthesis of biomass	0.565		$-(((\Delta G_{ic1}/\epsilon^{n1}) + (\Delta G_{pc}/\epsilon)) / (\Delta G_{r1} * \epsilon))$		Rittmann and McCarty (2012)
f_{e1}	The portion of electrons from acetate into the electron acceptor for energy generation	0.361		$A_1 / (A_1 + 1)$		Rittmann and McCarty (2012)
f_{s1}	The portion of electrons from acetate into biomass	0.639		$1 / (A_1 + 1)$		Rittmann and McCarty (2012)
R_{r1}	Final equation	See Table 1		$R_{r1} = R_{d1} + f_e * f_{e1} * R_{a1} + f_e * f_{s1} * R_{s1}$ (This equation is only valid for a Two-stage bioprocess system)		Rittmann and McCarty (2012)

Variables	Definition	Values	Units	Calculation	Assumption	Source
d_1	Degree of reduction of acetate	8	e^- eq/mol		Number of electron equivalents transferred from 1 mole of donor	
e_1	Moles of acetate consumed	0.121	moles	coefficient of acetate in R_{d1}		
f_1	Moles of biomass formed	0.031	moles	moles of biomass in $f_{s1} \cdot R_{s1}$		
Y_{d1}	Biomass yield per mol acetate	28.885	g/mol	$(f_1/e_1) \cdot M_{wt} \text{biomass}$		
Y_{e1}	Biomass yield per mol electron	3.611	g/e^- eq	Y_{d1}/d_1		
g_1	energy input into electrolyzer with a conversion efficiency of 80%	148.238	kJ/e^- eq	$((\Delta G^\circ_{\text{formation water-oxygen}} - \Delta G^\circ_{\text{formation hydrogen}}) / 0.8)$		
$Y_{\text{energy}1}$	Biomass yield based on input energy	24.356	mg/kJ	$(Y_{e1}/g_1) \cdot 1000$		

Table S4: Electrochemical reduction of carbon dioxide to acetate and the growth of heterotrophic microbes

Electron donor: Water; Electron acceptor: Carbon dioxide (CO₂)

Variable	Definition	Value	Units	Calculations	Assumptions	Source
$\Delta G^\circ_{\text{formation}}$ Acetyl-CoA (half-reaction)		30.900	kJ/e ⁻ eq			McCarty (2007)
$\Delta G^\circ_{\text{formation}}$ Acetate (half-reaction)		28	kJ/e ⁻ eq	Modified from the half-reaction of acetate synthesis in Table 2.3 (Chapter 2) in Source 1 to remove the bicarbonate species; Refer Table S1 for the half-reaction		Rittmann and McCarty (2012)
$\Delta G^\circ_{\text{formation}}$ Water-oxygen (half-reaction)		-78.720	kJ/e ⁻ eq			Rittmann and McCarty (2012)
E_a°	Standard reduction potential of half-reaction for water as a donor	0.816	V			Lide (2004)
E_b°	Standard reduction potential of half-reaction for acetate as product	-0.290	V			Lide (2004)
n_e	Number of electron equivalents transferred in the electrochemical reaction per mole of a reactant	8	mol e ⁻ eq			
F	Faraday Constant	96,485.330	C/mol			
$\Delta G^\circ A$	Gibbs free energy of acetate synthesis via electrochemical reduction	853.702	kJ	$(-n_e \cdot F \cdot (E_b^\circ - E_a^\circ)) / 1000$		Lide (2004)
$\Delta G^\circ_e A$	Gibbs free energy of acetate synthesis via electrochemical reduction per unit electron equivalent	106.713	kJ/e ⁻ eq	$\Delta G^\circ A / n_e$		
Mwt _{biomass}	Molecular weight of biomass	113	g/mol	C = 12 g/mol; H = 1 g/mol; O = 16 g/mol; N = 14 g/mol $C \cdot 5 + (H \cdot 7) + (O \cdot 2) + (N)$	The biomass composition is assumed to be C ₅ H ₇ O ₂ N	Rittmann and McCarty (2012)
V_{TN}	Voltage required for electrolysis to occur at constant temperature, without exchange of heat to the surroundings	1.132	V	$\Delta H / n_e \cdot F$, where ΔH is 874 kJ/mol		Gandia <i>et al.</i> (2013)
V_{TD}	The potential difference of standard reduction potential of half-reactions	1.106	V	$(E_a^\circ - E_b^\circ)$		Gandia <i>et al.</i> (2013)

Variable	Definition	Values	Units	Calculations	Assumptions	Source
E	Energy efficiency of electrolysis cells	0.97		V_{TD}/V_{TN}		Gandia <i>et al.</i> (2013)
STAGE 2: GROWTH OF HETEROTROPHIC MICROBES ON ACETATE: Electron donor: Acetate; Electron acceptor: Oxygen						
R _a	Reduction half-reaction of oxygen	See Table S1				Rittmann and McCarty (2012)
R _d	Oxidation half-reaction of acetate	See Table S1				Rittmann and McCarty (2012)
R _s	Half-reaction of cell synthesis	See Table S1				Rittmann and McCarty (2012)
R _f	Final equation	See Table 1		$R_f = R_d + f_e \cdot R_a + f_s \cdot R_s$		Rittmann and McCarty (2012)
ΔG_{ic}	Energy required to convert carbon source into acetyl-CoA	2.900	kJ/e ⁻ eq	$\Delta G^{\circ}_{\text{formation Acetyl-CoA}}$ (half-reaction) - $\Delta G^{\circ}_{\text{formation Acetate}}$ (half-reaction)		McCarty (2007)
ΔG_r	Free energy released per equivalent of acetate oxidized for energy generation	-106.720	kJ/e ⁻ eq	$\Delta G^{\circ}_{\text{formation Water-oxygen}}$ (half-reaction) - $\Delta G^{\circ}_{\text{formation Acetate}}$ (half-reaction)		Rittmann and McCarty (2012)
ΔG_{PcI}	ΔG of converting acetyl-CoA carbon to cellular biomass	3.330	kJ/g			McCarty (2007)
X	Number of electron equivalents transferred to ammonia for the synthesis of biomass	20	e ⁻ eq /mol			Rittmann and McCarty (2012)
Y	Amount of biomass obtained per unit electron	5.650	g/e ⁻ eq	Mwtbiomass/X		Rittmann and McCarty (2012)
ΔG_{Pc}	Amount of energy required for the reduction of ammonia into biomass	18.814	kJ/e ⁻ eq	$\Delta G_{PcI} \cdot Y$	We consider ammonia to be the nitrogen source.	Rittmann and McCarty (2012)
ϵ	Energy transfer efficiency	0.6			The energy lost during electron transfer for biomass synthesis	Rittmann and McCarty (2012)
n	Exponent for ϵ	1			Depending on whether ΔG_{ic} is positive or negative, energy is either required or lost during the conversion of the carbon source to acetyl-CoA	McCarty (2007)
A	Equivalents of acetate that must be oxidized for the synthesis of biomass	0.565		$-(((\Delta G_{ic} \cdot \epsilon^n) + (\Delta G_{Pc}/\epsilon))/(\Delta G_r \cdot \epsilon))$		Rittmann and McCarty (2012)

Variable	Definition	Values	Units	Calculations	Assumptions	Source
f_e	The portion of electrons from acetate into the electron acceptor for energy generation	0.361		$A/(A+1)$		Rittmann and McCarty (2012)
f_s	The portion of electrons from acetate into the electron acceptor for biomass synthesis	0.639		$1/(A+1)$		Rittmann and McCarty (2012)
d	Degree of reduction of acetate	8	$e^- \text{ eq} / \text{mol}$		Number of electrons equivalents transferred from 1 mole of this compound	
e	Moles of acetate consumed	0.125	moles	Coefficient of acetate in R_d		
f	Moles of biomass formed	0.032	moles	Coefficient of biomass in $f_s * R_s$		
Y_d	Biomass yield per mol acetate	28.883	g/mol	$(f/e) * \text{Mwtbiomass}$		
Y_e	Biomass yield per mol electron equivalent	3.610	$g/e^- \text{ eq}$	Y_d/d		
E_{in}	Amount of energy added in the form of electricity for generating acetate	110.013	$\text{kJ}/e^- \text{ eq}$	$\Delta G^\circ_e A/E$		
Y_{energy}	Biomass yield based on input energy	32.817	mg/kJ	$(Y_e/E_{in}) * 1000$		

Table S5: Hydrogenation of carbon dioxide to methanol and growth of methylotrophic microbesElectron donor: Hydrogen; Electron acceptor: Carbon dioxide (CO₂)

Variable	Definition	Value	Units	Calculations	Assumptions	Source
$\Delta G^\circ_{\text{formation}}$ Acetyl-CoA (half-reaction)		30.900	kJ/e ⁻ eq			McCarty (2007)
$\Delta G^\circ_{\text{formation}}$ Water-oxygen (half-reaction)		-78.720	kJ/e ⁻ eq			Rittmann and McCarty (2012)
$\Delta G^\circ_{\text{formation}}$ Hydrogen (half-reaction)		39.870	kJ/e ⁻ eq			Rittmann and McCarty (2012)
$\Delta G^\circ_{\text{formation}}$ Methanol (half-reaction)		36.840	kJ/e ⁻ eq			Rittmann and McCarty (2012)
$\Delta G^\circ_{\text{formation}}$ Formaldehyde (half-reaction)		46.530	kJ/e ⁻ eq			McCarty (2007)
ΔG water-splitting	Energy required to be invested per mole of electron to split H ₂ O	118.590	kJ/e ⁻ eq	$\Delta G^\circ_{\text{formation}}$ Hydrogen (half-reaction) - $\Delta G^\circ_{\text{formation}}$ Water-oxygen (half-reaction)		Rittmann and McCarty (2012)
ΔG Electrolysis	Total energy (kJ) that needs to be invested in the electrolyzer at 80 % efficiency	148.238	kJ/e ⁻ eq	ΔG water-splitting/0.8		
ΔG Step 1	ΔG at STP of conversion of 1 mole of CO ₂ → CH ₃ OH with Ga-Ni Catalyst	3.480	kJ/mol			Ahmad and Upadhyayula (2019a)
m1	Number of electrons involved in the reaction 'a'	6	e ⁻ eq/mol			
a	Conversion of 1 mole of CO ₂ to 1 mole of CH ₃ OH	0.580	kJ/e ⁻ eq	ΔG Step 1/m1		
ΔG Step 2	ΔG at STP of conversion of 1 mole of CO ₂ → CO with Ga-Ni Catalyst	28.600	kJ/mol			Ahmad and Upadhyayula (2019a)
m2	Number of electrons involved in the reaction 'b'	2	e ⁻ eq/mol			
b	Conversion of 1 mole of CO ₂ to 1 mole of CO	14.300	kJ/e ⁻ eq	ΔG Step 2/m2		
ΔG Step 3	ΔG at STP of conversion of 1 mole of CO → CH ₃ OH with Ga-Ni Catalyst	-25.100	kJ/mol			Ahmad and Upadhyayula (2019a)
m3	Number of electrons involved in the reaction 'c'	4	e ⁻ eq/mol			

Variables	Definition	Values	Units	Calculation	Assumption	Source
c	Conversion of 1 mole of CO (from step 2) to 1 mole of CH ₃ OH	-6.275	kJ/e ⁻ eq	$\Delta G_{\text{Step 3/m3}}$		
ΔG_{TOT}		0.582	kJ/e ⁻ eq	a+b+c		
E	Efficiency of CO ₂ hydrogenation to methanol at STP	0.100				Ahmad and Upadhyayula (2019b)
$\Delta G_{\text{TOT 2}}$	Total energy (kJ) that needs to be invested for CO ₂ hydrogenation to methanol with Ga-Ni catalyst after accounting for the efficiency	5.817	kJ/e ⁻ eq	$\Delta G_{\text{TOT/E}}$		
STAGE 2: GROWTH OF METHYLOTROPHIC MICROBES ON METHANOL; Electron donor: Methanol; Electron acceptor: Oxygen						
Mwtbiomass	Molecular weight of biomass	113	g/mol	C= 12 g/mol; H = 1 g/mol; O =16 g/mol; N = 14 g/mol $C*5 + (H*7) + (O*2) + (N)$	The biomass composition is assumed to be C ₅ H ₇ O ₂ N	Rittmann and McCarty (2012)
ΔG_{PCi}	ΔG of converting the acetyl-CoA to cellular biomass	3.330	kJ/g			McCarty (2007)
X	Number of electron equivalents transferred to ammonia for the synthesis of biomass	20	e ⁻ eq /mol			Rittmann and McCarty (2012)
Y	Amount of biomass obtained per unit electron equivalent	5.650	g/e ⁻ eq	Mwtbiomass/X		Rittmann and McCarty (2012)
ΔG_{PC}	Amount of energy required for the reduction of ammonia into biomass	18.814	kJ/e ⁻ eq	$\Delta G_{\text{PC}}*Y$	We consider ammonia to be the nitrogen source.	Rittmann and McCarty (2012)
$\Delta G_{\text{met} \rightarrow \text{fa}}$	Energy required to convert methanol into formaldehyde	9.690	kJ/e ⁻ eq	$\Delta G^{\circ}_{\text{formation}}$ Formaldehyde (half-reaction) - $\Delta G^{\circ}_{\text{formation}}$ Methanol (half-reaction)		
$\Delta G_{\text{fa} \rightarrow \text{Ac}}$	Energy required to convert formaldehyde into acetyl-CoA	-15.630	kJ/e ⁻ eq	$\Delta G^{\circ}_{\text{formation}}$ Acetyl-CoA (half-reaction) - $\Delta G^{\circ}_{\text{formation}}$ Formaldehyde (half-reaction)		McCarty (2007)

Variables	Definition	Values	Units	Calculation	Assumption	Source
ϵ	Energy transfer efficiency	0.6			The energy lost during electron transfer for biomass synthesis	Rittmann and McCarty (2012)
m	Exponent for ϵ for $\Delta G_{\text{met} \rightarrow \text{fa}}$	1		If $\Delta G_{\text{met} \rightarrow \text{fa}}$ is positive, then $m = 1$, otherwise $m = -1$		McCarty (2007)
n	Exponent for ϵ for $\Delta G_{\text{fa} \rightarrow \text{Ac}}$	-1		If $(\Delta G_{\text{formation Acetyl-CoA (half-reaction)} - \Delta G_{\text{formation Methanol (half-reaction)})} > 0$, is then $n = m$, otherwise $n = -1$		McCarty (2007)
ΔG_{r}	Free energy released per equivalent of donor oxidized for energy generation	-115.560	kJ/e ⁻ eq	$\Delta G_{\text{formation Water-oxygen (half-reaction)} - \Delta G_{\text{formation Methanol (half-reaction)}}$		Rittmann and McCarty (2012)
A	Equivalents of donor that must be oxidized for the synthesis of biomass	0.550		$-\left(\frac{\Delta G_{\text{met} \rightarrow \text{fa}}}{\Delta G_{\text{r}} \cdot \epsilon}\right) + \left(\frac{\Delta G_{\text{fa} \rightarrow \text{Ac}}}{\epsilon}\right) + (\Delta G_{\text{PC}} / \epsilon)$		McCarty (2007)
f_{e}	The portion of electrons from methanol into the electron acceptor for energy generation	0.355		$A/(A+1)$		Rittmann and McCarty (2012)
f_{s}	The portion of electrons from methanol into biomass synthesis	0.645		$1/(A+1)$		Rittmann and McCarty (2012)
R_{d}	Oxidation-half reaction of methanol	See Table S1				Rittmann and McCarty (2012)
R_{a}	Reduction-half reaction of oxygen	See Table S1				Rittmann and McCarty (2012)
R_{s}	Half-reaction of cell synthesis	See Table S1				Rittmann and McCarty (2012)
R_{f}	Final equation	See Table 1		$R_{\text{f}} = R_{\text{d}} + f_{\text{e}} \cdot R_{\text{a}} + f_{\text{s}} \cdot R_{\text{s}}$		Rittmann and McCarty (2012)
n_{e}	Degree of reduction of methanol	6	e ⁻ eq /mol		number of electron equivalents released when 1 mole of this compound is reduced	
e	Moles of methanol consumed	0.167	moles	R_{d}		
i	Moles of biomass formed	0.0323	moles	Coefficient of biomass in $f_{\text{s}} \cdot R_{\text{s}}$		
Y_{d}	Biomass yield per mol methanol	21.875	g/mol	$(i/e) \cdot \text{Mwt}_{\text{biomass}}$		
Y_{e}	Biomass yield per mol electron	3.646	g/e ⁻ eq	$Y_{\text{d}}/n_{\text{e}}$		
Y_{energy}	Biomass yield based on input energy	23.666	mg/kJ	$(Y_{\text{e}} / (\Delta G_{\text{TOT 2}} + \Delta G_{\text{Electrolysis}})) \cdot 1000$	Here, we assume that we can recover the energy that is being generated during the formation of methanol	

Table S6: Electrochemical reduction of carbon dioxide to methanol and growth of methylotrophic microbes

Electron donor: Water; Electron acceptor: Carbon dioxide (CO ₂)						
Variable	Definition	Value	Units	Calculations	Assumptions	Source
$\Delta G^\circ_{\text{formation}}$ Acetyl-CoA (half-reaction)		30.900	kJ/e ⁻ eq			McCarthy (2007)
$\Delta G^\circ_{\text{formation}}$ Water-oxygen (half-reaction)		-78.720	kJ/e ⁻ eq			Rittmann and McCarthy (2012)
$\Delta G^\circ_{\text{formation}}$ Hydrogen (half-reaction)		39.870	kJ/e ⁻ eq			Rittmann and McCarthy (2012)
$\Delta G^\circ_{\text{formation}}$ Methanol (half-reaction)		36.840	kJ/e ⁻ eq			Rittmann and McCarthy (2012)
$\Delta G^\circ_{\text{formation}}$ Formaldehyde (half-reaction)		46.530	kJ/e ⁻ eq			McCarthy (2007)
E_a°	Standard reduction potential of half-reaction for water as a donor	0.816	V			Lide (2004)
E_b°	Standard reduction potential of half-reaction for methanol as the product	-0.380	V			Lide (2004)
n_e	Number of electrons transferred in the electrochemical reaction per mole of methanol	6	mol e ⁻ eq			
F	Faraday Constant	96,485.33	C/mol			
ΔG°_M	Gibbs free energy of methanol synthesis via electrochemical reduction	692.378	kJ	$(-n_e * F * (E_b - E_a^\circ)) / 1000$		Lide (2004)
$\Delta G^\circ_e M$	Gibbs free energy of methanol synthesis via electrochemical reduction per unit electron	115.396	kJ/e ⁻ eq	$\Delta G^\circ_M / n_e$		
V_{TN}	voltage required for electrolysis to occur at constant temperature, without exchange of heat to the surroundings	1.254	V	$\Delta H / n_e * F$, where ΔH is 726 kJ/mol		Gandia <i>et al.</i> (2013)
V_{TD}	the potential difference of standard reduction potential of half-reactions	1.196	V	$(E_a - E_b^\circ)$		Gandia <i>et al.</i> (2013)
E	Energy efficiency of electrolysis cells	0.96		V_{TD} / V_{TN}		Gandia <i>et al.</i> (2013)
STAGE 2: GROWTH OF METHYLOTROPHIC MICROBES ON METHANOL; Electron donor: Methanol; Electron acceptor: Oxygen						
Mwtbiomass	Molecular weight of biomass	113	g/mol	$C^*5 + (H^*7) + (O^*2) + (N)$	The biomass composition is assumed to be C ₅ H ₇ O ₂ N	Rittmann and McCarthy (2012)

Variable	Definition	Value	Unit	Calculation	Assumption	Source
ΔG_{PCl}	ΔG of converting acetyl-CoA carbon to cellular biomass	3.330	kJ/g			McCarty (2007)
X	Number of electron equivalents transferred to ammonia for the synthesis of biomass	20	e ⁻ eq/mol			Rittmann and McCarty (2012)
Y	Amount of biomass obtained per unit electron	5.650	g/e ⁻ eq	Mwtbiomass/X		Rittmann and McCarty (2012)
ΔG_{PC}	Amount of energy required for the reduction of ammonia into biomass	18.814	kJ/e ⁻ eq	$\Delta G_{\text{PCl}} * Y$	We consider ammonia to be the nitrogen source.	Rittmann and McCarty (2012)
$\Delta G_{\text{met} \rightarrow \text{fa}}$	Energy required to convert methanol into formaldehyde	9.690	kJ/e ⁻ eq	$\Delta G^{\circ}_{\text{formation}} \text{ Formaldehyde (half-reaction)} - \Delta G^{\circ}_{\text{formation}} \text{ Methanol (half-reaction)}$		McCarty (2007)
$\Delta G_{\text{fa} \rightarrow \text{Ac}}$	Energy required to convert formaldehyde into acetyl-CoA	-15.630	kJ/e ⁻ eq	$\Delta G^{\circ}_{\text{formation}} \text{ Acetyl-CoA (half-reaction)} - \Delta G^{\circ}_{\text{formation}} \text{ Formaldehyde (half-reaction)}$		McCarty (2007)
ΔG_{r}	Free energy released per equivalent of methanol oxidized for energy generation	-115.560	kJ/e ⁻ eq	$\Delta G^{\circ}_{\text{formation}} \text{ Water-oxygen (half-reaction)} - \Delta G^{\circ}_{\text{formation}} \text{ methanol (half-reaction)}$		Rittmann and McCarty (2012)
ϵ	Energy transfer efficiency	0.6			The energy lost during electron transfer for biomass synthesis	Rittmann and McCarty (2012)
m	Exponent for ϵ for $\Delta G_{\text{met} \rightarrow \text{fa}}$	1		If $\Delta G_{\text{met} \rightarrow \text{fa}}$ is positive, then $m = 1$, otherwise $m = -1$		McCarty (2007)
n	Exponent for ϵ for $\Delta G_{\text{fa} \rightarrow \text{Ac}}$	-1		If $(\Delta G^{\circ}_{\text{formation}} \text{ Acetyl-CoA (half-reaction)} - \Delta G^{\circ}_{\text{formation}} \text{ Methanol (half-reaction)}) > 0$, is then $n = m$, otherwise $n = -1$		McCarty (2007)
A	Equivalents of methanol that must be oxidized for the synthesis of biomass	0.550		$-((\Delta G_{\text{met} \rightarrow \text{fa}} / \epsilon^m) + (\Delta G_{\text{fa} \rightarrow \text{Ac}} / \epsilon^n) + (\Delta G_{\text{PC}} / \epsilon)) / (\Delta G_{\text{r}} * \epsilon)$		McCarty (2007)
f_e	The portion of electrons from methanol into the electron acceptor for energy generation	0.355		$A / (A+1)$		Rittmann and McCarty (2012)
f_s	The portion of electrons from methanol into biomass synthesis	0.645		$1 / (A+1)$		Rittmann and McCarty (2012)
R_d	Oxidation-half reaction of methanol	See Table S1				Rittmann and McCarty (2012)

Variable	Definition	Values	Units	Calculation	Assumption	Source
R_d	Reduction-half reaction of oxygen	See Table S1				Rittmann and McCarty (2012)
R_s	Half-reaction of cell synthesis	See Table S1				Rittmann and McCarty (2012)
R_f	Final equation	See Table 1		$R_f = R_d + f_e \cdot R_d + f_s \cdot R_s$		Rittmann and McCarty (2012)
d	Degree of reduction of methanol	6	e ⁻ eq /mol	n_e	number of electrons equivalents transferred from 1 mole of this compound	
e	Moles of methanol consumed	0.1667	moles	Coefficient of methanol in R_d		
f	Moles of biomass formed	0.03227	moles	Coefficient of biomass in $f_s \cdot R_s$		
Y_d	Biomass yield per mol methanol	21.874	g/mol	$(f/e) \cdot M_{wt} \text{biomass}$		
Y_e	Biomass yield per mol electron	3.646	g/e ⁻ eq	Y_d/d		
E_{In}	Amount of energy added in the form of electricity for generating methanol	120.139	kJ/e ⁻ eq	$\Delta G_e M^* E$		
Y_{energy}	Biomass yield based on input energy	30.348	mg/kJ	$(Y_e/E_{In}) \cdot 1000$		

Table S7: Hydrogenation of carbon dioxide to methane and the growth of methanotrophic bacteriaElectron donor: Hydrogen; Electron acceptor: Carbon dioxide (CO₂)

Variable	Definition	Value	Units	Calculations	Assumptions	Source
$\Delta G^\circ_{\text{formation}}$ Methane (half-reaction)		23.530	kJ/e ⁻ eq			Rittmann and McCarty (2012)
$\Delta G^\circ_{\text{formation}}$ Water-oxygen (half-reaction)		-78.720	kJ/e ⁻ eq			Rittmann and McCarty (2012)
$\Delta G^\circ_{\text{formation}}$ Hydrogen (half-reaction)		39.870	kJ/e ⁻ eq			Rittmann and McCarty (2012)
$\Delta G^\circ_{\text{formation}}$ Acetyl-CoA (half-reaction)		30.900	kJ/e ⁻ eq			McCarty (2007)
$\Delta G^\circ_{\text{formation}}$ Formaldehyde (half-reaction)		46.530	kJ/e ⁻ eq			McCarty (2007)
$\Delta G^\circ_{\text{formation}}$ NADH		219.200	kJ/mol			McCarty (2007)
ΔG water-splitting	Energy required to be invested per mole of electron to split the corresponding amount of H ₂ O	118.590	kJ/e ⁻ eq	$\Delta G^\circ_{\text{formation}}$ Hydrogen (half-reaction) - $\Delta G^\circ_{\text{formation}}$ Water-oxygen (half-reaction)		Rittmann and McCarty (2012)
ΔG Electrolysis	Total energy (kJ) that needs to be invested in the electrolyzer at 80 % efficiency	148.238	kJ/e ⁻ eq	ΔG water-splitting/0.8		
ΔG CH ₄ hydrogenation	ΔG of conversion of 1 mole of CO ₂ into 1 mole of CH ₄ at STP	-114	kJ/mol			Koschany <i>et al.</i> (2016)
n_e	Number of electrons required for ' ΔG CH ₄ hydrogenation'	8	e ⁻ eq/mol			
ΔG TOT	Energy that needs to be invested into ' ΔG CH ₄ hydrogenation' per electron equivalent	-14.250	kJ/e ⁻ eq	ΔG CH ₄ hydrogenation/ n_e		
E	Efficiency of CO ₂ hydrogenation to methane at STP	0.90				Koschany <i>et al.</i> (2016)
ΔG TOT2	Total energy (kJ) that needs to be invested for CO ₂ hydrogenation to methane with NiAl(O) _x catalyst after accounting for the efficiency	-15.830	kJ/e ⁻ eq	ΔG TOT /E		
STAGE 2: GROWTH OF METHANOTROPHIC BACTERIA: Electron donor: Methane; Electron acceptor: Oxygen						
b	Moles of methane formed per unit e ⁻	0.125	moles	See Table S1		
Mwtbiomass	Molecular weight of biomass	113	g/mol	C = 12 g/mol; H = 1 g/mol; O = 16 g/mol; N = 14 g/mol C*5 + (H*7) + (O*2) + (N)	The biomass composition is assumed to be C ₅ H ₇ O ₂ N	Rittmann and McCarty (2012)
ΔG_{PCI}	ΔG of converting acetyl-CoA carbon to cellular biomass	3.330	kJ/g biomass			McCarty (2007)

Variable	Definition	Value	Units	Calculations	Assumptions	Source
X	Number of electron equivalents transferred to ammonia for the synthesis of biomass	20	e ⁻ eq/mol			Rittmann and McCarty (2012)
Y	Amount of biomass obtained per unit electron	5.650	g/e ⁻ eq	Mwtbiomass/X		Rittmann and McCarty (2012)
ΔG_{PC}	Amount of energy required for the reduction of ammonia into biomass	18.814	kJ/e ⁻ eq	$\Delta G_{PC} * Y$	We consider ammonia to be the nitrogen source.	Rittmann and McCarty (2012)
ϵ	Energy transfer efficiency	0.6				Rittmann and McCarty (2012)
$\Delta G_{\text{methane} \rightarrow \text{fa}}$	Energy required to convert methane into formaldehyde	23.000	kJ/e ⁻ eq	$\Delta G^{\circ}_{\text{formation}} \text{ formaldehyde (half-reaction)} - \Delta G^{\circ}_{\text{formation}} \text{ methane (half-reaction)}$		McCarty (2007)
$\Delta G_{\text{fa} \rightarrow \text{Ac}}$	Energy required to convert formaldehyde into acetyl-CoA	-15.630	kJ/e ⁻ eq	$\Delta G^{\circ}_{\text{formation}} \text{ Acetyl-CoA (half-reaction)} - \Delta G^{\circ}_{\text{formation}} \text{ formaldehyde (half-reaction)}$		McCarty (2007)
m	Exponent for ϵ for $\Delta G_{\text{methane} \rightarrow \text{fa}}$	1		If $\Delta G_{\text{methane} \rightarrow \text{fa}}$ is positive, then m = 1, otherwise m = -1		McCarty (2007)
n	Exponent for ϵ for $\Delta G_{\text{fa} \rightarrow \text{Ac}}$	-1		If $(\Delta G^{\circ}_{\text{formation}} \text{ Acetyl-CoA (half-reaction)} - \Delta G^{\circ}_{\text{formation}} \text{ Methane (half-reaction)}) > 0$, is then n = m, otherwise n = -1	But, if we proceed with further calculation using n = +1, we will over-estimate the energy going into biomass synthesis (with an ϵ of 0.6). Since, the conversion of formaldehyde to acetyl-CoA gives energy to the organism, we should multiply it by the energy transfer efficiency by taking n = -1 (McCarty, 2007)	McCarty (2007)
q	Constant	1		The number of times an oxygenase is used to perform the complete oxidation of a compound		McCarty (2007)
d	Degree of reduction of methane	8	e ⁻ eq/mol	n_c	number of electrons equivalents transferred from 1 mole of this compound	
ΔG_r	Free energy released per equivalent of methane oxidized for energy generation	-74.850	kJ/e ⁻ eq	$\Delta G^{\circ}_{\text{formation}} \text{ Water-oxygen (half-reaction)} - \Delta G^{\circ}_{\text{formation}} \text{ Methane (half-reaction)} - (q/d) * \Delta G^{\circ}_{\text{formation}} \text{ NADH}$		McCarty (2007)
A	equivalents of methane that must be oxidized for the synthesis of biomass	1.342		$-((\Delta G_{\text{methane} \rightarrow \text{fa}} / \epsilon^m) + (\Delta G_{\text{fa} \rightarrow \text{Ac}} / \epsilon^n) + (\Delta G_{PC} / \epsilon)) / (\Delta G_r * \epsilon)$		McCarty (2007)

Variable	Definition	Value	Units	Calculations	Assumptions	Source
f_e	The portion of electrons from methane into the electron acceptor for energy generation	0.573		$A/(A+1)$		Rittmann and McCarty (2012)
f_s	The portion of electrons from methane into biomass synthesis	0.427		$1/(A+1)$		Rittmann and McCarty (2012)
R_d	Oxidation-half reaction of methane	See Table S1				Rittmann and McCarty (2012)
R_a	Reduction-half reaction of oxygen	See Table S1				Rittmann and McCarty (2012)
R_s	Half-reaction of cell synthesis	See Table S1				Rittmann and McCarty (2012)
R_f	Final equation	See Table 1		$R_f = R_d + f_e \cdot R_a + f_s \cdot R_s$		Rittmann and McCarty (2012)
e	Moles of methane consumed	0.125	moles	Coefficient of biomass in R_d		
f	Moles of biomass formed	0.0213	moles	Coefficient of biomass in $f_s \cdot R_s$		
Y_d	Biomass yield per mol methane	19.296	g/mol	$(f/e) \cdot M_{wt} \text{biomass}$		
Y_e	Biomass yield per mol electron	2.412	g/e ⁻ eq	Y_d/d		
Y_{energy}	Biomass yield based on input energy	18.216	mg/kJ	$(Y_e/(\Delta G \text{ Electrolysis} + \Delta G \text{ TOT2})) \cdot 1000$	Here, we assume that we can recover the energy that is being generated during the formation of methane	

Table S8: Electrochemical reduction of carbon dioxide to methane and growth of methanotrophic bacteria

Variable	Definition	Value	Units	Calculations	Assumptions	Source
$\Delta G^\circ_{\text{formation}}$ Methane (half-reaction)		23.530	kJ/e ⁻ eq			Rittmann and McCarty (2012)
$\Delta G^\circ_{\text{formation}}$ Water-oxygen (half-reaction)		-78.720	kJ/e ⁻ eq			Rittmann and McCarty (2012)
$\Delta G^\circ_{\text{formation}}$ Hydrogen (half-reaction)		39.870	kJ/e ⁻ eq			Rittmann and McCarty (2012)
$\Delta G^\circ_{\text{formation}}$ Acetyl-CoA (half-reaction)		30.900	kJ/e ⁻ eq			McCarty (2007)
$\Delta G^\circ_{\text{formation}}$ Formaldehyde (half-reaction)		46.530	kJ/e ⁻ eq			McCarty (2007)
E_a°	Standard reduction potential of donor half-reaction	0.816	V			Lide (2004)
E_b°	Standard reduction potential of acceptor half-reaction	-0.240	V			Lide (2004)
n_e	Number of electrons transferred in the electrochemical reaction per mole of a reactant	8	mol e ⁻ eq			
F	Faraday Constant	96,485.33	C/mol			
$\Delta G^\circ M1$	Gibbs free energy of methane synthesis via electrochemical reduction	815.108	kJ	$(-n_e \cdot F \cdot (E_b^\circ - E_a^\circ)) / 1000$		Lide (2004)
$\Delta G^\circ_e M1$	Gibbs free energy of methane synthesis via electrochemical reduction per unit electron	101.888	kJ/e ⁻ eq	$\Delta G^\circ M1 / n_e$		
V_{TN}	Voltage required for electrolysis to occur at constant temperature, without exchange of heat to the surroundings	1.154	V	$\Delta H / n_e \cdot F$, where ΔH is 891 kJ/mol		Gandia <i>et al.</i> (2013)
V_{TD}	the potential difference of Standard reduction potential of half-reactions	1.056	V	$E_a^\circ - E_b^\circ$		Gandia <i>et al.</i> (2013)
E	Energy efficiency of electrolysis cells	0.920		V_{TD} / V_{TN}		Gandia <i>et al.</i> (2013)
STAGE 2: GROWTH OF METHANOTROPHIC BACTERIA: Electron donor: Methane; Electron acceptor: Oxygen						
Mwtbiomass	Molecular weight of biomass	113	g/mol	C = 12 g/mol; H = 1 g/mol; O = 16 g/mol; N = 14 g/mol $C \cdot 5 + (H \cdot 7) + (O \cdot 2) + (N)$	The biomass composition is assumed to be $C_5H_7O_2N$	Rittmann and McCarty (2012)
ΔG_{Pci}	ΔG of converting acetyl-CoA carbon to cellular biomass	3.330	kJ/g biomass			McCarty (2007)

Variable	Definition	Values	Units	Calculation	Assumption	Source
X	Number of electron equivalents transferred to ammonia for the synthesis of biomass	20	e ⁻ eq /mol			Rittmann and McCarty (2012)
Y	Amount of biomass obtained per unit electron	5.650	g/e ⁻ eq	Mwtbiomass/X		Rittmann and McCarty (2012)
ΔG_{PC}	Amount of energy required for the reduction of ammonia into biomass	18.814	kJ/e ⁻ eq	$\Delta G_{PC} * Y$	We consider ammonia to be the nitrogen source.	Rittmann and McCarty (2012)
ϵ	Energy transfer efficiency	0.6				Rittmann and McCarty (2012)
$\Delta G_{\text{methane} \rightarrow \text{fa}}$	Energy required to convert methane into formaldehyde	23.000	kJ/e ⁻ eq	$\Delta G^{\circ}_{\text{formation}}$ formaldehyde (half-reaction) - $\Delta G^{\circ}_{\text{formation}}$ methane (half-reaction)		McCarty (2007)
$\Delta G_{\text{fa} \rightarrow \text{Ac}}$	Energy required to convert formaldehyde into acetyl-CoA	-15.630	kJ/e ⁻ eq	$\Delta G^{\circ}_{\text{formation}}$ Acetyl-CoA (half-reaction) - $\Delta G^{\circ}_{\text{formation}}$ formaldehyde (half-reaction)		McCarty (2007)
m	Exponent for ϵ for $\Delta G_{\text{methane} \rightarrow \text{fa}}$	1		If $\Delta G_{\text{methane} \rightarrow \text{fa}}$ is positive, then m = 1, otherwise m = -1		McCarty (2007)
n	Exponent for ϵ for $\Delta G_{\text{fa} \rightarrow \text{Ac}}$	-1		If $(\Delta G^{\circ}_{\text{formation}}$ Acetyl-CoA (half-reaction) - $\Delta G^{\circ}_{\text{formation}}$ Methane (half-reaction)) > 0, is then n = m, otherwise n = -1	But, if we proceed with further calculation using n = +1, we will over-estimate the energy going into biomass synthesis (with an ϵ of 0.6). Since, the conversion of formaldehyde to acetyl-CoA gives energy to the organism, we should multiply it by the energy transfer efficiency by taking n = -1.	McCarty (2007)
q	Constant	1		The number of times an oxygenase is used to perform the complete oxidation of a compound		McCarty (2007)
d	Degree of reduction of methane	8	e ⁻ eq /mol	n_c	number of electrons equivalents transferred from 1 mole of this compound	
ΔG_r	Free energy released per equivalent of methane oxidized for energy generation	-74.850	kJ/e ⁻ eq	$\Delta G^{\circ}_{\text{formation}}$ Water-oxygen (half-reaction) - $\Delta G^{\circ}_{\text{formation}}$ Methane (half-reaction) - ((g/d) * $\Delta G^{\circ}_{\text{formation}}$ NADH)		McCarty (2007)
A	equivalents of methane that must be oxidized for the synthesis of biomass	1.342		$-((\Delta G_{\text{methane} \rightarrow \text{fa}} / \epsilon^m) + (\Delta G_{\text{fa} \rightarrow \text{Ac}} / \epsilon^m) + (\Delta G_{PC} / \epsilon)) / (\Delta G_r * \epsilon)$		McCarty (2007)
f_e	The portion of electrons from methane into the electron acceptor for energy generation	0.573		$A / (A + 1)$		Rittmann and McCarty (2012)
f_s	The portion of electrons from methane into biomass synthesis	0.427		$1 / (A + 1)$		Rittmann and McCarty (2012)

Variable	Definition	Value	Unit	Calculation	Assumptions	Source
R_d	Oxidation-half reaction of methane	See Table S1				Rittmann and McCarty (2012)
R_a	Reduction-half reaction of oxygen	See Table S1				Rittmann and McCarty (2012)
R_s	Half-reaction of cell synthesis	See Table S1				Rittmann and McCarty (2012)
R_f	Final equation	See Table 1		$R_f = R_d + f_e \cdot R_a + f_s \cdot R_s$		Rittmann and McCarty (2012)
e	Moles of methane consumed	0.125	moles	Coefficient of Methane in R_d		
f	Moles of biomass formed	0.0213	moles	Coefficient of biomass in $f_s \cdot R_s$		
Y_d	Biomass yield per mol methane	19.296	g/mol	$(f/e) \cdot M_{wt} \text{biomass}$		
Y_e	Biomass yield per mol electron	2.412	g/e ⁻ eq	Y_d/d		
E_{in}	Amount of energy added in the form of electricity for generating methane	110.748	kJ/e ⁻ eq	$\Delta G^\circ_{eM1/E}$		
Y_{energy}	Biomass yield based on input energy	21.779	mg/kJ	$(Y_e/E_{in}) \cdot 1000$		

References

- Ahmad, K., & Upadhyayula, S. (2019a). Conversion of the greenhouse gas CO₂ to methanol over supported intermetallic Ga–Ni catalysts at atmospheric pressure: thermodynamic modeling and experimental study. *Sustainable Energy & Fuels*, 3(9), 2509-2520.
- Ahmad, K., & Upadhyayula, S. (2019b). Greenhouse gas CO₂ hydrogenation to fuels: A thermodynamic analysis. *Environmental Progress & Sustainable Energy*, 38(1), 98-111.
- Gandia, L. M., Arzamedi, G., & Diéguez, P. M. (2013). *Renewable hydrogen technologies: production, purification, storage, applications and safety*: Newnes.
- Koschany, F., Schlereth, D., & Hinrichsen, O. (2016). On the kinetics of the methanation of carbon dioxide on coprecipitated NiAl (O) x. *Applied Catalysis B: Environmental*, 181, 504-516.
- Lide, D. R. (2004). *CRC handbook of chemistry and physics* (Vol. 85): CRC press.
- McCarty, P. L. (2007). Thermodynamic electron equivalents model for bacterial yield prediction: modifications and comparative evaluations. *Biotechnology and Bioengineering*, 97(2), 377-388. Retrieved from <https://onlinelibrary.wiley.com/doi/abs/10.1002/bit.21250>
- Rittmann, B. E., & McCarty, P. L. (2012). *Environmental biotechnology: principles and applications*: Tata McGraw-Hill Education.

2

Power-to-protein: converting renewable electric power and carbon dioxide into single cell protein with a two-stage bioprocess

Bastian Molitor¹, Akanksha Mishra¹ and Largus T. Angenent¹

1. Center for Applied Geosciences, University of Tuebingen, 72070 Tuebingen, Germany

Molitor, B., Mishra, A., & Angenent, L. T. (2019). Power-to-protein: converting renewable electric power and carbon dioxide into single cell protein with a two-stage bioprocess. *Energy & Environmental Science*, 12(12), 3515-3521.

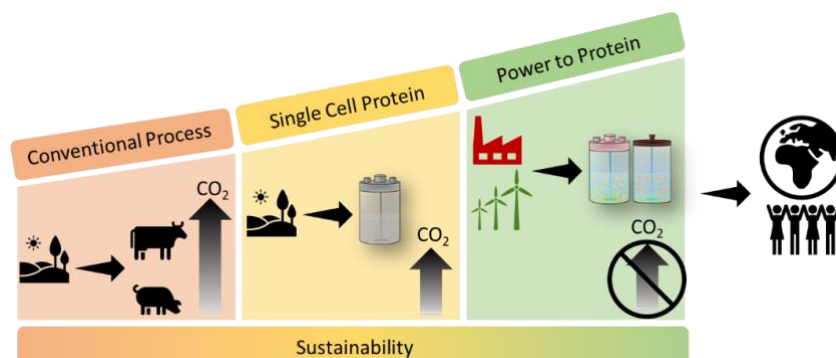
Power-to-protein: converting renewable electric power and carbon dioxide into single cell protein with a two-stage bioprocess

Author Contributions

The study was conceptualized by Largus T. Angenent, Dr. Hanno Richter and Dr. Bastian Molitor. Dr. Bastian Molitor performed the power-to-protein reactor experiments. Largus T. Angenent and Dr. Bastian Molitor wrote the manuscript. Akanksha Mishra performed the protein quantification in the biomass obtained from the power-to-protein reactor. She also drew the graphical abstract and Figure 1 for the manuscript. Largus T. Angenent performed the technical economic analysis, and the rest of the authors verified the calculations.

Abstract

To prevent an environmental collapse while feeding a future human population of 10 billion people, dilute nitrogen in waste streams as a nitrogen source and carbon dioxide as a carbon source should be recovered and recycled into edible protein as part of the circular economy. For this to work, however, ample renewable electric power would be necessary to provide hydrogen from water electrolysis as an electron donor. We developed a two-stage bioprocessing system as part of a power-to-protein approach to fix carbon dioxide in a first stage by anaerobic acetogenic bacteria, and grow yeasts or fungi in a second stage under aerobic conditions with acetate as the intermediate metabolite. We were able to obtain a carbon yield of 25% as yeast biomass with a protein mass-fraction of ~40-50% during a proof-of-concept experiment. We developed a technological solution to circumvent conventional agriculture for protein production, while still being able to provide protein for human consumption.



Broader Context

Single-cell protein production held a lot of promise to feed the rapid growing human population in the 1960s and 1970s. The green revolution, together with the Haber-Bosch process to produce massive quantities of ammonia, provided a matching supply of protein. As a result, single-cell protein was marketed only to vegetarians. However, a resurgence of single-cell protein work is at the forefront to prevent grave environmental impacts. To feed 10 billion people sustainably, ammonia and carbon dioxide must be recycled. We showed that ammonia, carbon dioxide, and hydrogen gas from electrolysis (water splitting) can be converted into yeast cells as a source of edible protein with a two-stage bioprocessing system. Our technological solution completely circumvents the need for conventional agriculture to produce protein. Even though it seems technologically feasible to provide protein for the entire world population this way, many social and ethical questions are raised on how to achieve this promise.

Introduction

To make our societies sustainable, we must refocus from a fossil-based and wasteful economy to a renewable and circular economy by closing nutrient and carbon cycles with renewable electric power. One important source of nutrients and carbon has to be human wastes, and it is not a surprise that resource recovery is starting to become an important pillar in environmental engineering research (El Abbadi & Criddle, 2019). Proteins are among many products that can be produced from wastes and can be used as animal feed or as human food.

A pertinent study recently has found that ammonia as a dilute nutrient in wastewater (nitrogen source) can be utilized with carbon dioxide (carbon source), hydrogen gas (electron donor), and oxygen (electron acceptor) with open cultures of autotrophic *Knallgas* bacteria (>97% *Sulfuricurvum* spp.) in a one-bioreactor gas-fermentation system to produce single-cell protein (SCP) as animal feed (Matassa *et al.*, 2016). The study, thus, focused on an alternative source of ammonia than what is now produced with the Haber-Bosch process from natural gas (Matassa *et al.*, 2015). Thereby, the authors envisioned a shift from an agriculture model with an inefficient and unsustainable application of ammonia as a nitrogen source to a biotechnology-production platform with microbes to recover dilute nutrients that are otherwise being wasted (Matassa *et al.*, 2015).

With both hydrogen gas and oxygen coming from electrolysis of water by renewable electric power, here, this biotechnology-production platform is referred to as power-to-protein (P2P) in

accordance to other technologies such as power-to-gas and power-to-chemicals (power-to-X). A re-imagination of our societies with an excess of renewable electric power and recovery of carbon dioxide is necessary for this to work on a vast scale. Carbon dioxide can be extracted from many sources, including biogas, pyrolysis/gasification exhaust, industrial off gases, and even air. *Knallgas* bacteria fix carbon dioxide into biomass by the Calvin-Benson-Bassham (CBB) cycle (Yu *et al.*, 2013), but oxygen has to be mixed into a bioreactor to produce cellular energy (*i.e.*, ATP) for biomass growth. However, introduction of hydrogen gas with oxygen will increase the complexity of the bioprocess due to safety concerns.

Another efficient pathway for carbon dioxide fixation is the Wood-Ljungdahl pathway (WLP) where autotrophic acetogenic bacteria are utilized under strict anaerobic conditions. These acetogens, such as *Clostridium ljungdahlii*, produce biomass and mainly acetate from: 1) ammonia (nitrogen source); 2) carbon dioxide (carbon source and electron acceptor); and 3) hydrogen gas (electron donor), including the formation of cellular energy (*i.e.*, ATP) without oxygen. However, the ATP production is limited (Molitor *et al.*, 2017), which results in a relatively low biomass (and thus protein) yield.

We circumvented this problem by utilizing a two-stage bioprocessing system consisting of: 1) a bioreactor with a pure culture of *C. ljungdahlii* to produce acetate from carbon dioxide, and hydrogen gas; and 2) another bioreactor with a pure culture of yeast or fungal cells to convert acetate with oxygen and a nitrogen source (*e.g.*, ammonia) into protein. Both, the hydrogen gas and oxygen from electrolysis will, therefore, be used in this P2P system. The ammonia can be sourced from dilute wastewater, but also from hydrolyzed urine (Udert & Wächter, 2012), to facilitate the envisioned circular economy. The two-stage process with yeast or fungi is advantageous compared to the study with an open-culture of *Knallgas* bacteria (Matassa *et al.*, 2015), because the produced edible protein can be used for human food instead of only animal feed, paving the way to circumvent conventional agriculture all together for the production of protein.

Here, we provide a proof-of-concept study of this two-stage bioprocessing system with two bioreactors in series to produce SCP with *Saccharomyces cerevisiae*. The use of microbes, such as yeast or fungi, as a SCP source for human food was studied considerably in the 1960s and 1970s mostly with sugars, such as molasses or glucose, as the substrate (Goldberg, 2013), resulting in at least one commercially viable product with glucose as the substrate (M. Wiebe, 2002; M. G. Wiebe, 2004). However, this still requires sugars from conventional agriculture, which we intend to completely circumvent for producing protein with our two-stage

bioprocessing system. Others have already successfully coupled extracted nitrogen from urine (Coppens *et al.*, 2016) or electrolysis (Szekeres *et al.*, 2001) to biological systems, including at the demonstration scale for power-to-methane (Bailera *et al.*, 2017), and therefore we did not yet integrate the full resource recovery system within this proof-of-concept study.

Experimental

Microbial strains and growth conditions

Clostridium ljungdahlii PETC (DSM 13528) in the Stage-A bioreactor (Stage A) was grown in modified 2xP7 medium (supplementary experimental procedures, **Figure 1**). During the initial batch-mode operating period of Stage A, the medium was supplemented with 1 g L⁻¹ yeast extract. *Saccharomyces cerevisiae* S288C (ATCC 204508) was pre-grown in YPD medium (per liter: 10 g yeast extract; 20 g peptone; and 20 g glucose) from frozen stocks. For flask experiments, YN medium, which does not contain yeast extract (supplementary experimental procedures), was supplemented up to a concentration of 150 mM acetate (YNA).

For flask experiments with gas-fermentation effluent, the effluent from a previous gas-fermentation study with *C. ljungdahlii* and 2xP7 medium without yeast extract similar to Richter *et al.*¹³ was collected, and used after filter sterilization. For the initial batch-mode operating period of the Stage-B bioreactor (Stage B), 500 mL of filter-sterilized effluent from Stage A was combined with 500 mL of 2-fold concentrated YN (2xYN) medium. During the continuous-mode operating period, Stage B was fed with filtered effluent from Stage A and an additional 2-fold or 4-fold concentrated YN (2x or 4xYN) medium (supplementary experimental procedures). Thus, yeast extract was not applied to the flask experiments and the continuous-mode bioprocessing experiments.

Bioprocessing set-up

A two-stage bioprocessing system was used to grow *C. ljungdahlii* in Stage A and *S. cerevisiae* in Stage B (**Figure 1**). A 2-L Biostat M chemostat (Braun, Allentown, PA) with a 1-L working volume was used as Stage A at 35°C and a pH of 5.7, while stirring at 300 rpm (supplementary experimental procedures). Stage A was inoculated with a glycerol stock that previously had been prepared from a *C. ljungdahlii*-rich broth, which was collected during a gas-fermentation study similar to Richter *et al.*¹³ The gas-flow rate (H₂:CO₂, 80:20 vol-%; Airgas East, Ithaca, NY) was adjusted from 50 up to 120 mL min⁻¹ to not be limiting when the gas consumption increased. Stage A was equipped with a Na₂S feed and a 100% cell guard (cell-retention filter

system) to retain bacterial cells and to filter the effluent (supplementary experimental procedures). In continuous-operating mode, a liquid-flow rate of 40 mL h⁻¹ was applied (0.04 h⁻¹ dilution rate).

A 1.5-L Celligen cell-culture unit (New Brunswick, Edison, NJ) with a working volume of 1 L was used as Stage B at 30°C and a pH of 5.4, while stirring at 200 rpm (supplementary experimental procedures). Stage B was inoculated to an OD₆₀₀ of 0.05 with a pre-culture of *S. cerevisiae* grown in YNA with a 100-mM acetate concentration. In continuous-operating mode when a flow-rate of 40 mL h⁻¹ was used, 20-mL h⁻¹ from Stage A was combined with 20-mL h⁻¹ from a 2xYN-bypass feed. When a flow-rate of 60 or 80 mL h⁻¹ was used, 40-mL h⁻¹ from Stage A was combined with 20- or 40-mL h⁻¹ from a 4xYN bypass feed, respectively. Thus, the dilution rate for Stage B varied between 0.04 and 0.08 h⁻¹. Oxygen was sparged at an 88.5 ± 19.6 mL min⁻¹ (n=60) air-flow rate to not be limiting, resulting in 69.5% ± 13.4% (n=58) of the oxygen remaining in the off gas.

Analytical procedures

Samples were collected from Stage A and Stage B on a daily basis to calculate the growth (OD₆₀₀), substrate consumption, and product formation (HPLC, GC; supplementary experimental procedures). Samples from both stages were also checked daily for potential contaminations with a phase contrast microscope (Nikon Labophot, Nikon, NY, USA). For protein determinations for Stage B, 2-mL samples were taken. The samples were collected by centrifugation at 13,000 rpm, washed with 1 mL of ddH₂O, dissolved in 1 mL of 1M NaOH, and stored at -20°C. Protein concentrations in the broth of Stage B were determined with the Lowry method (supplementary experimental procedures) (Lowry *et al.*, 1951). In addition, protein content of dried yeast biomass was determined with the Dumas method by an external laboratory (Dairy One Co-op, Inc., Ithaca, NY, USA). For this, the entire broth (effluent of Stage B) throughout the sampling period of 1 day (1 L at 40 mL h⁻¹ and 1.5 L at 60 mL h⁻¹) was collected, centrifuged, and dried. Finally, the dried biomass was grinded and sent for analysis of crude protein, lipid, and ash content.

Results and Discussion

C. ljungdahliae in Stage A achieved an industrially relevant acetate production rate from carbon dioxide and hydrogen without yeast extract

For this proof-of-concept study, we performed a bioprocessing experiment with Stages A and B in series (**Figure 1**). During a single operating period of 104 days for Stage A, carbon dioxide and hydrogen gas were continuously sparged into a pure culture of *C. ljungdahliae*. After a start-up period of 15 days that included two inoculation events during batch conditions, we operated Stage A in continuous mode (continuous feeding of medium at a dilution rate of 0.04 h^{-1} based on Richter *et al.* (2013)). This continuous mode was maintained even during a re-inoculation event on Day 82, which was triggered due to a faulty pH probe (**Figure S1**). We monitored Stage A daily except for a holiday period between Days 60–80 when only basic maintenance and some liquid sampling was performed (**Figure 2 and Figure S1**).

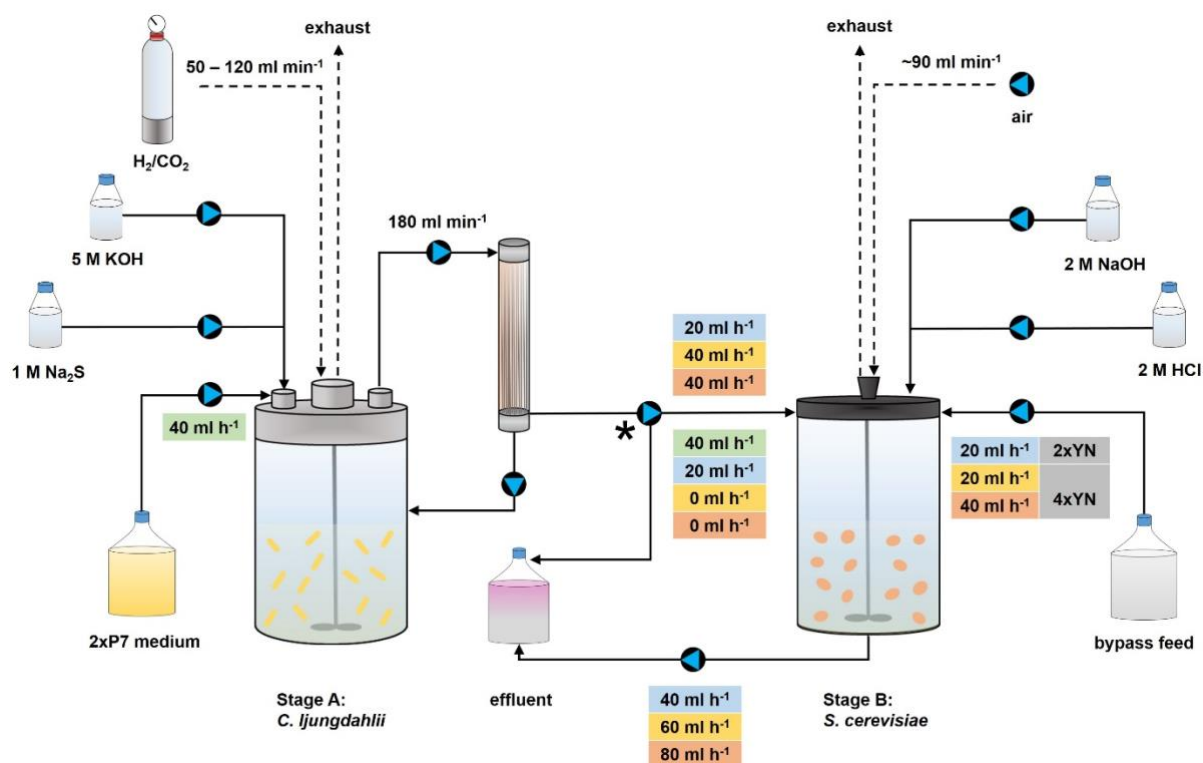


Figure 1: Schematic depiction of the bioprocessing set-up. A two-stage bioprocessing system with Stage A (*C. ljungdahliae*) and Stage B (*S. cerevisiae*) in series was used for our study. Stage A was continuously sparged with hydrogen and carbon dioxide (80:20 vol-%) at a flow rate of $50\text{--}120 \text{ mL h}^{-1}$. The pH was controlled with 5 M KOH. In continuous-operating mode, 2xP7 medium at a flow rate of 40 mL h^{-1} , and 1 M Na_2S at a flow rate of 0.84 mL h^{-1} was fed to Stage A. Stage A was equipped with cell recycling (180 mL min^{-1}) with a 100% cell guard to retain bacterial cells and to filter the effluent. The sterile effluent from Stage A, from the cell guard, was directed to the effluent tank, when only Stage A was active (green, 40 mL h^{-1} , Days 1–19; Days 62–84). The asterisk indicates that the flow was redirected from Stage A either to the effluent tank and/or to Stage B according to the color-code. Stage B was continuously sparged with air at a flow-rate of $\sim 90 \text{ mL min}^{-1}$. The pH was controlled with 2 M KOH

and 2 M HCl. In continuous operating mode, sterile effluent from Stage A plus 2xYN or 4xYN medium from a bypass feed, was fed to Stage B with flow rates according to the color-code (blue, 40 mL h⁻¹; yellow, 60 mL h⁻¹; red, 80 mL h⁻¹).

After Day 20 of the operating period when the volumetric acetate production rate for Stage A had leveled off to ~ 0.5 mol-C L⁻¹ d⁻¹ (0.61 g L⁻¹ h⁻¹) (**Figure 2B**), Stage B was integrated into the effluent line. Stage B was sterilized and inoculated twice with *S. cerevisiae* before Periods I/II and III (**Figure 2**). Throughout Periods I, II, and III, the performance of Stage A was stable (**Figure 2 and Table 1**). The total biomass amount for Stage A, which was based on cellular dry weight (CDW in **Figure 2A**), increased slowly until Day 39 after which a maximum volumetric acetate production rate of 0.78 mol-C L⁻¹ d⁻¹ (1.0 g L⁻¹ h⁻¹) was achieved (**Figure 2B**). The volumetric ethanol production rates remained low at ~ 0.01 mol-C L⁻¹ d⁻¹ (**Figure 2B**), which represented a carbon loss of $\sim 1.5\%$.

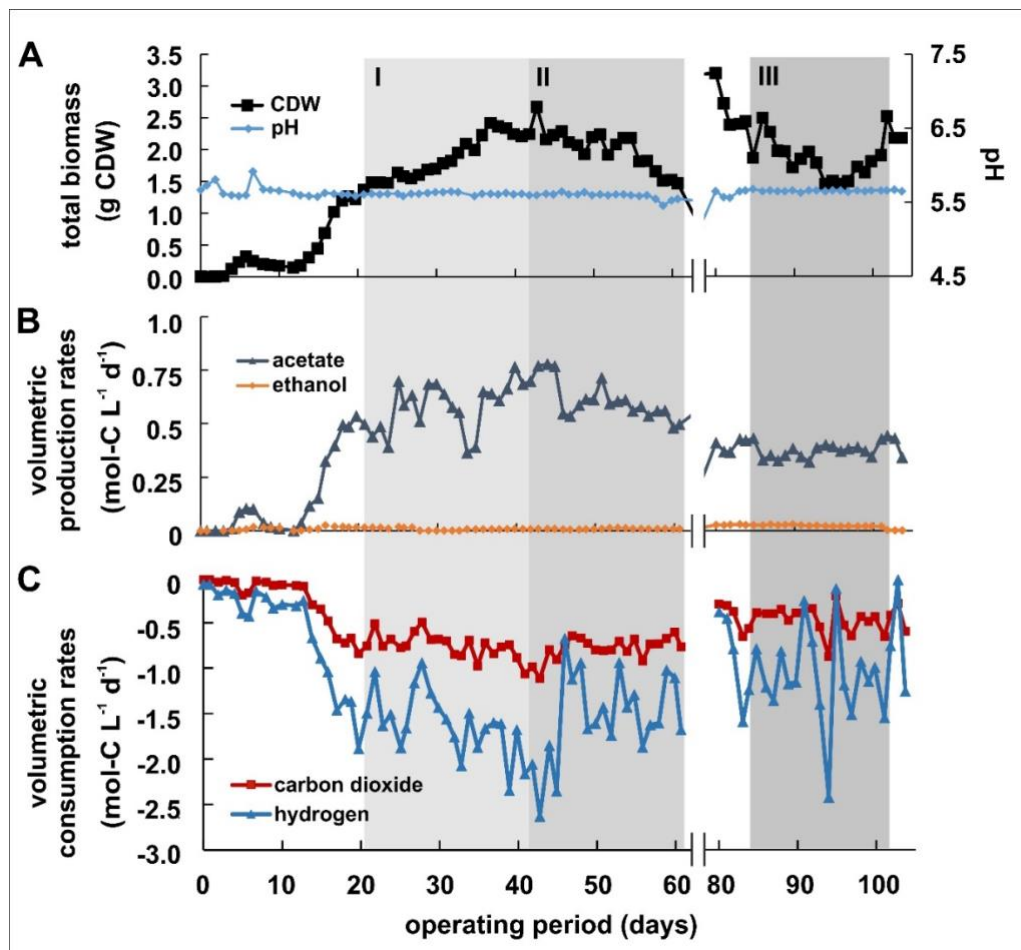


Figure 2: Performance of Stage A with *C. ljungdahlii* during the continuous operating period of 104 days. **A**, total biomass amount as grams cellular dry weight (CDW) and pH. **B**, production rates for acetate and ethanol in mol-C L⁻¹ d⁻¹. **C**, consumption rates for carbon dioxide and hydrogen in mol-C L⁻¹ d⁻¹. The period between day 60 and day 80 is left out for a clearer visualization (details in **Figure S1**). The grey areas that are labeled with I, II, and III indicate operating periods with batch or continuous feeding of Stage B (*S. cerevisiae*) with sterile-filtered Stage A effluent.

Our acetate production rate is lower compared to another study with the closely related acetogen *Clostridium autoethanogenum* (DSM 10061) for which also carbon dioxide and hydrogen gas was used as a substrate without the supplementation of yeast extract. Due to a higher dilution rate of 0.2 h^{-1} than 0.04 h^{-1} for our study, Mock *et al.* (2015) achieved a 210% higher volumetric flux through acetate production of $2.5 \text{ mol-C L}^{-1} \text{ d}^{-1}$ ($3.1 \text{ g L}^{-1} \text{ h}^{-1}$). Thus, we can anticipate a considerable increase in the volumetric acetate production by further optimizing the operating conditions, including changing the 80:20 vol-% $\text{H}_2:\text{CO}_2$ ratio to the stoichiometric ratio of 67:33 vol-%.

By adding yeast extract to promote bacterial growth, an additional increase in the volumetric acetate production rate in Stage A can be anticipated based on a study by Kantzow *et al.* (2015) with the acetogen *Acetobacterium woodii* (DSM 1030), although we know the caveats of a direct comparison between studies and bacterial strains. They achieved an additional increase in the volumetric acetate production rate of 100% to $5 \text{ mol-C L}^{-1} \text{ d}^{-1}$ ($6.2 \text{ g L}^{-1} \text{ h}^{-1}$) compared to Mock *et al.* (2015) at a similar dilution rate of 0.2 h^{-1} , while supplying 8 g L^{-1} yeast extract (0.8% w/v).¹⁶ However, with our main objective to produce yeast protein in Stage B, adding external yeast extract would be unwanted, which is further discussed below.

The average carbon dioxide consumption rates for Stage A were relatively stable during Periods I and II at $0.77 \pm 0.13 \text{ mol-C L}^{-1} \text{ d}^{-1}$ (n=42), but were lower with a factor of ~ 1.6 at $0.47 \pm 0.15 \text{ mol-C L}^{-1} \text{ d}^{-1}$ (n=20) during Period III after the operating problem for Stage A had been solved (**Figure 2C** and **Table 1**). These gas consumption rates resulted in average volumetric acetate production rates of $0.61 \pm 0.09 \text{ mol-C L}^{-1} \text{ d}^{-1}$ (n=42) and $0.38 \pm 0.04 \text{ mol-C L}^{-1} \text{ d}^{-1}$ (n=20) for Periods I/II and III, respectively, which represented a factor of ~ 1.6 difference (**Figure 2B**, **Table 1**). With these equal factors, the carbon yield from carbon dioxide to acetate for Stage A was similar during all three periods, with an average value of $81.7\% \pm 22.0\%$ (n=62; **Table 1**). The losses are associated to ethanol production ($\sim 1.5\%$) and accumulation of biomass due to growth (a cell guard maintained all biomass in the bioreactor).

Table 2: Growth data for steady-state periods under different conditions for stage A (*C. ljungdahlii*) and stage B (*S. cerevisiae*). Positive values indicate production, negative values indicate consumption. Data is given as average during the indicated periods \pm standard deviation.

^a Days 20-41; ^b Days 42-61; ^c Days 85-104; ^d Days 50-61; ^e Days 93-104; ^f biomass production rates for

	<i>C. ljungdahlii</i>			<i>S. cerevisiae</i>	
	Period I (n=22) ^a	Period II (n=20) ^b	Period III (n=20) ^c	12-day period, II (n=12) ^d	12-day period, III (n=12) ^e
CO₂ rates (mol-C L ⁻¹ d ⁻¹)	-0.76 \pm 0.13	-0.78 \pm 0.12	-0.47 \pm 0.15	0.34 \pm 0.06	0.20 \pm 0.05
	-0.77 \pm 0.13				
Acetate rates (mol-C L ⁻¹ d ⁻¹)	0.58 \pm 0.11	0.61 \pm 0.09	0.38 \pm 0.03	-0.55 \pm 0.06	-0.32 \pm 0.03
	0.59 \pm 0.04				
Biomass-C rates (mol-C L ⁻¹ d ⁻¹)	--- ^f	---	---	0.16 \pm 0.02	0.09 \pm 0.01
Protein rates (g L ⁻¹ d ⁻¹)	n/a ^g	n/a	n/a	1.56 \pm 0.29	0.86 \pm 0.07
Carbon yield product/substrate (mol-C basis) ^h	77.9 \pm 17.8	78.6 \pm 8.56	88.8 \pm 32.5	29.6 \pm 1.52	27.7 \pm 4.32
	81.7 \pm 22.0			28.7 \pm 3.30	
Carbon loss to CO₂ (mol-C basis)	n/a	n/a	n/a	61.6 \pm 9.78	65.1 \pm 15.4

C. ljungdahlii are not reported, because we used cell recycling with 100% cell retention. The amount of carbon from the substrate CO₂ going to biomass is, therefore, not detectable in a reliable way; ^g n/a, not applicable; ^h for *C. ljungdahlii*, acetate/CO₂; for *S. cerevisiae*, biomass carbon/acetate.

***S. cerevisiae* was able to grow in Stage B without yeast extract**

We performed initial experiments to optimize the growth of *S. cerevisiae* with acetate as the sole carbon source, and to find an appropriate dilution rate for our bioprocessing set-up (supplementary results and discussion S1; **Figure S2 and Figure S3**). From these experiments, we decided to bypass Stage A with additional fresh medium to Stage B in addition to the acetate-rich medium feeding line from Stage A to Stage B. This bypass was performed to prevent nutrient limitations for our Stage-B growth during bioprocessing experiments. Furthermore, because we observed a wash-out of yeast cells at a dilution rate of 0.08 h⁻¹, we decided to use a lower dilution rate of 0.06 h⁻¹ during the last 12 days of both Periods II and III for Stage B (supplementary results and discussion S1; **Figure 3**).

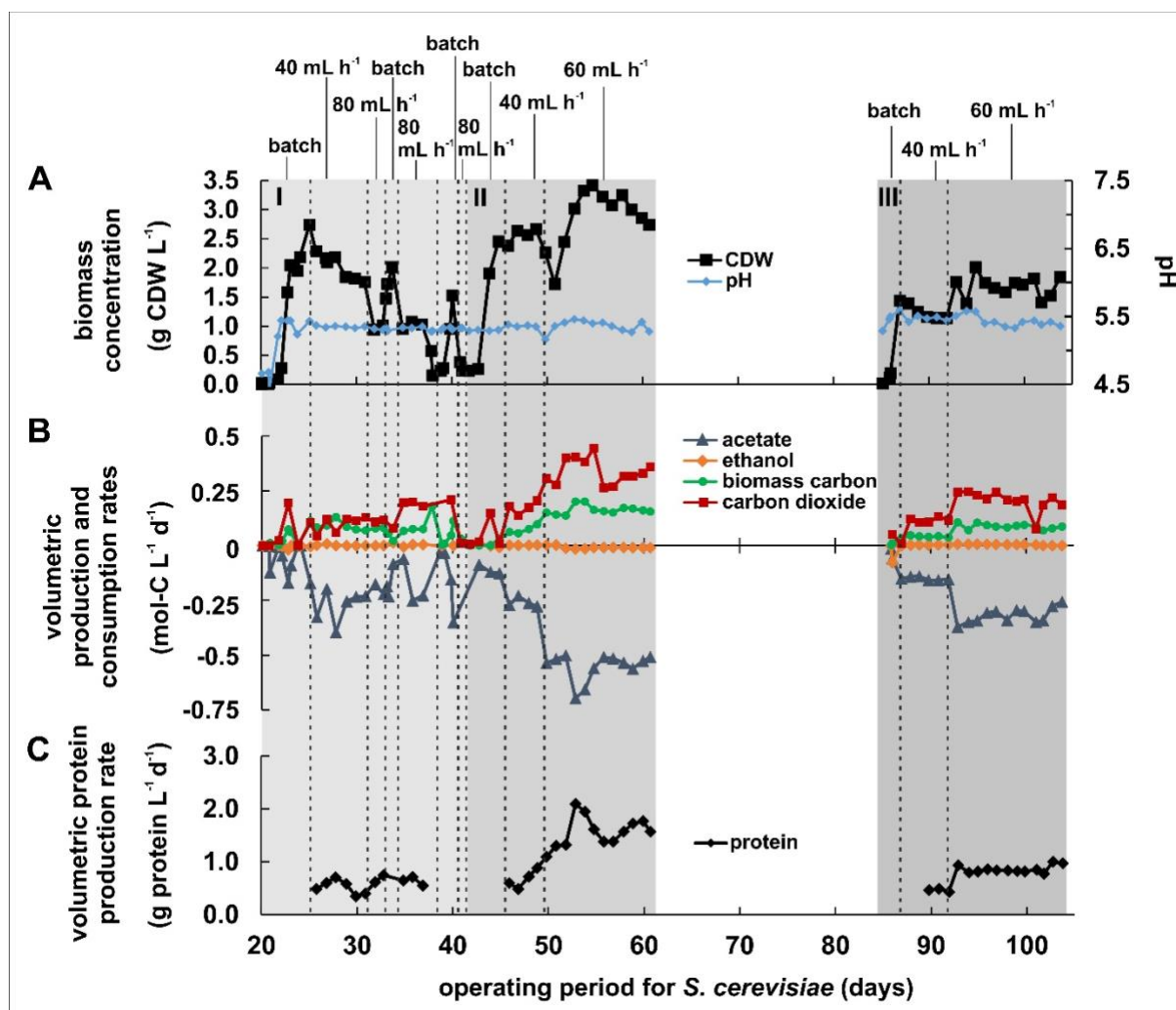


Figure 3: Performance of Stage B with *S. cerevisiae* during the continuous operating period of 62 days (Day 20-61 and Days 85-104). A, biomass concentration as grams cellular dry weight (CDW) per Liter and pH. B, production (positive) and consumption (negative) rates for acetate, ethanol, biomass carbon, and carbon dioxide in mol-C L⁻¹ d⁻¹. C, protein production rate in g protein L⁻¹ d⁻¹. The grey areas indicate operating periods for the preliminary test Period I and the experimental Period II and Period III. At the top of panel A, the flow rates for different operating periods are given.

A recent biofuel study had also developed a two-stage bioprocessing system to maximize lipid accumulation in yeast from acetate as the intermediate. Hu *et al.* (2016) grew the acetogen *Moorella thermoacetica* (ATCC 49707) in a first-stage anaerobic bioreactor at 60°C and an engineered yeast *Y. lipolytica* ACC-DGA in a second-stage aerobic reactor at 28°C. The yeast-protein production rates were not reported (Hu *et al.*, 2016), and were likely depressed due to the overexpression of lipids (Tai & Stephanopoulos, 2013). A considerable amount of yeast extract (10 g L⁻¹, 1% w/v), which includes many unspecified vitamins, was provided.

Yeast extract is relatively expensive to produce in off-site fermenters by feeding sugars, nutrients, and specific vitamins to *S. cerevisiae* before a lysis and drying step (Goldberg, 1985). Our objective here is different from bioenergy production – namely to produce yeast or fungal

protein, also in developing countries. Therefore, we should not procure valuable yeast extract with the goal to produce yeast or fungal cells as a human food, and instead we should only procure specific vitamins that are absolutely necessary. We had hypothesized that yeast can grow sustainably when placed in series after autotrophic bacteria, such as *C. ljungdahlii*, without yeast extract, because *C. ljungdahlii* produces the carbon source and additional amino-acids and vitamins. This assumption was found to be true in the continuous-mode operating periods II and III at a dilution rate of 0.6 h^{-1} , however, additional specific nutrients in the YN medium were necessary. More work is necessary to minimize the use of procured vitamins.

***S. cerevisiae* in Stage B achieved promising carbon yields per consumed carbon dioxide**

The different acetate production rates during the operating period for Stage A (**Figure 2B**), which were discussed above, caused different acetate loading rates to Stage B between Periods II and III. Because the acetate that was fed was also consumed by *S. cerevisiae* in Stage B (**Figure 3 and Figure S3**), we observed a factor of ~ 1.7 times higher average acetate consumption rate of $0.55 \pm 0.06 \text{ mol-C L}^{-1} \text{ d}^{-1}$ ($n=12$) compared to $0.32 \pm 0.03 \text{ mol-C L}^{-1} \text{ d}^{-1}$ ($n=12$) during the last 12 days of Period II and Period III, respectively (**Figure 3B**). The higher acetate consumption rate during Period II compared to Period III resulted also in higher: 1) biomass concentrations (**Figure 3A**); 2) volumetric biomass-carbon production rates (**Figure 3B**); and 3) volumetric protein production rates (**Figure 3C**).

A similar factor of ~ 1.9 as above was observed for the average volumetric biomass-carbon production rates, with $0.16 \pm 0.02 \text{ mol-C L}^{-1} \text{ d}^{-1}$ ($n=12$) compared to $0.09 \pm 0.01 \text{ mol-C L}^{-1} \text{ d}^{-1}$ ($n=12$) during the last 12 days of Period II and Period III (**Figure 3B**). As a result, the biomass yield per consumed acetate on a mol-C basis was similar between Period II and Period III at $29.6\% \pm 1.52\%$ ($n=12$) and $27.7\% \pm 4.32\%$ ($n=12$), respectively (**Table 1**). Thus, we observed a stable performance for yeast biomass production in continuous-operating mode (**Figure 3**).

To evaluate the overall biomass-carbon yield of our two-stage bioprocessing system (mol-C basis), we calculated how much of the carbon in carbon dioxide that was consumed in Stage A was converted eventually into biomass-carbon for Stage B. With the above mentioned average acetate-carbon yield of $81.7\% \pm 22.0\%$ ($n=62$) for Stage A and an average biomass-carbon yield of $28.7 \pm 3.30\%$ for yeast in Stage B, we calculated an overall biomass-carbon yield of $\sim 25\%$ (**Table 1**). A large average carbon loss of $63.3 \pm 12.8\%$ ($n=24$) was due to the production of carbon dioxide by the yeast from acetate in Stage B, because of high activation energy needs for this substrate (Verduyn *et al.*, 1991). Specifically, the carbon losses were $61.6\% \pm 9.78\%$

(n=12) and $65.1\% \pm 15.4\%$ (n=12) for Period II and Period III, respectively (**Table 1**). Since clean and concentrated carbon dioxide streams are already a commodity (Angenent *et al.*, 2018), this released carbon dioxide from Stage B would need to be recycled back to Stage A.

We determined the protein mass-fraction of the yeast biomass with the Lowry method under the various operating conditions and found it to be between 40-50% (g g^{-1}). The crude protein mass-fraction was higher and between 50-60% (g g^{-1}) as determined by an external laboratory with the Dumas method (supplementary results and discussion S2; **Table S1**). We used the lower (more conservative number) protein mass-fraction from the Lowry method to calculate the volumetric protein production rates for *S. cerevisiae*, with $1.56 \pm 0.29 \text{ g L}^{-1} \text{ d}^{-1}$ ($0.07 \text{ g L}^{-1} \text{ h}^{-1}$, n=12) and $0.86 \pm 0.07 \text{ g L}^{-1} \text{ d}^{-1}$ ($0.04 \text{ g L}^{-1} \text{ h}^{-1}$, n=12) during the last 12 days of Period II and Period III, respectively (**Figure 3C and Table 1**).

Technical, economical, and societal outlook

Considerable technical optimizations are necessary to reach industrially relevant protein production rates of approximately $1 \text{ g L}^{-1} \text{ h}^{-1}$, which is a 14 times increase from our study and a 3 times increase from the above-mentioned study with *Knallgas* bacteria (Matassa *et al.*, 2016). Very specific bioreactor configurations and optimized conditions for SCP production processes with yeast have already achieved these industrially relevant protein production rates from $0.7 \text{ g L}^{-1} \text{ h}^{-1}$ to $2.3 \text{ g L}^{-1} \text{ h}^{-1}$ at a commercial scale (Goldberg, 2013; Solomons & Litchfield, 1983). SCP production with yeast were performed in large-scale operations with a total reactor volume of up to $5,400 \text{ m}^3$ ($3 \times 1,800 \text{ m}^3$) and substrates such as waste streams from oil refining (*e.g.*, *n*-paraffin) or carbohydrate-rich substrates (*e.g.*, molasses) (Goldberg, 2013; Solomons & Litchfield, 1983). While technologically feasible, these SCP operations did not become commercial success stories. Marlow Foods Ltd in the UK is the one exception after isolating and optimizing a glucose-fed filamentous fungus strain (*Fusarium venenatum* A3/5). Marlow Foods showed that by using a special bioreactor design and by maintaining high concentrations of substrate and elements in the continuous bioreactor (M. Wiebe, 2002), an industrially relevant protein production rate was achieved. In 2014 (before the plant was enlarged (D. Moore *et al.*, 2019a)), this fungal strain was grown in a 310-m^3 ($2 \times 155 \text{ m}^3$) bioreactor volume at a dilution rate of 0.19 h^{-1} , achieving a protein production rate of $1.25 \text{ g L}^{-1} \text{ h}^{-1}$ (D. Moore *et al.*, 2019a). The produced myco-protein from Marlow Foods with a 44% protein mass-fraction (g g^{-1}) is commercially available for human consumption as vegetarian meat-replacement products under the name Quorn™ (M. Wiebe, 2002; M. G. Wiebe, 2004).

We estimated, based on the protein production rate of $1.25 \text{ g L}^{-1} \text{ h}^{-1}$, a bioreactor volume of 310 m^3 , and a plant run-time efficiency of 0.9, that Marlow Foods would produce 3,055 tons of dry weight protein per year in their Quorn™ process with 2014 information (**Table S2**). When we include anticipated protein losses due to post-treatment to remove unwanted RNA from yeast or fungal cells (~30% losses (M. Wiebe, 2002)), they would already have been feeding 105,000 people with an average weight of 70 kg to sustain their recommended dietary protein allowance, which is 56 g d^{-1} (Lupton *et al.*, 2002). With a supermarket price of approximately \$0.15 per g dry weight protein that we paid in Germany in 2019 for Quorn™, such a person would pay \$8.40 per day for their protein. The total revenue for Marlow Foods was reported for 2014 as \$245 million (**Table S2**). Based on published information and estimated parameters, we calculated each of the costs factors as percentages of the total revenue for 2014. Surprisingly to us, the glucose cost as part of the total revenue was relatively low at 3.4% with the cost of capital for the fermenters representing 6.5%. Other main cost categories and their percentages when corrected to the total revenue are: wastewater from fermenters (0.1%); water to fermenters (0.2%); ammonia (0.2%); electric power to fermenters (3.8%); profit to Marlow Foods (13%); all labor (22%); and the rest for the cost of capital and power needs of the packaging part of the factory; advertisement; research; and overhead (51%) (**Table S2**).

From this relatively simple economic model around the existing Quorn™ process, it becomes apparent that the fermentation costs represent a relatively small percentage of the total revenue (14% in **Table S2**). Next, we inserted the additional cost and credit of power-to-protein into the model for the Quorn process, including a similar size additional fermenter for acetate production. By replacing glucose (-3.4%) for carbon dioxide (+1.0%) and hydrogen gas (electric power [+2.3%]) as substrate, while adding the cost of capital for the electrolyzer (+0.3%); additional labor (+1.1%); and doubling the cost of capital for fermentation (+6.5%) and, while keeping all else the same, we increased the cost by a total 7.6% when corrected to the total revenue for 2014 (**Table S2**). This seems doable, especially because during a 10 times scale-up, as envisioned below, an increase in efficiency compared to the size of the 2014 Quorn™ process is anticipated. This also indicates that our proof-of-concept study already predicts a meaningful societal impact when a gaseous fermenter of equal size for acetate production (Stage A) would be placed in series with a yeast fermenter for protein production (Stage B). Our model is relatively simple, which is limited by the accuracy of the data input (**Table S2**), and therefore is only meant as a tool to compare with a currently economical SCP production system. We used a conservative procurement price for CO₂ even though in the future

companies could get paid to take their CO₂ as part of a carbon trade. Under these new trade conditions, the power-to-protein process will become more attractive.

If we envision a ten times scale up compared to the Quorn™ process, we achieve fermentation volumes that are comparable to the size of one conventional yeast-fermentation tank at a relatively small-sized corn-to-ethanol plant in the US. Then, we would be able to produce enough protein for 1.05 million people from a 3,100-m³ yeast fermenter placed in series after a similar volume gas-fermentation system. To feed 10 billion people in a future world, we would need approximately 10,000 of such two-bioprocessing systems (**Table S2**) when we assume that we can improve the production rates compared to this proof-of-concept study. This number of fermenters seems technically doable, which also explains the excitement for SCP research during the previous century (Goldberg, 2013). Of course, societal acceptance of protein produced *via* biotechnology is as important compared to the technological ability to shift toward sustainable food production.

One can often not predict environmental problems or societal consequences with new technologies on a vast scale, but the P2P system that is based on renewable electric power as proposed in our study, seem poised to circumvent many grave environmental problems. When implemented correctly, P2P should prevent: **1)** nutrient runoffs into rivers and oceans; **2)** greenhouse gas emissions, such as with methane, from animal husbandries; **3)** land use that produces a net positive greenhouse gas output; **4)** fossil-fuel requirements to produce ammonia *via* the Haber-Bosch method; and **5)** CO₂ uptake and recovery to further lower the carbon footprint. In addition to the environmental considerations, we have a moral obligation to empower all societies in producing protein this way, and to prevent one or more industrial or governmental entities of monopolizing human-food production. Another concern is livelihood of a large amount of small farmers with animals for human protein production.

We realize that intricate life-cycle and economic analyses are necessary to predict whether this two-stage bioprocessing system would be sustainable and economically viable on such a vast scale. Important to ascertain in future research will be the costs (or benefits) for the large quantities of: **1)** clean and concentrated carbon dioxide; **2)** renewable electric power to produce hydrogen gas; **3)** necessary nutrients and vitamins that cannot be recovered from wastewater; and **4)** urine collection and treatment to provide a clean nitrogen source, among many other important details about capital expenditures. A plethora of interdisciplinary studies are necessary on a technical and societal level before industrial-scale implementation can commence. Besides the above mentioned studies about: **1)** life-cycle and economic analyses;

2) improvements in volumetric protein production rates; 3) minimum requirements for nutrient and vitamins; 4) and societal acceptance, studies are necessary about the nutritional value and human health impacts of the produced yeast or fungi and how to improve it. Most importantly, studies are necessary to develop mechanisms on how all human societies can benefit and not only a few of them. Regardless, a possible rapid translation to an industrial scale may be foreseeable to provide human nutrition in locations where there is an acute need after, for example, environmental collapse.

Conflicts of Interest

There are no conflicts to declare.

Acknowledgements

L.T.A. acknowledges support from the Alexander von Humboldt Foundation in the framework of the Alexander von Humboldt Professorship endowed by the Federal Ministry of Education and Research in Germany. B.M. was funded through a postdoctoral research fellowship from the German Research Foundation (DFG, MO2933/1-1).

We acknowledge Dr. Hanno Richter, Erik Rasmussen, and Chase Brett for performing preliminary experiments in an early phase of the project. We are thankful to Dr. Juan Guzman for helping with maintaining and sampling the bioreactor (formerly all at Cornell University). Finally, we are thankful to Dr. Joseph Usack (University of Tübingen) and Dr. Marilyn Wiebe (VTT Technical Research Centre of Finland) for assistance with the economic model.

References

- Angenent, L. T., Usack, J. G., Xu, J., Hafenbradl, D., Posmanik, R., & Tester, J. W. (2018). Integrating electrochemical, biological, physical, and thermochemical process units to expand the applicability of anaerobic digestion. *Bioresource Technology*, *247*, 1085-1094.
- Bailera, M., Kezibri, N., Romeo, L. M., Espatolero, S., Lisbona, P., & Bouallou, C. (2017). Future applications of hydrogen production and CO₂ utilization for energy storage: Hybrid Power to Gas-Oxycombustion power plants. *International journal of hydrogen energy*, *42*(19), 13625-13632.
- Coppens, J., Lindeboom, R., Muys, M., Coessens, W., Alloul, A., Meerbergen, K., . . . Vlaeminck, S. E. (2016). Nitrification and microalgae cultivation for two-stage biological nutrient valorization from source separated urine. *Bioresource Technology*, *211*, 41-50.
- El Abbadi, S. H., & Criddle, C. S. (2019). Engineering the dark food chain. *Environmental science & technology*, *53*(5), 2273-2287.
- Goldberg, I. (1985). Fermentation Processes for Microbial SCP Production. In *Single Cell Protein* (pp. 67-128): Springer.
- Goldberg, I. (2013). *Single cell protein* (Vol. 1): Springer Science & Business Media.
- Hu, P., Chakraborty, S., Kumar, A., Woolston, B., Liu, H., Emerson, D., & Stephanopoulos, G. (2016). Integrated bioprocess for conversion of gaseous substrates to liquids. *Proceedings of the National Academy of Sciences*, *113*(14), 3773-3778.
- Kantzow, C., Mayer, A., & Weuster-Botz, D. (2015). Continuous gas fermentation by *Acetobacterium woodii* in a submerged membrane reactor with full cell retention. *Journal of Biotechnology*, *212*, 11-18.
- Lowry, O., Rosebrough, N., & Farr, A. (1951). Randall. RJ (1951) *J. Biol. Chem*, *193*, 265-275.
- Lupton, J. R., Brooks, J., Butte, N., Caballero, B., Flatt, J., & Fried, S. (2002). Dietary reference intakes for energy, carbohydrate, fiber, fat, fatty acids, cholesterol, protein, and amino acids. *National Academy Press: Washington, DC, USA*, *5*, 589-768.
- Matassa, S., Batstone, D. J., Hülsen, T., Schnoor, J., & Verstraete, W. (2015). Can direct conversion of used nitrogen to new feed and protein help feed the world? In: ACS Publications.
- Matassa, S., Verstraete, W., Pikaar, I., & Boon, N. (2016). Autotrophic nitrogen assimilation and carbon capture for microbial protein production by a novel enrichment of hydrogen-oxidizing bacteria. *Water research*, *101*, 137-146.
- Mock, J., Zheng, Y., Mueller, A. P., Ly, S., Tran, L., Segovia, S., Thauer, R. K. (2015). Energy conservation associated with ethanol formation from H₂ and CO₂ in *Clostridium autoethanogenum* involving electron bifurcation. *Journal of bacteriology*, *197*(18), 2965-2980.

- Molitor, B., Marcellin, E., & Angenent, L. T. (2017). Overcoming the energetic limitations of syngas fermentation. *Current opinion in chemical biology*, *41*, 84-92.
- Moore, D., Robson, G. D., & Trinci, A. P. (2019). *21st century guidebook to fungi*: Cambridge University Press.
- Richter, H., Martin, M. E., & Angenent, L. T. (2013). A two-stage continuous fermentation system for conversion of syngas into ethanol. *Energies*, *6*(8), 3987-4000.
- Solomons, G. L., & Litchfield, J. H. (1983). Single Cell Protein. *Critical Reviews in Biotechnology*, *1*(1), 21-58. doi:10.3109/07388558309082578
- Szekeres, S., Kiss, I., Bejerano, T. T., & Soares, M. I. M. (2001). Hydrogen-dependent denitrification in a two-reactor bio-electrochemical system. *Water research*, *35*(3), 715-719.
- Tai, M., & Stephanopoulos, G. (2013). Engineering the push and pull of lipid biosynthesis in oleaginous yeast *Yarrowia lipolytica* for biofuel production. *Metabolic engineering*, *15*, 1-9.
- Udert, K., & Wächter, M. (2012). Complete nutrient recovery from source-separated urine by nitrification and distillation. *Water research*, *46*(2), 453-464.
- Verduyn, C., Stouthamer, A. H., Scheffers, W. A., & van Dijken, J. P. (1991). A theoretical evaluation of growth yields of yeasts. *Antonie Van Leeuwenhoek*, *59*(1), 49-63.
- Wiebe, M. (2002). Myco-protein from *Fusarium venenatum*: a well-established product for human consumption. *Applied microbiology and biotechnology*, *58*(4), 421-427.
- Wiebe, M. G. (2004). Quorn™ Myco-protein-Overview of a successful fungal product. *Mycologist*, *18*(1), 17-20.
- Yu, J., Dow, A., & Pingali, S. (2013). The energy efficiency of carbon dioxide fixation by a hydrogen-oxidizing bacterium. *International journal of hydrogen energy*, *38*(21), 8683-8690.

Power-to-protein: converting renewable electric power and carbon dioxide into single cell protein with a two-stage bioprocess

Supplemental Information

Bastian Molitor¹, Akanksha Mishra¹ and Largus T. Angenent¹

1. Center for Applied Geosciences, University of Tuebingen, 72070 Tuebingen, Germany

Molitor, B., Mishra, A., & Angenent, L. T. (2019). Power-to-protein: converting renewable electric power and carbon dioxide into single cell protein with a two-stage bioprocess. *Energy & Environmental Science*, 12(12), 3515-3521.

Supplemental Information

Supplementary Figures

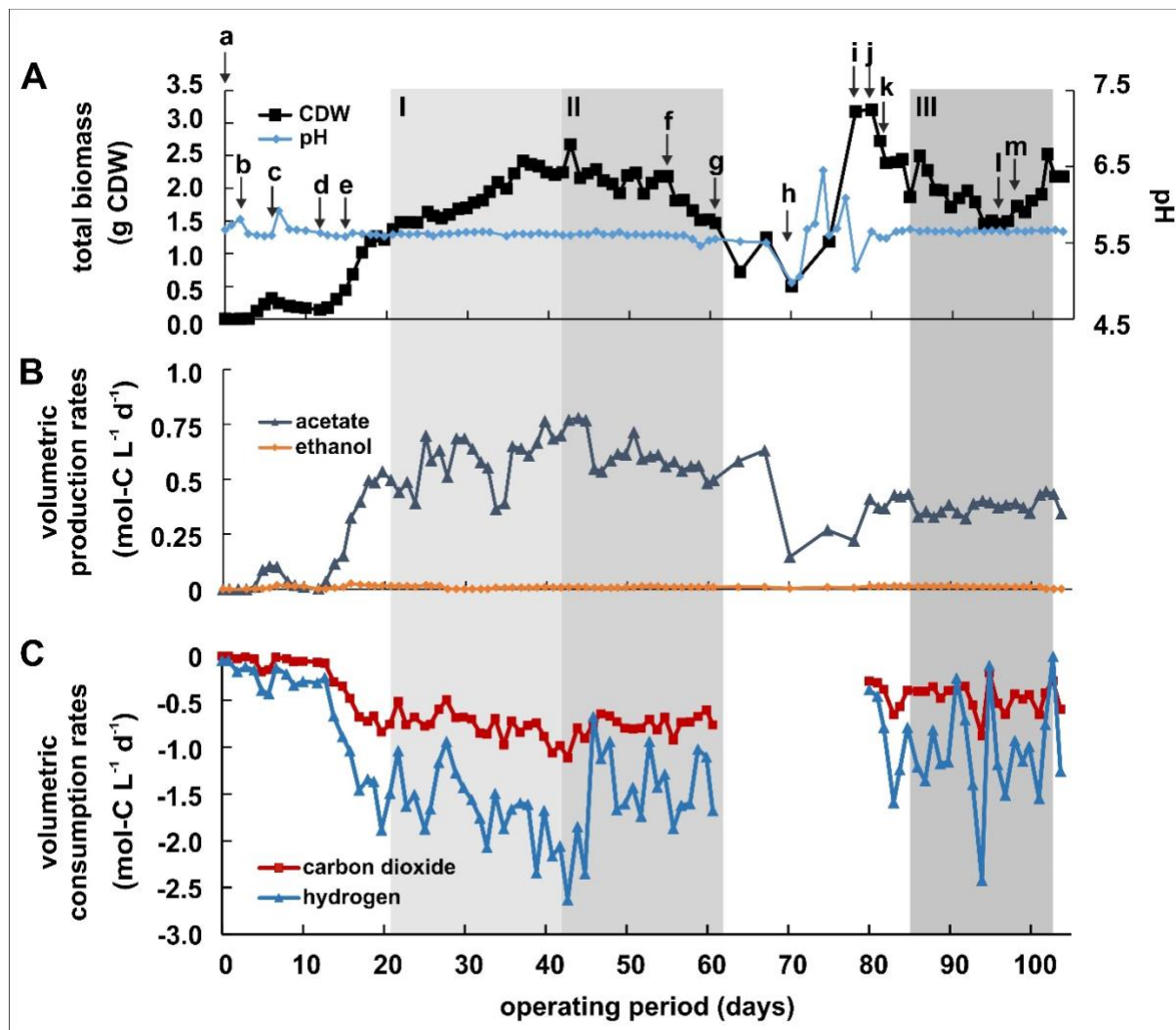


Figure S1. Details on the performance of Stage A with *C. ljungdahlii*. **A**, biomass concentration as grams cellular dry weight (CDW) and pH. **B**, production rates for acetate and ethanol in mol-C L⁻¹ d⁻¹. **C**, consumption rates for carbon dioxide and hydrogen in mol-C L⁻¹ d⁻¹. The grey areas labeled with I, II, and III indicate operating periods with batch or continuous feeding of Stage B (*S. cerevisiae*) with sterile-filtered Stage A effluent. Labels on the top of panel A indicate process changes and process perturbation: **a** (day 0), inoculate, batch, 200 rpm; **b** (day 2), re-inoculate, add 0.5 g L⁻¹ yeast extract; **c** (day 6), start cell recycling, start continuous, start Na₂S feed; **d** (day 12), batch, keep cell recycling, no Na₂S feed, add 0.5 g L⁻¹ yeast extract, 300 rpm; **e** (day 15), start continuous, start Na₂S feed; **f** (day 55), switch feed to medium without Vitamin B₁₂ and folate; **g** (day 61), switch feed to medium with Vitamin B₁₂ and folate; **h** (day 70), bad pH probe; **i** (day 78), black precipitate accumulating; **j** (day 80), exchange pH probe, OD measurements after addition of HCl to dissolve black precipitate; **k** (day 82), re-inoculate; **l** (day 96) OD measurements without addition of HCl (measurements with and without HCl are similar again); **m** (day 98), switch feed to medium without Vitamin B₁₂ and folate.

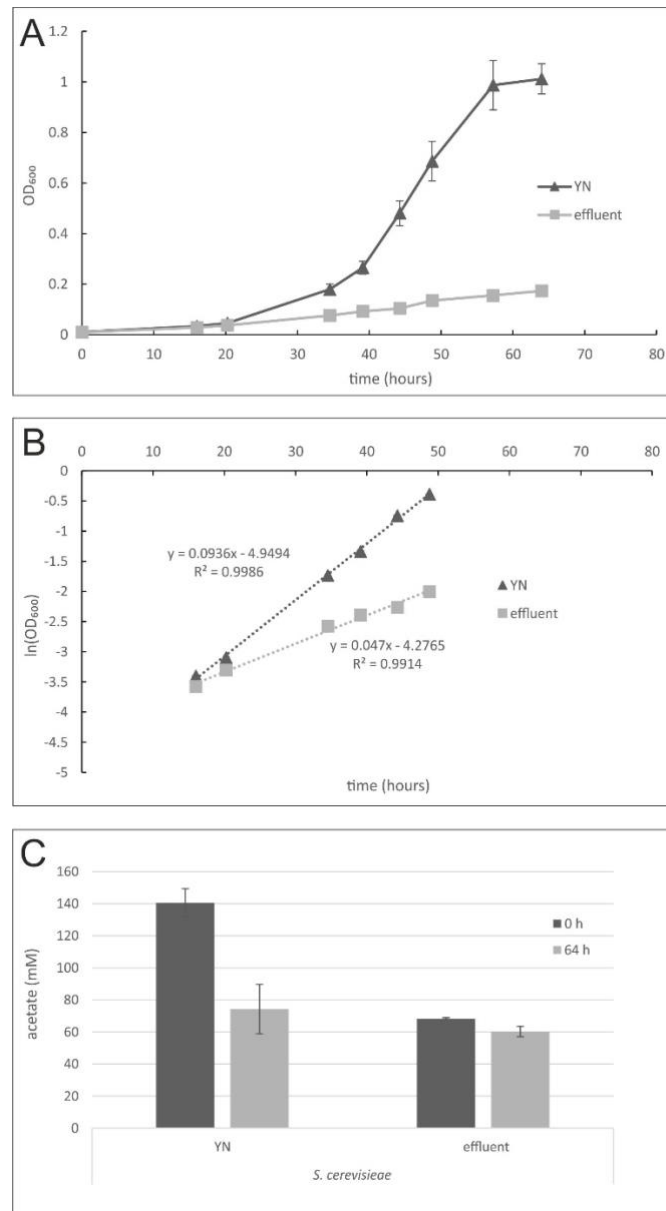


Figure S2: Growth and acetate consumption data for flask experiments with *S. cerevisiae*. A, cell concentrations given as OD₆₀₀ during the experimental period in YNA medium with a 150-mM acetate concentration (YN) and in gas-fermentation effluent with a 70-mM acetate concentration (effluent). B, determination of the growth rate by plotting the natural logarithm of the OD₆₀₀ during the exponential growth phase only. C, acetate concentration in the beginning (0 hours) and at the end (64 hours) of the experiment. Data is shown for biological triplicates. Error bars indicate standard errors.

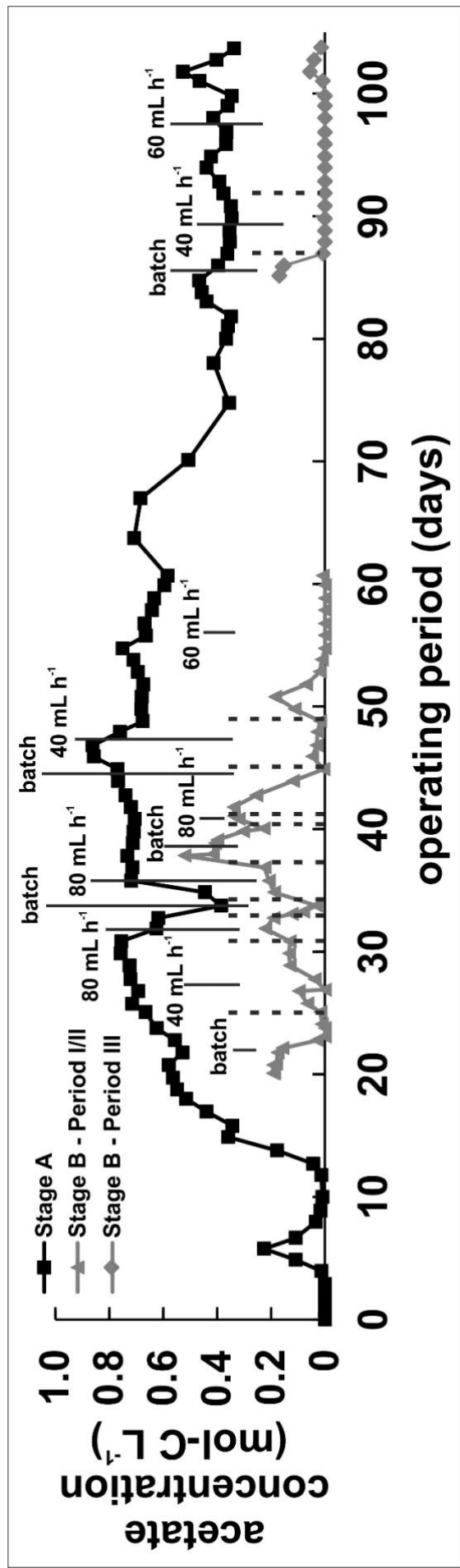


Figure S3: Acetate concentrations for Stage A (*C. ljungdahlii*) and Stage B (*S. cerevisiae*) during the continuous operating period of 104 days. Data is given in mol-C L⁻¹. For Stage B the flow rates of different operating periods are given.

Supplementary Tables

Table S1. Protein measurements for stage B (*S. cerevisiae*). Data for three technical replicates is given.

Operating period (days)	Dilution factor ^a	Concentration ^b ($\mu\text{g mL}^{-1}$)			Biomass concentration (g CDW L ⁻¹)	Specific concentration ($\mu\text{g mg CDW}^{-1}$)			Dairy One ^c ($\mu\text{g mg CDW}^{-1}$)	
		1	2	3		1	2	3		average
Period I										
26	1	1164	1086	1154	2.3	255	238	253	248	9.32
27	1	1186	1220	1211	2.2	274	282	279	278	4.10
28	1	1080	1017	939	2.2	247	232	215	231	16.1
29	1	1070	1055	1055	1.8	290	286	286	288	2.45
30	1	730	652	816	1.8	200	179	224	201	22.5
31	1	930	948	725	1.8	265	270	206	247	35.3
32	1	707	681	525	0.9	374	360	278	337	52.0
33	1	834	798	765	1.0	413	395	378	395	17.2
34	1	995	953	805	2.0	247	237	200	228	24.7
35	1	740	821	797	1.0	387	429	417	411	21.6
36	1	904	865	813	1.1	420	402	378	400	21.2
37	1	745	429	756	1.0	361	208	366	312	90.1
38	1	507	403	556	0.6	438	348	481	422	67.6
39	1	250	276	268	0.2	536	592	575	568	28.6
41	1	445	377	391	0.4	579	491	509	526	46.4
Period II										

42	1	259	212	202	0.2	557	456	434	482	65.7	
43	1	387	317	128	0.3	730	597	241	523	253	
44	2	1516	1462	1658	1.9	398	383	435	405	26.5	
45	2	1476	1853	1610	2.5	301	378	328	336	39.0	
46	2	1840	1995	2022	2.4	386	419	424	410	20.6	
47	2	1920	1698	2183	2.6	364	321	413	366	46.0	
48	2	2156	2197	1873	2.6	420	428	365	404	34.4	421
49	2	1725	2244	2210	2.7	324	421	415	387	54.5	
50	1	1428	1337	1434	2.3	315	295	317	309	11.9	
51	1	1356	1350	1350	1.7	393	392	392	392	1.01	
52	1	1901	2097	2007	2.4	388	429	410	409	20.0	544
53	2	2675	2789	2572	3.0	443	462	426	444	18.0	534
54	2	2699	2765	2771	3.3	406	416	417	413	6.04	547
55	2	2795	2916	2922	3.4	409	426	427	421	10.4	541
56	2	2576	2908	1730	3.2	399	451	268	373	94.2	
57	2	2410	2747	2041	3.1	392	447	332	390	57.5	
58	2	2456	2623	2472	3.2	378	404	381	388	14.1	547
59	2	2353	2612	2825	3.0	392	436	471	433	39.5	544
60	2	2711	2675	2654	2.9	474	468	464	469	5.06	554
61	2	2420	2223	2420	2.7	442	406	442	430	20.8	568
Period III											
90	1	1072	1182	1192	1.2	462	509	514	495	28.5	
91	1	1109	1096	1119	1.1	487	481	491	486	5.14	571
92	1	1091	1052	1166	1.1	479	462	512	484	25.5	
93	1	1259	1351	1341	1.8	359	385	382	375	14.5	

94	1	1194	1447	1387	1.4	430	521	500	484	47.6	
95	1	1408	1284	1346	2.0	350	319	334	334	15.4	534
96	1	1369	1423	1305	1.7	393	408	374	392	17.0	543
97	1	1274	1478	1354	1.7	384	446	408	413	30.9	557
98	1	1313	1380	1390	1.6	415	436	439	430	13.3	559
99	1	1315	1364	1367	1.7	377	391	392	387	8.33	
100	1	1256	1264	1279	1.7	367	369	374	370	3.45	
101	1	1508	1470	1449	1.8	415	404	398	406	8.27	597
102	1	1351	1354	1323	1.4	480	480	470	477	6.09	
103	1	1635	1735	1604	1.5	535	568	525	543	22.4	596
104	1	1741	1732	1782	1.8	473	471	484	476	7.21	

^a the necessary dilution was determined in a pre-measurement. The triplicate measurement was conducted with no dilution (1) or with a 1:2 dilution (2) to stay within measurement range of our standard curve; ^b 2 mL samples were collected from the bioreactor, pelleted, and resuspended/stored in 1 mL 1 M NaOH. The concentration given here is referred to 1 mL NaOH; ^c biomass from stage B was collected over a period of one day, pelleted, dried, and analyzed by Dairy One Co-op for crude protein content. When the amount of dried biomass was not enough to conduct a separate crude protein analysis, samples were combined, and the measurement given is an average of the combined samples; ^d SD, standard deviation.

Table S2. Data used for economic calculations, including calculations, explanation of assumptions, and references for an existing Quorn facility of 310,000 L.

Variable used in equations	Parameter	Value	Calculation (Variables in bold)	Assumptions	Reference
General considerations for 2014 Quorn process					
a	Quorn II Volume	155 m ³			(T. Finnigan <i>et al.</i> , 2017; M. Wiebe, 2002)
b	Quorn III Volume	155 m ³			(T. Finnigan <i>et al.</i> , 2017; M. Wiebe, 2002)
c	Quorn total Volume 2014	310 m ³	a + b		(T. Finnigan <i>et al.</i> , 2017; M. Wiebe, 2002)
d	Vol. Prod. Rate DW protein	1.25 g·L ⁻¹ ·h ⁻¹		We assume an average production rate given from the cited reference	(T. Finnigan <i>et al.</i> , 2017; M. Wiebe, 2002)
e	Vol. Prod. Rate DW protein	1.25 kg·m ⁻³ ·h ⁻¹	d ·(1kg/1000g)·(1000L/1m ³)		
f	Loss in protein to reduce RNA content	0.3			(T. Finnigan <i>et al.</i> , 2017; M. Wiebe, 2002)
g	Plant run-time efficiency	0.9		The process is operated for 6 weeks in continuous mode and then restarted	(T. Finnigan <i>et al.</i> , 2017)

h	Kilograms protein per kilogram biomass	0.44 kg·kg ⁻¹			with some down-time (~8 runs per year with each ~4 days down-time)	(T. Finnigan <i>et al.</i> , 2017)
i	Total DW protein produced per year	3055050 kg·yr ⁻¹	c·e·g ·(8760h/1yr)			
j	Total DW protein produced per year after RNA reduction	2138535 kg·yr ⁻¹	i ·(1- f)			
k	Quorn Supermarket price per kg protein	150 \$·kg ⁻¹			Sourced in German supermarket (www.rewe.de) in May 2019, converted with daily euro-to-dollar conversion rate in 2019	
l	Total revenue calc. from supermarket price in 2019	320,780,250 \$	j·k		l > n	
m	Total revenue reported in 2014 (£)	150,300,000 £				(Reuters, 2015)
n	Total revenue reported in 2014 (\$)	247,637,694 \$	m ·(1.648\$/£)		Average conversion rate £ to \$ in 2014	(X-rates, 2019)
o	Value ratio increase supermarket	30%	(l-n)/ n			
p	Dietary requirement of protein per person	0.056 kg·d ⁻¹			Average person with 70 kg body weight	(Lupton <i>et al.</i> , 2002)
q	How many persons can be fed per day?	105,000 d ⁻¹	j ·(1yr/365d)/ p			
r	One person spends how much daily?	8.40 \$·d ⁻¹	k·p			
s	How many persons can be fed per day after 10x scale-up?	1,050,000 d ⁻¹	q ·10			

t	How many 10x scaled-up plants are required to feed 10 billion people?	9558	10 ⁻¹⁰ /s	Assuming 10 billion people by 2050	
General considerations for 2010 Quorn process					
u	Total revenue reported in 2010 (£)	128,800,000 £			(D. Moore <i>et al.</i> , 2019b)
v	Profit reported in 2010 (£)	16,100,000 £			
w	Employees reported in 2010	600			(D. Moore <i>et al.</i> , 2019b)
TOT1	Profit ratio	13%	v/u		
General considerations for 1997 Quorn process					
x	Total revenue reported in 1997 (£)	74,000,000 £			(D. Moore <i>et al.</i> , 2019b)
y	Reported investment for fermenters in 1997	75,000,000 £			(D. Moore <i>et al.</i> , 2019b)
	Ratio of revenue to investment	99%	$(x/y) \cdot 100$		
Calculations on Quorn process in 2014 – comparing implemented Quorn process and hypothetical two-stage bioprocess					
z	Value of £ in 2014 (162.56 £) vs. 1997 (100 £)	1.6256	162.56£/100£		(Webster, 2019)
A	Investment cost of 1997 fermenter in 2014 (£)	121,920,000 £	$y \cdot z$		
B	Investment cost of 1997 fermenter in 2014 (\$)	200,878,162 \$	$A \cdot (1.648\$/£)$	Average conversion rate £ to \$ in 2014	(X-rates, 2019)
C	Investment cost for the two-stage bioprocess	401,756,324 \$	B ·2	Double investment cost for similar-sized second fermenter	

D	Weighted average cost of capital for UK food/beverage industry per year	8%				(WaccExpert, 2019)
E	Capital cost per year for Quorn process	16,070,253 \$	B·D			
F	Capital cost per year for two-stage bioprocess	32,140,506 \$	C·D			
TOT2	Capital cost ratio vs. revenue (Quorn process)	6.49%	(E/n)·100			
	Capital cost ratio vs. revenue (two-stage bioprocess)	12.98%	(F/n)·100			
G	Average cost per employee per year	90,949 \$·yr ⁻¹			Based on 27,600 £ average salary in UK in 2015, converted with average conversion rate (B); doubled to include additional cost for employer (insurance, health, pension)	(Buzz, 2019)
H	Labor cost per year (Quorn process)	54,569,264 \$·yr ⁻¹	w·G		Number of employees similar as in 2010	
I	Labor cost per year (two-stage bioprocess)	57,297,728 \$·yr ⁻¹	H+(H·5%)		5% more employees (30) for second fermenter	
TOT3	Labor cost ratio vs. revenue (Quorn process)	22.04%	(H/n)·100			
	Labor cost ratio vs. revenue (two-stage bioprocess)	23.14%	(I/n)·100			
J	DW protein yield per kg of glucose	0.136 kg·kg ⁻¹			This value includes that for DW protein production carbon also is “lost” as other biomass components and CO ₂	(D. Moore <i>et al.</i> , 2019b)

K	Glucose price	0.37 \$·kg ⁻¹			(Indexmundi, 2019)
L	Glucose cost per year in Quorn process	8,311,533 \$	i/J·K		
TOT4	Glucose cost ratio vs. revenue (Quorn process)	3.36%	(L/n)·100		
M	Kilogram Ammonia required per DW protein	0.33 kg·kg ⁻¹	0.27/(14g-N/mol)·(17g-NH ₃ /mol)	Based on average nitrogen content of dry biomass (0.12 kg/kg) and a protein content of 44% (kg/kg). This gives 0.27 kg-N/kg-DW protein	(Drapcho <i>et al.</i> , 2008)
N	Ammonia price	0.53 \$·kg ⁻¹			(solutions, 2019)
O	Ammonia cost per year in Quorn process	530,859 \$	i/M·N		
TOT5	Ammonia cost ratio vs. revenue (Quorn process and two-stage bioprocess)	0.21%	(O/n)·100		
P	Biotin required per DW protein	1.36·10 ⁻⁶ kg·kg ⁻¹			(T. Finnigan <i>et al.</i> , 2017)
Q	Biotin price	2000 \$·kg ⁻¹			(CMR, 2019)
R	Biotin cost per year in Quorn process	8,310 \$	i/P·Q		
TOT6	Biotin cost ratio vs. revenue (Quorn process and two-stage bioprocess)	0.00%	(R/n)·100		
S	Magnesium required per DW protein	4.20·10 ⁻³ kg·kg ⁻¹			(T. Finnigan <i>et al.</i> , 2017)
T	Magnesium price	8.55 \$·kg ⁻¹			(Ltd, 2019)
U	Magnesium cost per year in Quorn process	109,707 \$	i/S·T		

TOT7	Magnesium cost ratio vs. revenue (Quorn process and two-stage bioprocess)	0.04%						
V	Dilution rate in Quorn process per hour	0.19 h ⁻¹						(D. Moore <i>et al.</i> , 2019b; M. Wiebe, 2002)
W	Exchanges of reactor volume per day (dilution rate per day)	4.56 d ⁻¹			V ·(24h/1d)			
X	Water usage per year without recycling	464,368 m ³ ·yr ⁻¹			W · c · g ·(365d/1yr)			
Y	Recycling rate	50%					Similar to corn-to-ethanol industry	(Agler <i>et al.</i> , 2008)
Z	Water usage per year with recycling	232,184 m ³ ·yr ⁻¹			X · Y			
a1	Water cost	2.01 \$·m ⁻³					Location of Marlow foods (https://www.google.com/maps/search/marlow+foods/@54.522888,-1.497877,10z)	(BusinessElectricityPrices, 2019)
b1	Water cost per year	466,628 \$·yr ⁻¹			Z · a1			
TOT8	Water cost ratio vs. revenue (Quorn process)	0.19%						
c1	Water to wastewater	50%						
d1	Wastewater cost	1.74 \$·m ⁻³					Location of Marlow foods (https://www.google.com/maps/search/marlow+foods/@54.522888,-1.497877,10z)	(BusinessElectricityPrices, 2019)
e1	Wastewater cost per year	201,670 \$·yr ⁻¹			Z · c1 · d1			
TOT9	Wastewater cost ratio vs. revenue (Quorn process)	0.08%						

f1	Glucose used per year	22,463,603 kg·yr ⁻¹	iJ		
g1	Millimoles glucose per hour	14,233,987 mmol·h ⁻¹	f1 ·(1yr/8760h)/ (180.156g·mol ⁻¹)·(1000g/kg)· (1000mmol/mol)		
h1	Millimoles oxygen per Liter per hour needed for aeration without electrolyzer	275.49 mmol·(L·h) ⁻¹	g1 ·6·c·(1m ³ /1000L)	Stoichiometric need of 6 moles oxygen per 1 mole glucose	
i1	Kilograms oxygen per year	23,940,428 kg·yr ⁻¹	f1 ·(1000mmol/mol)/ (180.156g·mol ⁻¹) ·6·(32g·mol ⁻¹) ·(1kg/1000g)		
j1	Power to deliver oxygen to reactor per kg	2.75 kWh·kg ⁻¹		Extrapolated from data given Figure 3 in reference	(Humbird <i>et al.</i> , 2017)
k1	Power for aeration of reactor per year	6.58·10 ⁷ kWh·yr ⁻¹	i1 · j1		
	Amount of overall electric power in process used for aeration	50%		Similar to wastewater industry	(Drewnowski <i>et al.</i> , 2019)
l1	Power for other pumping, etc.	6.58·10 ⁷ kWh·yr ⁻¹		Same as for aeration, due to assumption that this is 50% of overall electric power needs	
m1	Whole sale kWh cost in UK in 2014	0.07 \$·kWh			(Ofgem, 2019)
n1	Electricity cost per year for Quorn process	9,330,830 \$·yr ⁻¹	(k1+l1) · m1		
o1	Millimoles oxygen per Liter per hour with oxygen from electrolyzer present	142.39 mmol·(L·h) ⁻¹	h1 · (C1/2)·(1000mmol/mol)/c·(1000L/m ³)	Offset by pressurized oxygen from electrolyzer; per two moles of H ₂ one mole of O ₂ is produced; the stoichiometric need of O ₂ for the	

					combustion is the same for glucose and acetate because carbon has the same oxidation number	(Humbird <i>et al.</i> , 2017)
p1	Power to deliver oxygen to reactor per kg with electrolyzer	2.3 kWh·kg ⁻¹			From data given Figure 3 in reference	
q1	Power for aeration of reactor per year with electrolyzer	5.51·10 ⁷ kWh·yr ⁻¹	i1·p1			
r1	Electricity cost per year with electrolyzer	8,567,398 \$·yr ⁻¹	(i1+q1)·m1			
TOT10	Electricity cost ratio vs. revenue (Quorn process)	3.77%	(n1/n)·100			
	Electricity cost ratio vs. revenue (two-stage bioprocess)	3.46%	(r1/n)·100		Offset by oxygen from electrolyzer	
s1	Kilograms carbon per kilogram protein	1.16 kg·kg ⁻¹			Based on average carbon content of dry biomass (0.51 kg/kg) and a protein content of 44% (kg/kg)	(Drapcho <i>et al.</i> , 2008)
t1	Carbon required for protein product produced per year	3,543,858 kg·yr ⁻¹	i·s1			
u1	Moles of carbon per year	295,321,500 mol·yr ⁻¹	t1/(12g/mol)·(1000g/1kg)			
v1	Moles of acetate required for protein production	147,660,750 mol·yr ⁻¹	u1/2		2 moles carbon per acetate	
w1	Carbon yield in gas fermentation	81.7%			Observation from this manuscript	
x1	Moles of CO ₂ required for gas fermentation per year	361,470,624 mol·yr ⁻¹	v1·2/w1		2 moles CO ₂ per acetate	

y1	Kilogram of CO ₂ required for gas fermentation per year	15,904,707 kg·yr ⁻¹	x1 ·(44g/mol)·(1000g/1kg)		
z1	CO ₂ cost	0.19 \$·kg ⁻¹			Independent on how carbon taxes may influence the cost or cost benefit of utilizing CO ₂ , there will be a cost for CO ₂ transportation infrastructure or shipping
A1	CO ₂ cost per year	3,053,704 \$·yr ⁻¹	y1 · z1		(California, 2019; Department for Business, 2018)
	CO ₂ cost ratio vs. revenue (two-stage bioprocess)	1.23%	(A1/n) ·100		
B1	Moles H ₂ required for gas fermentation per year	722,941,249 mol·yr ⁻¹	x1 ·2		(H. Richter, Molitor, Wei, <i>et al.</i> , 2016)
C1	Moles H ₂ required for gas fermentation per hour	82,528 mol·h ⁻¹	B1 ·(1yr/8760h)		
D1	Normal cubic meter H ₂ required per hour	1,849 Nm ³ ·h ⁻¹	C1 ·(22.4L/mol)·(1Nm ³ /1000L)		22.4 L·mol ⁻¹ of a gas under normal conditions
E1	Normal cubic meter H ₂ produced from 1 MWh electrolyzer per hour	200 Nm ³ ·h ⁻¹			(Electroarchea, 2019)
F1	Required electrolyzer capacity	9.24 MWh	D1/E1		
G1	Electrolyzer cost 1-10 MW per MW	1,000,000 \$·MW ⁻¹			(Electroarchea, 2019)
H1	Capital cost for electrolyzer	9,243,084 \$	F1 · G1		
I1	Capital cost for electrolyzer per year (two-stage bioprocess)	739,447 \$	H1 · D		

	Capital cost electrolyzer ratio vs. revenue (two-stage bioprocess)	0.30%	$(I1/n) \cdot 100$	
J1	Electricity required to operate electrolyzer	9243 kWh	F1 $\cdot (1000 \text{kWh}/1 \text{MWh})$	
K1	Cost to operate electrolyzer per hour	$655.00 \text{ \$} \cdot \text{h}^{-1}$	J1 ·m1	
L1	Cost to operate electrolyzer per year	$5,737,817 \text{ \$} \cdot \text{yr}^{-1}$	K1 ·(8760h/1yr)	
	Operation cost electrolyzer ratio vs. revenue (two-stage bioprocess)	2.32%	$(L1/n) \cdot 100$	
Summary of comparing implemented Quorn process and hypothetical two-stage bioprocess				
M1	Percentage of accountable revenue for 2014 Quorn process	36%	SUM(TOT1 to TOT10)	
N1	Residual revenue percentage for PR, research, packaging, overhead, eggs, etc. for 2014 Quorn process	64%	$100\% - \text{M1}$	
	Total accountable revenue per year for 2014 Quorn process	$89,814,920 \text{ \$}$	n ·N1	
	Total residual revenue per year for 2014 Quorn process	$157,822,775 \text{ \$}$	n ·M1	
	Glucose cost credit per year in two-stage bioprocess	$-8,311,533 \text{ \$}$	-L	
	Aeration cost credit per year by oxygen from electrolyzer in two-stage bioprocess	$-763,432 \text{ \$}$	$-(\text{n1} - \text{r1})$	
	Additional labor cost per year in two-stage bioprocess	$2,728,463 \text{ \$}$	I-H	

	Additional capital cost for fermenter per year in two-stage bioprocess	16,070,253 \$	F-E		
	Additional CO ₂ cost per year in two-stage bioprocess	3,053,704 \$	A1		
	Additional capital cost for electrolyzer per year in two-stage bioprocess	739,447 \$	II		
	Additional operating cost for electrolyzer per year in two-stage bioprocess	5,737,817 \$	L1		
O1	Total cost (required revenue) for two-stage bioprocess	266,892,414 \$	SUM(all above excluding M1 and N1)		
	Overall increase in cost to produce protein in two-stage bioprocess compared to Quom process	7.78%	(O1-n)/n·100		

Supplementary Experimental Procedures

Media compositions:

The 2xP7 medium was composed of mineral salts (per Liter: 2.4 g NaCl, 3 g NH₄Cl, 0.3 g KCl, 0.3 g KH₂PO₄, 1.01 g MgCl₂·6H₂O, 0.16 g CaCl₂·2H₂O), trace elements (per Liter: 20 mg NTA, 1.32 mg MnCl₂·4H₂O, 8 mg (NH₄)₂Fe(SO₄)₂, 2 mg CoCl₂·6H₂O, 3.56 mg ZnSO₄·7H₂O, 0.2 mg CuCl₂·2H₂O, 0.2 mg NiCl₂·6H₂O, 0.2 mg Na₂MoO₄·2H₂O, 0.27 mg Na₂SeO₃·5H₂O, 0.22 mg Na₂WO₄·2H₂O), and vitamins (per Liter: 0.1 mg pyridoxine, 0.05 mg thiamine, 0.05 mg riboflavin, 0.05 mg D-pantothenic acid hemicalcium salt, 0.05 mg thioctic acid, 0.02 mg aminobenzoic acid, 0.02 mg nicotinic acid, 0.1 mg vitamin B₁₂, 0.05 mg biotin, 0.05 mg folic acid, 0.05 mg mesna). The vitamin B₁₂ and folate was omitted from the vitamin solution during the last 6 days of Period II and III without noticeable changes in performance. Vitamins were added after autoclaving. Oxygen was completely removed from the medium by sparging with sterile nitrogen gas, and then adding cysteine (1 mM final concentration). Antifoam (Sigma 204) was added to the feed medium for Stage A according to the following scheme: below OD₆₀₀ of 5, no antifoam; above OD₆₀₀ of 5, addition of 10 μL L⁻¹ antifoam; and above OD of 7, addition of 20 μL L⁻¹ antifoam.

The YN medium for flask experiments was composed of mineral salts (per Liter: 1 g (NH₄)₂SO₄, 1 g KH₂PO₄, 1 g MgSO₄·7H₂O, NaCl 0.1 g, 0.033 CaCl₂·2H₂O), trace elements (per Liter: 5 mg Fe(II)SO₄·7H₂O, 1.6 mg ZnSO₄·7H₂O, 1.12 mg Mn(II)SO₄·1H₂O, 0.28 mg Na₂MoO₄, 0.18 mg Co(II)Cl₂, 0.18 mg Cu(II)Cl₂·2H₂O), and vitamins (per Liter: 20 mg myo-inositol, 4.4 mg thiamine, 1.2 mg pyridoxine, 1 mg D-pantothenic acid hemicalcium salt, 0.03 mg biotin). For the YN medium for the bioprocessing experiment, the (NH₄)₂SO₄ was replaced by 0.4 g NH₄Cl, and the MgSO₄·7H₂O was replaced by 0.82 g MgCl₂·6H₂O. Instead, we added 0.6 g L⁻¹ (2xYN) or 1.2 g L⁻¹ (4xYN) cysteine as the sulfur source. The by-pass feed was supplemented with antifoam (Sigma 204) according to the following scheme: 10 μL L⁻¹ in the 2xYN; 50 μL L⁻¹ in the 4xYN.

Stage A set-up:

The pH was controlled with the internal pH controller of the Stage A unit and a pH probe (Mettler Toledo, Columbus, OH). The temperature was controlled at 35 °C with a recirculating water bath. Stirring was at 300 rpm with two vertical flat-blade impellers each with four blades. The gas was

provided through a microsparger (0.5 microns, More Beer, Pittsburg, CA). The headplate was equipped with ports for pH control (5 M KOH), gas in and out, medium feed (40 mL h⁻¹), Na₂S feed, and cell recycling. The additional Na₂S feed was used during continuous operation to provide an additional source of sulfur and to keep Stage A anaerobic. The Na₂S feed pump was triggered with a timer (1 s on, 59 s off) resulting in a feed rate of 0.84 mL h⁻¹ with an anaerobic 1 M Na₂S stock, which resulted in an apparent concentration of 2 mM Na₂S per day at the 40 mL h⁻¹ medium feed rate. Cell recycling with full cell retention was performed through a Cellflo polyethersulfone hollow fiber module (cell guard) with 500-cm² membrane surface area and 0.2 μm pore size (C22E-011-01N, Spectrum Laboratories, Inc., Rancho Dominguez, CA) at 180 mL min⁻¹.

Stage B set-up:

The pH was controlled with an Alpha pH 800 controller (Eutech Instruments, Vernon Hills, IL) and a pH probe (Cole-Parmer, Vernon Hills, IL). The temperature was controlled at 30°C with the electric heating jacket from Stage B. Stirring was at 200 rpm with a magnetically coupled stirrer with two vertical flat-blade impellers each with six blades. Compressed air was provided through a microsparger (0.5 microns, More Beer, Pittsburg, CA) at an average flow-rate of 88.5 ± 19.6 mL min⁻¹ (n=60). The headplate was equipped with ports for pH control (2 M HCl, 2 M NaOH), gas in and out, medium feed from Stage A, and a by-pass feed for additional YN feeding.

Analytical Procedures:

The OD₆₀₀ for the flask experiments was measured in a plate reader (BioTek Synergy 2, Winooski, VT). The OD₆₀₀ for the bioprocessing experiments was measured using a photometer (Milton Roy Spectronic 1201, Houston, TX) in a quartz glass cuvette (SCC 282, 1.000, Hellma, Müllheim, Germany). Cell dry weight (CDW) was determined by using correlation factors of 242 mg CDW OD⁻¹ L⁻¹ for *C. ljungdahlii* (Perez *et al.*, 2013) and 270 mg CDW OD⁻¹ L⁻¹ for *S. cerevisiae* as determined in this study. For calculation of carbon in biomass a factor of 0.53 (bacterial biomass composition: C₅H₇O₂N) was used for *C. ljungdahlii*, and a factor of 0.51 (yeast biomass composition: C₁₀₀H₁₇₄O₄₅N₂₀) was used for *S. cerevisiae* (Drapcho *et al.*, 2008) considering the molecular weight for carbon of 12 g mol⁻¹. Ethanol and acetate concentrations were quantified by HPLC as described before (Richter *et al.*, 2016). Inlet and outlet gas flow rates were measured with water displacement flow-meters and bubble flow meters, respectively. Gas pressure was

measured with a digital pressure gauge (Cole Parmer, Vernon Hills, IL). Gas samples were collected at the inlet and the outlet of the gas lines to analyze the relative partial pressures of the gases (H_2/CO_2 for Stage A; $\text{N}_2/\text{O}_2/\text{CO}_2$ for Stage B) by GC as described before (Perez *et al.*, 2013). The oxygen and nitrogen peaks in our GC system overlapped. Therefore, the oxygen partial pressure was determined as the difference of the signal for air (78.09% nitrogen plus 20.95% oxygen) and the gas outlet, assuming that nitrogen is inert and at a constant concentration. Oxygen partial pressure in the gas outlet of Stage B was additionally determined with an electrochemical oxygen sensor that correlated the oxygen partial pressure to a potential (S101 Diffusion Sensor, Qubit Systems, Kingston, ON, Canada). The electrochemical oxygen sensor was calibrated with 100% nitrogen gas, and with compressed air. The partial pressures, the volumetric flow rates, and the gas pressure were used to determine the gas consumption and production rates.

Lowry determination of proteins:

Frozen samples were thawed at room temperature and samples were boiled for 10 min in a heating block at 105 °C. A 2 mg mL^{-1} BSA standard was mixed with 10 M NaOH to give a final concentration of 1 M NaOH with 1.8 mg mL^{-1} BSA. The standard was also boiled at 105°C in a heating block. Samples were either used directly or diluted further with 1 M NaOH. Standard dilutions were prepared with 1 M NaOH. 10 μL of standards and samples were loaded into a 96-well plate (265301, Nunc MicroWell 96-Well Plates, Thermo Scientific, Waltham, MA). 100 parts of Na_2CO_3 in 0.1 M NaOH were mixed with 1 part of 1% CuSO_4 and 1 part of 2% NaH-tartrate (*e.g.*, 10 mL + 100 μL + 100 μL). 200 μL of this mixture was added to every well. The plate was read in a plate reader (BioTek Synergy 2, Winooski, VT) at 750 nm. Then 20 μL of a mixture of 1 part water and 1 part Folin-Ciocalteu's phenol reagent was added to each well, and the plate was incubated at room temperature in the dark for 15 min. The plate was read again at 750 nm, and the background (first reading) was subtracted from the measurement (second reading).

Supplementary Results and Discussion

S1. Operating Stage B with *S. cerevisiae* during Period I to test for nutrient limitations and a feasible dilution rate

Only a few studies have been published with acetate as a substrate for SCP production. Goldberg *et al.* (1985) and Verduyn *et al.* (1991) reported growth of *S. cerevisiae* (CBS 8066) and *Candida utilis* (CBS 621; fodder yeast), respectively, in a continuously fed bioreactor without a cell guard (chemostat), while feeding a 125-mM acetate solution as the sole carbon source. Nevertheless, we performed a flask experiment to observe growth for *S. cerevisiae* under our conditions with: 1) a 150-mM acetate concentration in YNA medium (**Figure S2**); and 2) an acetate-rich effluent that we had obtained from a gas fermenter with *C. ljungdahlii* (**Figure S2**), which had been producing acetate concentrations of 70 mM from hydrogen and carbon dioxide (H₂:CO₂, 80:20 vol-%) during an experiment similar to (Richter *et al.*, 2013).

We found that for the YNA medium, 53% of the acetate remained, while this was 88% for the gas-fermentation effluent (**Figure S2C**). Since for both growth media the exponential phase of the growth curve had ended (**Figure S2A**), the presence of ample substrate indicated to us that one or more unknown nutrients had been limiting the growth of *S. cerevisiae*. Obviously, future studies would need to identify the growth-limiting nutrients to minimize unnecessary medium and nutrient usage.

Next, we used Period I to learn about bioprocessing of *S. cerevisiae* in Stage B with a filtered, acetate-rich Stage-A solution and a bypass of fresh medium without yeast extract. Unlike for the flask experiment (**Figure S2C**), the initial acetate concentration of 95 mM was completely diminished during the batch-mode operating condition for the first 5 days of the operating period for Stage B (**Figure S3**). Similarly, for all continuous-mode conditions the acetate was consumed efficiently with little residual acetate concentrations left in Stage B (**Figure S3**). Thus, with a bypass of fresh medium, growth nutrients were no longer limiting yeast growth.

An important bioprocessing parameter to determine is the dilution rate for maintaining high enough concentrations of cells. We had switched to continuous mode with an initial dilution rate of 0.04 h⁻¹ on Day 25 of the operating period (**Figure 3**), which was similar to the dilution rate of Stage A. Without a cell guard, the performance at this dilution rate was stable, indicating that the

growth rate could keep up with the dilution rate. To increase the yeast-protein production rate by providing more acetate and nutrients, the dilution rate was doubled to 0.08 h^{-1} . However, the growth rate was not sufficiently high enough, which ultimately led to a complete wash-out of the yeast cells during Period I (**Figure 3A**), although we had observed a growth rate of 0.09 h^{-1} in the flask experiment (**Figure S2B**). Verduyn *et al.* (1991) on the other hand, was able to achieve a dilution rate of 0.1 h^{-1} for an aerobic *S. cerevisiae* (CBS 8066) culture with acetate as the sole carbon substrate and without yeast extract. In our case and with a different *S. cerevisiae* strain, we decided to use a lower dilution rate of 0.06 h^{-1} during the last 12 days of both Periods II and III for Stage B (**Figure 3**).

S2. Determining the protein mass-fraction of the yeast biomass

The average protein mass-fraction for *S. cerevisiae* was $40.2\% \pm 3.65\%$ (n=16) and $53.3\% \pm 4.32\%$ (n=9) during Period II and $43.7\% \pm 5.95\%$ (n=15) and $56.5\% \pm 2.44\%$ (n=7) during Period III for the Lowry method and Dumas method, respectively (g g^{-1} in **Table S1**). In another study, Verduyn *et al.* (1991) measured a 47% protein mass-fraction (g g^{-1}) for *S. cerevisiae* CBS 8066 when grown aerobically with acetate and without yeast extract (by using a modified Biuret method). The protein mass-fraction during Period III was slightly higher than during Period II for *S. cerevisiae* by both methods in our study. This relatively high protein mass-fraction agrees with the relatively low crude-fat (lipid) mass-fraction during Period II ($0.59\% \pm 0.22\%$ [n=9]), and during Period III ($1.07\% \pm 0.35\%$ [n=7]), with ash values of $13.6\% \pm 1.14\%$ (n=9) and $14.2\% \pm 0.76\%$ (n=7) for Period II and Period III, respectively (all g g^{-1}). The remaining $\sim 30\%$ likely consisted of mainly fiber and nucleic acids, but this would need to be confirmed during future research.

Supplementary References

Agler, M. T., Garcia, M. L., Lee, E. S., Schlicher, M., & Angenent, L. T. (2008). Thermophilic anaerobic digestion to increase the net energy balance of corn grain ethanol. *Environmental science & technology*, 42(17), 6723-6729.

BusinessElectricityPrices. (2019). Retrieved from <https://www.businesselectricityprices.org.uk/water-prices/>

Buzz, R. (2019). Retrieved from <https://recruitmentbuzz.co.uk/average-wage-uk-salary-earning-age/>

- California, S. O. (2019). Retrieved from <https://ww3.arb.ca.gov/fuels/lcfs/credit/lrtweeklycreditreports.htm>
- CMR. (2019). Retrieved from <https://www.icis.com/explore/resources/news/1998/11/09/89463/biotin-prices-stabilize-after-months-of-decline/>
- Department for Business, E. I. S. (2018). Shipping carbon dioxide (CO₂): UK cost estimation study. Retrieved from <https://www.gov.uk/government/publications/shipping-carbon-dioxide-co2-uk-cost-estimation-study>
- Drapcho, C. M., Nghim, N. P., & Walker, T. (2008). *Biofuels engineering process technology*: McGraw-Hill Education.
- Drewnowski, J., Remiszewska-Skwarek, A., Duda, S., & Łagód, G. (2019). Aeration process in bioreactors as the main energy consumer in a wastewater treatment plant. Review of solutions and methods of process optimization. *Processes*, 7(5), 311.
- Electroarchea. (2019). Retrieved from <https://www.h2-international.com/2017/09/01/electrolyzer-target-100-megawatts/>
- Finnigan, T., Needham, L., & Abbott, C. (2017). Mycoprotein: a healthy new protein with a low environmental impact. In *Sustainable protein sources* (pp. 305-325): Elsevier.
- Goldberg, I. (1985). Fermentation Processes for Microbial SCP Production. In *Single Cell Protein* (pp. 67-128): Springer.
- Humbird, D., Davis, R., & McMillan, J. (2017). Aeration costs in stirred-tank and bubble column bioreactors. *Biochemical engineering journal*, 127, 161-166.
- Indexmundi. (2019). Retrieved from <https://www.indexmundi.com/commodities/?commodity=sugar&months=120>
- Ltd, I. (2019). Retrieved from <https://www.inoxia.co.uk/products/chemicals/inorganic-compounds/magnesium-carbonate>
- Lupton, J. R., Brooks, J., Butte, N., Caballero, B., Flatt, J., & Fried, S. (2002). Dietary reference intakes for energy, carbohydrate, fiber, fat, fatty acids, cholesterol, protein, and amino acids. *National Academy Press: Washington, DC, USA*, 5, 589-768.
- Moore, D., Robson, G. D., & Trinci, A. P. J. (2019). 21st Century Guidebook to Fungi. Retrieved from http://www.davidmoore.org.uk/21st_Century_Guidebook_to_Fungi_PLATINUM/Ch17_18.htm
- Ofgem. (2019). Retrieved from <https://www.ofgem.gov.uk/data-portal/all-charts/policy-area/electricity-wholesale-markets>
- Perez, J. M., Richter, H., Loftus, S. E., & Angenent, L. T. (2013). Biocatalytic reduction of short-chain carboxylic acids into their corresponding alcohols with syngas fermentation. *Biotechnology and Bioengineering*, 110(4), 1066-1077.

- Reuters. (2015). UPDATE 2-Philippines' Monde Nissin buying UK meat substitute firm Quorn for \$831 mln. Retrieved from <https://www.reuters.com/article/quorn-ma-idUSL5N1204C720151001>
- Richter, H., Martin, M. E., & Angenent, L. T. (2013). A two-stage continuous fermentation system for conversion of syngas into ethanol. *Energies*, 6(8), 3987-4000.
- Richter, H., Molitor, B., Diender, M., Sousa, D. Z., & Angenent, L. T. (2016). A narrow pH range supports butanol, hexanol, and octanol production from syngas in a continuous co-culture of *Clostridium ljungdahlii* and *Clostridium kluyveri* with in-line product extraction. *Frontiers in microbiology*, 7, 1773.
- solutions, I. (2019). Retrieved from <https://www.intratec.us/chemical-markets/ammonia-price>
- Verduyn, C., Stouthamer, A. H., Scheffers, W. A., & van Dijken, J. P. (1991). A theoretical evaluation of growth yields of yeasts. *Antonie Van Leeuwenhoek*, 59(1), 49-63.
- WaccExpert. (2019). Retrieved from <http://www.waccexpert.com/>
- Webster, I. (2019). CPI Inflation calculator. Retrieved from <https://www.in2013dollars.com/1997-GBP-in-2014?amount=100>
- Wiebe, M. (2002). Myco-protein from *Fusarium venenatum*: a well-established product for human consumption. *Applied microbiology and biotechnology*, 58(4), 421-427.
- X-rates. (2019). Retrieved from <https://www.x-rates.com/average/?from=GBP&to=USD&amount=1&year=2014>

3

Establishing a power-to-food platform by demonstrating the presence of cobalamin and folate in single-cell protein synthesized from renewable electric power and carbon dioxide

Akanksha Mishra¹, Mengle Wang³, Nadine Weber³, Bastian Molitor¹, Michael Rychlik³, Lars Angenent^{1,2}

1. Center for Applied Geosciences, University of Tuebingen, 72070 Tuebingen, Germany
2. Max Planck Fellow, Max Planck Institute for Developmental Biology, 72076 Tübingen, Germany
3. Analytical Food Chemistry, Technical University of Munich, 85354 Freising, Germany

In preparation

Establishing a power-to-food platform by demonstrating the presence of cobalamin and folate in single-cell protein synthesized from renewable electric power and carbon dioxide

Author Contributions

The experimental design in this study was conceptualized by Akanksha Mishra with advice from Largus T. Angenent. Akanksha Mishra wrote the manuscript and developed the microbiological analysis for quantifying the different forms of cobalamin in the biological samples. Nicolai Kliem-Kuster and Akanksha Mishra operated the power-to-food bioprocess system. Nadine Weber and Mengle Wang measured folate and cobalamin analogues, respectively and supported in the finalization of the overall discussion. Akanksha Mishra, Nadine Weber, and Mengle Wang interpreted the data from the instrumental analysis.

Abstract

The conventional practices of food production are responsible for one-third of the global carbon emission. They subsist on land-use, agricultural production, and transportation, thereby causing irreversible damage to non-renewable resources and utilization of fossil fuels. This issue is more persistent in developing countries, which are already at the risk of an impending food crisis. This motivated us to investigate an alternative technology for food production that is both sustainable as well as rich in nutrients. Therefore, in this study, we present the power-to-food platform, that converts CO₂ to microbial protein, while enhancing its nutritional composition. Inspired by the power-to-protein study from Molitor *et al.* (2019), we performed experiments under batch conditions to capture the production of cobalamin and folate by *Clostridium ljungdahlii*, followed by its uptake or accumulation by *Saccharomyces cerevisiae*. Then, we demonstrated a two-stage gas fermentation, with *C. ljungdahlii* in a Stage 1 bioreactor and *S. cerevisiae* in a Stage 2 bioreactor, to examine their fluxes under continuous operation. Unfortunately, due to several errors that occurred during the operation of the system and a high limit of detection of the analytical method, we were unable to confirm whether *C. ljungdahlii* had the capacity to synthesize

cobalamin, that is accumulated within the biomass of *S. cerevisiae*. Nevertheless, we are thrilled to report that *S. cerevisiae* was capable of producing folate when grown with acetic acid as a carbon source. We observed a volumetric productivity of $16.47 \mu\text{g L}^{-1} \text{d}^{-1}$ or a folate yield of $5.85 \mu\text{g g}^{-1} \text{d}^{-1}$ for an average biomass concentration of 1.7g L^{-1} in the Stage 2 bioreactor. With the findings from the operation of the power-to-food system, we have gained valuable insight into future optimization strategies that will support the actualization of a food production platform with zero or even negative net carbon emissions.

Introduction

The food industry relies on the consumption of fossil fuels to meet the demands of the growing population (Ladha-Sabur *et al.*, 2019). With a 60% increase in the global population by 2050, the energy requirements as well as the greenhouse gas emission of the food sector will also rise (Ladha-Sabur *et al.*, 2019). This calls for a major transformation in the food production and transportation process to make it more sustainable. In the context of meat cultivation, from livestock farming to its transportation and packaging, most of the emissions are due to land-use change (Crippa *et al.*, 2021). Breeding livestock causes and irreversible exploitation of the land and forest resources (Gerber & Opio, 2013). This is especially true in developing countries because of their inadequate renewable resource management strategies (Crippa *et al.*, 2021). In addition, most of the developing countries are also low-income countries with a nutrient deficiency from poor dietary diversity (Muthayya *et al.*, 2013). If we consider the statistics on greenhouse gas emission from the food sector (Crippa *et al.*, 2021), and combine it to the global hunger index (von Grebmer *et al.*, 2015) in lower income countries, we can attest to an urgent requirement of a sustainable food production system, especially for the developing countries.

The brand Quorn® is a successful illustration of a single-cell protein product that is currently being marketed as food. It has gained global attention as a meat substitute for people following a vegetarian and vegan diet. It primarily consists of mycoprotein that is derived from a fungal strain called *Fusarium venenatum*. Despite being more sustainable than conventional meat production practices, it is still reliant on agriculture for utilizing glucose as a substrate. In 2019, we demonstrated the synthesis of microbial protein from H₂ and CO₂ in a two-stage bioreactor system called power-to-protein (Molitor *et al.*, 2019). This system solely relies on the application of gas fermentation and CO₂ capture for single-cell protein production. Due to biological CO₂ fixation, operation of the power-to-protein system eliminates our reliance on agriculture. Although, the Quorn® process already has lower emissions than that of conventional food production processes, our technology is more sustainable with potentially zero or even negative net carbon emissions (Molitor *et al.*, 2019). The nutrient profile of Quorn® products is maintained by the external supplementation of vitamins and other co-factors during its operation (T. J. A. Finnigan, 2011). Therefore, there is still much room to enhance the sustainability and self-reliance of the food

production technologies by studying the composition of the nutrients that are inherently present within the microbial biomass, and how are they influenced by the operating parameters.

Cobalamin and folates (i.e., Vitamin B12 and B9, respectively) are essential for our neurological and cognitive development (Troen, 2012). They participate in vital biological reactions involving methylation (Troen, 2012) by acting as co-factors for forming methionine, which is a precursor for S-adenosylmethionine (SAM) (Selhub, 2002). SAM participates in key biological reactions by acting as a universal donor of methyl groups to DNA, protein, and membrane lipids etc (Selhub, 2002). Since, cobalamin participates in the methylation of homocysteine from methyl-THF to form methionine, its deficiency creates an unused pool of methyl-THF, prohibiting its oxidation to formyl-THF that is essential for forming the purines and pyrimidines during DNA synthesis. Consequently, a simultaneous deprivation in both the vitamins is linked to a damaged nervous system (Black, 2008), haematological abnormalities (Moll & Davis, 2017), and cognitive disorders (Bottiglieri, 1996). Moreover, several studies suggest that the functionality of these two vitamins is interlinked (Shane & Stokstad, 1985). An adequate intake of cobalamin is highly recommended during folic acid supplementation (Paul & Selhub, 2017). A deficiency in either one of these vitamins can be detrimental to the activity of the other (Paul & Selhub, 2017).

Despite its widespread functionality, only bacteria and archaea are one of the major producers of cobalamin. The structural complexity of this vitamin makes its chemical synthesis challenging. Microbial fermentation processes contribute to 10 t of cobalamin production (Martens *et al.*, 2002). Industry relies on *Propionibacterium*, *Pseudomonas*, and *Nocardia* for the synthesis of cobalamin (Fang *et al.*, 2017; Martens *et al.*, 2002). Multicellular organisms and higher-level organisms, such as plants and animals, are incapable of its *de-novo* synthesis. Since, cobalamin facilitates the enzymatic transfer of the methyl group in key biological reactions, bacteria use it either for the synthesis of methionine in the heme pathway or for the transfer of the methyl group from methyl-tetrahydrofolate to CO dehydrogenase in the acetyl Co-A pathway (Wood *et al.*, 1986, Ragsdale, 1991; Stupperich, 1993).

In nature, cobalamin follows an upward, unidirectional flow of the food chain starting at the bottom with microbes. A plethora of examples are available, wherein multicellular organisms rely on their interaction with bacteria or archaea to retrieve cobalamin. Such relationships can be seen as

illustrations of microbe-mediated biofortification, for which the enrichment of a certain micronutrient in a food product occurs due to its production by microbes. For instance, microbes present in the gastrointestinal tract of ruminants are responsible for the high occurrence of cobalamin in meat and dairy products (Gille & Schmid, 2015). The presence of cobalamin in plants is attributed to its direct contact with bacteria and is shown to be driven by diffusion (Mozafar, 1994, Lawrence *et al.*, 2018, Iguchi *et al.*, 2015). Watanabe *et al.* (2018) have proposed the transfer of cobalamin from soil microbes onto the fruiting bodies in mushrooms (Watanabe & Bito, 2018). Another prominent display of cobalamin accumulation along the food chain is witnessed in the aquatic environment. Cobalamin in aquatic environments accumulates in predatory fish bodies through its initial journey into Phytoplankton and Zooplankton (Bertrand *et al.*, 2015; Hayashi *et al.*, 2007). This results in its enrichment in the liver or kidney of tuna and salmon (Adachi *et al.*, 2005). Inspired by the role of bacteria in cobalamin synthesis, researchers are also investigating the microbe-mediated biofortification of legumes and cereals by incorporating selected strains of bacteria that are known to produce cobalamin during fermentation (Xie *et al.*, 2021).

Such interactions have been more intensively studied for algae. Croft *et al* (2005) performed a survey of 326 algal species and roughly 50% species showed cobalamin auxotrophy (Croft *et al.*, 2005). At the lab scale, microbe-mediated biofortification of cobalamin was demonstrated between an algae *Ostreococcus tauri*, and its heterotrophic bacterial partner *Dinoroseobacter shibae* (Cooper *et al.*, 2019). A recent study demonstrated that certain strains of microalgae were able to obtain pseudocobalamin from cyanobacteria, and convert it into its bioactive form (Grossman, 2016). In contrary to all the research promoting a bacterial-algae symbiosis for cobalamin acquisition (Sokolovskaya *et al.*, 2020), fewer studies target cobalamin transfer between bacteria and yeasts. However, it is still possible to enrich the cobalamin content of yeasts by supplementing it during fermentation process. This is shown by Jach *et al.* (2020) for *Yarrowia lipolytica* to present it as promising candidate to produce single-cell protein containing cobalamin. Moreover, in his comprehensive evaluation of yeast as animal feed, Czech *et al* (2016) stated that $5.44 \mu\text{g Kg}^{-1}$ of cobalamin was present in *Sachharomyces cerevisiae* compared to $60 \mu\text{g Kg}^{-1}$ in the *Y. lipolytica* (Czech *et al.*, 2016). At a commercial scale, a yeast-based spread called Marmite™ is supplemented with high amounts of cobalamin during its preparation. Its consumption on a regular basis improves cognitive functioning and increases the tolerance to anxiety and stress in the general adult population (Mikkelsen *et al.*, 2018).

Unlike cobalamin, multicellular organisms, such as plants (Rébeillé *et al.*, 2006), fungi (Revuelta *et al.*, 2018), and algae (Gorelova *et al.*, 2019), are capable of folate biosynthesis. The structural backbone of a folate consists of the pteridine molecule attached to para-aminobenzoic acid followed by the glutamate tail. Folate can be classified into five different forms depending on the functional group attached to the pteridine molecule. In this manuscript, we will collectively refer to these different forms that are naturally present in food as folates. However, it should be noted that the recommended dietary intake (RDI) of cobalamin is $2.4 \mu\text{g d}^{-1}$ per person (Herbert, 1987b), while that of folate is more than a 100-fold higher at $400 \mu\text{g d}^{-1}$ (Herbert, 1987a). The reason being that unabsorbed or unused amounts of folates are regularly washed out of your body through urination (Loew *et al.*, 1987). This mandates its constant replenishment to maintain the required levels in our body. Although, most of the organisms across the food chain are capable of biosynthesizing folates, because of a higher RDI, its abundance is still insufficient to maintain the required amount for humans. This has inspired several strategies to counter its deficiency in the world.

Folate supplementation refers to the consumption of an artificially synthesized form of folate in the form of pills (Radimer *et al.*, 2004). This form consists of a pteric acid molecule bound to a mono-glutamate residue and is known as folic acid. It is a popular choice for supplementation because of its stability. Unfortunately, this method of providing folate to an entire population is complicated to monitor and may have several other limitations. These can be in the form of unavailability of folic acid pills, a lack of general awareness, inconsistent and improper consumption, and an expensive production and purification process (De Steur *et al.*, 2014). Therefore, folate fortification and folate bioproduction emerges as the better alternative for large-scale production and administration. Folate fortification entails an enrichment of the natural food folates either during its breeding (Strobbe & Van Der Straeten, 2017), or by genetic manipulation (Strobbe & Van Der Straeten, 2017), or by microbe-mediated biofortification (Saubade *et al.*, 2017). Microbe-mediated biofortification of folate enhances the natural folate content in food by including microbes during the fermentation process that co-produce it (Laiño *et al.*, 2014, Liu *et al.*, 2016). Microbes that are capable of its biosynthesis are also used for folate bioproduction, during which, they are treated as cells factories from which folate is produced, extracted, and purified (Revuelta *et al.*, 2018). With a well-characterized pathway for folate synthesis (Cherest *et al.*, 2000), it has been demonstrated that *S. cerevisiae* is an ideal candidate to perform microbe-

mediated biofortification of food as well as folate bioproduction (Sofia Hjortmo *et al.*, 2008; S. Hjortmo *et al.*, 2008).

The aim of this study is to expand the applications of the power-to-protein study from single-cell protein into food. From here on, we will call this system power-to-food. In this process, the first bioreactor (Stage 1) will perform the conversion of an H₂/CO₂-gas mixture into acetic acid. The second bioreactor (Stage 2) will utilize the dilute acetic acid from Stage 1 bioreactor as a carbon source for the synthesis of single-cell protein (Molitor *et al.*, 2019). Stage 1 bioreactor will be operated under strictly anaerobic conditions for the cultivation of *Clostridium ljungdahlii*, which employs the Wood-Ljungdahl pathway (WLP), to convert CO₂ into acetic acid with reducing equivalents from H₂. Stage 2 bioreactor will contain an axenic strain of *S. cerevisiae* under aerobic conditions to grow biomass (and thus protein) with acetic acid as a carbon source.

We suspect that cobalamin production might occur in *C. ljungdahlii* during the synthesis of acetyl Co-A in the WLP pathway. Therefore, we will investigate whether it is released into the Stage 1 effluent during cell degradation and is eventually transported into Stage 2. This might result in an accumulation of cobalamin in the Stage 2 biomass, thereby, increasing its nutritional value. Moreover, as demonstrated across several studies, *S. cerevisiae* has an inherent capacity to synthesize folate. Hence, to further valorize the microbial product from power-to-protein as power to-food, we will examine the synthesis, transportation, and accumulation of both cobalamin and folate in the two-Stage system. In this preliminary study, we will closely observe the nutritional profile of the biomass obtained from Stage 2 bioreactor and determine future optimization strategies.

Material and Methods

Preparation of working cultures

For preparing a working culture of *C. ljungdahlii* PETC (DSM 13528) that can be used as an inoculum, we revived an anaerobic glycerol stock in a complex media called Robertson's cooked meat media (Supplementary information). This was further transferred into the P7 medium (Supplementary information) to slowly adapt the microbe to a mineral medium. The constituents and preparation for each medium are given within Supplementary Information. Cultures of *C.*

ljungdahlii were prepared in 100 ml serum bottles with a 1:1 headspace volume of N₂ gas. An anaerobic, sterile Fructose/MES solution (2%), an anaerobic 100X vitamin stock (1%), and L-Cysteine hydrochloride (1%) was added before adding the inoculum. Similarly, *S. cerevisiae* S288C (ATCC 204508) was first cultivated into a Yeast Peptone media (per liter: 10 g yeast extract; 20 g peptone) with 10 g L⁻¹ of glucose, from a cryo stock preserved in glycerol. It was then transferred into Yeast nitrogenous base (YN) media (Supplementary Information) with 100 mM of acetic acid as a carbon source. At this point, this culture was used as a working culture for inoculating either the Stage 2 bioreactor or the flasks.

Batch Cultivation Experiments

C. ljungdahlii was grown under batch conditions with two types of vitamin solutions in triplicates: (1) without cobalamin (**Figure 1A**); and (2) with cobalamin (**Figure 1B**). Since, the cultivation is performed with H₂/CO₂ as the substrate, it was carried out in six Duran Pressure Plus™ bottles to enable a pressurized headspace and maximize the availability of the gaseous substrate. Under autotrophic conditions, *C. ljungdahlii* requires at least 0.1 g L⁻¹ of yeast extract for its growth. Consequently, a certain amount of cobalamin was always present in the medium through the addition of yeast extract. The bottles were inoculated with a working culture that had been cultivated under heterotrophic conditions with 250 mM fructose. Before inoculation, the culture was centrifuged (Eppendorf centrifuge 5920R), and the pellet was collected and washed with PBS buffer under anaerobic conditions to remove any acetic acid or ethanol that could be introduced with the inoculum. The microbes grew until the pH turned acidic (< pH 4) due to the production of acetic acid. These cultures were then harvested, and the supernatant was collected under sterile conditions for performing further experiments with *S. cerevisiae*.

The supernatant containing acetic acid which had been obtained from the *C. ljungdahlii* cultures in the previous experiment, were transferred into six 250 ml Erlenmeyer flasks to act as carbon source for *S. cerevisiae*. This was divided into two categories: (1) three out of six flasks contained the supernatant from *C. ljungdahlii* cultures that had been cultivated without any cobalamin (**Figure 1A**); and (2) the rest contained supernatant that were derived from *C. ljungdahlii* cultures and that were grown with cobalamin (**Figure 1B**). To this, an equal volume of two-fold concentrated YN media was added. The pH was set between 5.9-6. The flasks were inoculated with 1% of the total volume from a *S. cerevisiae* working culture in YN media with 100 mM acetic

acid. After 48 h of growth, the cultures reached their stationary phase. The contents of the flasks were harvested, and centrifuged. The pellets and the supernatants were stored at -80°C to preserve the vitamins.

Experimental Setup: Without cobalamin in the vitamin solution

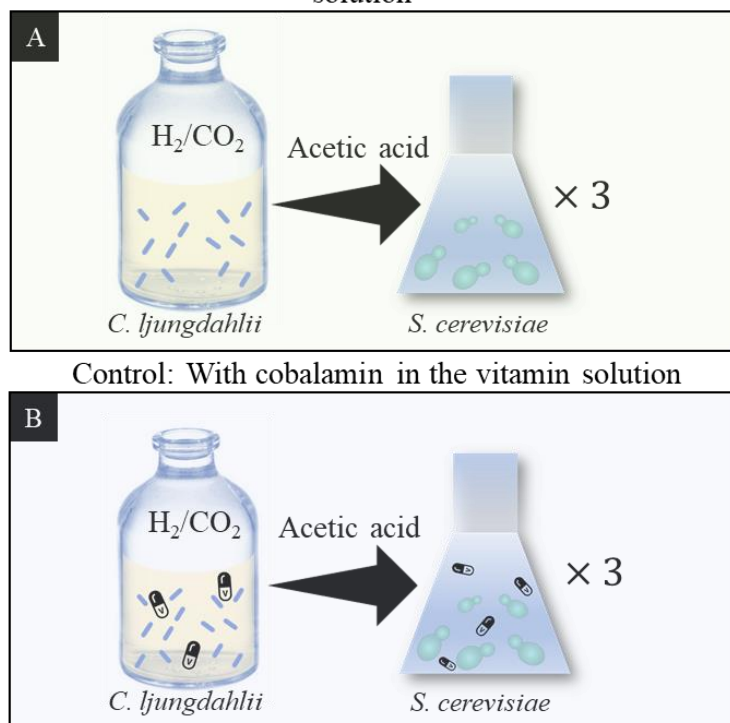


Figure 2: Cultivation of *C. ljungdahliae* and *S. Cerevisiae* under batch conditions in bottle experiments to detect the production of cobalamin and folate. (A) *C. ljungdahliae* was grown in a vitamin solution without any cobalamin in a set of triplicates. The effluent was transferred for the growth of *S. cerevisiae* without any cobalamin. (B) *C. ljungdahliae* was grown with a standard vitamin solution containing cobalamin in set of triplicates. The effluent was transferred for the growth of *S. cerevisiae* without any cobalamin. In the both the cases the media had to be supplemented with 0.1 g L^{-1} of yeast extract that may contain traces of cobalamin.

Power-to-food set-up

The Stage 1 bioreactor was operated under anaerobic conditions to cultivate *C. ljungdahliae* to produce acetic acid. This was conducted in a 2-L Biostat M Chemostat (Brown, Allentown, PA) with a 1-L working volume. The stirring was maintained at 300 revolutions per minute and the temperature was set to 37°C . The H_2/CO_2 gas flow rate ranged between 75 ml min^{-1} to 120 ml min^{-1} , depending on its consumption by the microbes at different stages of the reactor operation. Additionally, we incorporated a Na_2S feed (1 M) and a hollow-fiber cell recycling module to

separate the effluent for the Stage 2 bioreactor and retain the bacterial cells within the Stage 1 bioreactor. The functionality of the Stage 1 bioreactor was highly dependent on the maintenance of strict anaerobic conditions. We equipped it with temperature dependent optical O₂ sensors (PreSens Precision Sensing GmbH, Germany) in four locations where O₂ infiltration was expected- These were: (1) the anaerobic media tank; (2) the tubing through which Stage 1 media enters the bioreactor; (3) the connection between the recycling module; and (4) the headspace of the Stage 1 bioreactor.

For the Stage 2 bioreactor, we obtained a 3-L vessel and operated it with a working volume of 1.5-L to have a 1:1 ratio between the headspace and the media. The temperature and pH were kept constant at 30°C and 5.6, respectively. The vessel was stirred at 150 revolutions per minute with a magnetic stirring unit. The effluent from Stage 1 was continuously provided to Stage 2 through the hollow-fiber recycling module. The mineral salts for the Stage 2 microbe were given by using a bypass feed line. Since the Stage 2 bioreactor was an aerobic system, it was continuously sparged with air at a flow rate of 75-120 ml min⁻¹. The feeding rates of gas in both the bioreactors was always adjusted according to the growth rate of the microbes.

The goal behind this operation was to track cobalamin and folate production and accumulation in the power-to-food system. Unfortunately, we were unable to operate the system at a steady-state conditions without the addition of cobalamin. Therefore, it is important to note here that the bioreactor was always supplied with cobalamin throughout its operation. Details on how both the bioreactors were set up, and eventually integrated into the power-to-food system, has been provided in the Supplementary Information. The operation of Stage 1 and Stage 2 bioreactors was divided into the following three phases.

Phase 1 (0 – 4th day): During this phase, both the reactors were operated under batch conditions. The Stage 1 bioreactor was supplemented with yeast extract to reach a faster growth rate and achieve a higher biomass concentration.

Phase 2 (4th – 10th day): This phase entailed the continuous mode of operation for Stage 1 and Stage 2 bioreactor. The contents of the Stage 1 bioreactor were passed through a hollow-fiber recycling module. At this point, the cells were retained in Stage 1 bioreactor, while the filtered effluent was transported to Stage 2 at a flow rate of 40 ml h⁻¹, resulting in a dilution rate of 0.04 h⁻¹.

¹ in Stage 1 bioreactor. This was supplemented with a three-fold concentrated YN media through the bypass feed line. The effluent line from Stage 2 was operated with a flow rate of 60 ml h⁻¹, that also resulted in a dilution rate of 0.04 h⁻¹ for Stage 2.

Phase 3 (10th – 14th day): In this phase, the bioreactors were operated as described under Phase 2, without the supplementation of yeast extract in the Stage 1 medium. After reaching a high biomass concentration in Stage 1 bioreactor during Phase 1, and successfully initiating the continuous mode of operation for both the bioreactors, we attempted to wean the microbes off yeast extract. As mentioned at the beginning of this section, we were still feeding the Stage 1 bioreactor with cobalamin to maintain its steady-state operation. At this point, the effluent from Stage 1 bioreactor and the biomass from Stage 2 bioreactor were collected for estimating their vitamin composition. Additionally, elimination of yeast extract will minimize the influence of the folates and cobalamin that may enter the reactor system through it.

Sampling

The growth of the microbes in the bottle experiments and reactor experiments was recorded by measuring the optical density of the medium at 600 nm (Nanophotometer NP80, Implen, Germany). Acetic acid was quantified using the high-pressure liquid chromatography (HPLC) (LC20, Shimadzu, Japan) with an Aminex HPX-87H column operated with 5 mM sulfuric acid as an eluent. For the power-to-food system, samples were collected daily from the Stage 1 and Stage 2 bioreactors to check for contamination under phase contrast microscope. All the samples that were collected from the bottle experiments and the power-to-food system to determine the folate and cobalamin content were immediately stored at -80°C. For estimating the quantity and composition of folates and cobalamin, the frozen samples were sent to the Institute of Analytical Chemistry, at the Technical University of Munich in Freising. The quantification of total cobalamin content of the samples was performed in using a microbiological assay.

Analytical Methods

Cobalamin quantification using *Lactobacillus leischmanii*

The sum of all analogues of cobalamin was estimated using a microbiological assay. This assay was carried out with *L. leischmanii*. Due to its length, the protocol for this assay is provided in the Supplementary Information. Biomass samples which were collected from the bottle experiments and reactor experiments, were subjected to cell lysis by treating it with an ultrasonic probe for five minutes. The expected concentration of cobalamin in P7 media was $10 \text{ pg } \mu\text{L}^{-1}$, and therefore we prepared the standard concentrations to be in the range of $6 - 20 \text{ } \mu\text{g L}^{-1}$. We obtained a calibration curve from the growth of *L. leischmanii* to each standard and calculated the total cobalamin present in the sample (**Figure S3, Figure S4, Figure S5**).

Detection of different forms of cobalamin using the HPLC-MS/MS

Each sample was weighed according to the amount specified in **Table S1**. The biomass was boiled in a water bath for 30 minutes in the dark to release all the cobalamin from the cell. The supernatant was further purified using immunoaffinity columns. The eluent was dried under nitrogen at 40°C and was reconstituted in water. The sample was then passed through a filter and collected in HPLC vials for analysis. The samples were qualitatively analyzed using a HPLC (Shimadzu, Kyoto, Japan) in conjunction with a MS/MS, that confirmed the presence of certain forms of cobalamin.

Folate quantification using Isotope labelled standards

Approximately 100 mg of the biomass samples and 500 mg of the effluent or supernatant were taken. ^{13}C -Isotope labelled Internal standards (ITSD) as well as unlabeled standards are added to all the samples for all four analogues of folates: (1) $^{13}\text{C}_5\text{-PteGlu}$; (2) $^{13}\text{C}_5\text{-H}_4\text{folate}$; (3) $^{13}\text{C}_5\text{-5-CH}_3\text{-H}_4\text{folate}$; (4) $^{13}\text{C}_5\text{-5-CHO-H}_4\text{folate}$; and (5) $^{13}\text{C-10-CHO-PteGlu}$. The amount of ITSD that was added is usually evaluated based on the expected concentration within each sample. By using the response of a known concentration of an unlabeled analyte in the HPLC-DAD (Shimadzu, Kyoto, Japan), the concentration of labelled standards in the LC-MS/MS (Shimadzu Nexera X2 UHPLC system, Shimadzu, Kyoto, Japan) was quantified. This step was crucial to accurately determine the recovery of the folates during its purification or extraction.

Folates are usually present in the biological samples in their polyglutamic form. After the addition of the ITSDs, an enzymatic deconjugation of the polyglutamated form to its monoglutamic form was performed using chicken pancrease and rat serum (Striegel *et al.*, 2019). The chicken pancrease breaks down the lipid layer of the cells, while the rat serum degraded the polyglutamic forms into its monoglutamic forms. Afterwards, the folates were further purified through Solid Phase Extraction with an anion exchange column. The eluent from the column was filtered (PVDF, 0.22 μm) and placed in the LC-MS/MS for quantification. After accounting for the recovery of the internal standards, and the folate that was introduced while adding the enzymes, the concentration of all four analogues in each sample was calculated.

Results and Discussion

Stage 1 bioreactor requires optimizations for its stable performance

On day 10 of reactor operation, the Stage 1 bioreactor reached the maximum acetic acid production rate of 22.73 $\text{g L}^{-1} \text{d}^{-1}$ with a supplementation of 0.5 g L^{-1} of yeast extract (**Figure 2A**). In the power-to-protein study, we observed a value of 24 $\text{g L}^{-1}\text{d}^{-1}$ without the addition of yeast extract (Molitor *et al.*, 2019). Hu *et al.* (2016) demonstrated the production of lipids from gaseous substrates in an integrated two-stage system (Hu *et al.*, 2016). In their first bioreactor, *Moorella thermoacetica* was used to produce acetic acid under anaerobic conditions. This acetate was fed to the second bioreactor that was operated under aerobic conditions for synthesizing lipids through the cultivation of *Y. lipolytica* (Hu *et al.*, 2016). With a rate of 21.6 $\text{g L}^{-1} \text{d}^{-1}$, the overall average acetic acid productivity that was observed in this study was comparable to that observed in our Stage 1 bioreactor (Hu *et al.*, 2016). However, in the integrated system presented by Hu *et al.* (2016) the first bioreactor was supplemented with a 20-fold higher concentration of yeast extract than in the Stage 1 bioreactor in the power-to-food system (Hu *et al.*, 2016). With a goal of producing single-cell protein from yeast biomass, an external supplementation of yeast extract would diminish the self-sustenance of the system. The absence of yeast extract imparts a large advantage to the power-to-protein study and consequently to the power-to-food system proposed in this chapter.

Unfortunately, the production of acetic acid in the Stage 1 bioreactor was inhibited because of its exposure to O₂ through the Stage 1 medium into the bioreactor. Consequently, the acetic acid productivity was reduced to 7.67 g L⁻¹ d⁻¹. The O₂ concentration increased from 0.74 mg L⁻¹ on Day 10 to 1.24 mg L⁻¹ on Day 14, resulting in inhibitory effects on the survival and the metabolism of the *C. ljungdahlii*. The biomass concentration in the Stage 1 bioreactor was based on the cell dry weight (CDW) and followed a similar trend. It reached a maximum of 1 g CDW, and then decreased to 0.5 g on the final day of the operation because of O₂ infiltration. Since the Stage 1 bioreactor had just begun Phase 3 of the operation, the impact of the leak was exaggerated by the removal of yeast extract from the media. An exposure to O₂, along with the stress of adapting to a different media composition, affected the recovery of *C. ljungdahlii*, ultimately halting the activity of the Stage 1 bioreactor. Strict anaerobic conditions in the Stage 1 bioreactor were crucial for the survival and optimal functioning of the Stage 1 bioreactor. Since this bioreactor was also responsible for the administration of a carbon source to Stage 2, any change in the growth or production rate may have a negative influence on the growth behavior of *S. cerevisiae*. During this run, an exposure to O₂ was caused by a human error. In the future, we will take precautionary measures to manage the bioreactor run in addition to utilizing gas-tight fittings and connecting lines consisting of stainless steel.

Based on our findings, we have gathered several strategies for adjusting the operating parameters and reactor design to achieve higher acetic acid productivity. A higher dilution rates for Stage 1 may result in an even higher productivity of acetic acid. Mock et al. (2015) achieved an acetic acid production rate of 74.4 g L⁻¹ d⁻¹ with a ten times higher dilution rate of 0.2 h⁻¹ (Mock *et al.*, 2015) compared to our study. We attempted to test this in a stand-alone operation of the Stage 1 bioreactor, and we were able to see an acetic acid production rate of 10.25 ± 3.63 (n = 36), 13.92 ± 4.04 (n = 18), and 19.47 ± 0.84 (n = 2) g L⁻¹ d⁻¹ for dilution rates of 0.03, 0.04, and 0.05 h⁻¹ respectively (unpublished results). Furthermore, incorporating other design ideas into the power-to-food system which contributes to a more efficient H₂ mass transfer, will result in higher acetic acid production rates by enhancing the availability of reducing equivalents for CO₂ fixation. These solutions can be in the form of customized sparging stones to administer the H₂/CO₂ gas bubbles with a smaller size and a higher interfacial area (Riggs & Heindel, 2006). Alternatively, Stage 1 could be operated under pressurized conditions to achieve higher microbial growth and product formation rates (Van Hecke *et al.*, 2019).

The power-to-protein study already demonstrated that *S. cerevisiae* can grow when acetic acid is provided as a carbon source (Molitor *et al.*, 2019). We obtained a carbon yield of 25% as yeast biomass in their proof-of-concept experiment (Molitor *et al.*, 2019). Although, we need a 14-times increase in the protein productivity to arrive at industrially relevant rates. Hu *et al.* (2016) observed an average productivity of $18 \text{ g L}^{-1} \text{ d}^{-1}$ with *Y. lipolytica* (Hu *et al.*, 2016). The power-to-protein study only achieved an average productivity of $3.9 \text{ g L}^{-1} \text{ d}^{-1}$. However, it should be noted that Hu *et al.* (2016) had different operating conditions during their integrated run: (1) their first bioreactor was fed with 20-times higher concentration of yeast extract (Hu *et al.*, 2016); which mitigates the economic value of their product; and (2) they also provided their Stage 2 bioreactor with a hollow fiber recycling module to retain the cells (Hu *et al.*, 2016).

Table 3: Growth data for the Stage 1 and Stage 2 bioreactors under different Phases of operation. Data is given as the average value for each phase \pm standard deviation

Stage 1 bioreactor			Stage 2 bioreactor			
Phase	Duration (d)	Acetic acid production ($\text{g L}^{-1} \text{ d}^{-1}$)	Biomass (g CDW)	Time (d)	Acetic acid consumption ($\text{g L}^{-1} \text{ d}^{-1}$)	Biomass (g CDW)
I	4	1.44 ± 0.95 (n=4)	0.20 ± 0.13 (n=4)	5	0.13 (n=1)*	0.73 ± 1.39 (n=5)
II	4	10.12 ± 8.12 (n=4)	0.60 ± 0.42 (n=4)	4	3.04 ± 1.75	2.25 ± 0.54 (n=4)
III	5	15.04 ± 5.82 (n=5)	0.68 ± 0.22 (n=5)	5	4.00 ± 3.80	2.76 ± 0.63 (n=5)

*We saw acetic acid consumption in Stage 2 bioreactor on the 3rd day of Phase I. Until then, the microbes were present in their lag phase of growth.

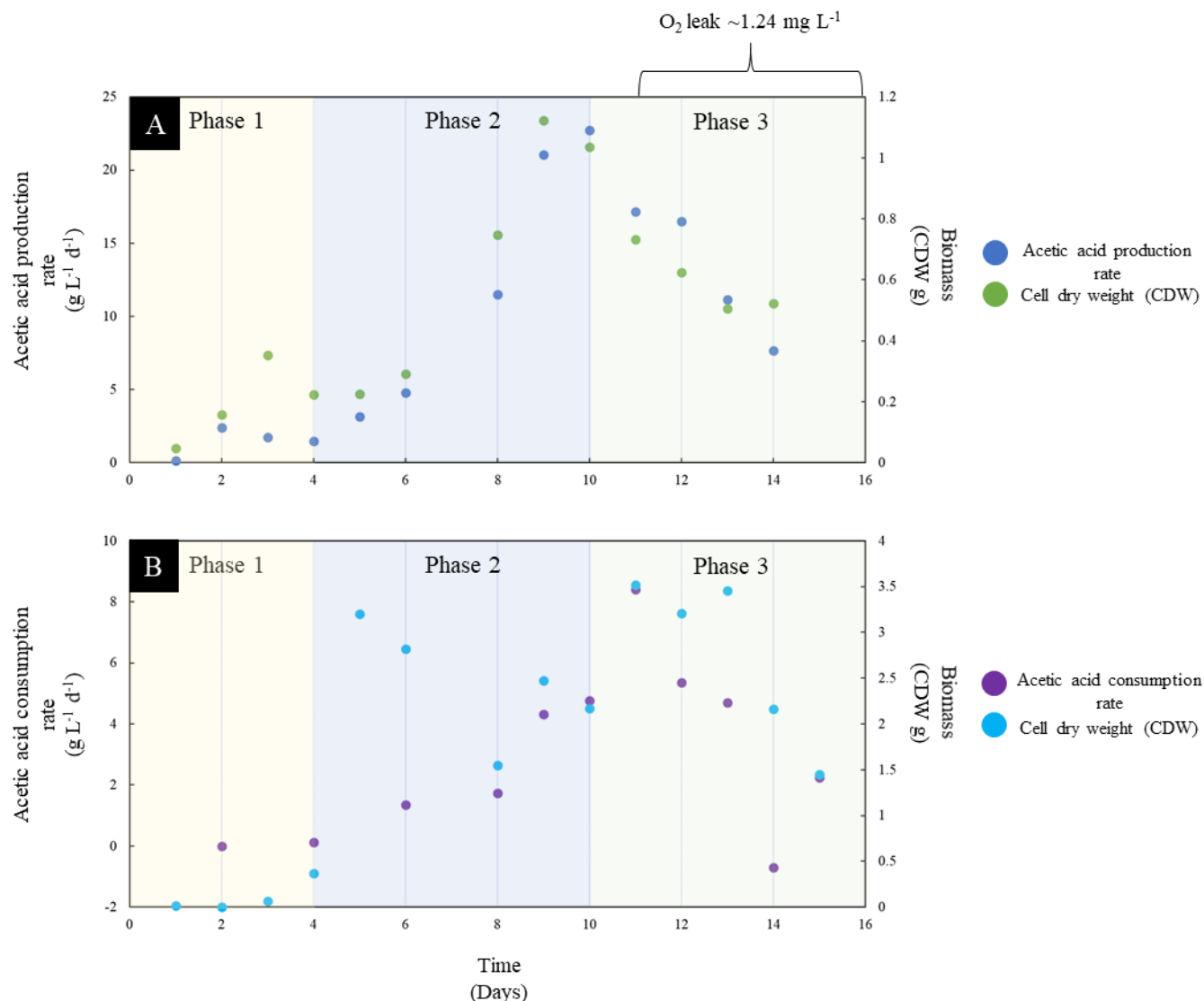


Figure 3: Reactor performance of Stage 1 and Stage 2 bioreactors in the power-to-food system for an operation period of 15 days. The operating period was divided into Phases 1-3 based on the medium composition. The system entered continuous mode of operation in Phase 2 on Day 4 and after samples were collected for quantifying vitamins in Phase 3 after the removal of yeast extract. (A) Acetic acid and biomass production rates in terms of cell dry weight (g) for Stage 1 bioreactor. An O_2 leak which started on from Day 11, reduced the acetic acid and biomass production rate. (B) Acetic acid consumption rate and biomass production for Stage 2.

Tracking cobalamin production and accumulation

One of the target products for us from the power-to-food system was cobalamin. We performed an LC-MS/MS analysis to confirm the presence of cobalamin and detect its different forms. In the meantime, we quantified its concentration by conducting a microbiological assay. The LC-MS/MS analysis revealed hydroxycobalamin and cyanocobalamin to be the predominant forms in most of

the samples (**Figure S1, Figure S2**). Unfortunately, we are lacking quantitative data on the concentration for each form because the microbiological assay is unable to differentiate between them. Previous experiments conducted in our lab, while developing the cobalamin protocol, revealed that the different forms of cobalamin have a similar effect on the growth of *L. leichmannii*. Therefore, in case, the sample contains a mix of different forms, the assay will give a cumulative value for all the bioactive forms in the sample without any information on their distribution.

Yeast extract and cobalamin supplementation obscures the detection of cobalamin from *C. ljungdahlii*

The bottle experiments always contained traces of cobalamin through the addition of 0.1 g L⁻¹ of yeast extract to initiate the growth of the cultures under autotrophic conditions. Nevertheless, we aimed to capture whether it is synthesized in a substantial amount by *C. ljungdahlii*. Therefore, we provided the microbes with two types of vitamin stock solutions. The only difference between these vitamin solutions was the addition of cobalamin (**Figure 1**). In the first set of experiments, the cultures were provided with a vitamin stock solution that was prepared without any cobalamin (**Figure 1A**). In the second set of experiments, the cultures were provided a standard vitamin stock solution containing 50 µg L⁻¹ of cobalamin (**Figure 1B, Table 2**). The biomass yield from both the experimental conditions under were low (**Table S3**). This was most likely due to autotrophic growth under batch fermentation condition, where *C. ljungdahlii* is limited by substrate availability due to a lower solubility of H₂ gas. The biomass from both experimental conditions were harvested for quantifying cobalamin using the microbiological assay. In the first experiment that was conducted without cobalamin in the vitamin solution (**Figure 1A**), the *C. ljungdahlii* cultures were centrifuged to retrieve its biomass for quantifying cobalamin, and the supernatant was taken for the flask experiments with *S. Cerevisiae*. This resulted in an estimation of 8 µg g⁻¹ of cobalamin in the biomass (**Table 3**). Since, cobalamin is present in such a small amount in this experiment, we suspect that it must be obtained from traces of cobalamin that were introduced because of the addition of 0.1 g L⁻¹ of yeast extract to media. Unfortunately, for the cultures that were grown with a vitamin solution containing cobalamin (**Figure 1B**), the biomass was insufficient to perform a microbiological analysis.

It is also likely that, the synthesis of minor concentrations of cobalamin in the Stage 1 bioreactor is masked by its supplementation in a concentration of 50 µg L⁻¹ in the Stage 1 media (**Table 2**).

From the data collected under Phase 3, i.e., the 10th – 12th day of reactor operation, we quantified a flux of 18 $\mu\text{g L}^{-1} \text{d}^{-1}$ (**Table 2, Figure S2, Table S3**) in Stage 1. We suspect that this value represents the cobalamin present in the Stage 1 media. Even if they are capable of its *de novo* synthesis, it is possibly made in trace amounts and utilized immediately in metabolic reactions. Although, yeast extract was removed from the Stage 1 media in Phase 3, it still contained cobalamin to maintain the operation of the bioreactor system. There might still be traces of this yeast extract from Phase 2 either within the cells of *C. ljungdahlii* or in the supernatant of the Stage 1 bioreactor. Although, this speculation warrants further investigation with quantitative measurements from an instrumental analysis.

In the next operation of the Stage 1 bioreactor, it is important to use the yeast extract from a fixed manufacturer throughout the entire run. The reason being that the addition of cobalamin during the preparation of yeast extract is unique to each brand. Additionally, it is imperative to perform a regular, quantitative analysis of the cobalamin concentration in the media after the addition of yeast extract. The bioavailability or the distribution of its different forms cobalamin in the yeast extract may vary with each media preparation step. For instance, exposure to a high temperature during sterilization process might impact the bioactivity of cobalamin. This information would be crucial to derive its path through the power-to-food system.

The biomass of *S. cerevisiae* from Stage 2 contained trace concentrations of cobalamin.

Once, *C. ljungdahlii* was cultivated under batch conditions in bottles, the supernatant containing acetic acid was provided to *S. cerevisiae*. In addition to acting as a source of acetic acid which was the only source of carbon, we want to determine whether the supernatant could potentially provide cobalamin and accumulate into the biomass of *S. cerevisiae*. As has been stated in the earlier sections, these experiments were conducted two types of vitamin solutions. One was prepared without any cobalamin, while the other followed a standardized recipe and contained cobalamin (**Figure 1**). According to the microbiological assay, cobalamin was absent in the supernatant taken from *C. ljungdahlii* culture that was prepared with a vitamin solution without cobalamin. Unfortunately, because of a low concentration of acetic acid from *C. ljungdahlii* in this setup, the amount of biomass retrieved from *S. cerevisiae* was insufficient to proceed with the

microbiological assay. This further suggests that the detection of cobalamin in the experiment conducted with a standard vitamin solution is most likely from the medium.

The microbiological assay detected a concentration of $21.5 \mu\text{g g}^{-1}$ in the biomass and $15 \mu\text{g g}^{-1}$ in the effluent from *S. cerevisiae* grown in the supernatant from *C. ljungdahlii* prepared with a vitamin solution containing cobalamin (**Table 3**). Although, we suspect that this was procured from the supplementation of either yeast extract or cobalamin instead of being produced by *C. ljungdahlii*. We calculated the volumetric concentration of cobalamin to be $97.4 \mu\text{g L}^{-1}$ in the biomass. If we compare this concentration to the amount of cobalamin that was added to the media, we observe a two-fold accumulation with a biomass concentration of 0.22 g L^{-1} . On the contrary, the *S. cerevisiae* biomass obtained from the Stage 2 bioreactor contained only $3 \mu\text{g g}^{-1}$ ($0.004 \mu\text{g L}^{-1}$) of cobalamin compared to $18.82 \mu\text{g L}^{-1}$ estimated for the reactor effluent. This implies that there may have been an uptake of cobalamin into the cells of *S. cerevisiae*, however, it did not result in an accumulation.

Altogether, due to the insufficient biomass concentrations observed in the batch experiments and the addition of yeast extract, the results pertaining to cobalamin production by *C. ljungdahlii* and accumulation by *S. cerevisiae* are inconclusive. Additionally, these results reveal a key limitation of the microbiological assay for quantifying the total amount of cobalamin. If these results were accompanied by their quantification using an LC-MS/MS, we would have successfully isolated the false positive signal obtained from the yeast extract. Furthermore, it is important to be cautious while analyzing the different forms of cobalamin. As only a few of the different forms of cobalamin are suitable for human food, we might overestimate its bioavailability in the Stage 2 biomass by only considering the evaluation from the microbiological assay. Moreover, degraded biomass, or even other biological samples may contain pseudo-analogs. Pseudo-analogs are compounds that resemble the structure of a cobalamin molecule without its biological functionality. It may yield a positive effect on the growth response of a *L. leischmanii*, leading to an overestimation of the actual content of cobalamin in the sample. We propose that in the future, a small fraction of the total sample collected should be periodically validated with an instrumental analysis to confirm the presence of relevant forms.

Elimination of cobalamin is necessary for detecting cobalamin production.

Once the reactor system is fully optimized and all the technical issues encountered in this operation by Stage 1 bioreactor have been resolved, we will attempt to enter Phase 4. This would entail the operation of the system without any supplementation of cobalamin in the media. There is a chance the microbes will initiate a higher productivity of cobalamin because of its absence in the media. It is now realized that acetogens are capable of growth without the addition of cobalamin (Annan *et al.*, 2019). They harbor the genes required for its biosynthesis (Köpke *et al.*, 2010). If the reactor can operate without cobalamin, we can explore the scope of its production under autotrophic conditions. It is likely that the formation of cobalamin by the Stage 1 bioreactor is masked by the incorporation of either yeast extract or cobalamin to the media. Therefore, to capture the extent of its production by *C. ljungdahlii*, it is mandatory to quantify and detect the different forms of cobalamin once the reactor has attained steady state after the elimination of yeast extract and cobalamin.

So far, we have failed to operate the Stage 1 bioreactor under Phase 4 during which the system is free of any yeast extract or cobalamin. Our previous experiments under continuous conditions in a reactor have shown that *C. ljungdahlii* is unable to surpass continuous operation after the elimination of both cobalamin and yeast extract. Although, there is evidence that *C. ljungdahlii* can sustain itself in a growth medium that is not supplemented with cobalamin (Annan *et al.*, 2019), we have only been to accomplish this in a bottle experiment with H₂/CO₂ with 0.1 g L⁻¹ of yeast extract. *C. ljungdahlii* is subjected to severe stress whenever the reactors are operating in continuous mode. These might be physical causes of stress, such as an incoming O₂ leak in the lines, or the shear stress created by their flow through the recycling module. This is succeeded by other biological causes of stress such as the adaptation of the microbe to a change in the media composition. We speculate that the removal of cobalamin from the media prior to their full recovery, exacerbates the negative effects resulting in their inactivity or death. Consequently, this would hinder the transition of the Stage 1 bioreactor into Phase 4 conditions. Most of the negative consequences exerted by such changes can be minimized by addressing the current technical difficulties. A sound bioprocessing unit may expediate the recovery of microbes, allowing us to transit into Phase 4. We are currently in the process of achieving this.

Tracking folate production and accumulation

S. cerevisiae can produce folate while using acetic acid as a carbon source

The Stage 1 medium was the only external source of folate in the power-to-food system. In the continuous mode of operation under Phase 2 and Phase 3, we provided folate at the rate of $20 \mu\text{g L}^{-1} \text{d}^{-1}$ to the Stage 1 bioreactor (**Table 2**). These folates would then enter the Stage 2 bioreactor during the transfer of the Stage 1 effluent through cell recycling module. Since the Stage 2 bioreactor also contains its own feed for all the necessary mineral salts, this would further dilute the folate, ultimately resulting in a final flux of only $6 \mu\text{g L}^{-1} \text{d}^{-1}$ of folate (**Table 2**). If we compare these values to the quantified concentration in the LC-MS/MS, the results are suggestive of folate synthesis by *S. cerevisiae* in the Stage 2 bioreactor. As per the analysis with the LC-MS/MS, the Stage 1 bioreactor received folate at a rate of $30 \mu\text{g L}^{-1} \text{d}^{-1}$ from the Stage 1 media (**Table 2**). This is equivalent to the theoretical flux of folate that was expected from the media (**Table 2**). With a standard deviation of $10 \mu\text{g L}^{-1}$ (**Table S4**) between the technical duplicates, we conclude that the difference between the quantified and theoretical values was caused by an instrumental error. The measurement of folate within the biomass of the Stage 2 bioreactor yielded promising results. We observed a productivity of $16.47 \mu\text{g L}^{-1} \text{d}^{-1}$ or $5.85 \mu\text{g g}^{-1} \text{d}^{-1}$ after accounting for the biomass yield of 1.7 g L^{-1} in the Stage 2 bioreactor. This was also evident in the bottle experiments where *S. cerevisiae* contained $\sim 60 \mu\text{g L}^{-1}$ in the biomass taken from the acetic acid containing supernatant of *C. ljungdahlii*.

Although, it is already known that *S. cerevisiae* can produce folates, the scope of this study was to determine whether it is still possible when the microorganism is grown with acetic acid as a carbon source. During its growth on acetic acid, *S. cerevisiae* initiates the gluconeogenesis pathway instead of their preferred pathway of glycolysis (Kelly, 2004). They synthesize hexoses by first converting acetic acid to oxalate and then to phosphoenolpyruvate (Kelly, 2004). As a result of the stress caused by an anabolic pathway of carbon assimilation, the carbon flow into folate synthesis might get affected, yielding a lower content of folate in the microbial cells. Nonetheless, folate production is evident in *S. cerevisiae* under both batch and continuous fermentation conditions. To the best of our knowledge, this is the first study demonstrating folate biosynthesis from yeasts cultivated in acetic acid. If we follow the flux of folate as shown in **Table 2**, we can state that: (1) consistent to the observations made for cobalamin, Stage 1 bioreactor is not an ideal source of

folate for Stage 2 bioreactor; and (2) *S. cerevisiae* is capable of folate prototrophy in the presence of acetic acid from Stage 1 bioreactor. The difference in the cell physiology between the batch experiments in bottles and the power-to-food reactor might have influenced the folate concentration of the cells. This has been discussed in more detail in the following sections.

Presence of favorable forms of folate for biofortification

The concentration of all folates in a food product is always a composition of different concentrations of each analogue. Upon consumption, the bioactivity of each of these would then determine its effect on human health. Classification of its forms are performed based on the functional group that is attached to the Pteric acid entity. This in turn affects their chemical properties and functionality. Straeten *et al.* (2017) declared the 5-CH₃-H₄ folate to be the most desirable form of folate for fortifying food products due to its stability and bioactivity. 5-CH₃-H₄ folate constituted for roughly 20 % of the total folates quantified in the Stage 2 biomass (**Figure 3**). The H₄ folate accounts for roughly 33 % of the total folates (**Figure 3**). Another dominant form of folate in all our samples is 5-CHO-H₄ folate (**Figure 3**). It is a precursor for the synthesis of 5-CH₃-H₄ folate that in turn acts as a co-factor for purine synthesis. The monoglutamic form, PteGlu, is absent in most of the samples (Maliepaard *et al.*, 2001). This is expected, as the folates that are naturally present in food products mostly exist as polyglutamates. The composition of the different folate analogues observed for *S. cerevisiae* in Stage 2 is consistent with that found in the other studies (Hjortmo *et al.*, 2005).

Several parameters determine the folate composition in a microbe. It could be influenced by the growth conditions, media composition, and nutrient availability (Revuelta *et al.*, 2018). For instance, the biomass samples collected from *S. cerevisiae* in bottle experiments that were grown in two different experimental conditions (**Figure 1**), showed comparable amounts of folate, but a different distribution of the analogues (**Figure 3**). The culture was grown in the sterile effluent of *C. ljungdahlii* in the absence (**Figure 1A**) and presence of cobalamin (**Figure 1B**). This difference in the media composition might have influenced the folate composition of the samples. This was especially evident for H₄ folate that accounted for 20% of the total distribution in the effluent without cobalamin in comparison to 51% with cobalamin (**Figure 3**). From the standpoint of valorizing the Stage 2 biomass by demonstrating the presence of folates, it is worth further

investigating the different operating conditions that enhance synthesis of the favorable forms such as 5-CH₃-H₄ folate and H₄ folate.

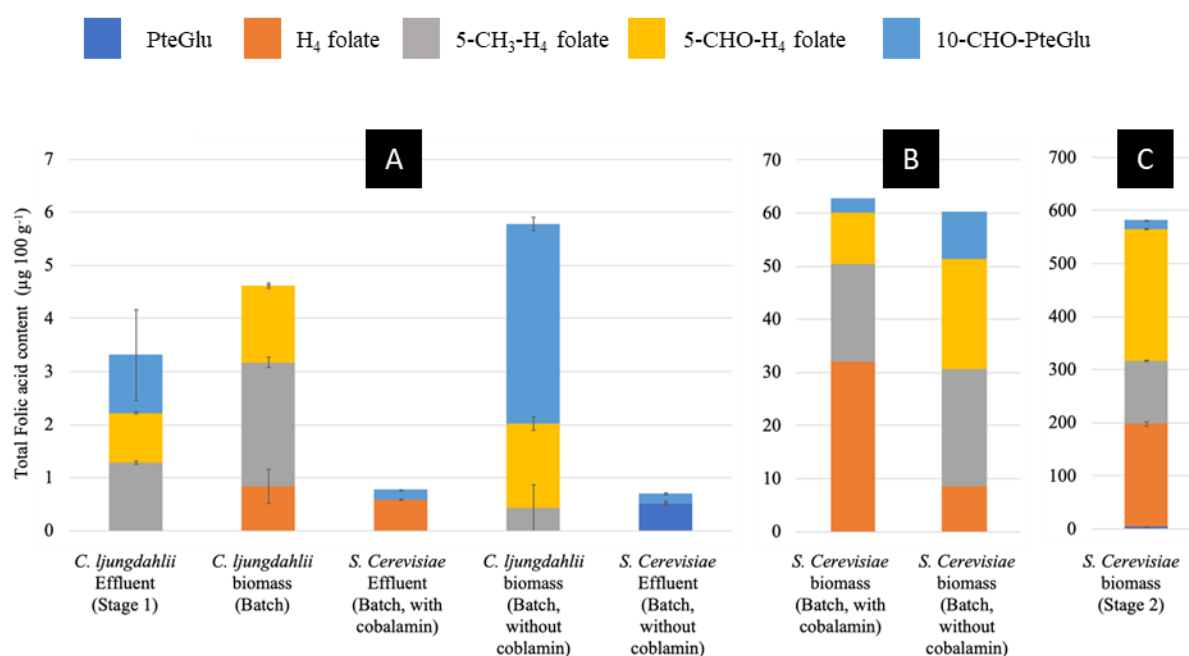


Figure 4: The distribution of all the forms of folate in $\mu\text{g } 100 \text{ g}^{-1}$ within each sample that was quantified with LC-MS/MS. Each extraction was conducted in duplicates and the standard deviation is given in **Table S4** under Supplementary Information. Each color represents specific form of folate. (A) All the experiments conducted under batch conditions as well the Stage 1 effluent showed minute concentrations of folate except for the biomass obtained from *S. cerevisiae* (B). (C) The folate concentration in the biomass from *S. cerevisiae* grown in Stage 2. The H₄ folate, 5-CH₃-H₄ folate and 5-CHO-folate are the predominant forms.

Intracellular folate content in the microbial cells depends on the growth phase of *S. cerevisiae*

Hjortmo *et al.* (2008) compared the folate content in *S. cerevisiae* in three media types: yeast peptone dextrose; molasses medium; and synthetic medium (Kazamia *et al.*, 2012). They observed the largest difference in the intracellular folate content between the different phases of growth when *S. cerevisiae* was cultivated in synthetic medium (Sofia Hjortmo *et al.*, 2008). Hjortmo *et al.* (2008) inferred from their studies in chemostats that the linear increase in the growth rate was proportional to the amount of intracellular folate that was extracted. They propose that high growth rates or the respiro-fermentative growth period appears to be the most ideal condition for achieving optimal folate productivity. This information is fundamental for the operation of the Stage 2 bioreactor, including the biosynthesis of folate. It emphasizes the importance of constantly

maintaining *S. cerevisiae* at their optimal growth rate in the Stage 2 bioreactor to achieve high intracellular folate concentrations. It is pivotal to closely study the correlation of its growth phase to the amount of folate produced. This investigation will aid in the identification of the respiro-fermentative growth period for *S. cerevisiae* with acetic acid, thereby, helping us attain the maximum intracellular folate productivity.

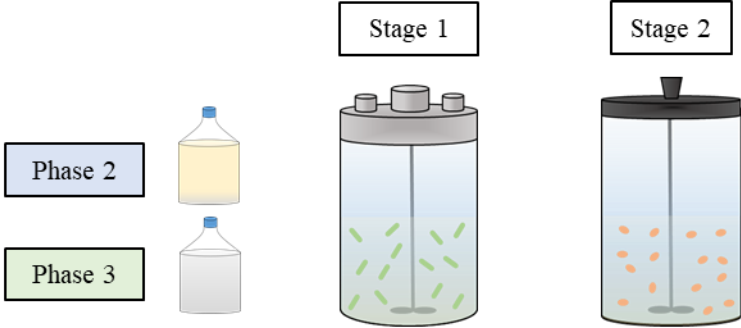
We can refer to the observations by Hjortmo *et al.* (2008) to justify the difference in the total folate concentration between the biomass obtained from the bottle experiments and the one harvested from the Stage 2 bioreactor. Under ideal conditions we expect a maximum growth rate of 0.05 h^{-1} (**Figure S5**) Even though, the growth rate in the Stage 2 bioreactor was still sub-optimal with a value of 0.02 h^{-1} , the growth rate in the bottle experiments were even lower at a rate of 0.01 h^{-1} . Moreover, the state of the cells is also influenced by the incoming concentration of acetic acid from the Stage 1 bioreactor. Observation of a higher growth rate can be linked to an abundance of substrate. The *S. cerevisiae* cultures in bottle experiments received an average of 1.79 ± 0.28 (n=6) g L^{-1} (**Table 2**) from *C. ljungdahlii* that was cultivated autotrophically in bottle experiments. Meanwhile, the Stage 1 bioreactor in the power-to-food system, provided $14.94 \pm 3.30 \text{ g L}^{-1} \text{ d}^{-1}$ (n=3) (**Table S5**) of acetic acid to the Stage 2 bioreactor. It is likely that the microbes were limited by the availability of the carbon substrate in the bottle experiments, ultimately resulting in a lower content of folates in the biomass.

These observations unravel the sensitivity of an integrated system such as power-to-food system. We are restricted to higher dilution rates to provide enough acetic acid to the Stage 2 bioreactor. However, low acetic acid productivity will result in cell-wash out. Moreover, high acetic acid productivity might cause substrate inhibition. Therefore, we would recommend a hollow-fiber cell recycling module for the Stage 2 bioreactor to enable intermittent cell retention (Hu *et al.*, 2016). From our experiments, we can state that *S. cerevisiae* is capable of synthesizing folate when provided with an unconventional carbon source such as acetic acid. However, there is a strong correlation of the intracellular folate concentrations to the physiology of the microbes. During the integrated operation of the system, the Stage 1 bioreactor is responsible for the continuity of optimal growth conditions in the Stage 2 bioreactor by providing the growth substrate. Maintaining this delicate balance between the two bioreactors is challenging and requires major modifications in the current system. So far, we can only conclude that initiating the continuous mode of operation

in the Stage 2 bioreactor at the optimal growth rate of *S. cerevisiae*, while maintaining a consistent supply of acetic acid from the Stage 1 bioreactor is imperative for preserving the intracellular productivity of folates.

Summary of cobalamin and folate quantification in the power-to-food system

Table 4: Each column shows the amount of yeast extract, cobalamin and folate that should be theoretically present in the media, Stage 1 bioreactor, and Stage 2 bioreactor in all three Phases of the reactor operation. Additionally, the amount of cobalamin and folate that was quantified using the instrumental analysis and the MBA during the Phase 3 of operation for Stage 1 effluent and Stage 2 biomass is shown alongside its theoretical volumetric concentrations.

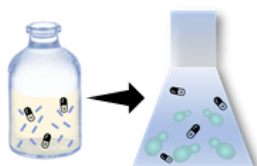


	Media	Stage 1	Stage 2
Phase 1 (Batch)	Yeast extract: 0.75 g L ⁻¹ Cobalamin: 50 µg L ⁻¹ Folic acid: 20 µg L ⁻¹	Yeast extract: 0.75 g L ⁻¹ Cobalamin: 50 µg L ⁻¹ Folic acid: 20 µg L ⁻¹	
Phase 2 (Continuous)	Yeast extract: 0.75 g L ⁻¹ Cobalamin: 50 µg L ⁻¹ Folic acid: 20 µg L ⁻¹	Yeast extract: 0.72 g L ⁻¹ d ⁻¹ Theoretical value for cobalamin: 50 µg L ⁻¹ d ⁻¹ Theoretical value for Folic acid: 19 µg L ⁻¹ d ⁻¹	Yeast extract: 0.24 g L ⁻¹ d ⁻¹ Theoretical value for cobalamin: 16 µg L ⁻¹ d ⁻¹ Theoretical value for Folic acid: 6 µg L ⁻¹ d ⁻¹
Phase 3 (Continuous) <u>Samples were collected for cobalamin and folate quantification</u>	Cobalamin: 50 µg L ⁻¹ Folic acid: 20 µg L ⁻¹	Theoretical value for cobalamin: 50 µg L ⁻¹ d ⁻¹ Theoretical Folic acid: 19 µg L ⁻¹ d ⁻¹ <u>Estimation in the Effluent</u> Cobalamin via MBA ^a : 18 µg L ⁻¹ d ⁻¹ Folic acid via LC-MS/MS ^b : 30 µg L ⁻¹ d ⁻¹	Theoretical value for cobalamin: 16 µg L ⁻¹ d ⁻¹ Theoretical Folic acid: 6 µg L ⁻¹ d ⁻¹ <u>Estimation in the Biomass</u> Cobalamin via MBA ^a : 8 µg L ⁻¹ d ⁻¹ Folic acid via LC-MS/MS ^b : 16.47 µg L ⁻¹ d ⁻¹

^a Errors observed during the microbiological assay of this sample is shown in **Table S2** under Supplementary Information. The chromatogram derived during its qualitative analysis in the MS is shown in **Figure S1**. ^b Folate extraction from this sample was performed in a set of duplicates and the error is between them is shown under **Table S4**

Summary of cobalamin and folate quantification in batch experiments

Table 5: A summary of the cobalamin and folate estimations from the experiments performed under batch conditions. The acetic acid concentration is given as the average value for the triplicates. The quantification of cobalamin and the distribution of its forms determined by the MBA and the HPLC-MS/MS for each sample. This is accompanied by the quantification of folate in all the samples by LC-MS/MS.



Sample Description	Acetic acid concentration (g L ⁻¹)	Cobalamin		Folates ^c
		MBA ^a	HPLC-MS ^b	
<i>C. ljungdahlīi</i> biomass (with Cobalamin)	1.91±0.27 (n=3)	Insufficient biomass		0.05 µg g ⁻¹
<i>S. cerevisiae</i> effluent (with cobalamin)	< 1 mM ^d	14.75 µg L ⁻¹	<ul style="list-style-type: none"> • Hydroxycobalamin • Cyanocobalamin 	0.01 µg g ⁻¹
<i>S. cerevisiae</i> biomass (with cobalamin)	< 1 mM ^d	21.45 µg g ⁻¹	<ul style="list-style-type: none"> • Hydroxycobalamin • Cyanocobalamin • Indistinguishable peaks/background noise of adenosylcobalamin and methylcobalamin 	0.63 µg g ⁻¹
<i>C. ljungdahlīi</i> biomass (without cobalamin)	1.60±0.23 (n=3)	0.81 µg g ⁻¹	<ul style="list-style-type: none"> • Hydroxycobalamin • Cyanocobalamin 	0.06 µg g ⁻¹
<i>S. cerevisiae</i> effluent (without cobalamin)	< 1 mM ^d	Not detected		0.01 µg g ⁻¹
<i>S. cerevisiae</i> biomass (without cobalamin)	< 1 mM ^d	Insufficient biomass		0.60 µg g ⁻¹

^a The calculated biomass yield and the error in the measurements are discussed in the Supplementary Information under **Table S3**. ^b The peaks observed in the MS for each form of cobalamin for all the samples is shown in the Supplementary Information under **Figure S2**. ^c The error observed during folate extraction protocol that was performed in duplicates as well as its quantification has been shown in **Table S4** in the Supplementary Information. ^d These values were below the limit of detection of 1 mM in the HPLC because of acetic acid consumption by the microbes

Conclusion

***C. ljundahlii* is incapable producing cobalamin in substantial amounts**

Based on our findings from the bottle experiments and the power-to-food system, we can primarily form two major conclusions. First, our original research question about cobalamin production from *C. ljundahlii* remains unresolved. The measurement of cobalamin in the effluent of the Stage 1 bioreactor and the biomass of the Stage 2 bioreactor, is because of its addition or the supplementation of yeast extract into the Stage 1 medium. This implies that *C. ljundahlii* is unable to produce cobalamin at a high concentration. This reduces the likelihood of any microbe-mediated biofortification of cobalamin from *C. ljundahlii* in the biomass of Stage 2 bioreactor. Second, we observed nearly a two-fold accumulation of cobalamin within the *S. cerevisiae* biomass. Nonetheless, we still require an in-depth investigation of the cell physiology and transporter proteins in the cell membrane of *S. cerevisiae* to discern why this observation was only witnessed in the bottle experiments.

We have also learned that in the future operations of the power-to-food reactor, it is crucial to regularly monitor the flux of cobalamin from the Stage 1 medium into the two bioreactors via LC-MS/MS and microbiological quantification. By doing so, we will be able to detect the production of trace concentrations of cobalamin by *C. ljundahlii*, as well as the amount of cobalamin introduced with yeast extract. Although, during Phase 3 of operation, yeast extract was eliminated from the Stage 1 media, it might have been present in trace amounts because of its addition in Phase 1 and Phase 2. This must have influenced the detection of the cobalamin in both analytical procedures. For future experiments, we should ideally wait for three hydraulic retentions¹ periods before collecting samples from the reactor for quantifying vitamins. This would ensure that all the yeast extract has been completely washed out of the two reactors. Additionally, since its concentration might differ from one manufacturer to the other, it is advisable to use a specific one throughout the course of the experiment.

¹ The hydraulic retention time is a measure of the average length of time that a soluble compound remains in a bioreactor

***S. cerevisiae* is capable of folate bioproduction with acetic acid as a carbon source**

There is no evidence of microbe-mediated biofortification of folate through *C. ljungdahlii* in Stage 1, however, *S. cerevisiae* was capable of folate bioproduction while using acetic acid as a carbon source. We also witnessed a variation in the total intracellular concentration of the folates amongst all the samples. This is because the microbes in each sample might be present in different physiological state. Nevertheless, we can implement these findings from the current power-to-food run to further optimize the system. For instance, we know that in an integrated system, such as power-to-food, a consistent supply acetic acid is from Stage 1 bioreactor of utmost importance to the health of the microbes in the Stage 2 bioreactor. Therefore, we should consider having an external supply of acetic acid, that is only activated in case the productivity in the Stage 1 bioreactor deteriorates. This will prevent any unwanted alterations in the growth phase of the microbes residing in the Stage 2 bioreactor, thereby, stabilizing the production of folates. On the contrary in case there is a very high productivity of acetic acid in Stage 1 bioreactor, it might have a toxic effect on the metabolism of *S. cerevisiae*. To account for this, a cell recycling module can be integrated into the Stage 2 bioreactor design to dilute the effluent while retaining the cells. This was also proposed in the integrated two-stage system of Hu *et al.* (2016) for lipid production from *Y. lipolytica*.

The overall performance of power-to-food is highly dependent on the optimal functioning and reliability of both the bioprocessing units. Cultivation of *C. ljungdahlii* in the Stage 1 bioreactor is challenging because it requires strict anaerobic conditions. In parallel to maintaining anaerobic and sterile conditions within the fermentation vessel, we must preserve similar conditions in the hollow-fiber membrane for cell-recycling. Often, O₂ infiltration at this location in the power-to-food system, led to the termination of Stage 1 bioreactor. It is crucial that we adapt our current system to these requirements to enable its operation for a longer period. In a study such as ours, testing various growth conditions in a reproducible way is key to validate its findings. Any technical issue that changes its biological attributes renders our speculations inconclusive and makes our data unaccountable. This is especially true for vitamins as they are highly sensitive. Therefore, to develop a detailed picture of the folate and cobalamin fluxes in the power-to-food system, we need to make it technically infallible.

Nutritional prospects of the power-to-food system

To appraise the marketability as well as the suitability of the biomass from power-to-food with its estimated nutritional profile from this study, we compared it to its more traditional alternatives (**Table 4**). The quantities of protein, folate, and cobalamin content in the three different meat products have been collected from the USDA Database². To account for the uptake of nutrients for when each product is consumed in its usual amount, we have normalized it to the Reference Amount Customarily Consumed (RACC) serving size. We have chosen beef, pork, and chicken as the traditional sources of protein because of their widespread consumption across the world. At this stage in our research, it is fundamental to compare the product of a contemporary system like power-to-food to a more widely accepted, and standardized food production system. This comparison would further reveal the competency of sustainable processes for food and nutrition administration.

One of the most common ways to consume yeast is in the form of powder or supplements (Monika E. Jach & Serefko, 2018). If we consider a serving size of 21 g for nutritional yeast, *S. cerevisiae* grown in a power-to-food system has the capacity to meet 15% of the RDA for protein. Consequently, this value is substantially lower when compared to beef, pork, and chicken that provide 39%, 41%, and 47% of the recommended values of protein per meal, respectively. However, the serving size of any microbial protein is unique to its preparation or processing. For instance, if we consume yeast extract as a spread (Kerr & Schulz, 2016), the nutrient and protein uptake is five times higher because of a larger serving size of 100 g³. Therefore, we can conclude that from the standpoint of protein content, it is as competent as the other traditional options.

If we compare, all the four options in terms of cobalamin, beef stands out by meeting 92% of the RDA. Meanwhile, pork and chicken only provide 25% and 11% of the total RDA needed for cobalamin. A high occurrence of cobalamin in beef can be attributed to its production by ruminants

² Database, USDA foods (2021). Reference Amounts Customarily Consumed (RACCs) (<https://www.fda.gov/media/99078/download>) accessed on 15.04.2021

³ Yeast extract spread nutrition facts and analysis (2021). Nutrition value (https://www.nutritionvalue.org/Yeast_extract_spread_nutritional_value.html) accessed on 14.06.2021

present in the animal's gut. Unfortunately, we suspect that the determination of elevated levels of cobalamin in our samples might be because of positive responses induced by the pseudo-analogues of cobalamin during the microbiological assay. We lack quantitative evidence from an instrumental analysis that can respectively confirm its production in Stage 1 bioreactor and its accumulation in Stage 2 bioreactor. Jach *et al.* (2020) has demonstrated that *Y. lipolytica* could accumulate 9 µg of cobalamin in 100 g of biomass. If we adapt the cobalamin content in the power-to-food output to that estimated for *Y. lipolytica* (Jach *et al.*, 2020), one serving size of nutritional yeast from power-to-food would have the capacity to meet 79% of the RDA for cobalamin. This provides a promising insight into the future of the power-to-food process, by exhibiting that the daily uptake of key nutrients like cobalamin and folate could be enriched by the inclusion of microbial protein in our diet.

In contrast to the high amount of cobalamin present in beef, the folate concentration is quite low in the animal-derived meat products. Overall, the folate concentration in the selected meat alternatives is within a range of 2-4 % of the RDA. However, the *S. cerevisiae* biomass obtained from the Stage 2 of the power-to-food process provides 31% of the total RDA of folate. It is likely that upon fortification with other dietary supplements such as cobalamin, one serving size of the microbial biomass from Stage 2 can meet the RDA for both protein and folate. Nevertheless, it is crucial to evaluate the highest quantity that should be consumed of such alternative sources of protein and nutrition without encountering any detrimental effect on human health (Jach & Serefko, 2018).

If we aim to mitigate carbon emissions from food production at a global scale, we must begin by targeting the developing countries. Such nations urgently require the establishment of a food production system like power-to-food to eradicate the wasteful usage of renewable resources while maintaining a steady supply of nutrients to the population. Despite its limitations, our investigations have encouraged its development by addressing the key nutritional elements such as, cobalamin and folate. These findings disclose a path for future research. After optimizing the protein productivity, the power-to-protein system claims to feed 10 billion people with ten-thousand fermenters with a capacity of 3100 m³ (Molitor *et al.*, 2019). This motivates the continuation of research to further upgrade it into a power-to-food process that focuses on overall nutrient administration in addition to protein.

Table 6: Comparison of the nutritional composition of the power-to-food biomass to other conventional products by traditional food production systems in terms of the RDA and the RACC

	Beef	% RDA	Pork	% RDA	Chicken	% RDA	PtF biomass as nutritional yeast	% RDA
Serving size	85.00 g		85.00 g		85.00 g		21.00 ^a g	
Protein	26.00 g	39%	27.00 g	41%	31.00 g	47%	40.00 g	15 %
Cobalamin	2.60 µg	92%	0.70 µg	25%	0.30 µg	11%	1.89 µg ^b	79%
Folate	9.70 µg	2 %	9.70 µg	2%	17.42 µg	4%	122.91 µg	31 %

^a The highest amount of nutritional yeast that is usually consumed (Berkheiser, 2019). ^b This value has been adapted from Jach *et al.* (2020)

References

- Adachi, S., Miyamoto, E., Watanabe, F., Enomoto, T., Kuda, T., Hayashi, M., & Nakano, Y. (2005). Purification and characterization of a corrinoid compound from a Japanese salted and fermented salmon kidney “Mefun”. *Journal of liquid chromatography & related technologies*, 28(16), 2561-2569.
- Annan, F. J., Al-Sinawi, B., Humphreys, C. M., Norman, R., Winzer, K., Köpke, M., Henstra, A. M. (2019). Engineering of vitamin prototrophy in *Clostridium ljungdahlii* and *Clostridium autoethanogenum*. *Applied microbiology and biotechnology*, 103(11), 4633-4648. doi:10.1007/s00253-019-09763-6
- Berkheiser, K. (Producer). (2019, August 8). Nutrition. *Healthline*. Retrieved from <https://www.healthline.com/nutrition/nutritional-yeast-dangers>
- Bertrand, E. M., McCrow, J. P., Moustafa, A., Zheng, H., McQuaid, J. B., Delmont, T. O., Xu, K. (2015). Phytoplankton–bacterial interactions mediate micronutrient colimitation at the coastal Antarctic sea ice edge. *Proceedings of the National Academy of Sciences*, 112(32), 9938-9943.
- Black, M. M. (2008). Effects of vitamin B12 and folate deficiency on brain development in children. *Food and nutrition bulletin*, 29(2_suppl1), S126-S131.
- Bottiglieri, T. (1996). Folate, Vitamin B12, and Neuropsychiatric Disorders. *Nutrition reviews*, 54(12), 382-390. doi:10.1111/j.1753-4887.1996.tb03851.x
- Cherest, H., Thomas, D., & Surdin-Kerjan, Y. (2000). Polyglutamylation of Folate Coenzymes Is Necessary for Methionine Biosynthesis and Maintenance of Intact Mitochondrial Genome in *Saccharomyces cerevisiae*. *Journal of Biological Chemistry*, 275(19), 14056-14063.
- Cooper, M. B., Kazamia, E., Helliwell, K. E., Kudahl, U. J., Sayer, A., Wheeler, G. L., & Smith, A. G. (2019). Cross-exchange of B-vitamins underpins a mutualistic interaction between *Ostreococcus tauri* and *Dinoroseobacter shibae*. *The ISME journal*, 13(2), 334-345.
- Crippa, M., Solazzo, E., Guizzardi, D., Monforti-Ferrario, F., Tubiello, F. N., & Leip, A. (2021). Food systems are responsible for a third of global anthropogenic GHG emissions. *Nature Food*, 2(3), 198-209. doi:10.1038/s43016-021-00225-9
- Croft, M. T., Lawrence, A. D., Raux-Deery, E., Warren, M. J., & Smith, A. G. (2005). Algae acquire vitamin B 12 through a symbiotic relationship with bacteria. *Nature*, 438(7064), 90-93.
- Czech, A., Smolczyk, A., Ognik, K., & Kiesz, M. (2016). Nutritional value of *Yarrowia lipolytica* yeast and its effect on growth performance indicators in piglets. *Ann. Anim. Sci*, 16(4), 1091-1100.
- Database, U. F. (2021). Reference Amounts Customarily Consumed (RACCs). Retrieved from <https://www.fda.gov/media/99078/download>

- De Steur, H., Feng, S., Xiaoping, S., & Gellynck, X. (2014). Consumer preferences for micronutrient strategies in China. A comparison between folic acid supplementation and folate biofortification. *Public health nutrition*, 17(6), 1410-1420.
- Fang, H., Kang, J., & Zhang, D. (2017). Microbial production of vitamin B(12): a review and future perspectives. *Microbial cell factories*, 16(1), 15-15. doi:10.1186/s12934-017-0631-y
- Finnigan, T. J. A. (2011). 13 - Mycoprotein: origins, production and properties. In G. O. Phillips & P. A. Williams (Eds.), *Handbook of Food Proteins* (pp. 335-352): Woodhead Publishing.
- Gerber, P., & Opio, C. (2013). Food and Agriculture Organization of the United Nations. *Animal Production and Health Division*.
- Gille, D., & Schmid, A. (2015). Vitamin B12 in meat and dairy products. *Nutrition reviews*, 73(2), 106-115.
- Gorelova, V., Bastien, O., De Clerck, O., Lespinats, S., Rébeillé, F., & Van Der Straeten, D. (2019). Evolution of folate biosynthesis and metabolism across algae and land plant lineages. *Scientific Reports*, 9(1), 1-16.
- Grossman, A. (2016). Nutrient Acquisition: The Generation of Bioactive Vitamin B12 by Microalgae. *Current Biology*, 26(8), R319-R321. doi:<https://doi.org/10.1016/j.cub.2016.02.047>
- Hayashi, M., Yukino, T., Watanabe, F., Miyamoto, E., & Nakano, Y. (2007). Effect of vitamin B12-enriched thraustochytrids on the population growth of rotifers. *Bioscience, biotechnology, and biochemistry*, 0612110228-0612110228.
- Herbert, V. (1987a). Recommended dietary intakes (RDI) of folate in humans. *The American journal of clinical nutrition*, 45(4), 661-670.
- Herbert, V. (1987b). Recommended dietary intakes (RDI) of vitamin B-12 in humans. *The American journal of clinical nutrition*, 45(4), 671-678.
- Hjortmo, S., Patring, J., & Andlid, T. (2008). Growth rate and medium composition strongly affect folate content in *Saccharomyces cerevisiae*. *International journal of food microbiology*, 123(1-2), 93-100.
- Hjortmo, S., Patring, J., Jastrebova, J., & Andlid, T. (2005). Inherent biodiversity of folate content and composition in yeasts. *Trends in food science & technology*, 16(6-7), 311-316.
- Hjortmo, S., Patring, J., Jastrebova, J., & Andlid, T. (2008). Biofortification of folates in white wheat bread by selection of yeast strain and process. *Int J Food Microbiol*, 127(1-2), 32-36. doi:10.1016/j.ijfoodmicro.2008.06.001
- Hu, P., Chakraborty, S., Kumar, A., Woolston, B., Liu, H., Emerson, D., & Stephanopoulos, G. (2016). Integrated bioprocess for conversion of gaseous substrates to liquids. *Proceedings of the National Academy of Sciences*, 113(14), 3773-3778. doi:10.1073/pnas.1516867113
- Iguchi, H., Yurimoto, H., & Sakai, Y. (2015). Interactions of methylotrophs with plants and other heterotrophic bacteria. *Microorganisms*, 3(2), 137-151.

- Jach, M. E., Maslyk, M., Juda, M., Sajnaga, E., & Malm, A. (2020). Vitamin B12-enriched *Yarrowia lipolytica* biomass obtained from biofuel waste. *Waste and Biomass Valorization*, *11*(5), 1711-1716.
- Jach, M. E., & Serefko, A. (2018). Chapter 9 - Nutritional Yeast Biomass: Characterization and Application. In A. M. Holban & A. M. Grumezescu (Eds.), *Diet, Microbiome and Health* (pp. 237-270): Academic Press.
- Kazamia, E., Czesnick, H., Nguyen, T. T. V., Croft, M. T., Sherwood, E., Sasso, S., . . . Smith, A. G. (2012). Mutualistic interactions between vitamin B12-dependent algae and heterotrophic bacteria exhibit regulation. *Environmental Microbiology*, *14*(6), 1466-1476. doi:<https://doi.org/10.1111/j.1462-2920.2012.02733.x>
- Kelly, J. (2004). The regulation of carbon metabolism in filamentous fungi. In *Biochemistry and molecular biology* (pp. 385-401): Springer.
- Kerr, E. D., & Schulz, B. L. (2016). Vegemite Beer: yeast extract spreads as nutrient supplements to promote fermentation. *PeerJ*, *4*, e2271.
- Köpke, M., Held, C., Hujer, S., Liesegang, H., Wiezer, A., Wollherr, A., Dürre, P. (2010). *Clostridium ljungdahlii* represents a microbial production platform based on syngas. *Proceedings of the National Academy of Sciences*, *107*(29), 13087-13092.
- Ladha-Sabur, A., Bakalis, S., Fryer, P. J., & Lopez-Quiroga, E. (2019). Mapping energy consumption in food manufacturing. *Trends in food science & technology*, *86*, 270-280. doi:<https://doi.org/10.1016/j.tifs.2019.02.034>
- Laiño, J. E., del Valle, M. J., de Giori, G. S., & LeBlanc, J. G. J. (2014). Applicability of a *Lactobacillus amylovorus* strain as co-culture for natural folate bio-enrichment of fermented milk. *International journal of food microbiology*, *191*, 10-16.
- Lawrence, A. D., Nemoto-Smith, E., Deery, E., Baker, J. A., Schroeder, S., Brown, D. G., Warren, M. J. (2018). Construction of Fluorescent Analogs to Follow the Uptake and Distribution of Cobalamin (Vitamin B12) in Bacteria, Worms, and Plants. *Cell Chemical Biology*, *25*(8), 941-951.e946. doi:<https://doi.org/10.1016/j.chembiol.2018.04.012>
- Liu, Y., Walkey, C. J., Green, T. J., Van Vuuren, H. J., & Kitts, D. D. (2016). Enhancing the natural folate level in wine using bioengineering and stabilization strategies. *Food Chemistry*, *194*, 26-31.
- Loew, D., Eberhardt, A., Hesecker, H., & Kübler, W. (1987). Plasma kinetics and elimination of folic acid. *Klinische Wochenschrift*, *65*(11), 520-524.
- Maliepaard, M., Scheffer, G. L., Faneyte, I. F., van Gastelen, M. A., Pijnenborg, A. C., Schinkel, A. H., Schellens, J. H. (2001). Subcellular localization and distribution of the breast cancer resistance protein transporter in normal human tissues. *Cancer research*, *61*(8), 3458-3464.
- Martens, J. H., Barg, H., Warren, M., & Jahn, D. (2002). Microbial production of vitamin B12. *Applied microbiology and biotechnology*, *58*(3), 275-285. doi:10.1007/s00253-001-0902-

- Mikkelsen, K., Hallam, K., Stojanovska, L., & Apostolopoulos, V. (2018). Yeast based spreads improve anxiety and stress. *Journal of Functional Foods*, *40*, 471-476. doi:<https://doi.org/10.1016/j.jff.2017.11.034>
- Mock, J., Zheng, Y., Mueller, A. P., Ly, S., Tran, L., Segovia, S., Thauer, R. K. (2015). Energy Conservation Associated with Ethanol Formation from H₂ and CO₂ in *Clostridium autoethanogenum* Involving Electron Bifurcation. *Journal of bacteriology*, *197*(18), 2965-2980. doi:10.1128/JB.00399-15
- Molitor, B., Mishra, A., & Angenent, L. T. (2019). Power-to-protein: converting renewable electric power and carbon dioxide into single cell protein with a two-stage bioprocess. *Energy & Environmental Science*.
- Moll, R., & Davis, B. (2017). Iron, vitamin B12 and folate. *Medicine*, *45*(4), 198-203. doi:<https://doi.org/10.1016/j.mpm.2017.01.007>
- Mozafar, A. (1994). Enrichment of some B-vitamins in plants with application of organic fertilizers. *Plant and Soil*, *167*(2), 305-311.
- Muthayya, S., Rah, J. H., Sugimoto, J. D., Roos, F. F., Kraemer, K., & Black, R. E. (2013). The global hidden hunger indices and maps: an advocacy tool for action. *PloS one*, *8*(6), e67860.
- Paul, L., & Selhub, J. (2017). Interaction between excess folate and low vitamin B12 status. *Molecular Aspects of Medicine*, *53*, 43-47. doi:<https://doi.org/10.1016/j.mam.2016.11.004>
- Radimer, K., Bindewald, B., Hughes, J., Ervin, B., Swanson, C., & Picciano, M. F. (2004). Dietary supplement use by US adults: data from the National Health and Nutrition Examination Survey, 1999–2000. *American journal of epidemiology*, *160*(4), 339-349.
- Ragsdale, S. W. (1991). Enzymology of the acetyl-CoA pathway of CO₂ fixation. *Critical reviews in biochemistry and molecular biology*, *26*(3-4), 261-300.
- Rébeillé, F., Ravel, S., Jabrin, S., Douce, R., Storozhenko, S., & Van Der Straeten, D. (2006). Foliates in plants: biosynthesis, distribution, and enhancement. *Physiologia Plantarum*, *126*(3), 330-342. doi:<https://doi.org/10.1111/j.1399-3054.2006.00587.x>
- Revuelta, J. L., Serrano-Amatriain, C., Ledesma-Amaro, R., & Jiménez, A. (2018). Formation of folates by microorganisms: towards the biotechnological production of this vitamin. *Applied microbiology and biotechnology*, *102*(20), 8613-8620. doi:10.1007/s00253-018-9266-0
- Riggs, S. S., & Heindel, T. J. (2006). Measuring carbon monoxide gas—liquid mass transfer in a stirred tank reactor for syngas fermentation. *Biotechnology progress*, *22*(3), 903-906.
- Saubade, F., Hemery, Y. M., Guyot, J.-P., & Humblot, C. (2017). Lactic acid fermentation as a tool for increasing the folate content of foods. *Critical Reviews in Food Science and Nutrition*, *57*(18), 3894-3910.
- Selhub, J. (2002). Folate, vitamin B12 and vitamin B6 and one carbon metabolism. *The journal of nutrition, health & aging*, *6*(1), 39-42.

- serving, Y. e. s. n. f. a. a. p. (Producer). (2021, June 14). Nutrition Value. Retrieved from https://www.nutritionvalue.org/Yeast_extract_spread_nutritional_value.html
- Shane, B., & Stokstad, E. R. (1985). Vitamin B12-folate interrelationships. *Annual review of nutrition*, 5(1), 115-141.
- Sokolovskaya, O. M., Shelton, A. N., & Taga, M. E. (2020). Sharing vitamins: Cobamides unveil microbial interactions. *Science*, 369(6499).
- Striegel, L., Brandl, B., Kopp, M., Sam, L., Skurk, T., & Rychlik, M. (2019). Quantitation of 5-methyltetrahydrofolic acid in plasma for determination of folate status and clinical studies by stable isotope dilution assays. *PLoS one*, 14(2), e0212255-e0212255. doi:10.1371/journal.pone.0212255
- Strobbe, S., & Van Der Straeten, D. (2017). Folate biofortification in food crops. *Current Opinion in Biotechnology*, 44, 202-211. doi:<https://doi.org/10.1016/j.copbio.2016.12.003>
- Stupperich, E. (1993). Recent advances in elucidation of biological corrinoid functions. *FEMS Microbiol Rev*, 12(4), 349-365. doi:10.1111/j.1574-6976.1993.tb00027.x
- Troen, A. M. (2012). Folate and vitamin B12: function and importance in cognitive development. *Nestle Nutr Inst Workshop Ser*, 70, 161-171. doi:10.1159/000337684
- Van Hecke, W., Bockrath, R., & De Wever, H. (2019). Effects of moderately elevated pressure on gas fermentation processes. *Bioresource Technology*, 293, 122129. doi:<https://doi.org/10.1016/j.biortech.2019.122129>
- von Grebmer, K., Bernstein, J., Prasai, N., Yin, S., Yohannes, Y., Towey, O., de Waal, A. (2015). The concept of the global hunger index. *IFPRI book chapters*, 6-11.
- Watanabe, F., & Bito, T. (2018). Vitamin B12 sources and microbial interaction. *Experimental Biology and Medicine*, 243(2), 148-158.
- Wood, H. G., Ragsdale, S. W., & Pezacka, E. (1986). The acetyl-CoA pathway: a newly discovered pathway of autotrophic growth. *Trends in Biochemical Sciences*, 11(1), 14-18.
- Xie, C., Coda, R., Chamlagain, B., Edelmann, M., Varmanen, P., Piironen, V., & Katina, K. (2021). Fermentation of cereal, pseudo-cereal and legume materials with *Propionibacterium freudenreichii* and *Levilactobacillus brevis* for vitamin B12 fortification. *LWT*, 137, 110431. doi:<https://doi.org/10.1016/j.lwt.2020.110431>

Establishing a power-to-food platform by demonstrating the presence of cobalamin and folate in single-cell protein synthesized from renewable electric power and carbon dioxide

Supplemental Information

Akanksha Mishra¹, Nadine Weber³, Mengle Wang³, Bastian Molitor¹, Michael Rychlik³, Largus T. Angenent^{1,2}

1. Center for Applied Geosciences, University of Tuebingen, 72070 Tuebingen, Germany
2. Max Planck Fellow, Max Planck Institute for Developmental Biology, 72076 Tübingen, Germany
3. Analytical Food Chemistry, Technical University of Munich, 85354 Freising, Germany

In preparation

Supplementary Material

Media Composition

Reinforced clostridia media (per liter):

Mineral salts and nutrients: 3 g yeast extract, 10 g beef extract, 10 g peptone, 5 g sodium chloride, 1 g soluble starch, 3 g sodium acetate, 4 mL Rezasurin solution (0.025 vol%)

Carbon source: 5 g Fructose

P7 media (per liter)

Mineral salts and nutrients: 0.8 g sodium chloride, 1 g ammonium chloride, 0.1 g potassium phosphate monobasic, 0.33 g magnesium sulphate, 0.04 g calcium chloride

Carbon source: Heterotrophic conditions: 5 g Fructose, Autotrophic conditions: 0.8 bar CO₂

Trace elements: 2 g nitrilotriacetic acid, 0.8 g manganese chloride, 0.8 g ferrous ammonium sulphate, 0.2 g cobalt chloride, 0.02 g copper chloride, 0.02 g nickel chloride, 0.02 g sodium molybdate, 0.018 g sodium selenite, 0.022 g sodium tungstate dihydrate

Vitamin solution: 0.01 g pyridoxine hydrochloride, 0.005 g thiamine hydrochloride, 0.005 g riboflavin, 0.005 g calcium pantothenate, 0.005 g Dithiooctanoic acid, 0.005 g Nicotinic acid, 0.005 g cobalamin, 0.002 g biotin, 0.002 g folic acid, 0.01 g mercaptothanesulfonic acid

The vitamin stock solution was passed through a sterile filter and stored in a container that was already autoclaved. It was made anoxic by flushing it with N₂ for 20 minutes

Buffer: 2-(N-morpholino) ethanesulfonic acid (MES)

Reducing agent (100 mL): 4 g L-Cystein hydrochloric acid and 0.9 g NaOH were dissolved in 100 mL of anaerobic water inside an anaerobic chamber. The solution was sterilized by autoclaving.

Yeast nitrogenous base (per liter):

Mineral salts and nutrients: 1 g ammonium sulphate, 1 g potassium phosphate monobasic, 1 g magnesium sulphate heptahydrate, 0.1 g sodium chloride, 0.33 g calcium chloride heptahydrate

Trace elements: 0.005 g iron (II) sulphate heptahydrate, 0.001 g zinc sulphate heptahydrate, 0.001 g manganese (II) sulphate monohydrate, 0.0002 g sodium molybdate, 0.00018 g cobalt (II) chloride, 0.00018 g copper (II) chloride dihydrate.

Vitamins: 0.02 g Myo-inositol, 0.004 g thiamine, 0.0012 g pyridoxine. 0.001 g D-pantothenic acid hemicalcium, 0.03×10^{-3} g biotin

Setting up the Stage 1 bioreactor

The Stage 1 bioreactor vessel was autoclaved containing appropriate amounts of mineral salts and trace elements. Once, the vessel cooled down to the room temperature, the vessel was connected to the H₂/CO₂ gas lines and left overnight to make in anaerobic. Next day, the vitamin and reducing agent were added to the Stage 1 bioreactor. Later, the bioreactor was inoculated with 1% (v/v) of *C. ljungdahlii* culture at its log phase of growth. The continuous mode of operation was initiated on day 4 with a cell-recycling module. The module was sterilized with 3 M KOH and rinsed thoroughly with sterile, anoxic distilled water.

Setting up the Stage 2 bioreactor

The Stage 2 bioreactor vessel was sterilized by autoclaving while containing an adequate volume of mineral salts and trace elements. It was connected to gas line providing compressed air. The vitamin solution and 100 mM of acetic acid was added once the Stage 2 bioreactor had cooled down to room temperature. Thereafter, it was inoculated with 1% (v/v) of *S. cerevisiae* culture grown in minimal media with acetic acid. Once, the culture reached an exponential phase of growth, the Stage 1 bioreactor was connected to the Stage 2 bioreactor through a multichannel pump. The multichannel pump was sterilized with bleach (10% v/v) and dried with air (through sterile filters). This step initiated the continuous mode of operation for the Stage 2 bioreactor. A

by-pass feed line containing three-fold concentrated mineral salt solution added to the Stage 2 bioreactor.

Analysis of the different forms of cobalamin in the bottle experiments and the power-to-food reactor

Table S1: Details on the quantity and injection volume of the samples that were analyzed for the presence of different forms of cobalamin using HPLC-MS/MS

Sample Description	Sample Weight	Injection volume
Stage 1 Reactor Effluent	40 ml	5 μ L
Stage 2 Reactor Biomass	514 mg	5 μ L
Supernatant from <i>S. cerevisiae</i> (with cobalamin)	40 ml	5 μ L
Cells from <i>S. cerevisiae</i> (with cobalamin)	15 mg	5 μ L
Cells from <i>C. ljungdahlii</i> (without cobalamin)	17 mg	5 μ L

Unfortunately, the biomass of *C. ljungdahlii* grown in the presence of cobalamin as well as the biomass from *S. cerevisiae* cultivated without cobalamin were insufficient to perform the microbiological assay (MBA) and the instrumental analysis, and therefore, are not included in this Table.

Results from the HPLC-MS/MS quantification

Power-to-food reactor experiments

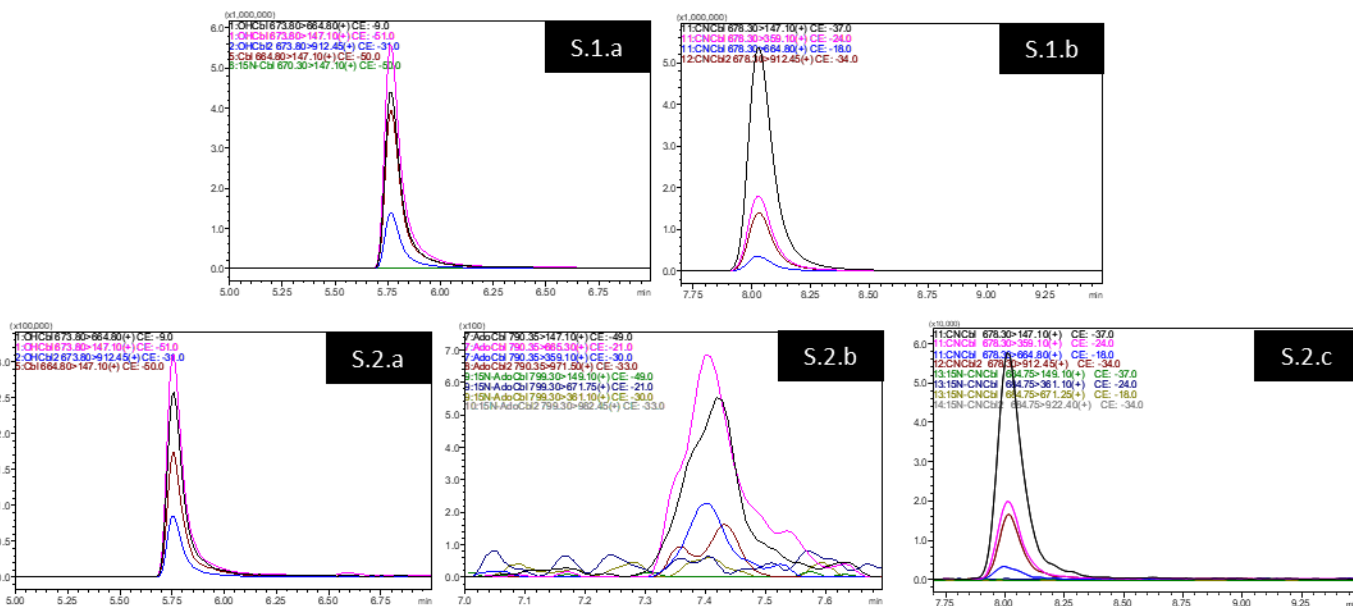


Figure S1: Confirmation of the presence of cobalamin in the samples collected from Stage 1 (S.1) as well as the biomass collected from Stage 2 (S.2). Highly intense peaks of Hydroxycobalamin (S.1.a) and cyanocobalamin (S.1.b) were primarily detected in Stage 1 effluent. Stage 2 showed traces of adenosylcobalamin (S.2.b) in addition to the peaks of hydroxycobalamin (S.2.a) and cyanocobalamin (S.2.c). The x-axis represents the retention time, and the y-axis shows the intensity of the peak.

Bottle experiments

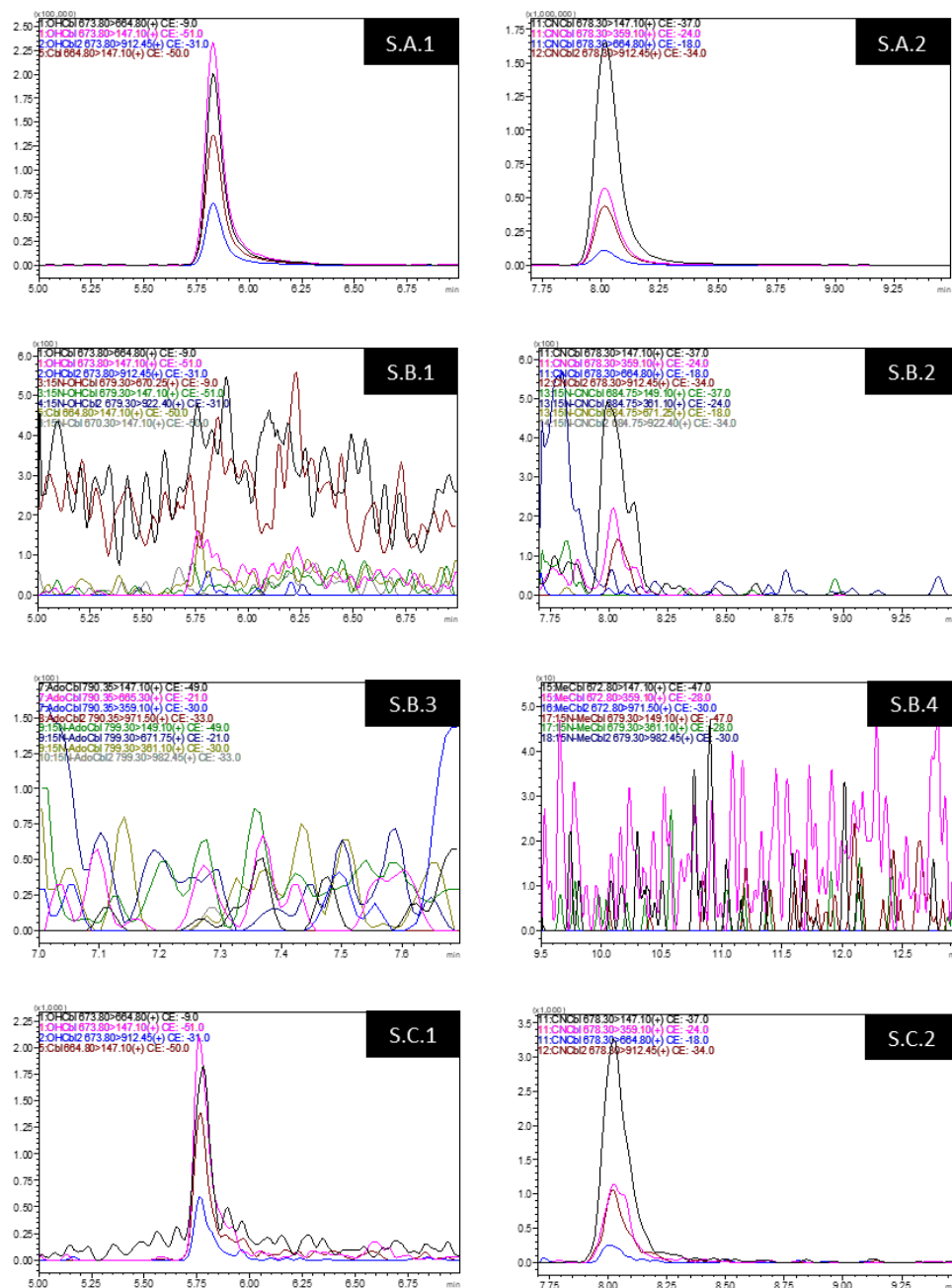


Figure S2: Different forms of cobalamin that were detected in the samples taken from bottle experiments under batch conditions with *C. ljungdahlii* and *S. cerevisiae*. Cyanocobalamin (S.A.1) and hydroxycobalamin (S.A.2) was detected in the effluent collected from *S. cerevisiae* that was cultivated in the presence of cobalamin. (S.B. 1-4) Minute traces of hydroxycobalamin (S.B.1), cyanocobalamin (S.B.2), adenosylcobalamin (S.B.3) and methylcobalamin (S.B.4) were detected in the *S. cerevisiae* biomass growth with cobalamin. However, due to its low concentration it is accompanied by strong noise signals (S.C.3) Hydroxycobalamin and cyanocobalamin (S.C.4) were detected in the biomass collected from *C. ljungdahlii* cultivated in the absence of cobalamin. The x-axis represents the retention time, and the y-axis shows the intensity of the peak.

Protocol for the Microbiological Assay

1. 20 ml of vitamin B12 assay medium was inoculated with 1 % of *L. leishmanii* cryo stock. It was allowed to grow for 48 hours at 37°C in the presence of 500 ng μL^{-1} until it reached an OD600 of 0.8.
2. The culture is then transferred into a 50 ml falcon tube and centrifuged. The supernatant is discarded and 45 ml of PBS buffer (pH:7) is added. The cells are thoroughly mixed with the buffer and centrifuged again. This step is repeated twice. The pellet was stored at -80°C for inoculating the medium during the assay.
3. The assay was performed in a sterile 96-well Microtiter plate. A fresh stock solution of cobalamin was prepared with a concentration of 100 pg μL^{-1} . A standard curve was derived by adding 20-60 μL volume of the 100x stock in each row of the 96-well plate in quadruplicates. To each standard, an appropriate amount of PBS buffer was added to have a volume of 100 μL . Immediately after this step, each well was given 200 μl of vitamin B12 assay medium inoculated with *L. leishmanii* cells that were obtained in the earlier steps (Figure S3).
4. The assay contained two groups of experimental control.
 - a. Traces of cobalamin might inherently be present within the cells due to its addition in the working culture. This was determined by adding 200 μL of inoculated media to 100 μL of PBS buffer.
 - b. The sterility of the 96-well plate was also assured by adding 200 μL of sterile Vitamin B12 assay medium to 100 μL PBS buffer.
5. For estimating the total cobalamin concentration in the samples, 200 μL of the vitamin B12 assay media inoculated with *L. leishmanii* culture (from Step 2) was added to 100 μL of samples.
6. After the preparation of the 96-well plate, it was placed in the 37°C incubator and incubated overnight.
7. The assay was analyzed using a spectrophotometer at a wavelength of 595 nm.

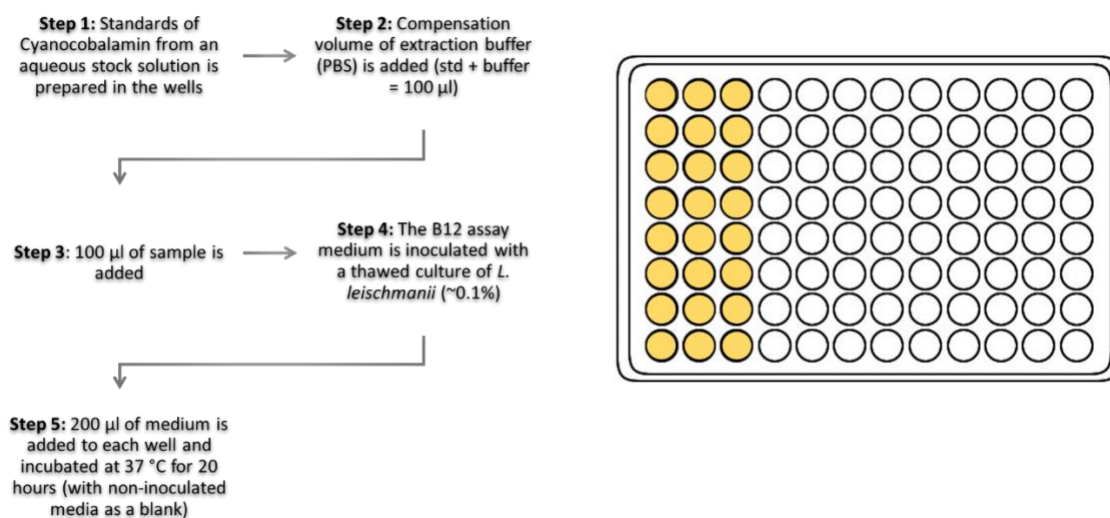


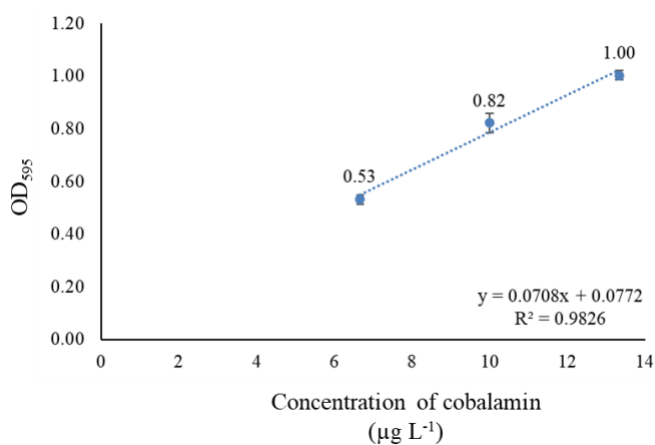
Figure S3: Protocol for performing the MBA for detecting the total Cobalamin content of the samples with *L. leishmanii*

Determination of the cobalamin concentration in each sample

We carried two sets of MBAs to quantify cobalamin concentrations for the samples that were analyzed with the HPLC-MS/MS in Freising.

The standard curve is shown as follows:

Figure S4: The calibration curve obtained with the growth of *L. leishmanii* to different concentrations of cobalamin for estimating its concentration in the reactor samples.



From the equation derived from the standard concentrations, the following values for the reactor samples and the batch experiments were calculated:

Table S2: Estimated concentrations of cobalamin from the MBA standard curve for the samples obtained from the power-to-food reactor during its operation in Phase 3

Sample Description	Estimated value ($\mu\text{g L}^{-1}$)	Biomass yield (if any) (mg mL^{-1})	Estimated value ($\mu\text{g g}^{-1}$)
Stage 1 Reactor effluent	18.82 ± 0.65 (n=8)	NA	NA
Stage 2 Reactor Biomass	3.74 ± 0.26 (n=8)	1.14	3.27 ± 0.23 (n=8)

Figure S5: The calibration curve obtained with the growth of *L. leischmanii* to different concentrations of cobalamin for estimating its concentration in the batch experiments

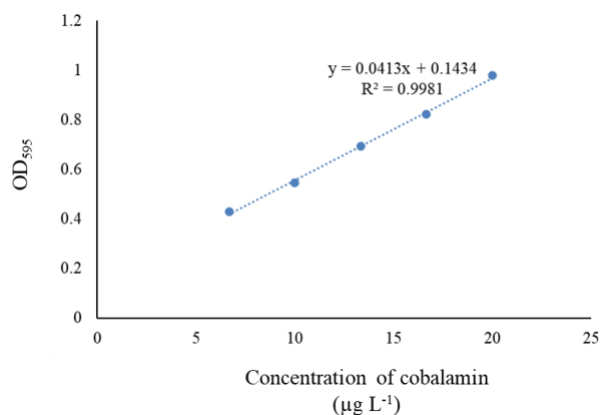


Table S3: Estimated concentrations of cobalamin from the MBA standard curve for the samples obtained from the batch experiments conducted with *C. ljungdahlii* and *S. cerevisiae* in bottles.

Sample Description	Estimated value ($\mu\text{g L}^{-1}$)	Biomass yield (if any) (mg mL^{-1})	Estimated value ($\mu\text{g g}^{-1}$)
<i>S. cerevisiae</i> Effluent	14.75 ± 3.35 (n=4)	NA	NA
<i>S. cerevisiae</i> Biomass (with Cobalamin)	4.72 ± 0.67 (n=4)	0.22 ± 0.02	21.45
<i>C. ljungdahlii</i> (Without B12)	0.17 ± 0.14 (n=4)	0.21 ± 0.01	0.81

Protocol for extracting and quantifying folates

1. Approximately ~100 mg of pellets and 500 mg of supernatant from each sample was taken.
2. Both unlabeled and labelled Standards (ITSD) were prepared with different analogues of folate:
3. The different types of standards were:
 - Labelled Pteroylmonoglutamic acid: $^{13}\text{C}_5\text{-PteGlu}$
 - Labelled Tetrahydrofolate: $^{13}\text{C}_5\text{-H}_4\text{folate}$
 - Labelled 5-Methyltetrahydrofolate: $^{13}\text{C}_5\text{-5-CH}_3\text{-H}_4\text{-folate}$
 - Labelled 5-formyltetrahydrofolate: $^{13}\text{C}_5\text{-5-CHO-H}_4\text{-Folate}$
 - Labelled Polyglutamic acid: $^{13}\text{C}_{10}\text{-CHO-PteGlu}$
 - And the unlabeled forms of each one
4. During sample preparation, ITSD were added to each sample according to its expected concentration to determine the recovery of the analytes in the process of its purification or extraction.
5. The concentration of the unlabeled analytes was analyzed using the HPLC-UV. The estimated concentration of each unlabeled analyte was then compared to its response in the LC-MS/MS to determine the concentration of the labelled analytes.
6. After adding the standards, Chicken pancreas and rat serum were added for deconjugation. The vials were incubated overnight to complete the enzymatic reaction.
7. To purify the folates, the supernatant is collected from these vials for solid phase extraction (SPE) using an anion exchange column.
8. Once, the folates were eluted from the column, they were quantified using the LC-MS/MS.
9. After accounting for the recovery of the internal standards and subtracting the folate that was introduced while adding the enzymes, the concentration of all the vitamers in each sample was calculated.

Quantified concentrations of folate in the power-to-food reactor and bottle experiments

Table S4: Details of all the forms of folate measured within each sample. Folate was extracted from the samples in duplicates. The coefficient of variance and the standard deviation has been provided for each vitamer in each sample

Sample Description	Number of extractions	PteGlu	H4Folate	5-CH3-H4Folate	5-CHO-H4Folate	10-CHO-PteGlu	σ $\mu\text{g/g}$
Supernatant <i>C. ljungdahlii</i> (Reactor)	1	0.00	0.00	1.32	0.92	1.94	0.04
	2	0.00	0.00	1.26	0.95	0.24	0.02
	σ $\mu\text{g/g}$	0.00	0.00	1.29	0.94	1.09	0.03
	SD [$\mu\text{g/g}$]	0.00	0	0.04	0.02	1.20	0.01
	CV %	#N/A	#N/A	3.19	1.75	110.30	37%
Cells of <i>S. Cerevisiae</i> (Reactor)	1	4.27	197.22	118.45	247.16	17.00	5.84
	2	3.93	190.42	119.80	248.09	17.38	5.80
	σ $\mu\text{g/g}$	4.10	193.82	119.13	247.63	17.19	5.82
	SD [$\mu\text{g/g}$]	0.24	4.81	0.95	0.66	0.27	0.03
	CV %	5.87	2.48	0.80	0.27	1.56	1%
<i>C. ljungdahlii</i> biomass (with cobalamin)	1	0.00	0.52	2.42	1.40	0.00	0.04
	2	0.00	1.16	2.23	1.50	0.00	0.05
	σ $\mu\text{g/g}$	0.00	0.84	2.33	1.45	0.00	0.05
	SD [$\mu\text{g/g}$]	0.00	0.45	0.13	0.08	0.00	0.00
	CV %	#N/A	53.99	5.75	5.19	#N/A	9%
<i>S. Cerevisiae</i> effluent (with cobalamin)	1	0.00	0.57	0.00	0.00	0.18	0.01
	2	0.00	0.60	0.00	0.00	0.19	0.01
	σ $\mu\text{g/g}$	0.00	0.59	0.00	0.00	0.18	0.01
	SD [$\mu\text{g/g}$]	0.00	0.02	0.00	0.00	0.01	0.00
	CV %	#N/A	3.84	#N/A	#N/A	3.38	4%
<i>S. Cerevisiae</i> biomass (with cobalamin)	1	0.00	32.01	18.37	9.71	2.65	0.63
	σ $\mu\text{g/g}$	0.00	32.01	18.37	9.71	2.65	0.63
<i>C. ljungdahlii</i> biomass (without cobalamin)	1	0.00	0.00	0.87	1.46	3.64	0.06
	2	0.00	0.00	0.00	1.71	3.89	0.06
	σ $\mu\text{g/g}$	0.00	0.00	0.43	1.58	3.77	0.06
	SD [$\mu\text{g/g}$]	0.00	0.00	0.61	0.18	0.18	0.00
	CV %	#N/A	#N/A	141.42	11.10	4.68	5%
<i>S. Cerevisiae</i> effluent (without B12)	1	0.48	0.00	0.00	0.00	0.17	0.01
	2	0.55	0.00	0.00	0.00	0.20	0.01
	σ $\mu\text{g/g}$	0.51	0.00	0.00	0.00	0.18	0.01
	SD [$\mu\text{g/g}$]	0.05	0.00	0.00	0.00	0.03	0.00
	CV %	8.91	#N/A	#N/A	#N/A	14.02	0.10
<i>S. Cerevisiae</i> biomass (without B12)	1	0.00	8.54	22.11	20.70	8.86	0.60
	σ $\mu\text{g/g}$	0.00	8.54	22.11	20.70	8.86	0.60

Growth behavior of *S. cerevisiae* in a preliminary operation of the Stage 2 bioreactor

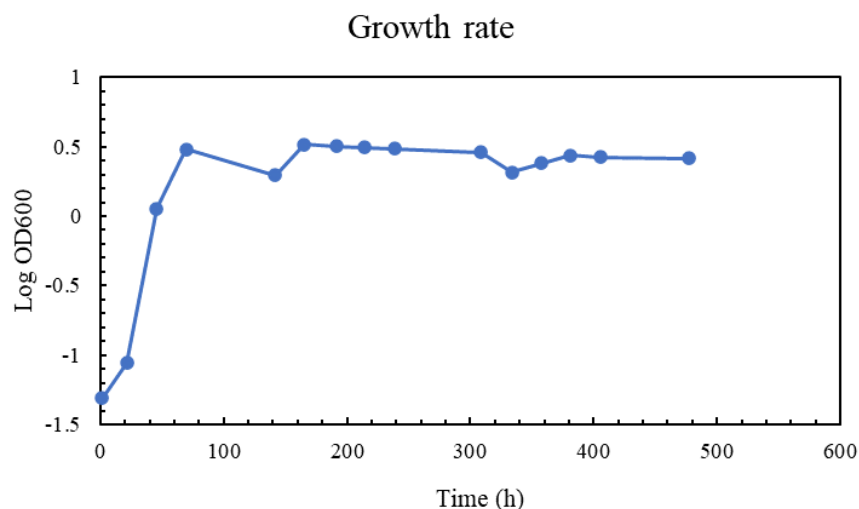


Figure S6: An OD₆₀₀ plot Vs time plot for a preliminary run of the Stage 2 bioreactor with *S. cerevisiae*. We observed a maximum growth rate of 0.05 h⁻¹ during this experiment. The growth rate presumably dropped to 0.04 h⁻¹ during the continuous mode of operation keeping a consistent concentration of biomass with a dilution rate of 0.04 h⁻¹.

Data collected from the Stage 1 bioreactor for all three periods

Table S5: Data collected during the operation of the Stage 1 bioreactor for 14 days through all the three periods. Phase I indicates the batch phase of operation when *C. ljungdahlii* was inoculated into the bioreactor. Phase II indicates the start of the continuous mode of operation with a medium that was prepared with a standard vitamin solution containing cobalamin as well as yeast extract. In Phase III of operation, the yeast extract was removed from the media.

Phases	Duration (d)	CDW (g)	Acetic acid production (g L ⁻¹ d ⁻¹)
I	0	#N/A	#N/A
	1	0.05	0.14
	2	0.16	2.41
	3	0.35	1.74
	4	0.22	1.47
II	5	0.23	3.13

	6	0.29	4.80
	8	0.75	11.52
	9	1.12	21.02
III	10	1.04	22.73
	11	0.73	17.17
	12	0.62	16.50
	13	0.51	11.15
	14	0.52	7.67

Data collected from the Stage 2 bioreactor for all three periods

Table S6: Data collected during the operation of the Stage 2 bioreactor for 15 days from Phase 1-III. Phase I indicates the batch phase of operation when *S. cerevisiae* was inoculated into the bioreactor with 100 mM of acetic acid. Phase II indicates the start of the continuous mode of operation with effluent from a Stage 1 bioreactor at a flow rate of 40 mL h⁻¹. During the Phase III of operation, the yeast extract was removed from the media that was being provided to the Stage 1 bioreactor.

Period	Duration (d)	CDW (g)	Acetic acid consumption (g L ⁻¹ d ⁻¹)	Production of biomass (g L ⁻¹ d ⁻¹)
I	0		#N/A	
	1	0.02	#N/A	
	2	0.00	0.00	
	3	0.06	#N/A	
	4	0.37	0.13	
	5	3.20	#N/A	
II	6	2.82	1.34	2.54
	8	1.55	1.73	1.39
	9	2.47	4.32	2.22
	10	2.17	4.75	1.95
III	11	3.52	8.42	3.50
	12	3.21	5.35	3.08
	13	3.46	4.71	3.32

	14	2.16	-0.71	2.08
	15	1.45	2.24	1.39

Discussion and Outlook

The syngas fermentation platform is gaining popularity as a leading solution to counter carbon emissions from industrial processes. Innovative coupling of such sustainable processes into a single lucrative bioprocess can have diverse applications. The objective behind this thesis was to apply this concept in a power-to-food system and to derive food and nutrition solely from gas fermentation. The reactor was operated as a two-stage process in which the Stage 1 bioreactor creates acetic acid from a mixture of H₂/CO₂ (80% H₂: 20% CO₂) using a carboxydophilic, acetogen as a biocatalyst under anaerobic conditions. The Stage 2 bioreactor of the power-to-food system utilized acetic acid as a substrate for the growth of yeast under aerobic conditions. The biomass retrieved from Stage 2 was then evaluated for its protein and vitamin content. In this section, we will summarize our findings and prospects from each step leading to the establishment of the power-to-food system.

Due to the limited solubility of syngas constituents, such as CO and H₂, several reactor optimization strategies have targeted the improvement of the gas-to-liquid mass transfer values in a gas fermentation system. This further inspired an auxiliary goal behind this thesis; The goal was to study the microbial influence on the bubble size properties of H₂/CO₂ bubbles during a gas fermentation experiment. We attempted to construct a series of methods and experiments to enable the user to inspect bubble size properties real-time in a gas fermentation system. Additionally, we propose an unconventional set-up for conducting gas fermentation that differentiates and captures both abiotic and biotic influences on bubbles during gas fermentation. Unfortunately, we were unable to execute them within the time allotted for the completion of this dissertation. Two major experiments concerning this topic have been described towards the end of the discussion. They will be pursued by other researchers in our lab soon.

Our findings from the Stage 1 bioreactor in the power-to-food system

Although the power-to-food system is conceptually simple, its operation was challenging. This was mainly because of the mandatory anaerobic and axenic conditions in the Stage 1 bioreactor. To facilitate a easier data correlation and validation, the Stage 1 bioreactor was reconstructed according to the original power-to-protein design (Molitor *et al.*, 2019a). The reactor was placed

inside an air-flow hood due to the utilization of a highly flammable H₂ gas. It was operated with a continuous flow of H₂/CO₂ gas mixture. Since its first operation in September 2018, it failed several times due to the intrusion of O₂. Afterwards, a bioreactor originally purchased from New Brunswick, was modified with new stainless-steel fittings to conduct gas fermentation experiments as the Stage 1 bioreactor. As a preliminary test, this reactor was operated from January 2019 until the beginning of May 2019. We conclude the following aspects from its continuous operation of approximately 90 days.

1. We witnessed limit in the concentration of biomass that the cells can reach (**Figure 1A**). This has also been observed in (Valgepea *et al.*, 2017). They hypothesized that high extracellular acetic acid concentration would lead to its diffusion into the cell, requiring higher ATP maintenance costs. However, to accomplish this task, the Rnf complex would require higher reducing equivalents, which cannot be met due to a limited capacity of the cell to consume H₂. Moreover, at a higher biomass concentration, the flux through acetyl Co-A is high, resulting in a depletion of the intracellular acetyl Co-A pool. The lack of enough reducing equivalents prevents its regeneration and CO₂ fixation, causing a crash in the biomass concentration as observed in our system (**Figure 1A**).
2. We can optimize acetate production rates by testing different dilution rates. For instance, we observed a production rate of 0.33 ± 0.12 (n = 51) mol-C L⁻¹ d⁻¹ and 0.47 ± 0.14 (n = 17) mol-C L⁻¹ d⁻¹ at dilution rates of 0.64 d⁻¹ and 0.96 d⁻¹, respectively (**Figure 1B (blue triangles)**). Moreover, when we further increased the dilution to 1.24 d⁻¹ in the last two days we saw an increase in the acetic acid production rate to 0.65 mol-C L⁻¹ d⁻¹ (**Figure 1B (blue triangles)**). Although, the operation time at this dilution rate was short, the result came close to the highest production rate of 0.78 mol-C L⁻¹ d⁻¹ that was observed in (Molitor *et al.*, 2019) (**Chapter 2**).
3. The optimal H₂:CO₂ ratio for carbon fixation by *C. ljungdahlii* is 2:1 (Müller & Wiechmann, 2017) Since we are using a ratio of 4:1, we are unable to consistently track H₂ consumption in the off-gas line. This is evident in **Figure 1C** in which we barely see any H₂ consumption. In the future run, we would like to switch to the optimal ratio for our H₂/CO₂ gas mixture tank to improve the usage of H₂ gas (**Figure 1C**). Moreover, the gas sampling method should be further improved to derive accurate consumption rates for H₂.

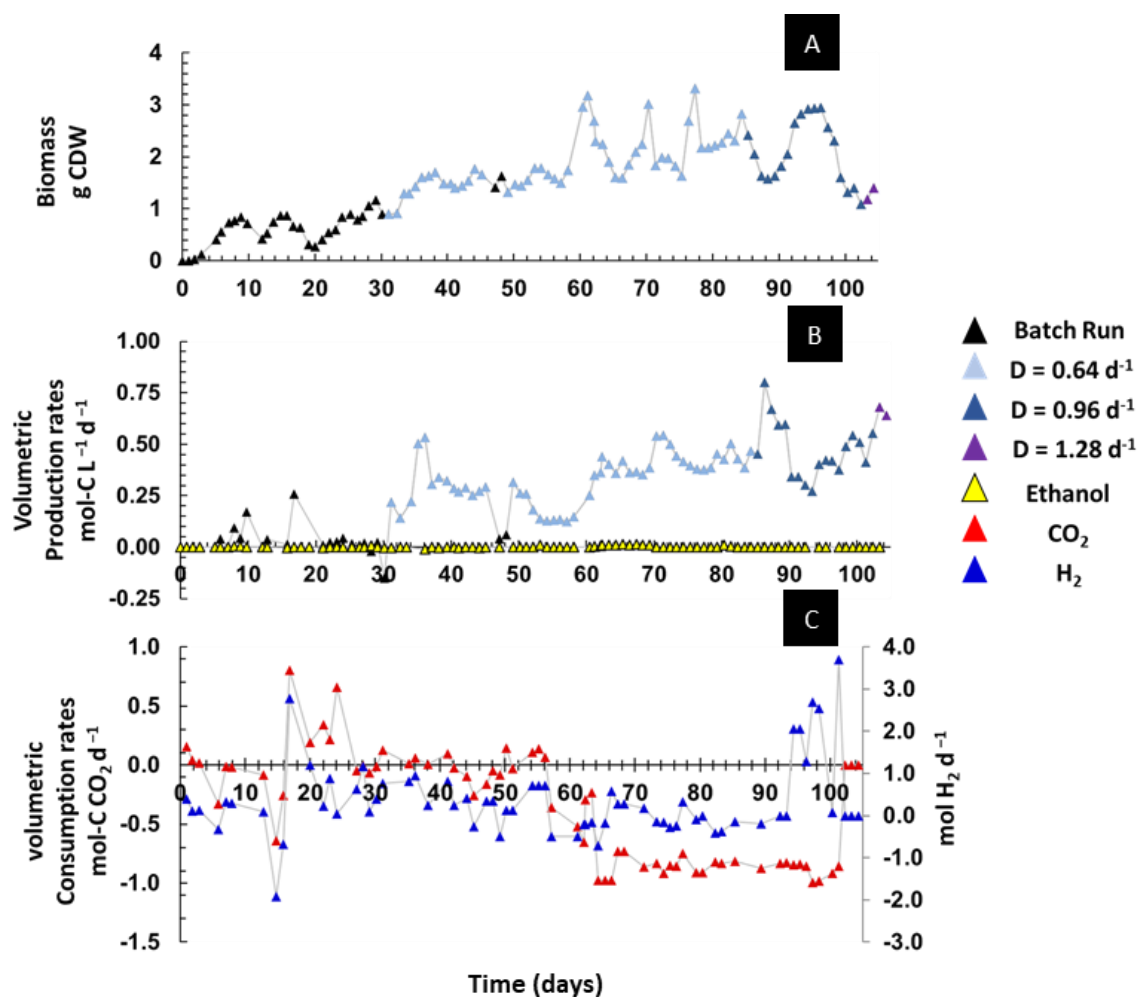


Figure 5: Data collected from a preliminary run of the Stage 1 bioreactor. A drop in the biomass concentration of *C. ljungdahlii* in the Stage 1 bioreactor (A) was accompanied by an increase in the volumetric acetic acid production rate (represented by blue) (B). These results also suggest that the consumption of H₂ can be optimized by switching to a stoichiometric ratio of H₂:CO₂ for the Wood-Ljungdahl pathway (C).

A successful demonstration of the power-to-food system requires technical and biological optimizations

Technical optimizations

As stated, and shown under Chapter 3, we experienced several difficulties while conducting experiments in the Stage 1 bioreactor. The presence of minute concentrations of O₂ was proven to be detrimental for the optimal functioning of the microbes. The infiltration of O₂ mainly occurred in two locations, thereby, halting the bioprocess system during its transition into continuous

operation. This occurred in: (1) The connection between the media bottle and the Stage 1 bioreactor (2) The hollow-fiber module for cell recycling connected between the Stage 1 to Stage 2 bioreactor. The bioreactor needs to be technically sound to prevent such leaks and ensure long-term operation. We aim to implement a stricter threshold for the overall quality control in the power-to-food system and be more critical of our own abilities to setup a bioreactor. The first strategy is the optimization of the hollow fiber module to maintain it under strict anaerobic conditions for a longer period of operation. We investigated actively gassing the hollow fiber module to prevent any O₂ intrusion because of changes in the pressure gradient (**Figure 2**). Furthermore, we highly recommend the utilization of stainless-steel lines that are highly impermeable to gases. For a strictly anaerobic system such as the Stage 1 bioreactor, we may consider replacing the peripheral connections with stainless-steel.

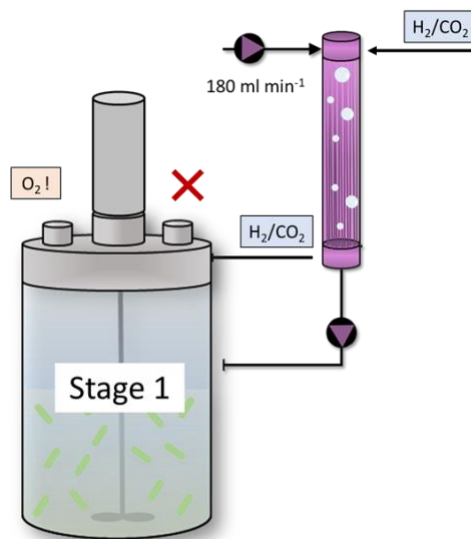


Figure 2: Introduction of a H₂/CO₂ gassing line to maintain the anaerobic conditions within the recycling module and facilitate its flow through the filtration module.

Furthermore, the gas sampling strategy will also be optimized for the power-to-food system. We can implement methods to measure the gas consumption *in-situ* during the fermentation using a gas chromatograph placed in series with a mass spectrometer. These in-line gas quantification will help us identify any fault in the system or any discrepancy in the biological activity as soon as it occurs. This will mitigate its negative impact on the productivity of acetic acid. Therefore, the nutrient composition and the biomass yield in the Stage 2 bioreactor in an integrated system will remain unhindered. It is of utmost importance to immediately identify any technical or biological

issue that affects the performance of the Stage 1 bioreactor and curb its effect at the source. An early detection of technical setbacks is pivotal for the consistent operation of an integrated system.

Biological optimizations

Genetic tools to amplify cobalamin synthesis in *C. ljungdahlii*

Unfortunately, with our experiments in Chapter 3, we were unable to find conclusive evidence of cobalamin production by *C. ljungdahlii*. Even if were possible for *C. ljungdahlii* to synthesize cobalamin, its concentration may have been masked because of the addition of yeast extract and cobalamin to the media. However, we can take advantage of an integrated system and include tools from synthetic biology to initiate or augment cobalamin synthesis in the Stage 1 bioreactor. First, we can use the ^{13}C -metabolic flux analysis to follow the path of carbon metabolism and its incorporation into the cobalamin structure (Z.-J. Wang *et al.*, 2012). This would reveal how the precursors of metabolic reactions, methyl groups, and different carbon assimilation pathways impact cobalamin production. Subsequently, this information can be manipulated with gene over-expression (Piao *et al.*, 2004), inactivation or down-regulation (Biedendieck *et al.*, 2010) to increase B12 production. All these methods have already been applied on the two popular candidates for B12 production in the industry, that are *Propiobacterium freundrichii* and *Bacillus megaterium* (Biedendieck *et al.*, 2010).

Based on the metabolic models present in Nagarjan *et al.* (2013) and Köpke *et al.* (2010) *C. ljungdahlii* has the genetic capacity to synthesize cobalamin (Section II, Chapter 1) (Köpke *et al.*, 2010; Nagarajan *et al.*, 2013). Annan *et al.* (2019) confirmed vitamin B12 prototrophy in *C. ljungdahlii* after its elimination from the media. We can adapt the strategies implemented on *B. megaterium* and *P. freundrichii* to increase B12 yield in *C. ljungdahlii* (Annan *et al.*, 2019). For instance, from the pathway illustrated in the KEGG database for *C. ljungdahlii*, it should be possible to redirect the metabolic flux from tetrapyrrole towards cobalamin synthesis. In a different study, the introduction of a plasmid expressing the *cbi* operon in *B. megaterium* enhanced cobalamin production to $200\ \mu\text{g L}^{-1}$ (S. J. Moore *et al.*, 2014). We can take advantage of the genetic system that is available for *C. ljungdahlii* to test whether this approach would yield similar results. Apart from the ones stated, several other genetic tools can be employed in *C. ljungdahlii* to initiate

or enhance the synthesis of B12. This can raise the scope of the power-to-food platform by providing an essential vitamin for the human diet.

Scope for media optimization in the power-to-food system to facilitate B12 production in *C. ljungdahlii*

Products of biological processes that have been manipulated with genetic tools often encounter severe scrutiny. This is especially true for substances that are directly consumed or utilized by humans. This has inspired several strategies to enhance the cobalamin content in such processes through media optimization. Cultivation of *B. megaterium* under different experimental conditions that were shown to be statistically favorable for B12 production resulted in the highest volumetric yield of 786.36 $\mu\text{g L}^{-1}$ (Mohammed *et al.*, 2014). Therefore, we can test similar strategies to first detect, and then increase the production of B12 in Stage 1. As suggested before in Chapter 3, our goal is to enter Phase 4 of power-to-food operation to isolate B12 production after its elimination from the media. This can be further be accompanied by the addition of specific micronutrients, trace elements, or precursors that augment specific pathways for its production (Chamlagain, 2016; P. Wang *et al.*, 2015). Addition of amino acids like glutamic acid, glycine and theonine have also been shown to stimulate the synthesis of B12 (Sych *et al.*, 2016). In the industry, CO^{2+} and DMB are popular supplements for enhancing B12 production (P. Wang *et al.*, 2015). It is worthwhile to investigate whether such a simple strategy in the form of an additive can provide an immense benefit to the Stage 1 bioreactor for B12 production.

Extrapolating the power-to-food concept to other systems

Production of cobalamin in a two-stage system was first shown by Quesada Chanto *et al.* (1994) (Quesada-Chanto *et al.*, 1994). They achieved a production rate of 1.47 $\text{mg L}^{-1} \text{h}^{-1}$ when supplemented with cobalt (Co^{2+}) and 5,6-dimethylbenzimidazole (DMB). Their technique motivated a two-step process for the synthesis of B12 with *Propionibacterium* at an industrial scale (Balabanova *et al.*, 2021). The first step promotes the structural synthesis of cobalamin under anaerobic conditions and is later switched into aerobic conditions for the attachment of the DMB ligand (Balabanova *et al.*, 2021). Although the power-to-food system is also operated in two-stages, its uniqueness lies in the administration of a gaseous substrate.

Therefore, as shown in Chapter 1, this concept is adaptable to several pathways of carbon assimilation. For instance, H₂-oxidizing bacteria can grow with H₂/CO₂ to generate methane and a high yield of cobalamin (Zhang, 2002). It would be rewarding to investigate the nutrient composition of a two-stage system, wherein H₂ oxidizing bacteria produce methane and cobalamin from H₂/CO₂ in the first stage, while the second stage consumes the methane to yield biomass that capable of accumulating cobalamin. Another illustration of a two-stage process to create microbial biomass enriched in B12 for human consumption could be with algae and cyanobacteria. This system would then become an adaptation of their symbiotic exchange of B12, as observed in nature. This is especially true now that higher fungi and algae are proven to be capable of accumulating B12 and converting it into its active forms (Koyyalamudi *et al.*, 2009). Moreover, some microalgae are even shown to convert the less available pseudocobalamin to the form active for humans (Nef *et al.*, 2019).

Outlook-I

At a commercial scale, microbial protein from gas fermentation is currently being considered for H₂-oxidizing bacteria. They have a lipid, carbohydrate, and protein content 4 - 5%, 28- 56%, and 33 -37% respectively (Nyyssölä *et al.*, 2021). In comparison, to address the overall scope of the power-to-food project, we require a similar evaluation of its output for human consumption. Fortunately, utilization of yeast as SCP is widely accepted, but its consumption in a serving size comparable to other sources of protein may create severe problems in our body (Monika E. Jach & Serefko, 2018). Moreover, its downstream processing, packaging, and fortification warrants further evaluation before being subjected to a rigorous, legislative procedure for acceptance. After a thorough investigation of ten years, Marlow Foods finally received the approval from U.S Food and Drug administration for selling *F. venenatum* as a meat alternative (T. J. A. Finnigan *et al.*, 2019). Nevertheless, despite the effort pledged by the scientific community, followed by a wearisome process and legislation, the extent to which such technologies can mitigate the CO₂ emissions makes the research worthwhile. It will transform the food industry into a circular economy. This leads us to the following questions to envision the prospects of this project:

- Will the inclusion of synthetic biology/metabolic engineering in Stage 1 operation, initiate an industrially competitive production of vitamin B12?

- What measures can be taken to maintain a stable performance of the power-to-food system after its scaled-up?

Gaining an in-depth knowledge of microbial gas fermentation by studying bubble size properties

One of the key parameters that govern substrate availability to the microbes in a gas fermentation system is the gas-to-liquid mass transfer coefficient (K_L). The gaseous substrate is introduced into the fermentation system in the form of bubbles. These bubbles are surrounded by a layer of stagnant liquid film containing the dissolved gas components. The amount of gas within this liquid film is mainly dictated by the interfacial area of the gas bubble and Henry's constant of the residing gas. Therefore, the dissolution and transfer of gas from a bubble to the surrounding liquid film become the primary determinant of substrate availability, emphasizing the importance of a bubble's physical characteristics. This phenomenon has inspired extensive research on the dynamics of bubble behavior and size properties, particularly while dealing with gaseous substrates.

Furthermore, in one of the syngas fermentation experiments carried out in the Angenent lab in Cornell, a considerable reduction in the radius of the gas bubbles was recorded (Martin *et al.*, 2016). This may have corresponded to a lower interfacial area, resulting in a higher gas to liquid mass transfer value. As this observation was absent in a non-inoculated fermenter, it indicated the influence of an unknown biotic component (Martin *et al.*, 2016). Therefore, it was speculated that surface-active metabolites were secreted into the fermentation broth during autotrophic acetogenesis. Therefore, we propose a few experimental designs that could inspire a researcher to pursue this objective in our lab. These experiments are specifically designed to distinguish between the contribution of both biotic and abiotic parameters that influence mass transfer dynamics by governing the bubble size properties during gas fermentation.

1st Setup: Visually tracking bubbles *in-situ* during fermentation

Visually tracking the bubble characteristics inside the fermenter during its operation will capture the gradual modifications in the bubble diameter. Additionally, we will be able to correlate the amount of product formed or substrate consumed to the size of the bubbles. The setup consists of

a camera that is attached to a microscope to attain the required magnifying power. The camera will collect the images of gas bubbles formed at the wall of the reactor vessel in regular intervals. These images can be processed by an image processing algorithm such as Matlab or the ImageJ software to quantify the radius, area, and circumference of the bubbles. The estimated values of mass transfer co-efficient (K_{La}) will be compared with the experimental values of K_{La} , calculated from the partial pressure of CO_2 in the headspace (**Figure 3**). This comparison will validate the data obtained from our image analysis algorithm. This step might also reveal a correction factor that should be incorporated to reduce the error between the calculated and experimental K_{La} values (**Figure 3**).

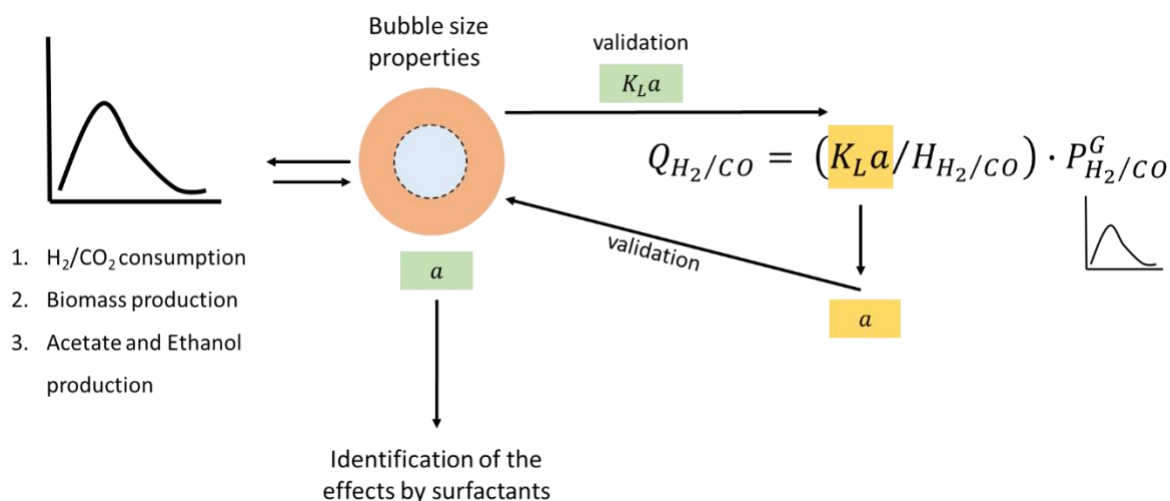


Figure 3: This figure shows how the physical properties of the bubbles are connected to mass transfer parameters obtained during fermentation. Apart from isolating the effects exerted by a biosurfactant, we can study bubble size properties to understand their impact on substrate consumption and the type of products formed. We will also compare the K_{La} values derived from the estimated radius of the bubbles to the values obtained experimentally to test the accuracy of the method proposed to visually study bubbles.

Analysis

The data will be analyzed based on statistics. Once the radius for each bubble is calculated, a histogram will be generated from every image collected at pre-determined sampling time points. This will enable the visualization of the bubble size properties. Based on the interpretations from the histogram, a one-way ANOVA test would be performed for confirming whether the mean from the samples collected at different time points within the same run is significantly different. Additionally, the average radius of the bubble will be used to calculate the K_{La} values for those

sampling time points. This will help in deriving a correlation between bubble size properties and the volumetric production and consumption rates during a continuous gas fermentation process.

2nd Setup: Determining the extent to which a surface-active metabolite affects the total gas mass transfer in the gas fermentation system

Measurements carried out in the previous design only reveal the cumulative effect of both biotic and abiotic variables on the bubble dimensions. However, this experiment is designed to record the bubble size properties under different test conditions to minimize and isolate the influence of such variables. We propose a pseudo-2D bubble column reactor for conducting multiple gas fermentation experiments for facilitating optical analysis. The design is very similar to that of the flat photo-bioreactors used for algae cultivation (Shahriar *et al.*, 2016). The two large flat surfaces on either side of the reactor provide enough surface area for a stronger and uniform illumination. The dimensions for each part have been stated in Figure 4. It is designed to contain a volume of 1 L with a 50:50 headspace to liquid ratio. Additionally, a needle sparger will be placed at the bottom of the column for the introduction of the H₂/CO₂ gas. Steps will be taken to make the reactor gas-tight and capable of tolerating a maximum positive pressure of 0.8 bar.

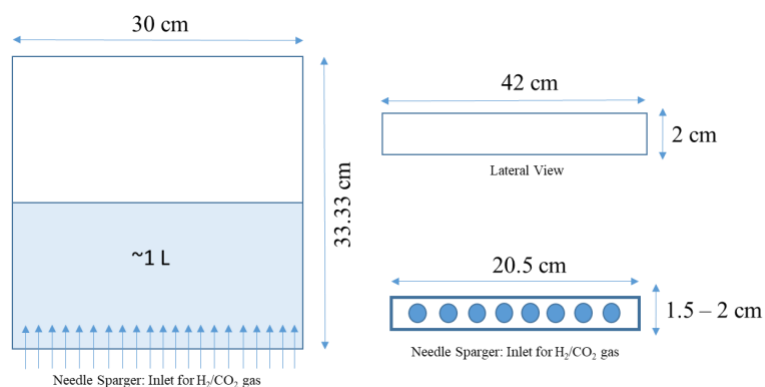


Figure 6: A preliminary design of the pseudo-2D bubble column reactor. It is subject to modification depending on the outcome of the preceding experiments

Several studies conducted on bubble size properties, dynamics, and behavior have opted for pseudo-2D columns to facilitate visualization in turbid solvents (Laupsien *et al.*, 2017). The biggest obstacle in most optical measurement techniques is the error introduced from the variation in depth of the different bubbles while being captured in a 2D focal plane. This gives rise to inaccurate estimations of bubble dimensions. With a 2D reactor, we will reduce these errors that

are otherwise unaccounted for in a 3D setup. An additional advantage of a 2D reactor is the opportunity to eliminate other factors that also lead to biased observations but are crucial for maintaining optimal fermentation conditions, such as the effects caused by continuous stirring.

We suggest three types of gas fermentation experiments in parallel to each other to test the impact of all the biotic/abiotic parameters on the bubble size properties. The three parameters we are interested in are electrolytes, direct contact of the microbial cells, and the strength of a surface-active metabolite. All the gas fermentation experiments will be carried out in the pseudo-2D bubble column under the following treatments (**Figure 4**),

1. The first treatment will act as the cell-free control by only containing the mineral medium generally used in our gas fermentation experiments.
2. The second treatment will contain the *C. ljungdahlii* cells.
3. The third treatment will contain a filtered fermentation effluent derived from gas fermentation.

The images will be collected from one of the two larger flat surfaces of the 2D reactor using a high speed camera ([340M-USB](#) camera; MVL50TM23 lens, Thor Labs). The camera will be placed directly in front of the reactor and will be automated to capture images at regular time points. The same camera will be transferred between each treatment for collecting visual data.

Analysis

Parameters like bubble radii and bubble velocity can be quantified with a Matlab code and the ImageJ software. The range for the observed bubble radii will be calculated by developing a histogram plot for each sampling time-point. Furthermore, the difference between the various treatments will be confirmed using a One-way ANOVA test. If these results show significant difference amongst the treatments, a post-hoc analysis (e.g. Tukey's test) will be performed to compare the different treatments. The K_{ia} will be estimated from the observed bubble radius as well as the H_2/CO_2 partial pressure in the headspace. The concentration of the biosurfactant will be measured via HPLC-MS (Agilent Technologies, Inc., CA) or GC-MS (SRI Instruments, CA) using the method developed earlier. The K_{ia} values as well the application of some qualitative assays will help us compare the tensio-activity of the extracted biosurfactant to the synthetic surfactant. *C. ljungdahlii* cells show auto-fluorescence between a wavelength 515 - 560 nm. We can exploit

this property to visually capture the direct physical interaction of the microorganism to the gas bubbles by the formation of a fluorescing outline around the gas bubble.

Outlook-II

So far, to the best of our knowledge, a very small amount of research has been dedicated to the detection of surface-active metabolite and its effect on gas fermentation. Consolidating the outcomes from all these studies, we will be able to create a complete picture of this crucial interaction and recognize all its regulating parameters. (Domingues *et al.*, 2017) stated that in some cases, the presence of an insoluble solute stimulates the generation of surfactants in microorganisms. If this is proven to be consistent with our findings, it will lead us to novel optimization strategies for the syngas platform, facilitating an even higher gas mass transfer. Consequently, the scope for expanding the product spectrum derived from syngas fermentation will be even larger.

Conclusion

Microbial production platforms have two major competitive advantages in comparison to the existing conventional processes. First, they have a substantially lower carbon footprint. For instance, breeding livestock for meat production consumes a large proportion of natural resources in addition to emitting greenhouse gases. Second, in most cases, the food supplements obtained from microbial processes also contain the nutritional elements that are unavailable in plant-based food sources, leading to their deficiencies in a vegetarian diet. Furthermore, unlike the pharmaceutical industry, where a highly purified form of a single vitamin is manufactured, the food industry benefits from a heterogeneous synthesis of different vitamins occurring simultaneously along with the production of biomass and lipid. The feedstock for these processes can be diverse and is often manipulated to mass-produce commercial compounds resulting in a cost-effective operation. Maintenance of bioreactors is a multifaceted task. The user requires to have a strong foundation of both, technical and microbiological expertise. This further translates into superior bioreactor designs and operation. Although the establishment of an integrated system is highly challenging, once it's proven to be a sustainable source of nutrition and vitamins, it will create a novel use of the Syngas platform, that has so far, been unexplored.

References

- Annan, F. J., Al-Sinawi, B., Humphreys, C. M., Norman, R., Winzer, K., Köpke, M., Henstra, A. M. (2019). Engineering of vitamin prototrophy in *Clostridium ljungdahlii* and *Clostridium autoethanogenum*. *Applied microbiology and biotechnology*, *103*(11), 4633-4648. doi:10.1007/s00253-019-09763-6
- Balabanova, L., Averianova, L., Marchenok, M., Son, O., & Tekutyeva, L. (2021). Microbial and Genetic Resources for Cobalamin (Vitamin B12) Biosynthesis: From Ecosystems to Industrial Biotechnology. *International Journal of Molecular Sciences*, *22*(9), 4522. Retrieved from <https://www.mdpi.com/1422-0067/22/9/4522>
- Biedendieck, R., Malten, M., Barg, H., Bunk, B., Martens, J. H., Deery, E., Jahn, D. (2010). Metabolic engineering of cobalamin (vitamin B12) production in *Bacillus megaterium*. *Microb Biotechnol*, *3*(1), 24-37. doi:10.1111/j.1751-7915.2009.00125.x
- Chamlagain, B. (2016). Fermentation fortification of active vitamin B12 in food matrices using *Propionibacterium freudenreichii*: Analysis, production and stability.
- Domingues, P. M., Almeida, A., Leal, L. S., Gomes, N. C., & Cunha, Â. (2017). Bacterial production of biosurfactants under microaerobic and anaerobic conditions. *Reviews in Environmental Science and Bio/Technology*, *16*(2), 239-272.
- Finnigan, T. J. A., Wall, B. T., Wilde, P. J., Stephens, F. B., Taylor, S. L., & Freedman, M. R. (2019). Mycoprotein: The Future of Nutritious Nonmeat Protein, a Symposium Review. *Curr Dev Nutr*, *3*(6), nzz021. doi:10.1093/cdn/nzz021
- Jach, M. E., & Serefko, A. (2018). Chapter 9 - Nutritional Yeast Biomass: Characterization and Application. In A. M. Holban & A. M. Grumezescu (Eds.), *Diet, Microbiome and Health* (pp. 237-270): Academic Press.
- Köpke, M., Held, C., Hujer, S., Liesegang, H., Wiezer, A., Wollherr, A., Dürre, P. (2010). *Clostridium ljungdahlii* represents a microbial production platform based on syngas. *Proceedings of the National Academy of Sciences*, *107*(29), 13087-13092.
- Koyyalamudi, S. R., Jeong, S. C., Cho, K. Y., & Pang, G. (2009). Vitamin B12 is the active corrinoid produced in cultivated white button mushrooms (*Agaricus bisporus*). *J Agric Food Chem*, *57*(14), 6327-6333. doi:10.1021/jf9010966
- Laupsien, D., Cockx, A., & Line, A. (2017). Bubble Plume Oscillations in Viscous Fluids. *Chemical Engineering & Technology*, *40*(8), 1484-1493. doi:<https://doi.org/10.1002/ceat.201600690>
- Martin, M. E., Richter, H., Saha, S., & Angenent, L. T. (2016). Traits of selected *Clostridium* strains for syngas fermentation to ethanol. *Biotechnol Bioeng*, *113*(3), 531-539. doi:10.1002/bit.25827
- Mohammed, Y., Lee, B., Kang, Z., & Du, G. (2014). Development of a two-step cultivation strategy for the production of vitamin B12 by *Bacillus megaterium*. *Microbial cell factories*, *13*(1), 102. doi:10.1186/s12934-014-0102-7

- Molitor, B., Mishra, A., & Angenent, L. T. (2019). Power-to-protein: converting renewable electric power and carbon dioxide into single cell protein with a two-stage bioprocess. *Energy & Environmental Science*.
- Moore, S. J., Mayer, M. J., Biedendieck, R., Deery, E., & Warren, M. J. (2014). Towards a cell factory for vitamin B12 production in *Bacillus megaterium*: bypassing of the cobalamin riboswitch control elements. *New biotechnology*, *31*(6), 553-561.
- Müller, V., & Wiechmann, A. (2017). Synthesis of Acetyl-CoA from Carbon Dioxide in Acetogenic Bacteria. In O. Geiger (Ed.), *Biogenesis of Fatty Acids, Lipids and Membranes* (pp. 1-18). Cham: Springer International Publishing.
- Nagarajan, H., Sahin, M., Nogales, J., Latif, H., Lovley, D. R., Ebrahim, A., & Zengler, K. (2013). Characterizing acetogenic metabolism using a genome-scale metabolic reconstruction of *Clostridium ljungdahlii*. *Microbial cell factories*, *12*(1), 118. doi:10.1186/1475-2859-12-118
- Nef, C., Jung, S., Mairet, F., Kaas, R., Grizeau, D., & Garnier, M. (2019). How haptophytes microalgae mitigate vitamin B12 limitation. *Scientific Reports*, *9*(1), 8417. doi:10.1038/s41598-019-44797-w
- Nyssölä, A., Ojala, L. S., Wuokko, M., Peddinti, G., Tamminen, A., Tsitko, I., Lienemann, M. (2021). Production of Endotoxin-Free Microbial Biomass for Food Applications by Gas Fermentation of Gram-Positive H₂-Oxidizing Bacteria. *ACS Food Science & Technology*, *1*(3), 470-479. doi:10.1021/acsfoodscitech.0c00129
- Piao, Y., Yamashita, M., Kawaraichi, N., Asegawa, R., Ono, H., & Murooka, Y. (2004). Production of vitamin B12 in genetically engineered *Propionibacterium freudenreichii*. *J Biosci Bioeng*, *98*(3), 167-173. doi:10.1016/s1389-1723(04)00261-0
- Quesada-Chanto, A., S.-Afschar, A., & Wagner, F. (1994). Microbial production of propionic acid and vitamin B12 using molasses or sugar. *Applied microbiology and biotechnology*, *41*(4), 378-383. doi:10.1007/BF01982523
- Shahriar, M., Monir, M. I., & Deb, U. K. (2016). Comparative Analysis of Hydrodynamics Behavior of Microalgae Suspension Flow in Circular, Square and Hexagonal Shape Photo Bioreactors. *American Journal of Computational Mathematics*, *6*(04), 320.
- Sych, J. M., Lacroix, C., & Stevens, M. J. (2016). Vitamin B12—Physiology, Production and Application. *Industrial biotechnology of vitamins, biopigments, and antioxidants*.
- Valgepea, K., de Souza Pinto Lemgruber, R., Meaghan, K., Palfreyman, R. W., Abdalla, T., Heijstra, B. D., . . . Marcellin, E. (2017). Maintenance of ATP Homeostasis Triggers Metabolic Shifts in Gas-Fermenting Acetogens. *Cell Systems*, *4*(5), 505-515.e505. doi:https://doi.org/10.1016/j.cels.2017.04.008
- Wang, P., Zhang, Z., Jiao, Y., Liu, S., & Wang, Y. (2015). Improved propionic acid and 5,6-dimethylbenzimidazole control strategy for vitamin B12 fermentation by *Propionibacterium freudenreichii*. *Journal of Biotechnology*, *193*, 123-129. doi:https://doi.org/10.1016/j.jbiotec.2014.11.019

Wang, Z.-J., Wang, P., Liu, Y.-W., Zhang, Y.-M., Chu, J., Huang, M.-z., Zhang, S.-L. (2012). Metabolic flux analysis of the central carbon metabolism of the industrial vitamin B12 producing strain *Pseudomonas denitrificans* using ¹³C-labeled glucose. *Journal of the Taiwan Institute of Chemical Engineers*, 43(2), 181-187. doi:<https://doi.org/10.1016/j.jtice.2011.09.002>

Zhang, T. M. Y. (2002). United States Patent No. US7018815B2.

Acknowledgement

I would like to express my deepest gratitude to Prof. Largus. T. Angenent, who accepted me as his first PhD student in his working group in Tübingen, Germany. We were both immensely inspired by outcome of this thesis and its potential to revolutionize the food industry. This has encouraged me to bring this thesis to a completion. I am thankful to him for always recognizing that I wanted to make an impact through my dissertation, and supporting me accordingly with all his resources. He taught me how to be thorough to attain perfection, the value of working hard, and communicating with precision. This dissertation has not resulted in the outcome we hoped for, but I believe that it will establish a solid foundation for the successor of this project.

I acknowledge the support from the Alexander Von Humboldt foundation for funding my position. I would also like to express my gratitude to the Max-Planck Institute of Developmental Biology for their support during the early years of my PhD. I was fortunate to have received an incredible amount of guidance from the IT, electrical, and mechanical workshop for establishing the lab. I would like to specifically acknowledge the efforts of Luis Antonetti and Klaus Schneider for helping me build the power-to-food system. Furthermore, I must also thank Dr. Bastian Molitor for supervising the building of the reactor system and for teaching me how to conduct data collection and analysis. I am extremely grateful to Nicolai Kliem-Kuster for preparing and operating the power-to-food system always with perfection and optimism.

I would like to express my deepest appreciation to our collaborators at the Technical University of Munich in Friesing. This mainly includes Nadine Weber and Mengle Wang for helping me generously with their experience and knowledge for analyzing folate and cobalamin. Thank you for taking the time out to conduct the analysis of my biological samples with high precision and sensitivity. I have benefitted substantially from our discussions regarding this topic, and it has elevated the overall quality of this dissertation. Furthermore, I have learned to appreciate the importance of analytic skills towards the overall success of a multidisciplinary project such as this one. I am deeply indebted to Prof. Michael Rychlik for making this possible by accepting our request for collaboration and giving us the confidence to pursue this project.

The completion of my dissertation would not have been possible without the support and nurturing of my colleagues in the lab, who within a span of four and half years became my family in Germany. Thank you for supporting me through all difficult moments of self-doubt and distress. Without your sense of humor, friendship, and wisdom, it would have been impossible for me to witness the end of this journey. I am especially grateful for Christian Fink, Patrick Schweizer, Isabella Casini, Dr. Sofia Esquivel Elizondo, Ginés Martínez Cano, Nicolai Kliem-Kuster and Dr. Richard Hegner. Thank you for supporting me so generously and for looking after me. All of you have inspired me with your perseverance and determination in your personal/professional lives. I hope to acquire this into my next endeavor.

I cannot begin to express my thanks to my family, who have endured innumerable sacrifices and separation to help me reach this point. I dedicate this dissertation to the prayers and blessings of my grandparents and parents. Lastly, I would like to thank my greatest support system, my partner, for compensating the absence of my family by gladly taking over their role. Thank you for loving me unconditionally through all the highs and lows of this journey. You will always be my most favorite cheerleader! I am extremely grateful for him and his family for keeping me healthy and sane throughout this process. Going forward, I hope to make you all proud for everything you have done to support me.

Statement of contribution

Chapter 1: Power-to-Protein: Carbon Fixation with Renewable Electric Power to Feed the World

Largus T. Angenent led the discussion and oversaw the writing. Akanksha Mishra and Largus T. Angenent wrote the manuscript. Akanksha Mishra calculated the stoichiometric equations with advice from Dr. Tiaran Sun and Dr. Sofia Esquivel Elizondo about the electrochemical calculations and the applications of the electron equivalent model, respectively. Jean Nepomuscene Ntihuga drew the figure and validated all the calculations. Bastian Molitor organized the paper and edited the manuscript.

Chapter 2: Power-to-protein: converting renewable electric power and carbon dioxide into single cell protein with a two-stage bioprocess

The study was conceptualized by Largus T. Angenent, Dr. Hanno Richter and Dr. Bastian Molitor. Dr. Bastian Molitor performed the power-to-protein reactor experiments. Largus T. Angenent and Dr. Bastian Molitor wrote the manuscript. Akanksha Mishra performed the protein quantification in the biomass obtained from the power-to-protein reactor. She also drew the graphical abstract and Figure 1 for the manuscript. Largus T. Angenent performed the technical economic analysis, and the rest of the authors verified the calculations.

Chapter 3: Establishing a power-to-food platform using renewable electric power and carbon dioxide by demonstrating the presence of essential vitamins in single-cell protein

The experimental design in this study was conceptualized by Akanksha Mishra with advice from Largus T. Angenent. Akanksha Mishra wrote the manuscript and developed the microbiological analysis for quantifying the different forms of cobalamin in the biological samples. Nicolai Kliem-Kuster and Akanksha Mishra operated the power-to-food bioprocess system. Nadine Weber and Mengle Wang measured folate and cobalamin analogues, respectively and supported in the finalization of the overall discussion. Akanksha Mishra, Nadine Weber, and Mengle Wang interpreted the data from the instrumental analysis.

Publications

Published

Mishra A., Ntihuga J. N., Molitor B. and Angenent L. T. (2020). Power-to-protein: Carbon fixation with renewable electric power to feed the world. *Joule*, Vol. 4, No. 6, pp. 1142-1147.

Molitor B., Mishra A and Angenent L. T. (2019). Power-to-protein: converting renewable electric power and carbon dioxide into single cell protein with a two-stage bioprocess, *Energy and Environmental Science*, Vol. 21, No. 12, pp. 3515-3521.

In preparation

Mishra A., Weber N., Wang M., Molitor B., Rychlik M. and Angenent L. T. (2021). *Manuscript in preparation*